



Batas, Anastasios (2018) *Protein trafficking and autophagy in the moulting cycle of C. elegans*. PhD thesis.

<https://theses.gla.ac.uk/8856/>

Copyright and moral rights for this work are retained by the author

A copy can be downloaded for personal non-commercial research or study, without prior permission or charge

This work cannot be reproduced or quoted extensively from without first obtaining permission in writing from the author

The content must not be changed in any way or sold commercially in any format or medium without the formal permission of the author

When referring to this work, full bibliographic details including the author, title, awarding institution and date of the thesis must be given

Enlighten: Theses

<https://theses.gla.ac.uk/>
research-enlighten@glasgow.ac.uk

Protein trafficking and autophagy in the moulting cycle of *C. elegans*.

A thesis submitted to the INSTITUTE OF MOLECULAR, CELL AND SYSTEMS
BIOLOGY

For the degree of DOCTOR OF PHILOSOPHY

by **Anastasios Batas**

College of Medical, Veterinary and Life Sciences Institute of Molecular, Cell and Systems
Biology University of Glasgow

January 2018

Abstract

Endosomal trafficking and autophagy are two fundamental processes of eukaryotic cell biology, from unicellular organisms such as yeast to multicellular metazoans such as *C.elegans* and Humans. Both processes are involved in a diverse number of physiological processes and implicated in a number of pathologies. A recent study has exhibited a mutation on the SM protein Vps45 as a cause of severe congenital neutropenia in humans. The same mutation in yeast causes defects in endosome to vacuole trafficking in *S.cerevisiae* as well as a temperature sensitive lethality at the non-permissive temperature. A null allele of *vps-45* in *C.elegans* results in developmental arrest during the highly secretory phase of moulting in a similar temperature conditional manner to yeast and defects in yolk protein trafficking. The work presented in this thesis aims to provide basic understanding in an animal model of the impact of loss of Vps45 function that might be informative of the reason for the death of the highly secretory neutrophil cells under the absence of a functional Vps45 protein. The *vps-45* and *unc-51* mutants as well as a novel *unc-51 vps-45* double mutant where possible, were characterised for lifespan, duration of post- embryonic development as well as moulting duration. Reduced embryonic viability, reduced lifespan as well as delays in the moulting process were identified. Data suggested that both autophagy and protein trafficking play a role in *C.elegans* development through *unc-51* and *vps-45* respectively.

In addition to this, the seam cells of both the *vps-45* and *unc-51* defective *C.elegans* were observed during the moult using an autophagy marker. An increase in autophagic activity during the moult was observed, which was more pronounced in the case of the *vps-45* mutant. As such the obtained data suggest autophagy and endosomal trafficking play an important role in the moulting process.

Following up to previous work conducted in our lab in yeast defective for Vps45 trafficking which exhibited increased sensitivity to oxidative stress, the redox state of the *vps-45* and *unc-51* animals as well as their sensitivity to oxidative stress was assessed using a set of ER and cytosolic GFP markers and killing assays. Both the *vps-45* and *unc-51* mutants showed a higher sensitivity to oxidative stress, with the *unc-51* exhibiting the more pronounced phenotype overall. These results came in agreement with the shorter lifespan phenotypes exhibited by both mutants in the previous experiments, possibly as a result of accumulation of ROS, as well as the severe defects of the double mutant.

Finally, a suppressor identified for the moulting death of the *vps-45* mutant was characterized for a set of phenotypes, in order to exclude suppression of any of the other phenotypes identified for the *vps-45* mutant. Furthermore, the suppressor was identified as being autosomal and recessive and as thus an SNP full genome sequencing technique was employed, which gave rise to two suppression loci in two different chromosomes, along with two different subpopulations corresponding to these loci which exhibited different growing patterns.

Contents

Abstract	2
List of Tables	8
List of Figures	9
Acknowledgements	14
Authors Declaration	15
Abbreviations	16
Measurements	19
Chapter 1: Introduction	21
1.1 An introduction to <i>C. elegans</i>	21
1.1.1 <i>C. elegans</i> embryonic development	22
1.1.2 <i>C. elegans</i> post-embryonic development	23
1.1.3 <i>C. elegans</i> cuticle	24
1.1.4 Expression of cuticle collagen genes	26
1.1.5 Molting	26
1.1.6 The seam cells and their role in <i>C. elegans</i> development and molting	27
1.1.7 <i>C. elegans</i> genetics	29
1.1.8 Next generation sequencing	31
1.1.9 RNAi	34
1.2 The endocytic pathway	34
1.2.1 SM proteins and SNARE complexes	36
1.2.2 The SM protein Vps45	39
1.2.3 Loss of VPS45 as a cause for Neutropenia	40
1.2.4 VPS-45 and its role in <i>C. elegans</i>	41
1.3 Autophagy	42
1.3.1 The cytoplasm to vacuole targeting pathway	43
1.3.2 Induction of autophagy by the mTORC1 pathway	44
1.3.3 Induction of autophagy and autophagosome assembly	45
1.3.4 Fusion of the autophagosome and the lysosome	48
1.3.5 Autophagy in <i>C. elegans</i>	49
1.3.6 Autophagy an endocytic trafficking in molting	50
1.3.7 Autophagy in Disease	50
1.4 Project aims	51
Chapter 2: Materials and Methods	53
2.1 Solutions and media	53
2.2 Other Materials	55

2.2.1 Electrophoresis Markers	55
2.3 Methods	56
2.3.1 E.Coli OP50 bacteria culturing	56
2.3.2 Nematode culture in solid media	56
2.3.3 Nematode Handling	57
2.3.4 Freezing and thawing nematode stocks	59
2.3.5 Decontamination of <i>C. elegans</i> stocks	59
2.3.6 Nematode synchronous cultures	59
2.3.8 <i>C. elegans</i> crosses	61
2.3.9 Routine microscopy	61
2.3.10 Quantification of whole body <i>C. elegans</i> fluorescence	62
2.3.11 <i>C. elegans</i> lysis and genomic DNA extraction	63
2.3.12 <i>C. elegans</i> lysis and genomic DNA extraction for full genome sequencing	63
2.3.13 Quantitation of DNA	64
2.3.14 Preparation of samples for full genome sequencing	64
2.3.15 Restriction endonuclease digestion of DNA fragments.....	64
2.3.16 Polymerase chain reaction (PCR)	65
2.3.17 DNA Gel electrophoresis.....	74
2.3.18 Detecting the ER redox state of nematodes using a 96-well plate reader.....	74
2.3.19 Scoring <i>C. elegans</i> adult lifespan.....	76
2.3.20 Scoring <i>C. elegans</i> viability under oxidative stress	76
2.3.21 Quantifying GFP expression under oxidative stress.....	76
2.3.22 RNAi of <i>C. elegans</i> by bacterial feeding method	77
2.3.23 Western blots	78
2.3.24 Immunolocalisation of <i>C. elegans</i> proteins.....	80
2.4 Graphs and statistical analysis.....	81
Chapter 3: Phenotypic characterisation and comparison of <i>vps-45</i> (tm246) and <i>unc-51</i> (e369) mutants and identification of a functional relationship between autophagy and the endosomal trafficking pathway in <i>C. elegans</i> molting	82
3.1 Overview and aims	82
3.2 The <i>vps-45</i> (tm246) endosomal trafficking mutant at 25°C exhibiting defects in molting.....	85
3.3 The <i>vps-45</i> (tm246) and <i>unc-51</i> (e369) mutant strains exhibit embryonic lethality during development	85
3.4 The autophagy defective <i>unc-51</i> (e369) mutant strain does not die by molting when cultured at 25°C.....	87
3.5 The <i>unc-51</i> (e369) V; <i>vps-4 5</i> (tm246) X double homozygotic mutant exhibits a synthetic effect	88

3.6 Genetic analysis of the unc-51(e369) vps-45(tm246) double homozygotic mutant ..	94
3.7 Size comparison of the vps-45 (tm246), unc-51 (e369) and unc-51 (e369) V; vps-45 (tm246) X double mutant	99
3.8 Phenotypic analysis of internal and cuticular structures of vps-45 (tm246), unc-51 (e369) and unc-51 (e369) V; vps-45 (tm246) X mutants	100
3.9 Characterisation of the moult and intermoult periods on vps-45 (tm246) and unc-51 (e369) mutants	108
3.10 Determination of lifespan for vps-45 (tm246) and unc-51 (e369) mutants	113
3.11 Chapter summary	116
Chapter 4: The role of autophagy and protein trafficking during embryonic development and molting	118
4.1 Overview and aims	118
4.2 Introduction of the LGG-1::GFP and AJM-1::GFP markers in unc-51 (e369) and vps-45 (tm246) backgrounds	120
4.3 LGG-1 accumulates in the seam cells during molting	121
4.4 Assessment of the retention of the LGG-1 autophagy marker in the seam cells in vps-45 (tm246) and unc-51 (e369) mutants	130
4.5 Assessment of the autophagy levels in the seam cells of wild type, vps-45 (tm246) mutant and unc-51 (e369) mutant <i>C. elegans</i>	134
4.6 LGG-1 is expressed in the seam cells in <i>C. elegans</i> embryos at the 3 fold stage and is retained for longer in the unc-51 (e369) mutant post-hatch	138
4.7 LGG-1 expression in the seam cells and seam cell division are two distinct processes	145
4.8 vps-45 (tm246) and unc-51 (e369) mutant embryos demonstrate higher levels of LGG-1 marker at the 3-fold stage	147
4.9 vps-45 (tm246) and unc-51 (e369) mutants exhibit higher levels of expression of the LGG-1 protein outside of the molt	149
4.10 Chapter summary	151
Chapter 5: Investigating oxidative imbalances and resistance to oxidative stress in unc-51 (e369) and vps-45 (tm246) mutants	153
5.1 Overview and aims	153
5.2 The roGFP ER3 marker and its introduction in the vps-45 (tm246) and unc-51 (e369) mutant backgrounds	155
5.3 The roGFP ER3marker can detect changes in ER redox state in <i>C. elegans</i>	157
5.4 Assessing the survival of vps-45 (tm246) and unc-51 (e369) mutants under oxidative stress	162
5.5 Assessing the oxidative response of vps-45 (tm246) and unc-51 (e369) mutants under oxidative stress	165
5.6 Chapter summary	176

Chapter 6: Characterisation and identification of the vps-45 (tm246) molting death suppressor.....	178
6.1 Overview and aims	178
6.2 Characterization of the svp (ij117) vps-45 (tm246) suppressed mutant	178
6.3 svp (ij117) suppresses the vps-45 (tm246) molting death at 25°C.....	179
6.4 The suppressor does not change the body size of vps-45 (tm246) mutants	179
6.5 The svp (ij117) suppressor allele does not suppress embryonic lethality	181
6.6 Characterisation of the molt and intermolt periods on the IA773 strain	183
6.7 Determination of lifespan for the IA773 strain	188
6.8 The svp (ij117) suppressor follows a recessive and autosomal inheritance pattern.	191
6.9 Introduction of the vps-45 (tm246) deletion allele and svp (ij117) suppressor, into ‘Hawaiian’ genetic background for whole genome sequencing analysis.....	195
6.10 Next generation sequencing analysis of the svp (ij117) vps-45 (tm246) suppressed mutants in Hawaiian background	197
6.11 Identification of candidate suppressors for the vps-45 (tm246) molting arrest....	202
6.12 Testing of the candidate genes for suppression of the vps-45 (tm246) using RNAi	203
6.13 Identification of two different genetic subpopulations within the vps-45 (tm246) suppressed lines	206
6.14 A second linkage area on chromosome V suggest the existence of a second suppressor for the vps-45 (tm246) molting arrest	209
6.15 At least two phenotypic sub-populations exist within the 40 suppressed sequencing lines exhibiting different growth patterns	212
6.16 Chapter summary	214
Chapter 7: Discussion	216
7.1 Characterisation and identification of the vps-45 (tm246) molting death suppressor	218
7.2 Phenotypic characterisation of unc-51 (e369), vps-45 (tm246) and unc-51(e369) vps-45 (tm246) synthetic lethal double mutant.....	220
7.3 Autophagy is developmentally regulated during molting and is required for the survival of vps-45 (tm246) mutants.	223
7.4 Investigating oxidative imbalances and resistance to oxidative stress in unc 51 (e369) and vps-45 (tm246) mutants.....	226
7.5 Concluding remarks and future work.....	230
References	232
Appendices.....	255

List of Tables

Table 2.1: List of <i>C.elegans</i> strains used in this study.....	57
Table 2.2: Components of general mix used for digestion of DNA	65
Table 2.3: List of the primers used in this study for the detection of mutant alleles and Hawaiian and Bristol SNPs	66
Table 2.4: Components of general mix used for PCR amplification using two primers ...	68
Table 2.5: Components of the mix used for PCR amplification of the <i>vps-45</i> allele and the mutant <i>vps-45 (tm246)</i> allele, using two forward and one reverse primers in a single reaction	69
Table 2.6: Primers used for the distinction of Hawaiian and Bristol sequences in <i>C.elegans</i> on chromosomes I and IV	71
Table 2.7: Primers used for the distinction of Hawaiian and Bristol sequences in <i>C.elegans</i> on several regions of chromosome II	72
Table 2.8: Primers used for the distinction of Hawaiian and Bristol sequences in <i>C.elegans</i> on several regions of chromosome V	73
Table 2.9: Settings used by the plate reader for the detection of the redox state of the roGFP marker in nematodes.....	75
Table 2.10: List of RNAi strains used in this study	77
Table 3.1: Table 3.1: Table of progeny from five IA900 parents	97
Table 3.2: Table of showing the number of double mutant progeny dying during larval development	98
Table 4.1: Analytical tables of the onset of LGG-1 expression during the molt for individual <i>C.elegans</i> for each strain	131
Table 6.1: Inheritance pattern of the <i>svp (ij117)</i> suppressor allele	193
Table 6.2: List of candidate suppressors retrieved from sequencing results for the <i>C.elegans</i> Chromosome II	204
Table 6.3: Visual representation of homozygosity of Bristol (red) or Hawaiian (green) sequences of each of the suppressed lines for Chromosome II	208

Table 6.4: Visual representation of homozygosity of Bristol (red) or Hawaiian (green) sequences of each of the suppressed lines for chromosome V	211
Appendix 6: Table showing the concentration of each sample from the 40 sequencing lines genomic isolates, as it was quantified from the gel pictures.....	262
Appendix 9: Table showing the concentration of each sample from the genomic isolates, as it was quantified from the gel pictures for the second round for full genome sequencing	266

List of Figures

Figure 1.1: Major changes in body appearance of <i>C.elegans</i> during embryonic development	23
Figure 1.2: <i>C.elegans</i> larval development	24
Figure 1.3: Schematic of an adult <i>C.elegans</i> cuticle depicting its multi-layered structure	25
Figure 1.4: Position of the seam cells in the hypodermis of <i>C.elegans</i>	28
Figure 1.5: Schematic of the arrangement of the seam cells in an adult <i>C.elegans</i> with respect of the hypodermis and the cuticle	29
Figure 1.6 Schematic depicting the chromosomal recombinations that can occur between the wild type Bristol strain and the highly polymorphic Hawaiian strain	33
Figure 1.7: Schematic representation of the endosomal system	36
Figure 1.8: Schematic representation of the SNARE and SM proteins in membrane fusion during protein trafficking	38
Figure 1.9: Depiction of the steps for the initiation of autophagy and formation of autophagosome	43
Figure 1.10: Regulation of autophagy in mammals	45
Figure 3.1: DIC microscopy, moulting arrest of IA757 animals when cultured at 25°C ...	86
Figure 3.2: Progeny of young adult <i>C.elegans</i> which were hatched 48h hours after egg laying as a percentage of total number of eggs laid	89
Figure 3.3: Survival of <i>C.elegans</i> after 120 hours of culturing, from L1 arrest at 25°C. ..	90

Figure 3.4: PCR samples run on 2% agarose gels for the detection of <i>unc-51 (369)</i> and <i>vps-45 (tm246)</i> alleles	92
Figure 3.5: Cuticular defects of the <i>vps-45(tm246) unc-51(e369)</i> double homozygotic hermaphrodite	93
Figure 3.6: DIC microscopy of <i>unc-51 (e369) vps-45 (tm246)</i> double homozygotic animals at various larval stages	95
Figure 3.7: Length comparison of wild type, IA757, CB369 strains and <i>unc-51 (e369) vps-45 (tm246)</i> double mutant_	101
Figure 3.8: DIC microscopy, of the pharynx of adults cultured at 15°C	102
Figure 3.9: DIC microscopy, of intestine of adult animals cultured at 15°C	103
Figure 3.10: DIC microscopy, of adult cuticular alae (white arrows)	104
Figure 3.11: Immunolocalisation of <i>C.elegans</i> DPY-7 cuticular collagen	106
Figure 3.12: Immunolocalisation of DPY-7 cuticular collagen, in <i>vps-45 (tm246)</i> mutants during moulting arrest when cultured at 25°C	107
Figure 3.13: Moulting profiles of N2 , IA757, CB369 strains during the L1-L2 molt at 15°C	109
Figure 3.14 Duration of moult and development time to adulthood for N2, IA757 and CB369 strains	111
Figure 3.15 Developmental stage of N2, IA757, CB369 animals in cultures after 72h of development, from L1 arrest at 15°C	113
Figure 3.16 Lifespan of adult N2, IA757 and CB369 <i>C.elegans</i> at 15°C and 25°C	115
Figure 4.1: UV microscopy DA2123 L1 larvae before (24 hours), during (27 and 30 hours) and after (31 hours) of the L1-L2 moult	126
Figure 4.2: UV microscopy of IA903 animals before (24 hours), during (26 and 28 hours) and after (31 hours) the L1-L2 moult	127
Figure 4.3: UV microscopy of IA888 larvae before (25 hours), during (29 and 35 hours) and after (36 hours) of the L1-L2 moult.	128
Figure 4.4: UV microscopy of IA897 L1 larvae before (25 hours), during (29 and 31 hours) and after (34 hours) of the L1-L2 moult	129

Figure 4.5: Average time of retention of LGG-1 in the seam cells after the end of the moult	133
Figure 4.6: Overall levels of LGG-1::GFP in N2, IA888 and IA897 adult <i>C.elegans</i>	135
Figure 4.7: Representative images of DIC and UV (200ms) images of coma stage, two-fold and three-fold stage embryos along with hatching embryos of DA2123[<i>adIs2122 [lgg-1p::GFP::lgg-1 rol-6(su1006)]</i>] strain	141
Figure 4.8: Representative images of DIC and UV (200ms) images of coma stage, two-fold and three-fold stage embryos along with hatching embryos of wild type IA903 [<i>adIs2122 [lgg-1p::GFP::lgg-1 rol-6(su1006)]</i>]; <i>jcIs1 [ajm-1::GFP unc-29(+)</i> <i>rol-6(su1006)] IV</i> strain	142
Figure 4.9: Representative images of DIC and UV (200ms) images of coma stage, two-fold and three-fold stage embryos along with hatching embryos of IA888 [<i>adIs2122 [lgg-1p::GFP::lgg-1 rol-6(su1006)]</i>]; <i>vps-45 (tm246) X</i>] strain. 63x magnification.....	143
Figure 4.10: Representative images of DIC and UV (200ms & 100ms exposure) images of coma stage, two-fold and three-fold stage embryos along with hatching embryos of IA897 [<i>adIs2122 [lgg-1p::GFP::lgg-1 rol-6(su1006)]</i>]; <i>unc-51 (e369) V</i>] strain	144
Figure 4.11: DIC and UV images of L1 larvae seam cells, 5 hours post hatching	146
Figure 4.12: Total levels of LGG-1::GFP in 3 fold DA213, IA888 and IA897 embryos .	148
Figure 4.13: Overall levels of LGG-1::GFP in N2, IA888 and IA897 adult <i>C. elegans</i> ..	150
Figure 4.14: Representative images of DIC and UV (200ms) images of coma stage, two-fold and three-fold stage embryos along with hatching embryos of IA897 strain	142
Figure 4.15: Total levels of LGG-1::GFP in 3 fold DA213, IA888 and IA897 embryos .	144
Figure 4.16: DIC and UV images of L1 larvae seam cells, 5 hours post hatching	145
Figure 5.1: The roGFP ER3 marker	151
Figure 5.2: Western blot of roGFP ER3 protein resolved on a 10% tricine gel	157
Figure 5.3: Test of roGFP ER3 oxidation state in <i>C.elegans</i>	160
Figure 5.4: roGFP oxidation state in TP198, IA881 and IA880 strains	161
Figure 5.5: Survival fractions of wild type <i>C.elegans</i> over 4 hour time period under the influence of 0, 0.1, 0.5, 1 and 5mM hydrogen peroxide	163

Figure 5.6: Survival fractions of N2, IA757 and CB369 <i>C.elegans</i> over a 4 hour time period under the influence of 1mM and 5mM hydrogen peroxide	164
Figure 5.7: Assessment of oxidative response in CF1553, IA887 and IA896 strains using the SOD-3::GFP marker	170
Figure 5.8: Assessment of oxidative response in wild type, <i>vps-45 (tm246)</i> and <i>unc-51 (e369)</i> strains using the GST-4::GFP marker	172
Figure 5.9: Assessment of oxidative response in wild type, <i>vps-45 (tm246)</i> and <i>unc-51 (e369)</i> strains using the GCS-1::GFP marker	174
Figure 6.1: Assessment of the moulting death of the suppressed <i>vps-45 (tm246)</i> mutant at 25°C	180
Figure 6.2: Length measurement of the suppressed <i>vps-45 (tm246)</i> mutant	182
Figure 6.3: Embryonic lethality assessment of the IA773 strain	184
Figure 6.4: Moulting profiles of wild type N2, IA757, IA773 during the L1-L2 moult at 15°C	185
Figure 6.5: Moulting duration and development time characterisation of the IA773 strain	187
Figure 6.6: Developmental stage of N2, IA757, IA773 strains after 72h of development, from L1 arrest, at 15°C	189
Figure 6.7: Life span of N2, IA757, IA773 <i>C.elegans</i> at 15°C and 25°C	190
Figure 6.8: Representative gel for detection of <i>vps-45 (tm246)</i> allele	196
Figure 6.9: Representative PCR for the detection of “Hawaiian” and “Bristol” DNA	198
Figure 6.10: Cloudmap results as retrieved by the analysis of the full genome sequencing data obtained by the Galaxy software for the identification of the <i>svp (ij117)</i> suppressor allele	195
Figure 6.11: Survival fraction of animals under a period of 6 days, under the influence of RNAi for each of the candidate suppressor genes	205
Figure 6.12: Detection of Hawaiian and Bristol SNPs across the <i>C.elegans</i> chromosome II.	207

Figure 6.13: Detection of Hawaiian and Bristol SNPs across the <i>C.elegans</i> chromosome V	210
Figure 6.14: Two sub populations exhibiting different growth phenotypes within the isolated Hawaiian <i>svp (ij117)</i> suppressed lines prepared for the sequencing experiment	213
Appendix 1: Moulting profiles of wild type (N2), <i>vps-45 (tm246)</i> (IA757), <i>unc-51 (e369)</i> (CB369) strains during the L1-L2 moult at 15°C	256
Appendix 2: Moulting profiles of adult wild type (N2), <i>vps-45 (tm246)</i> strain (IA757), <i>svp</i> (<i>ij117</i>) strain (IA773) during the L1-L2 moult at 15°C	257
Appendix 3: Average percentage of animals at a specific developmental stage for each strain after 72 hours of culturing at 15°C	258
Appendix 4: 40 homozygotic lines for the <i>vps-45(tm246)</i> after cross with the Hawaiian strain verified by PCR	259
Appendix 5: Genomic isolates of the 40 suppressed lines for the <i>vps-45 (tm246)</i> moulting death at 25°C, after treatment with RNase	260
Appendix 7: Sample pools prior to final mix for full genome sequencing	263
Appendix 8: Genomic isolates of the 35 suppressed lines for the <i>vps-45 (tm246)</i> moulting death at 25°C excluding the five slow growing lines, after treatment with RNase	264
Appendix 10: Sample pools prior to final mix for the second round of full genome sequencing	267

Acknowledgements

I would like to thank my supervisors, Dr. Iain Johnstone and Prof. Nia Brynat, for giving me the opportunity to perform this study and for their help and support throughout the course of the project. I am also grateful to my assessors Prof. Sireen Davis and Prof. Neil Bulleid for their helpful discussion and advice. I would also like to thank Prof. Gwyn Gould and his group for their help and support throughout this project.

I would like to acknowledge Prof. Tony Page (University of Glasgow, Glasgow, UK) for the kind gift of the strain TP198 as well as the cosmid clones he provided. Dr. Graham Hamilton (Glasgow Polyomics, University of Glasgow, Glasgow UK) for his help with the analysis of the full genome sequencing data.

Special thanks to my lab buddy Alexandra Kaupisch for her advice and help in the lab and the amazing and compulsory «stress relief» days and nights out.

I would also like to thank Kati Batista. Vielen Dank für die schöne Zeit, das viele Lachen, die Ü Eier und die Unterstützung.

I would also like to express my gratitude to Evdokia Michalopoulou for tolerating me all these years. Ευδοκάκι μου δεν θα είχα φτάσει ως εδώ αν δεν ήσουν εσύ, σε ευχαριστώ για την υποστήριξη, καθώς και τη Δέσποινα Ασλάνογλου για τις αμέτρητες ώρες ψυχανάλυσης. Επίσης να πω ένα μεγάλο ευχαριστώ στη Στεφανία, τη Χρύσα και το Λευτέρη, για τα όμορφα διαλείμματα από το χάος του Διδακτορικού. Ακόμη θα ήθελα να ευχαριστήσω φίλο μου Χάρη Μπαρκαγιάννη που με στήριζε όλα αυτά τα χρόνια και με «έπρηζε» να γυρίσω πίσω.

Τέλος, θέλω να ευχαριστήσω την οικογένειά μου. Σας ευχαριστώ πολύ για την υποστήριξη σε όλη τη διάρκεια του Διδακτορικού. Αυτή η διατριβή είναι αφιερωμένη σε εσάς, σας ευχαριστώ που με βοηθήσατε να φτάσω ως εδώ. Σας αγαπώ πολύ!

Authors Declaration

I declare that the work presented in this thesis has been carried out by me, unless otherwise cited or acknowledged. It is entirely of my own composition and has not, in whole or in part, been submitted for any other degree.

Anastasios Batas

January 2018

Abbreviations

ATG	autophagy related gene
Act	ACTin
BO ₃	Borate
BSA	bovine serum albumin
CaCl ₂	calcium chloride
<i>C.elegans</i>	<i>Caenorhabditis elegans</i>
CGC	<i>Caenorhabditis</i> Genetic Centre
COG	conserved oligomeric complex
Col	Collagen related mutant
Cvt	cytoplasm-to-vacuole targeting
Dic microscopy	Differential interference contrast microscopy
dH ₂ O	distilled water
ddH ₂ O	double distilled water
DABCO	1,4-diazabicyclo octane
DIC	differential interference contrast
DNA	deoxyribonucleic acid
Dpy	dumpy
dNTP	deoxyribonucleotide
dsRNA	Double stranded RNA
DTT	dithiothreitol dTTP
<i>E.coli</i>	<i>Escherichia coli</i>
EtOH	ethanol
ECM	extracellular matrix
EDTA	ethylenediamine tetra-acetic acid
EGTA	ethylene glycol-bis(β-aminoethyl ether)-N,N,N',N'-tetraacetic acid
EMS	ethyl methasulfonate
ER	endoplasmic reticulum
F1	first filial generation
F2	second filial generation

F3	third filial generation
GCS	gamma GlutamylCysteine Synthetase related gene
GFP	green fluorescent protein
GST	Glutathione S transferase related gene
HOPS	Homotypic fusion and protein sorting
H ₂ O	Water
H ₂ O ₂	hydrogen peroxide
Ifb	Intermediate Filament, B
Ifo	Intermediate Filament Organize
IgG	Immunoglobulin G
IPTG	Isopropyl β-D-1-thiogalactopyranoside
KCl	Potassium Chloride
KH ₂ PO ₄	Monopotassium phosphate
K ₂ HPO ₄	Dipotassium phosphate
KOH	Potassium hydroxide
LAMP	Lysosome-associated membrane protein
LB	Lysogeny broth
LC3	microtubule-associated protein 1 light chain 3
LGG	LC3, GABARAP and GATE-16 related gene
Lin	abnormal cell LINEage
Lon	long
L1-4	larval 1-4 stages
MEF	Mouse embryonic fibroblast
MgSO ₄	Magnesium sulphate
Mlt	MoLTing defective
MVB	multivesicular body
NaCl	sodium chloride
NaOH	sodium hydroxide
NaOCl	sodium hypochloride

NEM	N-Ethylmorpholine
NGM	nematode growth media
NP-40	nonyl phenoxyethoxyethanol
Nuo	NADH Ubiquinone Oxidoreductase
PAGE	polyacrylamide gel electrophoresis
PAS	Phagophore assembly site/ pre-autophagosomal structure
PBS	phosphate buffered saline
PBST	PBS tween
PCR	polymerase chain reaction
Peel	Paternal-effect Epistatic Embryonic Lethal
PI3K	Phosphoinositide 3 -kinase
PI(3)P	Phosphatidylinositol 3-phosphate
Ptc	PaTChed family
PtdIns	phosphatidylinositol
Rabs-5	Rabenosyn 5
RFB	Ruvkuv Finney Buffer
RNA	Ribonucleic acid
RNAi	RNA- mediated interference
mRNA	messenger RNA
<i>S.cerevisiae</i>	<i>Saccharomyces cerevisiae</i>
SOD	superoxide dismutase related gene
SNARE	soluble NEM sensitive factor attachment protein receptor
SNP	single nucleotide polymorphism
Snt	SyNapTotagmin
SWLB	single worm lysis buffer
TBE	Tris borate buffer
TE	Tris-EDTA
Tlg	target-SNARE of the late Golgi compartment protein
TORC	target of rapamycin complex
TTB	Tris-Triton Buffer

t-SNARE	target-SNARE
ULK1	unc-51 Like Autophagy Activating Kinase 1
UNC	uncoordinated movement related gene
UPR	Unfolded protein response
UTR	untranslated region
UV	ultraviolet
UVRAG	UV radiation resistance-associated gene
VAMP	Vesicle associated membrane proteins
Vha	Vacuolar H ATPase
VPS	Vacuolar protein sortin related gene
v-SNARE	vesicle-SNARE
WLB	worm lysis buffer
w/v	weight per volume
zeel	Zygotic Epistatic Embryonic Lethal
ZNF	Zinc Finger Nuclease

Measurements

bp	base pair
cm	centimetre
g	gram
h	hour
Kb	kilobase
Kda	kilodalton
L	litre
M	Molar
ml	millilitre
mM	millimolar
ng	nanogram

nm	nanometre
rpm	revolution per minute
sec	second
V	volt
μg	microgram
μm	micromolar
μl	microliter
°C	degree centigrade
%	per cent

Chapter 1: Introduction

Autophagy is a cellular housekeeping mechanism which plays an important role in energy homeostasis and cell viability (Reggiori & Klionsky 2002). Studies have associated autophagy and embryonic development in the past along with apoptosis (Agnello et al. 2015). Biogenesis of autophagosomal membranes is aided by machinery in the endocytic system, including SNARE (soluble NSF-attachment protein receptors) and SM (Sec1/Munc18) proteins. While it is clear that SM proteins play an important role in regulating SNARE-mediated membrane fusion, their mechanism of action is not well understood. It is, however well-documented that they function in homotypic fusion of membranes in the endocytic system, being required for exocytosis, endocytosis and lysosomal/vacuolar delivery (Gengyo-Ando et al. 2007; Solinger & Spang 2014; Zhu et al. 2015; Wartosch et al. 2015). Loss of SM protein function can result in a multitude of defects. For example, it has been shown that neutrophil cells with impaired action of the SM protein VPS45 undergo rapid apoptosis (Vilboux et al. 2013; P. Stepensky et al. 2013). Furthermore, in *Caenorabditis elegans* (*C. elegans*) knockout of the *vps-45* gene resulted in defects during early embryonic and post embryonic development (Gengyo-Ando et al. 2007). Like other SM proteins, Vps45 is perhaps best characterised for its regulation of SNARE-mediated membrane traffic; via Syntaxin 16 in mammalian cells, Tlg2 in yeast and SYN-16 in *C. elegans* (Bryant & James 2001; Gengyo-Ando et al. 2007; Struthers et al. 2009; Shanks et al. 2012)). Collectively, numerous studies on Vps45 in various systems have implicated a role for the SM protein in endosomal membrane traffic, autophagy and entry into apoptosis. In this project, I sought to use the model organism *Caenorhabditis elegans* to investigate relationships between endosomal trafficking and autophagy in the development of this small multi-cellular model animal.

1.1 An introduction to *C. elegans*

C. elegans is a small, free-living, transparent nematode approximately 1.2 millimetres (mm) in length (Brenner 1974). *C. elegans* has been used as a model organism for developmental and genetic studies and consequently a wide variety of mutants have been described to date and are broadly categorised based on the phenotype they exhibit

(Hodgkin 2005). Some of these phenotypes include: uncoordinated (Unc), roller (Rol), dumpy (Dpy), small (Sma) and long (Lon). Uncoordinated phenotypes range in severity from paralysis to small abnormalities in movement. Roller mutants rotate around their longitude axis during motion whereas dumpy and small mutants are typically shorter and wider than their wild type counterparts, respectively. On the other hand, long mutants are longer and thinner than wild type nematodes.

C. elegans can exist in two sexual forms, either as males or self-fertilizing hermaphrodites [reviewed in (Zarkower 2006)]. Hermaphrodites are the predominant sexual form. Self-fertilizing hermaphrodites can be used to readily generate homozygotic strains. Heterozygosity can be introduced to homozygotic mutant strains via mating with appropriate genotype males.

C. elegans embryogenesis takes normally approximately 16 hours under standard laboratory conditions (20°C). This can be faster at higher temperatures (25°C) or slower at lower (15°C) temperatures (Byerly et al. 1976). After hatch larvae develop through four larval stages (L1-L4) before reaching the adult stage. Each larval stage ends with the shedding of the exoskeleton and the production and secretion of the new one. An egg-to-egg developmental cycle takes approximately 3.5 days at 20°C [(Brenner 1974; Singh & Sulston 1978)]. Under starvation conditions, L2 larvae enter an alternative stage termed the dauer. The animal can survive at this stage for many months, and they exhibit higher resistance to environmental and chemical stresses due to an altered metabolism (KLASS & HIRSH 1976; Cassada & Russell 1975; Dalley & Golomb 1992; Vanfleteren & De Vreese 1995) .

1.1.1 *C. elegans* embryonic development

Embryogenesis in *C. elegans* can be subdivided in two stages, cellular proliferation and organogenesis/morphogenesis (Sulston et al. 1983). Proliferation takes roughly 5.5-6 hours under standard laboratory conditions. The first phase of proliferation occurs in the uterus, lasting 2.5-3 hours, with the remainder of this stage taking place outside the parent's body. During proliferation, the embryonic founder cells are generated during the first phase, with cell divisions and gastrulation taking place during the second phase [(Sulston et al. 1983), reviewed in (Bucher & Seydoux 1994)]. At the organogenesis/morphogenesis stage the terminal differentiation of cells occurs, and animals acquire their final, elongated form.

During this second embryogenesis stage, the embryo goes through several distinct morphological changes which themselves can be subdivided into four stages: the comma stage, the 1.5-fold, the 2-fold and the 3-fold stage. Morphogenesis lasts approximately 10 hours. At the end of embryogenesis, the general body morphology of the animals is established and does not change during post embryonic development (Figure 1.1) (Sulston et al. 1983).

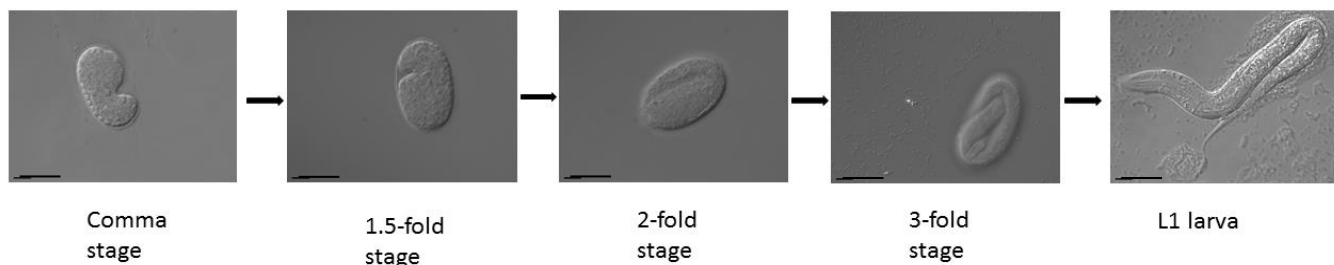


Figure 1.1: Major changes in body appearance of *C. elegans* during embryonic development. *C. elegans* goes through the second part of embryonic development with the elongation of the embryo starting with the comma stage, and proceeding to the 1.5-fold, 2-fold and 3-fold stages. At the 3-fold stage elongation stops. The worm hatches as the L1 larva after the cuticle has secreted.

1.1.2 *C. elegans* post-embryonic development

C. elegans is a eutelic organisms, this means that wild type (N2) adult hermaphrodites contain a constant number of somatic cells, in this case 959, once cell division has stopped and maturity is reached (Sulston et al. 1983). From that point on, both the number and the position of the cells remain unchanged, and *C. elegans* growth is achieved via enlargement of the cells.

After embryonic development, *C. elegans* proceeds through the four larval (L) stages, L1 to L4, before reaching adulthood. The end of each of the four larval stages is defined by shedding of the old cuticle and synthesis of the new one, a process termed moulting. A new cuticle is synthesised five times during the lifespan of the animal, once in the embryo and subsequently at the end of each of the four larval stages prior to moulting (Singh & Sulston 1978) (Figure 1.2). The cuticle is composed predominantly of collagen proteins; cuticle protein synthesis peaks during each moult, and is much reduced during the inter-moult period (Cox, Kusch, et al. 1981; Cox, Staprans, et al. 1981).

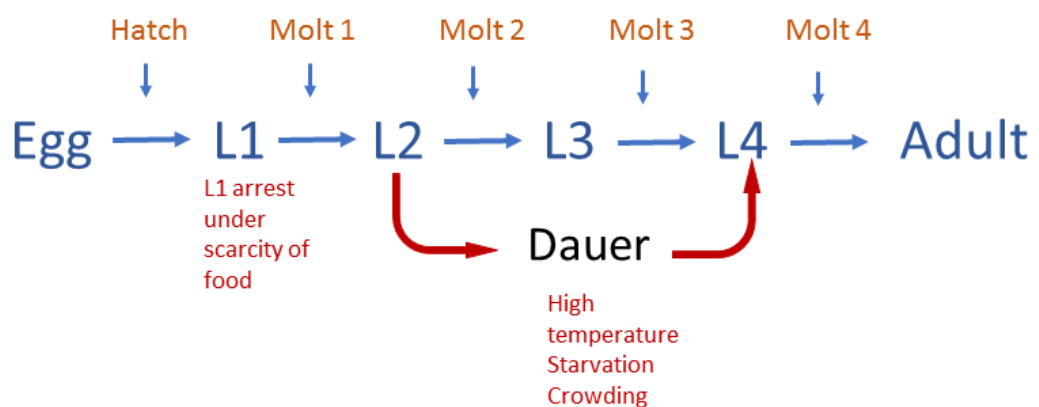


Figure 1.2: *C. elegans* larval development.

C. elegans proceed through four larval stages (L1 to L4) prior to reaching adulthood. The cuticle is synthesised five times during development and is shed four times during this time. Egg-to-egg duration in wild type N2 nematodes grown at 20°C is approximately 3 days. Worms arrest development at the L1 stage under scarcity of nutrients. Under stress worms take an alternate developmental path at the L2 stage by moulting into the dauer larva. Upon removal of the stressful conditions worms moult straight to the L4 larva and continue development normally.

1.1.3 *C. elegans* cuticle

The cuticle is an exoskeleton which encloses the body of all nematodes. The major component of the extracellular matrix which forms the cuticle is collagen. The cuticle is composed of six layers: the epicuticle, external cortical, internal cortical, intermediate (median), fibrous and basal layers. The median layer is considered to be fluid

filled and contains columns of filamentous material, termed struts, which connect the cortical and basal layers by fibres with a particular arrangement. The fibrous layer comprises two sublayers of fibres that spiral around the animal in opposite directions. The basal layer has a loosely organised fibrillar appearance (Figure 1.3). The cortical or outer layer exhibits a striped pattern, formed from circumferential ridges called annuli. Annuli are present in all developmental stages (Cox, Staprans, et al. 1981; Peixoto et al. 1997).

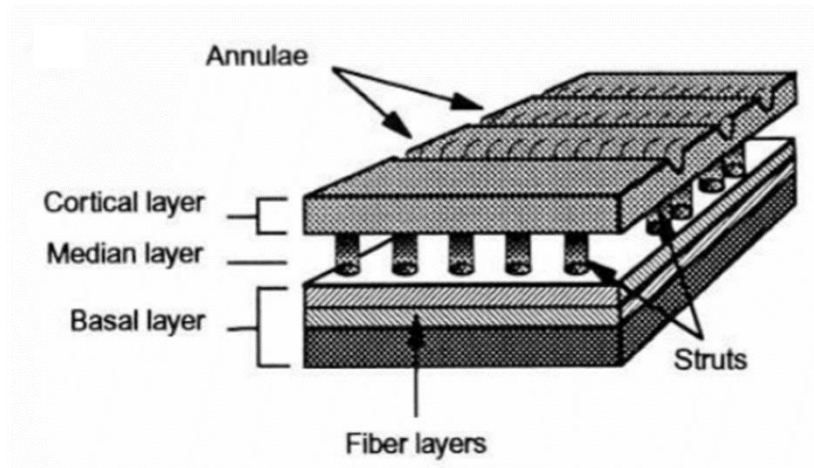


Figure 1.3: Schematic of an adult *C. elegans* cuticle depicting its multi-layered structures.

Scheme representing the different layers that constitute the cuticle: cortical (which includes the epicuticle, external and internal cortical), intermediate, fibrous, and basal along with the struts of the median layer. Reproduced from (Johnstone, 1994), permission granted from the publisher.

Cuticle components are synthesised by an underlying hypodermal cell layer, known as the hypodermis surrounding the animal's body (Cox, Staprans, et al. 1981; Johnstone 1994). The cytoplasm of the hypodermal cells exhibits smooth appearance during the inter-moult period (Singh & Sulston 1978), and a granular appearance during each moult. This granularity reflects an increased formation of Golgi bodies, likely to aid processing and secretion of new cuticle. After the end of each moult, the increase of intracellular membranes and vesicles, observed during the pre-moult period, is rapidly cleared (Singh & Sulston 1978). The molecular mechanisms underlying this clearance of secretory apparatus after each period of new cuticle synthesis have not been established, but are pertinent to research presented in this thesis. The apical membrane of the hypodermal cells secretes the components of the new cuticle. During the period of the synthesis and secretion of the

new cuticle, actin filaments are organised circumferentially around the body of the animal. They are disbanded after the end of each moult (Costa et al. 1997). This actin localisation corresponds to invaginations forming on the apical membrane of the hypodermal cells and subsequently form the furrows which intervene the annuli. The cuticular collagens DPY-7 and DPY-10 both localise within or just beneath the annular furrows and are required for their continued persistence (McMahon et al. 2003).

1.1.4 Expression of cuticle collagen genes

Cuticle collagen genes are expressed periodically during cuticle secretion; initially at the end of embryogenesis, and subsequently during each moult period of *C. elegans* post-embryonic development. Depending on precisely when individual collagen genes are expressed during the cuticle synthesis period (in post-embryonic development termed lethargus) they can be classified as early, intermediate or late expression, based on mRNA peak abundance, for instance *dpy-2*, *dpy-3*, *dpy-7*, *dpy-8* and *dpy-10* genes are early expressed whereas *dpy-5* and *dpy-13* genes are intermediate expressed. It is possible that the reason for this temporal expression of genes is that different substructures of the cuticle are synthesized at different times hence the requirement for the expression of the genes associated with them at those appropriate times (Johnstone & Barry 1996).

1.1.5 Moulting

Moulting is the process in the development of *C. elegans* during which, after the secretion and synthesis of the new cuticle, the old cuticle is shed. Moulting can, itself, be divided into three stages: lethargus, apolysis and ecdysis (Singh & Sulston 1978). During lethargus there is a gradual decrease in general activity and feeding of the worm, until the animal essentially stops moving altogether. The second stage is apolysis, defined by the separation of the old cuticle from the new cuticle. Finally, during ecdysis the worm starts moving again and rapidly rotates around its longitudinal axis to loosen the old cuticle. The worm breaks the old cuticle and emerges from it, leaving it behind to complete the process.

It is not entirely clear how the moulting process and the cuticle synthesis is controlled, however there is evidence suggesting cholesterol and steroid hormones are involved (Yochem et al. 1999; Kuervers et al. 2003; Matyash et al. 2004; Frand et al. 2005).

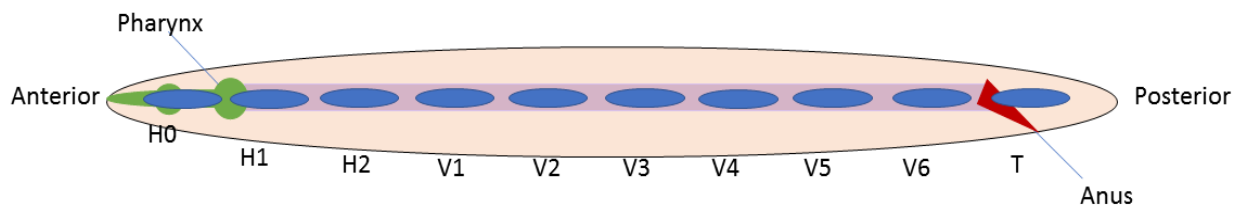
Furthermore, RNAi screens have identified 159 genes involved in moulting, which include transcription factors, secreted peptides, transmembrane proteins, proteases and peroxidases (Frand et al. 2005). Furthermore, it seem probable that the endosomal system must be involved in some way in the moulting process, either during the secretion of the cuticle or during the apolysis or the ecdysis by trafficking the appropriate molecules to the basal membrane or the cuticle to aid the process.

1.1.6 The seam cells and their role in *C. elegans* development and moulting

Epidermal cells assemble early in embryonic development into three rows on either side of the worm's body. As such, they can be subdivided into dorsal, lateral and ventral depending on their position (Sulston et al. 1983). During embryogenesis, the dorsal and the anterior and posterior ventral cells fuse and form several large cytoplasmic masses which enclose the nuclei of the individuals cells that gave rise to them termed the syncytia (Podbilewicz & White 1994). The central cells in the ventral row don't fuse, and neither do the lateral cells. The lateral cells give rise to seam cells which exhibit stem cell-like features in that they continue to divide and differentiate asymmetrically as larval development proceeds, giving rise to one daughter cell that will continue to proliferate carrying the stem like features, and a second daughter that ceases to proliferate and will differentiate to a specific cell type [reviewed in (Brabin & Woollard 2012)]. In the newly hatched animals, seam cells are arranged as ten bilateral pairs (H0-H2, V1-V6 and T) (Figure 1.4). Seam cells can divide both assymmetrically and symmetrically; following symmetric divisions, the two daughter cells differentiate and fuse with the hyp7 syncytium, whereas the daughter cells resulting from symmetric divisions maintain their stem-cell-like characteristics and contribute to the increase in number of seam cells. This symmetric division takes place in the second larval stage and increases the number of the seam cells from 10 to 16 pairs (division of V1-V4, V6 and T). During larval development, between the L2 and L4 moults, the seam cells divide (at the end of each moult) generating an anterior daughter cell which subsequently fuses with the hyp7, and a posterior daughter cell which divides again at the end of the next moult. At the end of the final moult (L4-adult), the 16 seam cells stop dividing and fuse together to form a single longitudinal syncytium (Sulston & Horvitz 1977; Singh & Sulston 1978)

Seam cells exhibit increased biosynthetic activity at the end of each moult (Sulston & Horvitz 1977; Singh & Sulston 1978), and likely play a role in the secretion of cuticular components such as *dpy-5* and *col-19* (Thein et al. 2003) and other secreted molecules required for the moult. Additionally, seam cells are responsible for correct formation of the cuticle alae at the adult stage. The alae are positioned over the seam cells at the two sides of the *C. elegans* body mirroring the underlying seam syncytia (Figure 1.5). Mutants defective for seam cell fusion at the adult stage exhibit alae irregularities (Shemer et al. 2004). Finally in male animals the V5 and V6 seam cells generate daughter cells that give rise to the male sensory rays instead of the alae (Hunter et al. 1999; Waring et al. 1990).

A)



B)

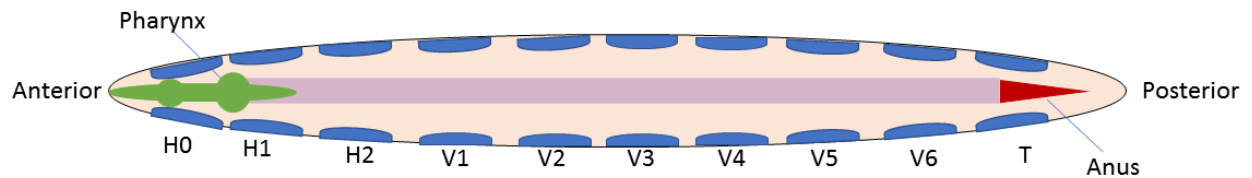


Figure 1.4: Position of the seam cells in the hypodermis of *C. elegans*.

A) Cartoon of an L1 larvae depicting the positioning of each of the 10 seam cells along the length of the animal prior to their division. B) Cartoon of Dorsal view of an L1 larvae showing the pair of seam cells body along the length of the animal.

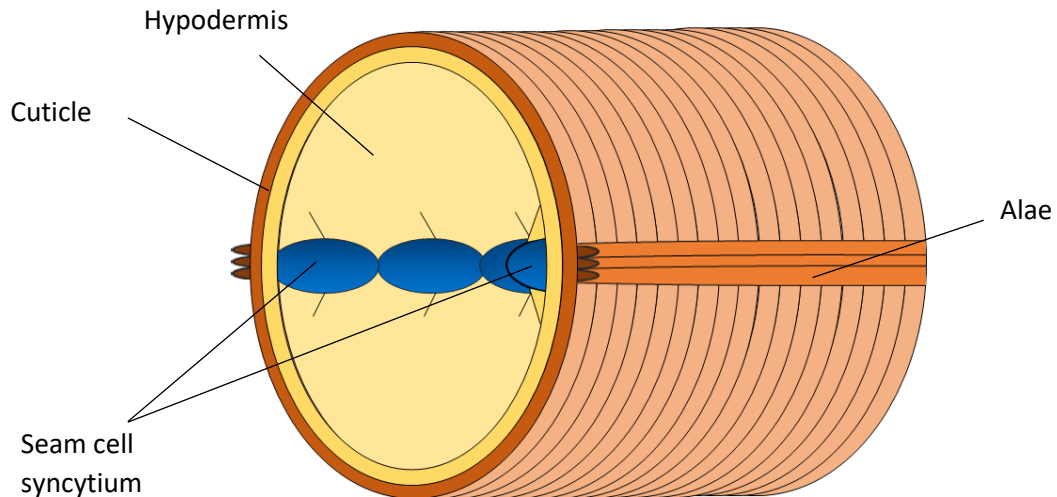


Figure 1.5: Schematic of the arrangement of the seam cells in an adult *C. elegans* with respect of the hypodermis and the cuticle. The seam cells are embedded in the hypodermis and are organised in a syncytium. The cuticular alae of the adult animals are formed in accordance to the position of the seam cells.

1.1.7 *C. elegans* genetics

The wide range of genetic tools available for studies using *C. elegans* make it a very attractive model organism. Its appeal was further increased after its genome was fully sequenced and annotated in 1998 (*C. elegans* Sequencing Consortium 1998). *C. elegans* exhibit a low level of genetic diversity as a result of their ability to self-reproduce (Hodgkin & Doniach 1997). Molecular polymorphism has been studied in a number of natural isolates collected worldwide. Isolates originate from North America, Australia and Western Europe from where the N2 (Bristol) reference strain originates. The CB4856 isolate which was first identified in Hawaii (Termed the Hawaiian strain) and closely related to the N2 isolate (Hodgkin & Doniach 1997) in particular has been previously used in SNP (single nucleotide polymorphism) (Minevich et al. 2012) mapping.

C. elegans can reproduce through self-fertilisation. All animals carry 5 pairs of autosomal chromosomes (LGI-LGV) and one pair of sex determining chromosome (LGX).

Hermaphrodites carry two copies of the X chromosome, whereas males have only one X

chromosome. During self-fertilisation, hermaphrodites first produce sperm and then their oocytes through meiotic divisions. In a population, hermaphrodites cannot cross-fertilize, as such males are required for outcrossing. Males can be produced by non-disjunction of the X chromosome at meiosis in hermaphrodite animals. Spontaneous non-disjunction of the X chromosome occurs at a low rate in laboratory conditions as a result of genetic variation even in the cases of higher brood production [(Hodgkin & Doniach 1997), reviewed in (Zarkower 2006)]. The rate of X chromosome non-disjunction can be increased via alteration of environmental factors such as increased temperature. After crossing of the N2 males with N2 hermaphrodites, the early generations will produce a 50% frequency of males. That frequency is reduced in subsequent generations due to low mating abilities of the N2 males as well as the ability of hermaphrodites to self-reproduce prior to/ or without mating with males. However, in the case of the CB4856 strain the males exhibit a higher mating ability (Hodgkin 1983; Hodgkin & Doniach 1997; Chasnov & Chow 2002; Cutter et al. 2003).

The advantages of the above methods of reproduction are apparent when it comes to maintaining mutants. Homozygotic hermaphrodite mutants that are viable and fertile can be maintained as homozygous stocks since the parents produce genetically identical offspring. With lethal mutations or mutations causing sterility, which are recessive as well it is possible to be maintained in a heterozygotic state. As such only 25% of the offspring population will die, and thus making it possible to analyse these mutants.

A common way of generating *C. elegans* mutants is through treatment with ethyl methanesulfonate (EMS), a strong mutagen that can commonly produce G to A and C to T transitions, and less commonly other point mutations and deletions (Brenner 1974). For targeted gene conversion and deletions transposon based methods are utilised either by insertions or by excisions. G4 DNA induced deletion mutagenesis which utilises the G-quadruplex DNA secondary structure can also be used for generation of deletions. A range of other chemicals as well as radiation has also been utilised for the generation of mutants (Kutscher & Shaham 2014). Recently more modern methods have been developed to generate *C. elegans* mutants. These are the Zinc finger nucleases (ZNFs) (Kim et al. 1996) and the CRIPSR/Cas system methods (Friedland et al. 2013).

After a mutant has been isolated, the specifics of its gene function can be investigated through the phenotypes manifested on the animals that carry it. There are two approaches

to this. The forward genetic approach involves identifying the said mutant phenotype first and proceeding to the characterisation and mapping of the mutation in order to identify the exact gene producing these phenotypes. This used to be quite a lengthy and difficult process requiring several steps of crossing between the mutant strain and the Hawaiian strain and then SNP testing via PCR. This has been made much simpler with the potential of producing more accurate and much faster results through next generation sequencing [(Bazan & Hillers 2011; Minevich et al. 2012), reviewed in (Fay 2013)]. After the annotation of the *C. elegans* genome it has become possible, to follow an alternative approach; the reverse genetics approach going from a gene sequence to characterising the mutant phenotype.

1.1.8 Next generation sequencing

As previously mentioned, next generation sequencing is a fast and cost effective method to identify genetic mutations in organisms such as *C. elegans*. The use of single nucleotide polymorphisms (SNPs) is the most commonly used mapping strategy in *C. elegans*. SNPs can function as genetic markers for two- and three-factor mapping in order to measure recombination across whole chromosomes and hence identify the position of the phenotype causing mutation [reviewed in (Fay 2013)]. Commonly this strategy employs DNA sequence polymorphisms between the wild-type *C. elegans* Bristol strain (N2) and the closely related Hawaiian strain (CB4856) (Hodgkin & Doniach 1997). The Hawaiian SNPs in general display no phenotype and as a result, mutations which do cause an associated phenotype, even a subtle one, can be mapped via the utilisation of the SNPs (Bazan & Hillers 2011; Wicks et al. 2001).

Traditional mapping involves a cross set up between the mutant isolate and the polymorphic strain of the same species. For instance, a mutation in a strain with Bristol genetic background is crossed with the wild type Hawaiian polymorphic strain. In the F1 generation all of the progeny will be heterozygotic for the mutation as well as the Hawaiian SNPs. In the subsequent F2 generation 25% of the progeny will be homozygotic for the mutation causing allele. In this case, that 25% will display the mutant phenotype. SNPs in this case will be distributed approximately equally at 50% Hawaiian/ Bristol across most of the genome due to the random recombination that occurs between the chromosomes during meiosis. However, this ratio will tend towards 0% for Hawaiian polymorphisms near the mutation. The reason for this difference is that SNPs which are

physically close to the causal mutation are linked to it, and hence are much less likely to take part in a chromosomal recombination event compared to others which are further away. As such the region which carries a long stretch of parental SNPs, in this case Bristol, will incorporate the genetic mutation in question. This method is very time consuming as it requires several strains to be checked for SNP in question via PCR (Williams et al. 1992; Wicks et al. 2001).

The first stage of the above method involves identification of the relevant chromosome, and a rough position of the gene of interest. In the second stage, a more specific positioning of the gene of interest is identified and the aim is to identify the interval between two SNPs on which the mutation is located. PCR can be used for the amplification of the SNP is followed by digestion with the appropriate enzyme. Depending on the combination of bands acquired in the end after the electrophoresis the on whether they are of Bristol or Hawaiian origin can help in assessing whether recombination has not occurred hence the region is linked or not, to the mutation (Wicks et al. 2001).

With the aid of deep genome sequencing technologies however the process of gene mapping and identification can be considerably sped up. The basic principle is the same as in the traditional SNP mapping method with the only difference being that instead of performing PCR, restriction enzyme digestions and finally gel electrophoresis to identify each SNP individually, all of them can be identified as once (Figure 1.6). The method was initially tested in *Arabidopsis thaliana* for the identification of a non-synonymous codon change that caused slow growth and different pigmentation of the leaves (Schneeberger et al. 2009). The method has since then, been adapted and applied for the identification of mutations in *C. elegans* (Doitsidou et al. 2010a; Minevich et al. 2012).

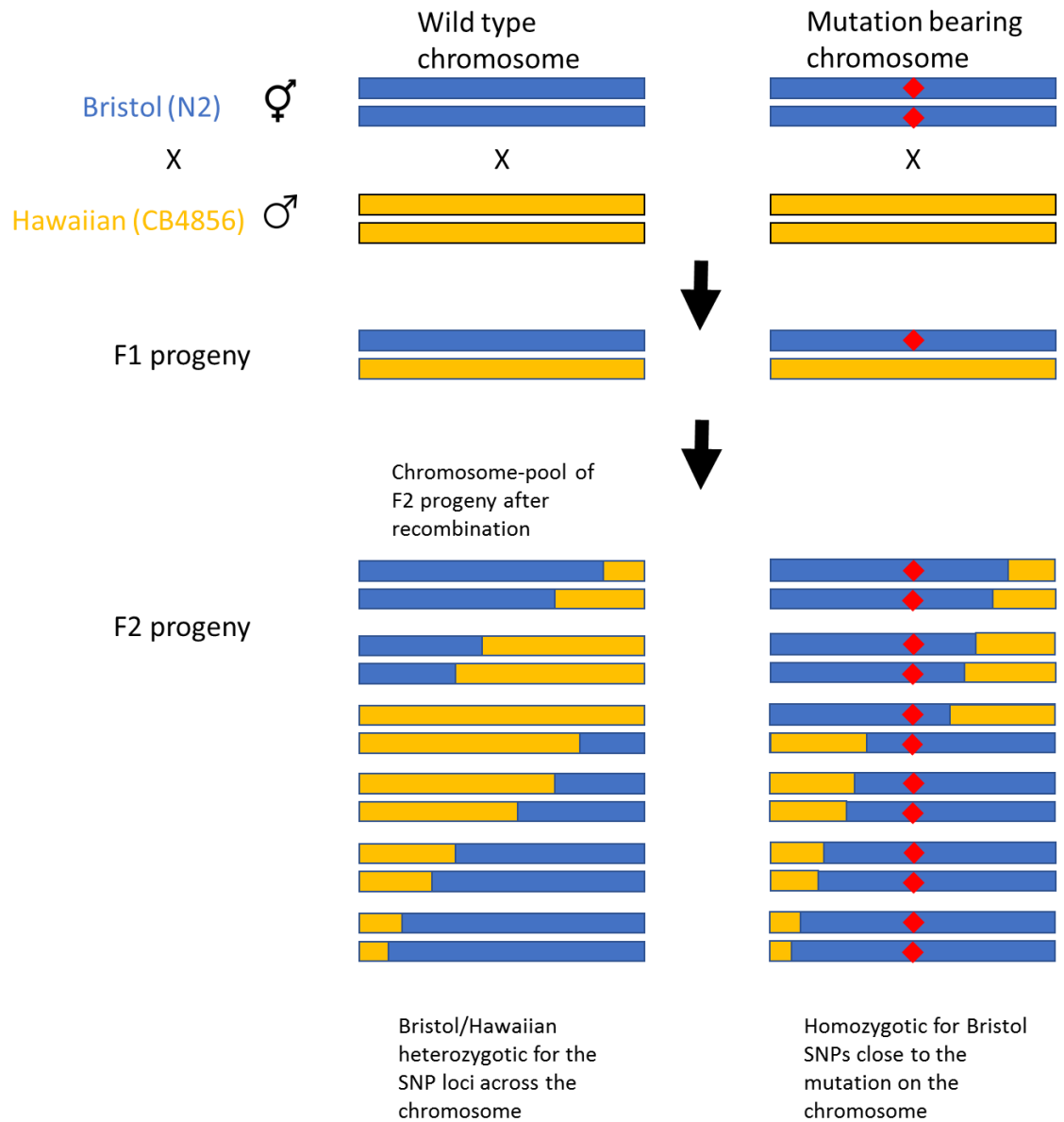


Figure 1.6: Schematic depicting the chromosomal recombinations that can occur between the wild type Bristol strain and the highly polymorphic Hawaiian strain.

The reference strain (N2) is shown in blue, the polymorphic Hawaiian strain (CB4856) in yellow and the presence or absence of a mutation by the red diamond shape. In the F1 progeny all progeny will be heterozygous for the Hawaiian sequences. At the F2 and subsequent generation Hawaiian DNA will be equally represented across the genome of the animals if no mutation is present. If a mutation is present, the area surrounding it should remain Bristol (blue). Adapted from (Minevich et al. 2012).

1.1.9 RNAi

In 1998, it was discovered that the injection of double stranded RNA (dsRNA) in *C. elegans* can lead to degradation of the corresponding mRNA. This process was termed RNA interference or RNAi (Fire et al. 1998). Since the full genome sequencing and annotation of the *C. elegans* genome RNAi is being used as a complementary approach to the creation of genetic knockouts. Other methods, apart from injection of dsRNA in adult worm gonads, include soaking the worms in dsRNA solutions (Tabara et al. 1998) or by feeding worms with *E.coli* expressing the desired dsRNA (Timmons et al. 2001). The latter two can be done in worms of any stage, however it is important to keep in mind that depending on the stage the animals will be fed can produce different phenotypes.

1.2 The endocytic pathway

Endocytosis is the process by which a portion of a cell's plasma membrane invaginates to form a vesicle that buds off into the cytoplasm facilitating transport of extracellular material including nutrients, and cell surface components into the cell via the endocytic system. The initial vesicle that buds from the cell surface forms, engulfing the material to be internalised in the process. These vesicles fuse with the early/sorting endosomes which can subsequently mature to late endosomes. The internalised material in the early endosomes, can be delivered back to the plasma membrane via the recycling endosome, or can be targeted to the vacuole/lysosome for degradation to the lysosomes via the late endosomes. [reviewed in (Elkin et al. 2016)] (Figure 1.7). As with all membrane trafficking pathways in eukaryotic cells, fidelity of fusion of vesicles with the appropriate target organelle is critical. Proteins required for proper regulation of membrane trafficking are conserved between different trafficking steps and also between all eukaryotes (from yeast to humans). Like all trafficking pathways membrane fusion in the endocytic pathway involves SNARE (soluble N-ethylmaleimide-sensitive factor attachment protein receptor), SM (Sec1/Munc18), Rab and tethering proteins. Tethering complexes such as CORVET (class C core vacuole/endosome tethering), HOPS (Homotypic fusion and protein sorting), or COG (conserved oligomeric complex) act , in the tethering/connection of the endosomal vesicle and the target membrane (Jiang et al. 2014; Solinger & Spang 2014; Seals et al. 2000; Solinger & Spang 2013; Yen et al. 2010). Each of the tethering complexes appears to be involved in fusions at different parts of the endocytic system. The CORVET complex acts as a tethering factor for the fusion of the endocytic vesicles with the early endosomes

(Solinger & Spang 2013; Solinger & Spang 2014), the HOPS complex regulates the fusion of mature endosomes and autophagosomes to lysosomes (Solinger & Spang 2014; Jiang et al. 2014). Finally COG is thought to act mainly in Golgi retrograde trafficking, ER to Golgi transport as well as during the formation of autophagosomes as a membrane tethering factor (Yen et al. 2010; VanRheenen et al. 1998; Bruinsma et al. 2004; Zolov & Lupashin 2005; VanRheenen et al. 1999). SNARE/SM protein complexes mediate the fusion of the vesicle and target organelle. SNARE proteins provide the force for the membrane fusion via their association into SNARE complexes and SM proteins interact with SNARE proteins to regulate the formation of these complexes [reviewed (Jahn & Scheller 2006)] as described below (Section 1.2.1). Finally, Rab GTPases mediate the transport and correct targeting of vesicles through the endocytic system, as well as the fusion of the membranes via direct interaction with tethering complexes or via indirect interaction with SNAREs through their effectors (Nielsen et al. 2000; Simonsen et al. 1999).

Other pathways that intersect with the endocytic system, include the exocytic pathway (delivering both previously endocytosed material through recycling endosomes (Ward et al. 2005) and newly synthesized material (Futter et al. 1995; Ang et al. 2004; Chen et al. 1998; Harsay & Schekman 2002) to the plasma membrane, the autophagic pathway (Ganley et al. 2011; Jiang et al. 2014; Itakura & Mizushima 2010), and the Cytoplasm to vacuole trafficking (Cvt) pathway in yeast (Baba et al. 1997; Scott et al. 1996) (Figure 1.7).

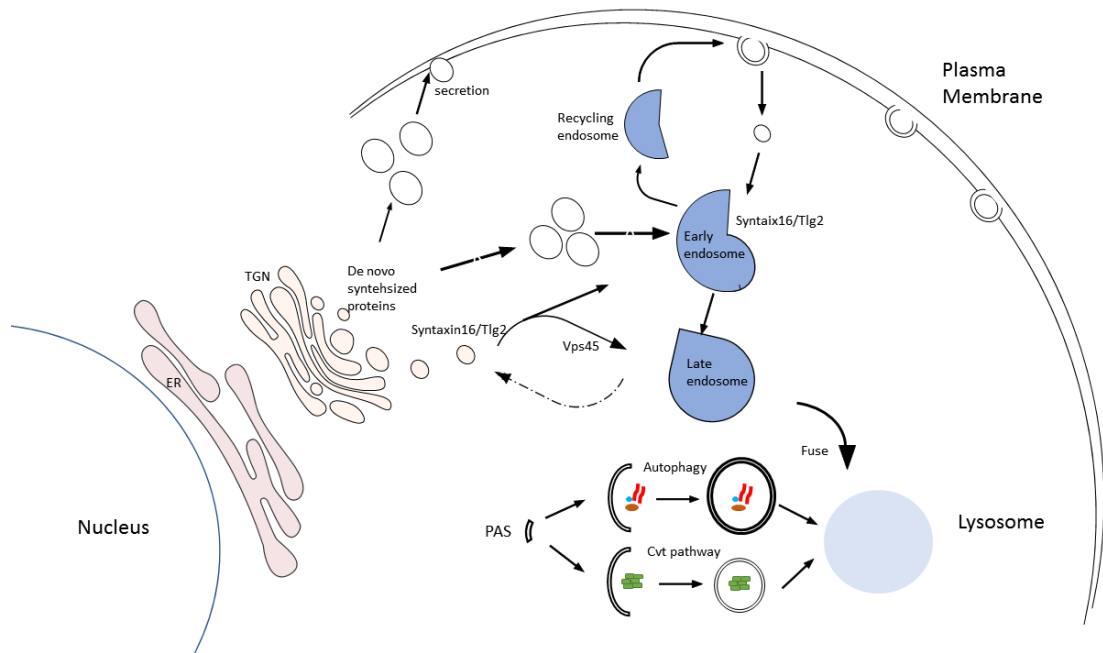


Figure 1.7: Schematic representation of the endocytic system.

Endosomes form at the plasma membrane and can target cargo protein for degradation to the lysosome by fusing with it. Autophagy/Cvt vesicles are formed at the PAS and transfer their respective cargo (Macromolecules, organelles, enzymes) to the lysosome. De novo synthesized proteins are secreted through the secretory pathway which can intersect with the endocytic system at the early endosomes. The Tlg2/Syntaxin 16 SNARE localises at the early endosome and the TGN. Vps45 is required for the transfer of cargo proteins between the TGN and the endosomal system.

1.2.1 SM proteins and SNARE complexes

SM (Sec1/Munc18) proteins regulate the assembly of SNARE (soluble N-ethylmaleimide-sensitive factor attachment protein receptor) complexes which are central to membrane trafficking in all eukaryotes. SNARE proteins are localised on vesicle membranes and the membranes of target organelles, and form complexes via their carboxy (C) termini (Bennett et al. 1992; Séron et al. 1998; Gurunathan et al. 2000). Formation of SNARE complexes between cognate SNAREs on opposing lipid bilayers is the minimal requirement for membrane fusion [reviewed in (Jahn & Scheller 2006)].

SNARE proteins are evolutionary conserved with their defining characteristic being the cytosolic SNARE motif (Jahn & Südhof 1999; Lin & Scheller 2000). Most SNAREs are

C-terminally tail anchored membrane proteins [reviewed in.(Hong, 2005; Sudhof *et al*, 2009)]; ~60-70 amino acid residue stretch containing a heptad repeat. A functional SNARE core complex, forms when four SNARE motifs are arranged in a tight, parallel helical bundle. This paralleled arrangement requires one arginine- SNARE (R-SNARE) and three glutamine SNARES (Qa, Qb, Qc SNAREs) (Weimbs et al. 1997; Antonin et al. 2002). This classification of the SNARE proteins depends on their amino acid contribution (glutamine or arginine) to the ionic layer (termed “0” layer) of the SNARE complex (Fasshauer et al. 1998). In general R SNAREs are anchored on the vesicle membrane (v-SNAREs) and the Q-SNAREs on the membrane of the target organelle (t-SNAREs) (Sudhof & Rothman 2009).

Syntaxins are a subfamily of SNARE proteins, usually Qa SNAREs, that carry an N-terminal domain, the Habc domain, that autonomously folds into a three-helix bundle. This Habc domain can bind to the syntaxin’s SNARE motif, an interaction that inhibits SNARE complex formation (Hanson et al. 1995; Burkhardt et al. 2008). This state is termed ‘the closed conformation’. When the Habc domain is not bound at the C-terminus and the SNARE is in its open conformation, the SNARE domain is accessible and can form the SNARE complex along with the other three snare domains of the cognate snare proteins (Dulubova et al. 2002). The open and closed conformations of the syntaxin SNARE proteins is regulated by Sec1/Munc-18 (SM) proteins. One example of such regulation of SNARE proteins is the case of Vps45 and its binding partner Tlg2/Syntaxin 16 in yeast and mammals (Dulubova et al. 2002; Yamaguchi et al. 2002).

The Sec1/Munc18 (SM) family of proteins regulates membrane fusion via association with distinct subsets of SNAREs. Although the mechanism of action for SM protein regulation is not clear, it is certain that these proteins are universally required for functional SNARE complex assembly (Carr & Rizo 2010). SM proteins have an arch-shaped structure (Misura et al. 2000) and can interact with SNAREs in three distinct modes. The first mode, which was originally characterised via the interaction of syntaxin1a and the neuronal SM protein Sec1. In this mode, the SM protein binds all four helices of the SNARE protein (3 Helices from the Habc domain and 1 helix for the SNARE motif) and bring them together in a bundle. As such the syntaxin adopts a closed conformation and cannot form the SNARE complex require for the membrane fusion (Figure 1.8A) (Dulubova et al. 1999; Misura et al. 2000). In the second mode, the SM protein binds to the N-terminus of the syntaxin at a specific peptide sequence, thus allowing for the syntaxin to adopt an open conformation (Figure 1.8B). At this point the three remaining helices of the

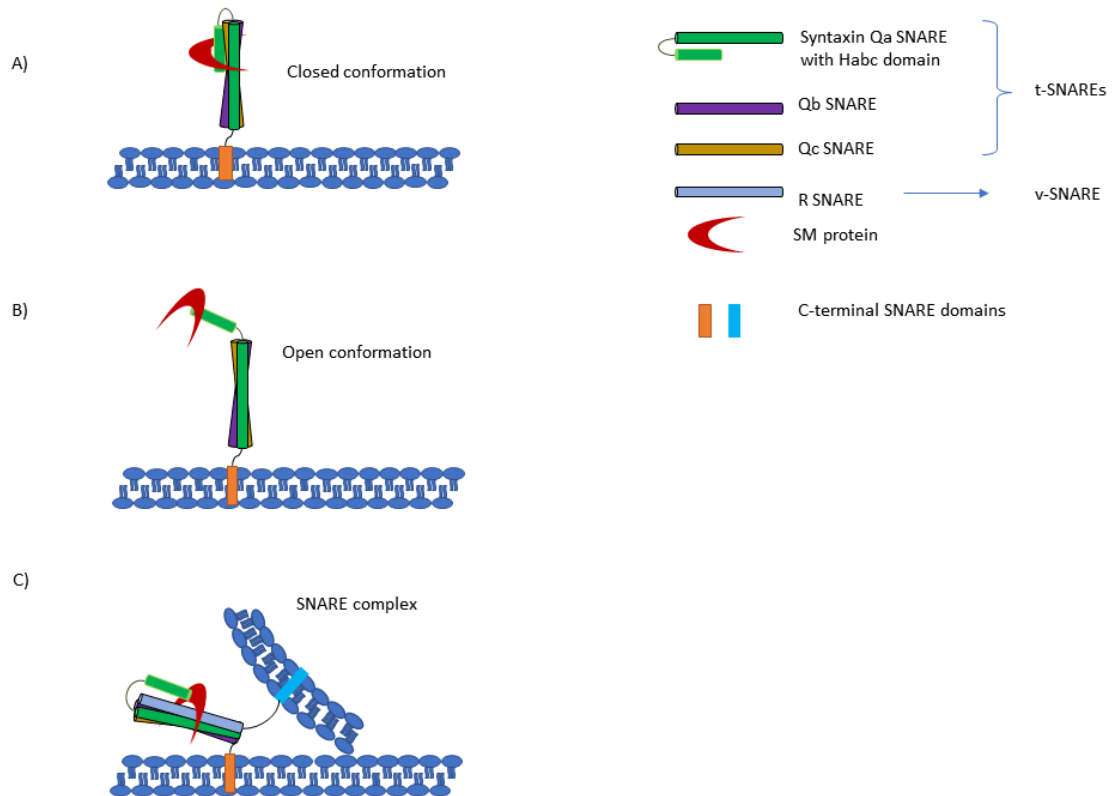


Figure 1.8: The different binding modes of SM proteins with syntaxins

A) The SM protein binds the four-helix bundle composed of the syntaxins own Habc N-terminal domain resulting in the closed conformation of the syntaxin. B) The SM protein binds to the N-peptide present at the Habc domain allowing for association of the t-SNAREs with the v-SNARE. C) SM protein binding SNARE complex consisting of the three t-SNAREs and the v-SNARE which will guide the fusion of the membranes. Adapted from (Jahn & Südhof 2003).

t-SNARE can form a complex with the single helical v-SNARE which is stabilised by the “clasping” of all four helices by the SM protein, similar to how it would previously clasp the four helix bundle of the “closed” conformation syntaxin (Figure 1.8C) (Yamaguchi et al. 2002; Dulubova et al. 2002).

As the SNARE complex has now formed it can bring the two membranes (vesicle and target membrane) together in close proximity, and provide the force for the fusion.

1.2.2 The SM protein Vps45

Vps45 was originally identified through genetic screens for yeast defective in vacuolar protein sorting (*vps* mutants) (Robinson et al. 1988), and has been shown to be essential for delivery of proteins from the *trans* Golgi network (TGN) into the endosomal system (Cowles et al. 1994; Piper et al. 1994).

In *Saccharomyces cerevisiae*, the Sec1/Munc-18 protein Vps45 activates the Syntaxin Tlg2 by facilitating a change in its conformation from closed to open. Once Tlg2 is in its open conformation it can form a functional SNARE complex with its binding partner t-SNAREs Tlg1, Vti1 and the v-SNARE Snc2 (Bryant & James 2001; Carpp et al. 2007). Vps45 binds directly to Tlg2, as well as to the v-SNARE, Snc2, and the assembled SNARE complex (Carpp et al. 2007; Furgason et al. 2009). Vps45 is required for the stable expression and function of its Tlg2 in yeast (Bryant & James 2001).

As mentioned above, Vps45, and the SNARE complex whose assembly it regulates, mediates traffic from the TGN through the endosomal system, and was originally identified as being required for the biosynthetic pathway in yeast. It is also required for the endocytic, autophagic pathways as well as the autophagy-related Cvt (Section 1.3.1) pathway. However the actual mechanism of this regulation is still unknown (Brickner *et al*, 2001; Ohashi and Munro, 2010; Nair and Klionsky, 2011).

Furthermore, Vps45 was originally reported to regulate membrane traffic through the syntaxin Pep12 (Burd et al. 1997; Webb et al. 1997), but no physical interaction has ever been identified (Bryant & James 2001), and the significance of the functional interactions demonstrated remain to be fully understood.

Vps45 yeast mutants belong to the class D group, one of the six groups (A-F) of *vps* mutants as classified based on the morphology of their vacuoles. The class D group mutants, exhibit defective segregation of the vacuole from the mother cells to the budding daughter cells. This classification further suggest the existence of 6 separate processes which when disrupted result in the miss sorting of vacuolar hydrolase carboxy peptidase Y (CPY) (Raymond et al. 1992). Unlike most *vps* mutants, *vps45* mutant yeast have a significantly longer doubling time compared to wild type strains and are temperature sensitive for growth. Importantly, this is an unusual case of temperature sensitivity in that null alleles are temperature sensitive meaning that the function of *vps45* is not essential for

growth at low temperature, but it is at high temperatures. Of note here is the observation that mutations in *VPS* genes encoding proteins with which Vps45 interacts and/or function in the same specific trafficking step (class D Vps proteins) do not share these growth phenotypes (Shanks et al. 2012).

1.2.3 Loss of VPS45 as a cause for Neutropenia

Severe congenital neutropenia is a group of genetic disorders which show great heterogeneity. Among all of them however, the common denominator is the increased susceptibility of neutrophil precursors to undergo apoptosis. Neutrophils are part of the initial line of immune defense of most mammals against invading pathogens such as bacteria. In humans they represent 40%-60% of the white blood cells and they exist in healthy adults in a resting state ready to be activated. When in this state, the cells are prevented from secreting any of their toxic intracellular components which can potentially damage host tissue. Upon infection neutrophils are activated and migrate to the site of infection where they attack and phagocyte pathogens. After this is complete they can act as antigen presenting cells for T-cells and also secrete a large number of inflammatory mediators such as chemokines and cytokines which attract more immune cells to the site (Fielding et al. 2008; Wright et al. 2010). Patients with neutropenia suffer recurring infections as a result of the reduction in neutrophil population.

Recently a loss of function mutation (Thr224Asn) in the Sec1/Muc18 protein (SM protein) VPS45 in humans was identified as a cause for neutropenia. It is proposed that disruption of the VPS45 function in neutrophils could result in a perturbed delivery of cargo from the TGN to the endosomal system, which could be blocking the earlier secretory pathway and result to ER stress which would eventually trigger apoptosis (P. Stepensky et al. 2013). A similar model through which neutropenia can develop has been reported in patients with mutations in the *ELA2* gene, which encodes for neutrophil elastase (NE) (Grenda et al. 2007). In this case ER stress develops from the accumulation of misfolded NE protein (P. Stepensky et al. 2013; Benson et al. 2003; Grenda et al. 2007; Grenda et al. 2009), which would activate the UPR response and eventually apoptosis [(Grenda et al. 2007; Grenda et al. 2009), reviewed in (Ron 2002)]. Further to this, previous experiments by members of our lab have demonstrated that yeast cells harbouring the analogous mutation (T238N) exhibit higher sensitivity to H₂O₂ mediated killing (Cowan, 2014), suggesting possibly a

sensitivity to oxidative stress as a result of a pre-existing ER stress (Plaisance et al. 2016; Malhotra & Kaufman 2007a; Harding et al. 2003).

1.2.4 VPS-45 and its role in *C. elegans*

A similar temperature sensitive behaviour to that identified in Vps45 yeast mutants (section 1.2.1) is associated with a null allele of *vps-45* *Caenorabditis elegans*. The *vps-45* gene is located on the X-chromosome of the *C. elegans* genome. Strains carrying a deletion at the *vps-45* gene are viable at 15°C but die during the moult when cultured at 25°C.

When the same mutant is cultured at 15°C it can survive and moult through to adulthood, but with a small body size phenotype. Furthermore, a role of VPS-45 was identified for the uptake of the yolk protein YP170, by the oocytes in *C. elegans*. The process was disrupted in mutants at the non-permissive temperature. Additionally, a defect at the transport of cargo from the endosomes to lysosomes was identified. As previously stated, in yeast Vps45 directly interacts with Tlg2 and functionally interacts with Pep12 and their orthologues syntaxin 13 and syntaxin 16 in mammals. Similarly in *C. elegans* VPS-45 has also been shown to interact with the *C. elegans* orthologues SYN-13 in co-IP experiments and SYN-16 in co-IP and yeast-two hybrid experiments. Single and double knockouts of those two syntaxins in *C. elegans* exhibited none of the above described phenotypes suggesting that their binding to VPS-45 is not essential for its function or might not be acting on the same endocytic pathway (Gengyo-Ando et al. 2007).

On the other hand, VPS-45 does physically interact with Rabenosyn-5 (RABS-5), which is the effector of the tethering factor RAB-5, both in mammals and in *C. elegans* (Nielsen et al. 2000; Gengyo-Ando et al. 2007) is generally believed, that Rab GTPase proteins such as Rab5 are responsible for specific tethering and docking reactions and SM proteins such as Vps45 are what drives the fusion of the two membranes (Mayer & Wickner 1997; Zerial et al. 1999; Nielsen et al. 2000). No interaction has been identified between VPS-45 and RAB-5. In addition to this, rabenosyn-5 (*rabs-5*) mutants, were no different than the *vps-45* suggesting an interaction between the two molecules in a RAB-5 mediated homotypic fusion. Experiments in *C. elegans* demonstrated that the murine orthologue (VPS45) is functionally interchangeable with *vps-45* and can rescue the defects caused by its deletion. However, the yeast orthologue had no such effect. As such it is speculated, that VPS-45 has evolved in multicellular organisms to gain additional endocytic functions due to the higher complexity exhibited in their transport pathways (Gengyo-Ando et al. 2007).

1.3 Autophagy

Autophagy is a vital cellular process involving the degradation of intracellular components such as proteins and organelles. Autophagy can be subdivided to macroautophagy, microautophagy and chaperone-mediated autophagy. Macroautophagy and microautophagy can engulf large structures in a selective and non-selective manner. On the other hand, chaperone mediated autophagy can only degrade soluble protein and in a selective way. All three autophagic mechanisms include the use of membrane organelles for the transfer of intracellular cargo to be degraded to the lysosome [reviewed in (Mizushima et al. 2008)].

It has been demonstrated that autophagy can act both as a cytoprotective mechanism as well as a deleterious one. The pathway has been shown to aid in the survival of yeast under starvation conditions (Tsukada & Ohsumi 1993). Induction of autophagy in *Drosophila* through overexpression of the autophagy regulator Atg1 can lead to cell death (Scott et al. 2007). On the other hand, in *C. elegans* lacking *bec-1*, which is the mammalian orthologue of beclin1 and the yeast ATG6 and mice lacking beclin 1 or ATG5, display increased numbers of apoptotic cells in embryonic tissue (Takacs-Vellai et al. 2005; Qu et al. 2007). This suggests that tight control of autophagy is a requirement to promote cell survival. Mutations in a variety of genes related to autophagy demonstrate the importance of this pathway in a number of physiological processes and pathologies (Section 1.3.6). The first step in this process is the formation of the membranes for these organelles termed phagophores or isolation membrane. The proposed site for the formation of the phagophore is the phagophore assembly site/pre-autophagosomal structure (PAS) in yeast (Kirisako et al. 1999; Suzuki et al. 2001; Kim et al. 2002) where the autophagic machinery colocalises. In other eukaryotes multiple sites of autophagosome assembly have been identified such as the ER, the Golgi, mitochondria and the plasma membrane (Lamb et al. 2013), however the current consensus is that the autophagosomes arise from the omegasome, an omega shape compartment of the ER where autophagy regulators ULK1, ATG14 and PI(3)P are localised (Itakura & Mizushima 2010; Matsunaga et al. 2010; Axe et al. 2008; Karanasios et al. 2013).

The phagophore/isolation membrane has a crescent like shape. This is then elongated to enclose and assimilate the cytosolic cargo. Subsequently the autophagosome fuses with the

lysosome to form the autolysosome, where degradation of the cytosolic content takes place [reviewed in (Mizushima 2007)] (Figure 1.9).

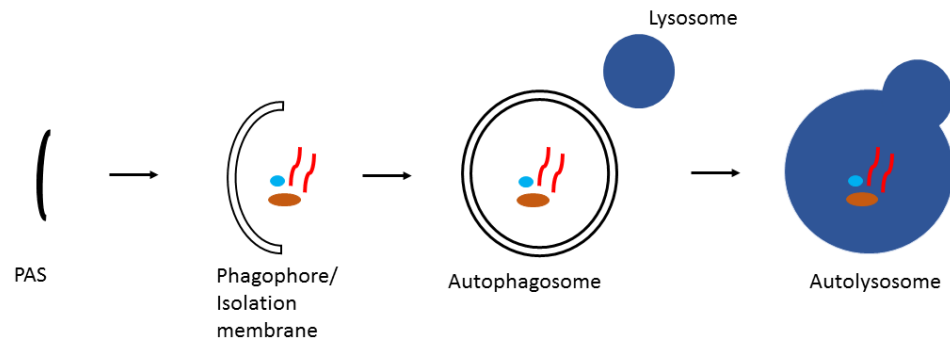


Figure 1.9: Depiction of the steps for the initiation of autophagy and formation of autophagosome.

Autophagy is initiated at a pre-autophagosomal structure (PAS) by the formation of the phagophore/isolation membrane. This membrane expands and engulfs cytosolic components in the process. The two leading edges of the isolation membrane fuse, resulting in the formation of a double-membrane vesicle termed the autophagosome. Fusion between the autophagosome and the lysosome results in the formation of the autolysosome. The contents of the autolysosome are subsequently degraded by the proteolytic enzymes and recycled by the cell.

1.3.1 The cytoplasm to vacuole targeting pathway

The cytoplasm to vacuole targeting (Cvt) pathway is a constitutively active biosynthetic pathway which is responsible for the transport of hydrolase enzymes, such as aminopeptidase I (ApeI) to the yeast vacuole (equivalent of the lysosome in higher organisms) under nutrient rich conditions [reviewed in (Khalfan & Klionsky 2002)]. The Cvt pathway utilizes, to a great extent the same molecular machinery as autophagy, and as a result it is considered to be an autophagy related pathway (Baba et al. 1997; Scott et al. 1996). However, unlike autophagy it is constitutively active, whereas autophagy is inducible under stress or starvation. Cvt vesicles, much like autophagic vesicles arise from the PAS (Suzuki et al. 2002; Kim et al. 2002), however they have a much smaller size of 140-160 nm (Kim et al. 2002) compared to 400-900 nm for the autophagosomes (Takeshige et al. 1992).

1.3.2 Induction of autophagy by the mTORC1 pathway

The key regulator of autophagy in yeast is the Atg1 kinase. ULK1 and UNC-51 are its orthologues in mammals and *C.elegans* respectively. The action of the Atg1 kinase is explained in detail in section 1.3.3. In mammals the target of rapamycin complex (TORC) is known to regulate autophagy via the ULK1 kinase (J. Kim et al. 2011).

The mammalian target of rapamycin or mechanistic TOR (mTOR) is a highly conserved serine/threonine kinase which interacts with a multitude of signals such as amino acid levels, growth factors and oxygen in order to coordinate cell growth and regulate metabolic homeostasis (Laplante & Sabatini 2012). In mammals two mTOR complexes exist, mTORC1 and mTORC2. It is mTORC1 that has been shown to be sensitive to both growth factors and nutrients which is essential for the activation of the mTORC1 kinase (Jewell et al. 2013), whereas mTORC2 has been shown to be sensitive only by growth factors and has been shown to control their flux via the Akt/PKB (Protein KINASE B) pathway in mitochondrial associated ER membranes (Betz et al. 2013).

It is widely accepted that mTORC1 acts as repressor of autophagy in eukaryotes. It has been shown that just the inhibition of mTORC1 is enough to induce autophagy even when there is abundance of nutrients both in yeast and mammalian cells (Noda & Ohsumi 1998; Kanazawa et al. 2004; Thoreen et al. 2009).

The ULK1/Atg1/UNC-51 complex (Section 1.3.3) is suppressed by mTORC1 which in turn represses autophagy. Suppression of the ULK1 results in the inhibition of autophagy and is conserved across eukaryotes. In mammalian cells the ULK1-ATG13-FIP200 complex (ATG1-ATG13-ATG17 in yeast) is formed regardless of the nutrient status (Kamada et al. 2000; Mizushima & Klionsky 2007).

The mTORC1 inhibits the ULK1 kinase activity, by phosphorylating the ATG13 and ULK1 subunits of the ULK1 complex. Inhibition of mTORC1 binding, allows ULK1 to autophosphorylate and in turn further phosphorylates its binding partners ATG13 and FIP200 and thus activating the kinase complex under starvation (Figure 1.10) (J. Kim et al. 2011) which in turn recruit the rest of the components for the formation of the

autophagosome. Similarly in yeast the ATG genes have been demonstrated to act downstream of TOR (Ohsumi 2000; Kamada & Ohsumi 2010).

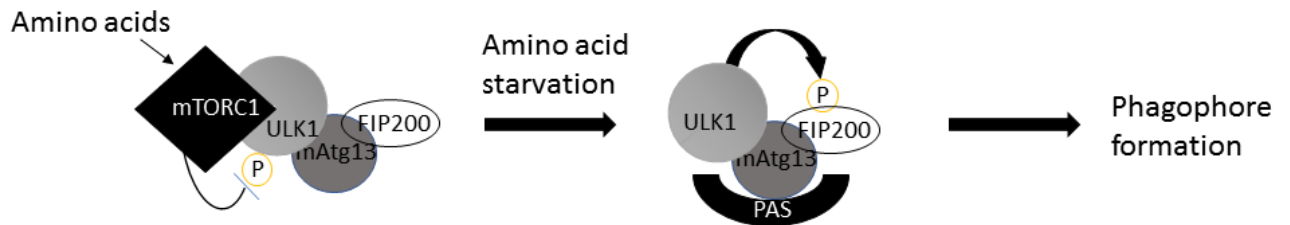


Figure 1.10: Regulation of autophagy in mammals.

Phosphorylation by mammalian-TOR complex 1 (mTORC1) of ULK1 inhibits ULK1 and initiation of autophagy. Amino acid starvation or rapamycin treatment causes dissociation of mTORC1 and ULK1 can phosphorylate and activate FIP200 allowing formation of the phagophore at the phagophore assembly site/pre-autophagosomal structure (PAS).

1.3.3 Induction of autophagy and autophagosome assembly

The autophagosome is a double membrane organelle which required for the sequestering of cargo destined for degradation in cells as part of the autophagic process. The autophagosomal membrane is rich in lipids and poor in proteins since it only has one specialised function which is the delivery of cytosolic components to the lysosome/vacuole (Baba et al. 1995) where the two fuse and the autophagosome is degraded rapidly (Suzuki et al. 2002). Autophagy related protein (Atg) are the main regulators and components in the formation of the autophagosome and can be classified into six functional groups i) the Atg1 kinase complex (Atg1-Atg13-Atg17-Atg29-Atg31), ii) Atg9, iii) the class II phosphatidylinositol (PI)3P- kinase complex (Atg6/Vps30-Atg14-Vps15-Vps34), iv) The PI(3)P- binding Atg2-Atg18 complex, v) the Atg12 conjugation system (Atg12-Atg5-Atg16) and finally vi) the Atg8 conjugation system with the involvement of phosphatidylethanolamine (Atg8-PE) (Suzuki et al. 2007; Suzuki & Ohsumi 2007). The formation of the autophagosome can be subdivided into two steps the nucleation which can

form a minimum size autophagosome, termed the phagophore or isolation membrane, and the expansion to achieve a normal size organelle (Abeliovich et al. 2000; Biazik et al. 2015). The Atg2-Atg18 complex, the Atg12 conjugation system the PI(3)P kinase complex are involved in the nucleation step, whereas Atg8-PE is required for expansion [reviewed in (Suzuki & Ohsumi 2007)].

Studies in yeast have provided the hierarchy through which the protein acts in the PAS for the formation of the autophagosome. Atg17 is essential for the recruitment of the rest of the Atg protein to the PAS. In the absence of Atg17 localisation of downstream Atg to the PAS protein is abolished (Suzuki et al. 2007). Atg17 forms a complex with Atg29 and Atg31 (Kabeya et al. 2009) and subsequently recruit Atg1-Atg13 to the PAS via the direct interaction of Atg17 and Atg13 (Kabeya et al. 2005). The formation of complexes between Atg1-Atg13 and Atg17-Atg29-Atg31 is what gives Atg1 its kinase activity (Kabeya et al. 2005; Ohsumi 2000). The PI(3)P kinase complex is subsequently recruited via direct interaction of between its own Atg14 and Atg13 from the Atg1 kinase complex (Jao et al. 2013). The complex then acts in the initial recruitment to the PAS via recruitment of Atg8-PE and the Atg12 conjugation system and Atg2-Atg18 complex. Atg9 is recruited via a direct interaction with Atg11 (He et al. 2006) which can form complexes with Atg1 kinase complex via Atg17 (Yorimitsu & Klionsky 2005). Atg11 however, has been identified to operate exclusively in the Cvt pathway in yeast via the interaction of autophagy receptors (Kim et al. 2001; Kamber et al. 2015) and it is unclear if a component is present in the autophagic pathway.

The mammalian homologue of Atg1, known as ULK1, also form a complex at the initiation of autophagy in mammals termed the ULK1 complex. It has been shown to mediate localisation of Atg9 in an AMPK (Adenosine monophosphate-activated protein kinase) dependent manner (Young et al. 2006; Mack et al. 2012). Atg-8 is subsequently recruited by Atg9 (Suzuki & Ohsumi 2007; Suzuki et al. 2001). The Atg12 conjugation system subsequently localises to the developing autophagosome where it facilitates the correct localisation and lipidation of Atg8 to aid in the expansion of the autophagosomal membrane (Hanada et al. 2007; Nakatogawa et al. 2007). Furthermore ATG9 has been shown to function in aiding in the transport of membranes from the PAS to non-PAS structures, a process required for the expansion of the phagophore membrane and the formation of the autophagosome in yeast (Reggiori et al. 2004; Yen et al. 2007; Reggiori & Klionsky 2006).

A similar mechanism has been identified in mammals. The formation of ULK1 (mammalian homologue of yeast Atg1) complex puncta is one of the first events to occur as part of autophagy initiation (Itakura & Mizushima 2010; Kuroyanagi et al. 1998; Mizushima et al. 1998; Yan et al. 1998). There is evidence to suggest that ULK1/Atg1 is recruited before any of the other ATG proteins and as such acts as the initiation for the maturation of the phagophore. ULK1 is required for recruitment of VPS34 to the phagophore (Itakura & Mizushima 2010; Koyama-Honda et al. 2013). VPS34 forms a complex along with VPS15, Beclin-1 and ATG14 forming the mammalian PI(3)P complex. The complex is recruited to the phagophore where it phosphorylates phosphatidylinositols (PtdIns), thus producing PtdIns(3)P (Matsunaga et al. 2010; Fan et al. 2011; Koyama-Honda et al. 2013; Itakura & Mizushima 2010). Phosphorylation of PtdIns results in the stabilisation of ULK1 at the omegasome which are membrane extensions of the ER within which some autophagosomes form (Karanasios et al. 2013; Matsunaga et al. 2010; Biazik et al. 2015). At the same time as the ULK1 complex forms the ATG12-ATG5-ATG16 complex also forms with the aid of the ubiquitin like conjugation system which requires the action of ATG7 and ATG10 (Geng & Klionsky 2008). The ATG12-ATG5-ATG16 complex is required for the conjugation of LC3 to phosphatidylethanolamine (Kabeya et al. 2000). LC3 is the mammalian homologue of the yeast Atg8 (and *C. elegans* LGG-1) and is required for the expansion of the phagophore membrane (Kabeya et al. 2000; Tanida et al. 2002; Meléndez et al. 2003; Kirisako et al. 1999). LC3-phosphatidylethanolamine is considered to play an important role in aiding the closure of the expanding autophagosomal membrane during the formation of the autophagosome from the phagophore (Fujita et al. 2008). Finally, ATG9 takes part in the autophagosome formation however it is not a stable component of the membrane (Orsi et al. 2012; Itakura & Mizushima 2010), acting as a mediator for the trafficking of membranes from non-PAS to PAS structures similar to yeast (Orsi et al. 2012).

Many of the genes regulating the formation of the autophagosome have orthologues in *C. elegans* [reviewed in (Meléndez & Levine 2009)], such as *bec-1* which is the orthologue of the yeast ATG6 and *unc-51* which is the *C. elegans* orthologue of ATG1. In some cases multiple orthologues for certain genes have been identified as in the case of *lgg-1* and *lgg-2*, both of which are orthologues of the yeast ATG8. It has been shown however, that only *lgg-1* has a role in autophagy (Meléndez et al. 2003). It is believed that general mechanism remains the same in *C. elegans* with a number of the *C. elegans* homologues exhibiting the

same functions in autophagy as in yeast (Meléndez et al. 2003; Matsuura et al. 1997; Tian et al. 2009; Yang & Zhang 2011).

1.3.4 Fusion of the autophagosome and the lysosome

The newly formed autophagosome must travel to the lysosome and fuse with it to deliver its cargo for degradation. It is believed that the mature autophagosome is characterized by the absence of the proteins involved in the autophagy initiating machinery from the outer membrane via Atg4 dependent deconjugation of Atg8-PE as it has been demonstrated in yeast (Yu et al. 2012; Nair et al. 2012; Kirisako et al. 1999). After arrival of the autophagosome, it is believed to fuse with the lysosome via the action of Rab7 in conjunction to the HOPS tethering complex (Ganley et al. 2011).

It is probable that the recruitment of Rab7 is mediated by Rab conversion. Rab5 has previously been associated with the initiation of autophagy under the absence of growth factors (Dou et al. 2013). As a result Rab5 could be part of the mature phagosome membrane. It is possible that the Rab5 could recruit the HOPS complex in the autophagosome and under the action of the VPS39 subunit, which acts as guanine exchange factor (GEF), activate Rab7 which will result in the replacement of Rab5 in the membrane [(Poteryaev et al. 2010) reviewed in (Stenmark 2009)]. PI(3)P is also important for the Rab5-Rab7 conversion and is catalysed by the action of the phosphoinositide 3 - kinase (PI3K) VPS34 (Gillooly et al. 2000; Shin et al. 2005; Poteryaev et al. 2010).

VPS34 itself can form a complex with the UV radiation resistance-associated gene (UVRAG). UVRAG can also bind VPS16 which is part of the HOPS complex. Furthermore, the protein Rubicon which negatively regulates VPS34 by binding to UVRAG, has been shown to inhibit endosomal and autophagosome fusion to lysosomes. It is interesting that an activated Rab7 promote dissociation of Rubicon and UVRAG, which allows the second to bind to HOPS and in turn further activate Rab7 and promote fusion of membranes (Sun et al. 2010; Liang et al. 2008). The SNARE proteins that have been shown to function in the fusion of the autophagosome and the lysosome are VAMP8 and Vtib (Furuta et al. 2010), along with VAMP3 and VAMP7 (Fader et al. 2009). Furthermore, In addition to this the Q-SNARE Syntaxin 17 has been shown to be recruited to the autophagosome and act exclusively in autophagosome fusion as its loss only disrupts the autophagosomal fusion and not the endosomal fusion with the lysosome.

Further to this, it has been shown to interact with the Q-SNARE SNAP-29 and the R-SNARE VAMP8. (Itakura et al. 2012).

After the autophagosome and the lysosome have fused, the inner membrane of the previously independent autophagosome along with its cargo is degraded by hydrolases. Monomeric units of the degraded macromolecules are exported to the cytosol for reuse (Mizushima 2007).

1.3.5 Autophagy in *C. elegans*

The autophagic machinery appears to be implicated with endosomal trafficking (Djeddi et al. 2012). In an early publication on the process of moulting in *C. elegans*, a rapid loss of secretory membranes immediately after secretion of a new cuticle and subsequent completion of moulting was described (Singh & Sulston 1978). Although the molecular basis of this rapid reduction in intercellular membranes inside hypodermal seam cells is not known, the possibility that this is by autophagy is a reasonable hypothesis.

Autophagy was previously explained in detail with regards to its molecular mechanism in yeast and mammalian cells. However, as it is a highly conserved process amongst organisms, understanding this process in those organisms can also aid our knowledge in other organisms such as *C. elegans*. UNC-51 is the *C. elegans* ortholog of the yeast Atg1. Atg1 is required for the induction of autophagy through its association with Atg13 (Kijanska et al. 2010). The *unc-51* mutants are paralyzed (uncoordinated phenotype) and exhibit developmental problems, namely a smaller body size. The smaller body size in *unc-51* mutants can be attributed to cells having a decreased size (Aladzcity et al. 2007). They also exhibit defective formation of LGG-1, (orthologue of the mammalian LC3 protein) punctae which act as a marker of autophagy (Meléndez et al. 2003; Aladzcity et al. 2007; Sato et al. 2011). Additionally, silencing of the gene through RNAi has resulted in animals with reduced levels of autophagy (Cheng et al. 2013). Finally it is possible, as hypothesized in this work, that autophagy contributes to the removal of membranes from the old cuticle as well as structures that appear during the molt, such as Golgi Bodies, but are no longer required after its completion (Singh & Sulston 1978).

1.3.6 Autophagy an endocytic trafficking in molting

It has been previously demonstrated that, *unc-51; dpy-10* and *vps-45 dpy-10* double mutants are both synthetically lethal (Cowan, 2014). Considering DPY-10 is a secreted collagen component of the cuticle this points to some possible link between the processes of autophagy, endocytic trafficking and moulting. In addition to this VPS-45 defective mutants in yeast have been shown to exhibit defects in selective autophagy accompanied by the accumulation of clusters of autophagosomes (Chen et al. 2014). In addition to this, Tlg2 which is stabilized by Vps45 (Bryant & James 2001), has been proposed to play a role in the recruitment of Atg9 in the PAS in yeast (Abeliovich et al. 1999; Nair et al. 2011; Ohashi & Munro 2010). Thus possibly suggesting that components of the endocytic pathway could be also be having an effect in moulting through autophagy.

1.3.7 Autophagy in Disease

A multitude of human diseases have been associated with autophagy. Among others these include, cancer, neurodegenerative diseases, cardiovascular and metabolic diseases.

Autophagy has been shown to be associated with cancer, as well as the effect of potential therapeutic approaches on the disease. In several human cancers altered expression of autophagy proteins has been observed. For instance, ATG5 expression is up-regulated in prostate carcinomas (Kim et al. 2011), and it has generally been shown that autophagy can promote survival of cancer cells (Degenhardt et al. 2006). Additionally chromosomal abnormalities in autophagy genes have often been observed in human cancers (Levine & Kroemer 2008). Furthermore, elevated levels of autophagy have been identified in human tumours. Autophagy levels have been shown to increase in response to chemotherapy in mouse tumour cells (Ladoire et al. 2012).

Neurodegenerative diseases such as Alzheimer's and Huntington's, commonly involve accumulation of protein aggregates. Increased aggregates are formed with increasing age. Autophagy can remove such aberrant protein aggregates, and deregulation of the autophagic process could be one of the contributing factors of the disease along for the

causative mutations for the disease (Ma et al. 2010; Goedert et al. 2010). It has been shown that in mice deficient for the autophagic process, age dependent neurodegenerative diseases have been promoted via the increased accumulation of protein aggregates (Hara et al. 2006).

Finally, autophagy can affect metabolism since through the process itself several metabolites are produced such as lipids and amino acids (Rubinsztein et al. 2012). Increased levels of autophagy under exercise further support this idea. Experiments in mouse models have shown that increased autophagy as a result of exercise can have protective effects against glucose intolerance (He et al. 2012).

In all cases, it is suggested that diseases can arise as a result of autophagic impairment. As such in all of the above cases autophagy can be considered a pro survival process.

1.4 Project aims

Endocytosis and autophagy are both important cellular processes promoting the survival of cells through homeostasis. Disruption of either of these processes can result in severe pathologies. Both processes have been previously investigated in yeast and *C. elegans*. A link between autophagy and endosomal trafficking has also been suggested in yeast via the involvement of the COG tethering complex and Tlg2 (Yen et al. 2010). During molting in *C. elegans* synthesis and secretion of the new stage specific cuticle takes place. The cuticular components are synthesized and secreted by the hypodermal cells, at the end of each larval stage accompanied by the synthesis peak of cuticle proteins. Synthesis of these cuticular proteins is highly reduced during the intermoult periods (Johnstone & Barry 1996). This oscillation in the synthesis of the cuticular proteins and their secretion coincides with the appearance of dense Golgi structures during the moult, followed by the rapid disappearance of these Golgi after moulting is completed (Singh & Sulston 1978). As a result, one of the aims of this project is to investigate and identify how the disruption of endosomal trafficking and autophagy affects *C. elegans* in their development, with a focus on the moulting/cuticle synthesis processes. Initially, the endosomal trafficking defective *vps-45* mutant and the autophagy defective *unc-51* mutant were phenotypically characterised and compared for moulting and developmental defects. In addition to this, autophagy in these mutants was quantified during the moulting process and during embryonic development.

Mutation in *vps-45* have been shown in to be a cause for severe congenital neutropenia in humans, this in addition to data previously collected in our lab (Cowan, 2014) where yeast carrying an analogous mutation of *vps-45* exhibited high sensitivity to H₂O₂ led to the investigation of the sensitivity of *vps-45* and *unc-51* mutants to oxidative stress.

Finally, to further elucidate the role of endosomal trafficking and more specifically *vps-45* in the moulting process of *C. elegans* and previously isolated suppressed strain carrying the null mutation investigated in this project was characterised phenotypically and full genome sequencing was employed in order to identify the gene responsible for the suppression.

.

Chapter 2: Materials and Methods

Unless stated otherwise, all chemicals and reagents used in this study were purchased from BioRad Laboratories Ltd. (Hemel Hempstead, UK), Fisher Scientific Ltd. (Loughborough, UK), Invitrogen Ltd. (Paisley, UK), Melford Laboratories Ltd. (Suffolk, UK), Qiagen Ltd. (Crawley, UK), Roche Diagnostics Ltd. (Burgess Hill, UK), Sigma-Aldrich Ltd. (Poole, UK) and VWR Prolabo (Lutterworth, UK).

Enzymes and reagents used for molecular biology were purchased from New England Biolabs Ltd. (Hitchin, UK), Promega Ltd. (Southampton, UK), Roche Diagnostics Ltd. (Burgess Hill, UK), and Yorkshire Bioscience Ltd. (York, UK).

Bacterial [*Escherichia coli* (*E.coli*)], and nematode [*C. elegans*] growth media components were purchased from ForMedium™ (Norfolk, UK) and Melford Laboratories Ltd. (Suffolk, UK).

2.1 Solutions and media

Ampicillin sodium salt: 100 mg/ml in dH₂O Stock solution. 100µg/ml working solution.

BO₃ buffer (Borate buffer) (40x): 618 mg H₃BO₃, 5 ml 1M NaOH, ddH₂O to 10 ml. Adjust pH to 9.2.

Bleach solution: NaOCl 12ml, 5M KOH 5ml, dH₂O to 100ml

C. elegans Freezing solution: S-Basal + 30% Glycerol(v/v)

IPTG: 1M stock in sterile H₂O. Stored at -20°C

LB agar: 10g bacto-tryptone, 5 g bacto-yeast extract, 5 g NaCl and 15 g agar in 1 L of dH₂O, pH adjusted to 7.5 by the addition of HCl and/or NaOH, and autoclaved. If required, antibiotics were added to the cooled medium before aseptically pouring onto 9 cm plates. Unused plates were stored at 4°C for short periods.

LB (L-broth): 10g bacto-tryptone, 5 g bacto-yeast extract, 5 g NaCl, dH₂O to 1 L. pH adjusted to 7.0 with NaOH. Sterilised by autoclaving (121°C at 15 psi for 15 minutes).

Microscopy Mounting solution: For 100 ml of solution, 50 µl glycerol, 10 µl DABCO and 40 µl 1 x PBS were mixed by vortex. Made fresh before use.

M9 buffer (10x): 30 g KH₂PO₄, 60 g Na₂HPO₄, 50 g NaCl, 1 ml 1 M MgSO₄ in 1 L dH₂O. Mixed and autoclaved. Nematode growth medium (NGM) agar: 0.3% NaCl, 0.25% of Bacto-peptone, 1.7% agar, 0.0005% cholesterol (1 ml of 5 mg/ml stock in EtOH), in dH₂O. Autoclaved and, after the medium cooled, the following solutions were added using sterile technique: 400µl of 1M CaCl₂, 400µl of 1 M MgSO₄ and 10 mL of 1 M potassium phosphate pH 6.0, prior to pouring petri plates.

Phosphate buffered saline (PBS): 800 g NaCl, 20 g KCl, 144 g Na₂HPO₄ · 2H₂O, 24 g KH₂PO₄, 8L of dH₂O, pH 7.4

PBST: 1x PBS and 0.2% Tween-20.

Potassium phosphate buffer (1M, pH 6): obtained by mixing 13.2 ml of 1 M KH₂PO₄ and 86.8 ml of 1M K₂HPO₄ to reach pH 6.0 in a 100ml solution.

Ponceau S solution: (0.1% (w/v) Ponceau S, 5% (v/v) acetic acid)

RFB (Ruvkun Finney Buffer) (2x): 1.6 ml 1M KCl, 80µl 5M NaCl, 0.4ml 0.5M EGTA, 0.6 ml 0.5M PIPES (pH 7.4), 0.1 ml spermidine, 5ml Methanol, 2.22 ml ddH₂O

Streptomycin sulfate salt: 12.5 mg/ml in dH₂O 12.5 µg/ml

S-Basal buffer: 0.1M NaCl, Potassium Phosphate pH 6.0 0.05M, Cholesterol 5µg/ml

Single worm lysis buffer (SWLB): 50 mM Tris-HCl pH 8.0, 100 mM NaCl, 50 mM EDTA, 1% SDS, 30 mM β-mercaptoethanol, 100 µg/ml proteinase K. Buffer was freshly made just before use.

Streptomycin sulfate: salt 12.5 mg/ml in dH₂O 12.5 µg/ml stock solution, 12.5 µg/ml working solution.

TTB (Tris-Triton Buffer): 1 ml 1M Tris HCl, p H7.4, 100 µl Triton-X-100, 20 µl 0.5M EDTA, ddH₂O to 10 ml

TE buffer: 10 mM Tris and 1mM EOTA in dH₂O. pH7.5.

10 x Tris borate buffer (TBE): 465.2 g TRIS base and 205.2 g boric acid dissolved in 4 L of dH₂O by stirring. Then 14.88 g of EDTA added and mixed. The working solution was 1x TBE.

2.2 Other Materials

2.2.1 Electrophoresis Markers

DNA markers:

NEB (New England BioLabs) 100bp DNA Ladder, 500µg/ml (Lot: 1081504)

BIO-RAD EZ Load 1 kb Molecular Ruler, 500 µl, 0.08 µg/µl, #1708355

Protein markers:

BIO-RAD Precision Plus Protein Standards # 161-0373

Antibodies:

Primary antibodies

anti-DPY-7 Mouse monoclonal antibody 1:100 in PBST (McMahon et al., 2003)

GFP Antibody (FL) rabbit polyclonal IgG 1:200 in PBST Santa Cruz

Biotechnologies (sc-8334)

Secondary antibodies

Donkey anti rabbit 800 1:10 000 in LI-COR blocking buffer 1:1 PBST infrared dye-labelled secondary antibodies against rabbit IgG from donkey LICOR Biosciences (926-32213) used for western blotting.

Alexa Fluor Fluorophore conjugated whole IgG from goat 1:200 Invitrogen Ltd. 488 anti-rabbit used for immunolocalisation.

2.3 Methods

2.3.1 *E. coli* OP50 bacteria culturing

LB agar with streptomycin (12.4 mg/ml) was used for streaking of isolated colonies of *E. coli* OP50 bacteria (Uracil auxotroph). A single OP50 colony each time was used to inoculate 50 ml batches of liquid medium containing 1g LB, and H₂O up to 50 ml. 50 µl of streptomycin (stock: 12.4 mg/ml) was also added to the liquid media prior to inoculation. Sigma LB broth was made in batches of 50 ml (1 g LB in 50ml of LB). Inoculated medium was left overnight in room temperature to grow and was then subsequently stored at 4°C for up to two months (Stiernagle 2006).

2.3.2 Nematode culture in solid media

Nematodes were grown on solid Nematode growth medium (NGM). 400 ml volumes of NGM were made containing 1.2 g NaCl, 6.8 g agar, 1 g peptone, 0.4 ml cholesterol (stocks: 5 mg/ml in EtOH), and H₂O to 390 ml. To this, 0.4ml 1M CaCl₂, 0.4 ml 1M MgSO₄, and 10 ml 1M potassium phosphate (pH 6.0) were added into the medium before pouring the plates. 200 µl of OP50 inoculated LB broth were spread on each NGM agar plates. Plates were left overnight in room temperature to produce a thin lawn of OP50. On occasions where synchronous cultures were needed the bacteria were spread using a glass spreader under sterile conditions for the medium (5.5 cm diameter) and large petri dishes (9cm diameter). A drop of 200µl liquid culture OP50 was added to large petri dishes (9cm) and 50µl added to the medium (5.5cm) petri dishes in all other occasions. 15µl of OP50

liquid culture was added in the small (3cm diameter) petri dishes in all cases (Stiernagle 2006).

2.3.3 Nematode Handling

Individual animals were manipulated with a worm pick, which consists of a piece of platinum wire with a flattened, arrow-shaped end, sealed into a broken Pasteur pipette. The platinum wire cools quickly when flamed, allowing sterilisation of the pick on a Bunsen burner between worm transfers. For handling, large amounts of animals, agar chunks were cut out from old NGM cultures and transfer onto fresh, seeded plates with the aid of a sterilised scalpel. N2 Bristol and most other strains were maintained in a 20°C incubator (Stiernagle 2006). Temperature sensitive mutants were also placed at 15°C or 25°C according to their characteristics and the aims of the study. Strains carrying the *vps-45* (*tm246*) allele in particular had to be regularly tested for lethality at 25°C since it was proven that it was very easily suppressed after a long culturing.

<i>C. elegans</i> strains used in the experiments	Description
N2	<i>C. elegans</i> wild isolate (Bristol)
CB4856	<i>C. elegans</i> wild isolate (Hawaiian)
IA757	<i>vps-45</i> (<i>tm246</i>)
IA773	<i>svp</i> (<i>ij117</i>) -suppressor of <i>vps-45</i> (<i>tm246</i>)
TP198	<i>kaIs6</i> [<i>pADW0083</i> (<i>pdi-2prom::roGFP-ER3::phy-1 unc-119(+)</i>)]
CB369	<i>unc-51</i> (<i>e369</i>)
LD1171	<i>ldIs3</i> [<i>gcs-1p::GFP rol-6(su1006)</i>]
CF1553	<i>muIs84</i> [<i>(pAD76) sod-3p::GFP rol-6(su1006)</i>]
CL2166	<i>dvIs19</i> [<i>(pAF15)gst-4p::GFP::NLS</i>] III

DA2123	<i>adIs2122 [lgg-1p::GFP::lgg-1 rol-6(su1006)]</i>
SU93	<i>jcIs1 [ajm-1::GFP unc-29(+)] rol-6(su1006)] IV</i>
IA880	<i>kaIs6 [pADW0083 (pdi-2prom::roGFP-ER3::phy-1 unc-119(+))];unc-51 (e369) V</i>
IA881	<i>kaIs6 [pADW0083 (pdi-2prom::roGFP-ER3::phy-1 unc-119(+))];vps-45 (tm246) X</i>
IA882	<i>vps-45 (tm246) in Hawaiian background (back cross with CB4856)</i>
IA887	<i>muIs84 [(pAD76) sod-3p::GFP rol-6(su1006)]; vps-45 (tm246) X</i>
IA888	<i>adIs2122 [lgg-1p::GFP::lgg-1 rol-6(su1006)]; vps-45 (tm246) X</i>
IA889	<i>ldIs3 [gcs-1p::GFP rol-6(su1006)]; vps-45 (tm246) X</i>
IA890	<i>dvIs19 [(pAF15) gst-4p::GFP::NLS] III; vps-45 (tm246) X</i>
IA896	<i>muIs84 [(pAD76) sod-3p::GFP rol-6(su1006)]; unc-51 (e369) V</i>
IA897	<i>adIs2122 [lgg-1p::GFP::lgg-1 rol-6(su1006)]; unc-51 (e369) V</i>
IA898	<i>ldIs3 [gcs-1p::GFP rol-6(su1006)]; unc-51 (e369) V</i>
IA899	<i>dvIs19 [(pAF15) gst-4p::GFP::NLS] III; unc-51 (e369) V</i>
IA900	<i>unc-51(e369)/unc-51 (e369) V; vps-45(tm246)/+</i>
IA903	<i>adIs2122 [lgg-1p::GFP::lgg-1 rol-6(su1006)]; jcIs1 [ajm-1::GFP unc-29(+)] rol-6(su1006)] IV</i>

Table 2.1: List of *C. elegans* strains used in this study

2.3.4 Freezing and thawing nematode stocks

The wild-type and mutant strains can be stored indefinitely in liquid nitrogen (-196°C). Two large (9cm) petri dishes of the desired strain for storing were left to grow close to starvation with the purpose of having populations mainly constituted by L1 larvae. At this stage nematodes are most likely to survive the freezing. Each plate was then washed with 3 ml of M9 buffer to make three or four 0.5 ml aliquots to which an equal volume of freezing solution was added. Tubes were mixed and immediately placed in a polystyrene box at -70°C. After at least a day, one tube was thawed and plated as a tester and the remainder of the tubes were passed to two different liquid nitrogen tanks (Stiernagle 2006).

2.3.5 Decontamination of *C. elegans* stocks

Contamination of cultures by fungi, yeast, or undesirable bacteria happened occasionally. This problem could be rectified by transferring individual *C. elegans* onto a fresh plate, at which point they were allowed to move before repeating the operation at least one more time. Yeast and bacteria could also be removed by treatment with alkaline hypochlorite solution, as eggs are resistant to bleach. *C. elegans* treated with bleach solution and subjected to vortexing are fragmented and eggs are harvested (section 2.3.5.1) (Stiernagle 2006).

2.3.6 Nematode synchronous cultures

2.3.6.1 Harvesting nematode eggs

Nematodes were washed off NGM plates using S-Basal buffer (into a 15ml tube). *C. elegans* were left to form a pellet in the tube for 5 minutes on the bench. The

excess buffer was removed. Bleach solution was added to about 20x the volume of the worm pellet. Samples were vortexed several times during 5-minute incubation. They were checked under the microscope for release of eggs and fragmentation of adult bodies. If the nematodes did not fragment and mostly dissolve, the amount of alkaline hypochlorite solution was doubled, and incubation time was doubled for another 3 minutes. Samples were centrifuged at 1000xg for 5 minutes, to pellet eggs. Bleach solution was removed. Eggs were washed 3 times with centrifugation using S-basal buffer (Stiernagle 2006).

2.3.6.2 Synchronous cultures in liquid media

Embryos were transferred in a sterile 2L flask containing 60 ml of S-basal buffer plus MgSO₄ and CaCl₂. The low volume of buffer was used in order to achieve a high surface to volume ratio so that animals would get enough oxygen. Embryos hatching would arrest at the L1 stage (Kaplan & Baugh 2016). After 24 hours all of the larvae were in sync for the wild type strain. For the *vps-45* (tm246)/IA757 and *unc-51* (e369)/CB369 mutants larvae were in sync after 48 hours (Stiernagle 2006).

2.3.6.3 Synchronous cultures in solid media

NGM plates with 100µl of OP50 bacteria evenly spread across the surface of the agar were used. The desired number of L1 arrested larvae were added onto each plate. When cultured this way, wild type *C. elegans* remained in synchrony throughout their development to adulthood.

2.3.7 Observation of nematodes during the molt

Synchronised L1 larvae in liquid cultures were obtained and were seeded on NGM plates with an evenly spread lawn of OP50 bacteria, as previously described in material methods (section 2.3.6). All mutants were cultured in the NGM petri dishes until they entered lethargus at which point they started moulting. At this stage they were accounted for or they were transferred on slides to be observed

under the high magnification microscope (section 2.3.8). Cultures were observed, and images were acquired at several points during the moult, from the onset of lethargus until ecdysis (end of moult) depending on the aim of the experiment.

2.3.8 *C. elegans* crosses

5-10 L4 or young adult males and 1 L4 or young adult hermaphrodite were placed on a NGM plate for each mating. A ratio of approximately 50% males to hermaphrodites at the F1 generation suggested that that the cross was successful. Animals from the parental generation were transferred from their original plate to a fresh plate after 24-48 hours of egg laying depending on the needs of the experiment. When accurate counting of progeny was needed transfer of the parents was repeated one more time. This way the entire brood of one adult could be followed and counted if necessary. Thus, numbers of F1 progeny were more easily scored for each cross. Animals were counted separately for each plate of each cross and were then summed up. For each successful cross single F1 hermaphrodites were picked and transferred to new plates and were left to self-reproduce. Depending on the aim of the experiment the animals from the F2 generation were either further crossed or transferred to new plates in order to produce the F3 generation. All proceeding generations were monitored for the desired phenotype (Fay 2013). All procedures were done near the bunsen flame to maintain sterile conditions. In cases where genotyping was required at any of the crossing stages, *C. elegans* were lysed for DNA for PCR analysis, as described below.

2.3.9 Routine microscopy

C. elegans on NGM plates were visualised with Zeiss stereo dissecting microscopes. The handling of transgenic animals expressing GFP was carried out with a Stemi SV-6 Zeiss microscope with fluorescence attachment. For closer examination of nematodes, specimens were collected and placed on 2% agarose pads on standard glass microscope slide. They were prepared with, 10 ml of 2% Agar, containing 0.2% sodium-azide. Sodium azide was

used to anesthetize the animals and stop them from moving. Agar was heated, to molten, then 30 μ l was added to the centre of a microscope slide and a second slide placed on top to create a “sandwich” of agar which was allowed to set. Slides were separated so the agar pad was on one of the two slide. *C. elegans* were transferred onto the agar pad and a 5 μ l drop of S-Basal (0.1M NaCl, 0.05M potassium phosphate buffer (pH 6.0), 1ml/ L cholesterol) was added to prevent nematodes from drying. A cover slip was placed and the animals were observed using an Axioskop 2 microscope (Carl Zeiss, Jena, Germany) equipped with Normaski optics at 10X, 63X and 100 magnification with a 0.63X or 1X reducing lens depending on the requirements of the experiment. The camera used was a Hamatsu Orca C4742-95 digital camera (Hamatsu Photonic, Hamatsu City, Japan). Openlab 4.0.2 software (Improvision, Coventry, United Kingdom) was used to capture pictures of the srains. Images were processed using the ImageJ software (<https://imagej.nih.gov/ij/>).

2.3.10 Quantification of whole body *C. elegans* fluorescence

Images from the microscope were manipulated using ImageJ software (Schneider et al. 2012). The worm was outlined on the picture of interest using any of the drawing/selection tools (i.e. rectangle, circle, polygon or freeform). AREA, INTEGRATED DENSITY and MEAN GRAY VALUE were selected to be measured for each image. “Measure” was selected from the analyse menu. A different region was selected on the same image next or close to the *C. elegans* that had no fluoresce. This was the background measurement. The steps were repeated for all pictures and the corrected total worm fluorescence (CTCF) was calculated using the following formula

$$\text{CTCF} = \text{Integrated Density} - (\text{Area of selected worm} \times \text{Mean fluorescence of background readings}) \text{ (McCloy et al. 2014)}$$

The value obtained was divided by the total selection area to correct for the difference in size between individual animals.

2.3.11 *C. elegans* lysis and genomic DNA extraction

The same method was used for single *C. elegans* genomic lysates as well as preps which required a larger number of animals. In the first instance, a single worm was picked from each plate and was placed in a sterile 0.5 ml tube with 12.5 μ l single worm lysis buffer. Samples were incubated at -70°C for 10 minutes to freeze-fracture. They were then removed and put for 1 hour at 60°C for lysis, followed by 15 minutes at 95°C for proteinase K inactivation. Samples were stored at -20°C as DNA for PCR.

For lysates from multiple animals, *C. elegans* were washed off plates in sterile H_2O and were transferred to a sterile 1.5 ml tube. They were left to sediment for 5 minutes or until an obvious worm pellet could be formed. Most of the supernatant was removed using a pipette without disturbing the pellet. 1 ml of H_2O was added at this stage to wash the nematodes. *C. elegans* were left again to sediment for 5 minutes and the supernatant was removed. Single worm lysis buffer was added at approximately five times the volume of the *C. elegans* pellet. Same incubation times and temperatures as described above. EDTA was added to the sample to 10 mM final concentration to preserve DNA for multiple uses. Lysis was carried out at the same temperatures as described above. Samples were then diluted 4-fold in TE and were frozen at -20°C as DNA for PCR.

2.3.12 *C. elegans* lysis and genomic DNA extraction for full genome sequencing

The DNeasy Blood and Tissue kit from Qiagen (Cat No. 69504) was used to extract pure genomic DNA for full genome sequencing. A modified protocol of the kit was used. Nematodes were washed off their plates and were gathered in 1.5ml Eppendorf tubes, until a *C. elegans* pellet of 100 μ l was collected. 180 μ l of buffer ATL were added with 20 μ l of proteinase K provided by the kit. The kit protocol was followed from step 2 onward. After purification samples were treated with 2.5 μ l RNase 30mg/ml + TRIS pH 7.5 mixed at a ratio of 1:4. Samples were incubated for 30 minutes at 37°C . All samples were passed through the column a second time to remove the enzyme.

2.3.13 Quantitation of DNA

The following methods were used to estimate the concentration of DNA in samples. For approximate estimations, a percentage of the sample was electrophoresed in an agarose gel with size standards at known concentrations. A comparison of fluorescent intensity after ethidium bromide staining permitted an estimation of the DNA concentration of the sample. For accurate quantifications, the Nanodrop system was employed.

2.3.14 Preparation of samples for full genome sequencing

Pure DNA was isolated from all the required lines as described on section 2.3.10. DNA was quantified as on section 2.3.11. Samples were mixed in equal amounts based on that in one master mix and were sent for sequencing. About 100 ng of DNA were required for the sequencing procedure. Sequencing was carried out using the illumina technology.

2.3.15 Restriction endonuclease digestion of DNA fragments

DNA digestion reactions were prepared in 200µl Eppendorf tubes and in a total volume of 10 µl. These were routinely incubated for 2-4 hours or overnight at 37°C depending on the activity of the enzyme. DNA fragments were analysed by agarose gel electrophoresis (refer to section 2.3.15). An example of all the components included in a standard single restriction endonuclease digest is shown in table 2.2.

Component	Volume (µl)
DNA sample	5
10X Buffer	1
dH2O	3

Restriction enzyme	1
Final volume	10

Table 2.2: Components of general mix used for digestion of DNA

2.3.16 Polymerase chain reaction (PCR)

2.3.16.1 Design of primers for PCR

Primers for PCR were designed using the Vector NTI software (ThermoFisher scientific). A collection of the primers used in this study is shown on table 2.2. General characteristics of the desired primers were 15-22 nucleotides in length, and a melting temperature of 55°C-65°C, as well as GC content of 40%-60%. Oligonucleotide primer pairs were designed to amplify desired DNA sequences by PCR. All primers used in this study are listed in Table 2-. Primers were synthesised by Yorkshire Bioscience Ltd. and were routinely diluted to 50 picomoles (pmol) in TE buffer prior to storage at -20°C. The PCR reaction mix was typically made up to a total volume of 20 µl in a 0.2 ml thin-walled PCR tube. Taq DNA polymerase combined with its buffer was used. All PCR products were analysed by agarose gel electrophoresis (described in section). Where required the PCR products were digested with the appropriate enzyme. An example of a standard PCR mix used in this study is shown in Table 2.3. In the case of the *vps-45* (tm246) primers a 50µl mix was prepared as shown on table 2.4.

Primer name	Primer Sequence (5'-3')
<i>vps-45</i> TM246 sense 2	ATAGGGACAGAAGGACCGC
<i>vps-45</i> TM246 anti sense 2	AAGCTGCGAAACACTCTCTA
<i>vps-45</i> WT sense	GAGCCAAGATTCAGCCAGT
roGFP forward	GTGCGTGGAGAGGGAGAGGG
roGFP reverse	TGTAGAGTTCATCCATTCCG
<i>unc-51</i> Forward	AGGTCCCGTTTGCTG TAC TC

<i>unc-51</i> Reverse	TCGTGACTTGACTTTTCGCCT
Chromosome ID Forward	ATCATTCTCCAGGCCACGTTAC
Chromosome ID Reverse	CTGAACTAGTCGAACAAACCCC
Chromosome IVE Forward	ACGAAAAATCACAGAGCGGG
Chromosome IVE Reverse	AATCAACAACGGACGACGAG
Chromosome IIA Forward	CGGAGATAGTCTCGTGGTACTG
Chromosome IIA Reverse	CAGTCATGCTCCAAACATTCTC
Chromosome IIB Forward	TCCATCTTCGCAATCAGATTTC
Chromosome IIB Reverse	AACGTA CTGCTTCCCATGCTC
Chromosome IIC Forward	TCATCTGTGAGTGCTTTTG
Chromosome IIC Reverse	CGATCGCTCAAATGGTTG
Chromosome IID Forward	TTCTCACA ACTTCTTTTCCAAG
Chromosome IID Reverse	TTCACTATTTCCCTCGCTGG
Chromosome IIE Forward	TAGGAAAGTTGTGTCCACCTGG
Chromosome IIE Reverse	TGATGACTCCTTCTTCAGCTGC
Chromosome IIF Forward	GATTCGGAATGGGTGTTG
Chromosome IIF Reverse	TCTTGAATGCGTGGTGTG
Chromosome VA Forward	TGTAGGGCGAGTAACCAAGC
Chromosome VA Reverse	CCGCACTTCCTTCAGAAATG
Chromosome VB Forward	ATTGATCCCATGATCTCGG
Chromosome VB Reverse	AATCGCTACTTCCGATAACTTC
Chromosome VC Forward	ATCAATCACATGATGCCGT
Chromosome VC Reverse	TTTCAGCTAGACCTCCCATG
Chromosome VD Forward	GGCGGAAAGCAATTTCTATC
Chromosome VD Reverse	AGCTGCAACCAACTGCTC
Chromosome VE Forward	GCTTTGGAGACATTGAGCCGTG

Table 2.3: List of the primers used in this study for the detection of mutant alleles and Hawaiian and Bristol SNPs.

2.3.16.2 Detection of TM246 null *vps-45* (tm246) mutant and wild type *vps-45* alleles

For the detection of the *vps-45* (tm246) allele a 50µl reaction was prepared as shown on table unlike the standard reactions of the other primers (Table 2.4). The *vps-45* (tm246) mutant allele carries a 1178bp deletion compared to the wild type *vps-45* allele. *Vps-45* WT sense primer along with the *vps-45* (tm246) anti sense 2 primer produce an amplified 629bp fragment of WT DNA. On the other hand, *vps-45* (tm246) sense 2 primer along with *vps-45* (tm246) anti sense 2 produces a 480bp fragment of the mutant allele. There is no amplification of a mutant allele when the *Vps-45* WT sense primer along with the *vps-45* (tm246) anti sense 2 primer for a wild type strain, nor is there amplification of the wild type allele when *vps-45* (tm246) sense 2 primer along with *vps-45* (tm246) anti sense 2 are combined for a IA757 strain.

The PCR routine used, was as follows:

- 1 cycle of initial denaturation at 94°C for 3 minutes.
- 35 cycles of denaturation at 94°C for 30 seconds, annealing at 50°C for 30 seconds, extension at 72°C for 2 minutes.
- 1 cycle of final annealing at 50°C for 2 minutes.
- 1 cycle of final extension at 72°C for 4 minutes

Component	Volume (μl)
DNA lysate	1
dNTPs (2 mM)	2
10x Taq buffer	2
MgSO ₄ (25 mM)	1
Forward primer	1
Reverse primer	1
Taq polymerase	0.5
dH ₂ O	14.5

Table 2.4: Components of general mix used for PCR amplification using two primers.

Component	Volume (μ l)
DNA lysate	5
dNTPs (2 mM)	5
10x Taq buffer	5
MgSO ₄ (25 mM)	2.5
Vps-45 WT sense (20 μ M)	2.5
vps-45 (tm246) sense 2 primer (20 μ M)	2.5
Vps-45 (tm246) anti-sense primer (20 μ M)	2.5
Taq polymerase	0.5
dH ₂ O	24.5

Table 2.5: Components of the mix used for PCR amplification of the *vps-45* allele and the mutant *vps-45* (tm246) allele, using two forward and one reverse primers in a single reaction.

2.3.16.3 Detection of the *unc-51* (e369) allele

The *unc-51* (e369) allele has a single point mutation at the 5 untranslated region (UTR) of the *unc-51* gene (Ogura et al. 1994). The CAG to TAG substitution changes the cut site of the restriction enzyme PvuII. Thus, the enzyme can no longer cut the mutated region allowing for identification of the mutant allele through digestion of the amplified PCR fragment. A standard PCR mix was used to amplify the region. Enzyme digestion was carried out as described on 2.3.15. As such the wild type allele, would produce two band (330bp, 51bp) and the mutated allele a single band (851bp), (Table 2.8).

The PCR routine used, was as follows:

- 1 cycle of initial denaturation at 94°C for 2 minutes.
- 35 cycles of denaturation at 94°C for 20 seconds, annealing at 58°C for 30 seconds, extension at 72°C for 40 seconds.
- 1 cycle of final extension at 72°C for 5 minutes.
-

2.3.16.4 Detection of Bristol N2 or Hawaiian CB4856 genome

A combination of PCR amplification and enzyme digestions was also employed in order to identify the presence of Hawaiian or Bristol DNA utilising the SNP which would create or erase restriction endonuclease cut sites (Bazan & Hillers 2011). The primers along with the enzymes used to detect between Hawaiian and Bristol DNA across chromosomes I, II, IV and V of the *C. elegans* genome are shown on table. A standard PCR reaction mix was used as described on section 2.3.14. After amplification, each sample was digested with the appropriate restriction enzyme as shown on tables 2.5, 2.6, 2.7.

- 1 cycle of initial denaturation at 94°C for 2 minutes.
- 35 cycles of denaturation at 94°C for 20 seconds, annealing at 60°C for 30 seconds, extension at 72°C for 40 minutes.
- 1 cycle of final extension at 72°C for 10 minutes.

Chromosome I, IV
primers

SNP	Cosmid	Map position	Primer sequence (5'-3')	Restriction enzyme	N2 restriction fragments	CB4856 restriction fragments
ID	T07D10	13.6	F:ATCATTCTCCAGGCCACGT TAC R:CTGAACTAGTCGAACAAA CCCC	NdeI	594	300,294
IVE	D2096	3.8	F:ACGAAAAATCACAGAGCG GG R:AATCAACAACGGACGACG AG	EcoRI	648,326	852

Table 2.6: Primers used for the distinction of Hawaiian and Bristol sequences in *C. elegans* on Chromosomes I and IV.

The enzymes in each can recognise a specific base sequence on the DNA. The number of restriction sites available changes depending on SNP of the Hawaiian and the Bristol DNA. The restriction fragments generated in each genome are indicated and are in bp.

Chromosome II primers

SNP	Cosmid	Map position	Primer sequence (5'-3')	Restriction enzyme	N2 restrictions fragments	CB4856 restriction fragments
IIA	T25D3	-17.9	F:CGGAGATAGTCTCGTGGTACTG R:CAGTCATGCTCCAAACATTCTC	DraI	336, 93	288, 93, 48
IIB	R52	-14.5	F:TCCATCTTCGCAATCAGATTTC R:AACGTACTGCTTCCCATGCTC	AluI	368	203, 165
IIC	M03A1	-4	F:TCATCTGTCGAGTGCTTTTG R:CGATCGCTCAAATGGTTG	TaqI	291,81,80	210, 81, 80, 70
IID	F37HB	3.3	F:TTCTCACAACCTCTTTTCCAAG R:TTCCTATTTCCTCGCTGG	TaqI	572, 112, 15	382, 190, 112, 15
IIE	Y38F1	13.6	F:TAGGAAAGTTGTGTCCACCTGG R:TGATGACTCCTTCTTCAGCTGC	HinfI	449	288, 160
IIF	Y51HI	20.9	F:GATTCGGAATGGGTGTTG R:TCTTGAATGCGTGGTGTG	TaqI	482	340, 142

Table 2.7: Primers used for the distinction of Hawaiian and Bristol sequences in *C. elegans* on several regions of Chromosome II.

The enzymes in each can

recognise a specific base sequence on the DNA. The number of restriction sites available changes depending on SNP of the Hawaiian and the Bristol DNA. The restriction fragments generated in each genome are indicated and are in bp.

Chromosome V primers						
SNP	Cosmid	Map position	Primer sequence (5'-3')	Restriction enzyme	N2 restrictions fragments	CB4856 restriction fragments
VA	Y38C9B	-20.0	F:TGTAGGGCGAGTAACCAAGC R:CCGCACTTCCTTCAGAAATG	BamHI	318	268,50
VB	H10D18	-7.9	F:ATTGATCCCATGATCTCGG R:AATCGCTACTTCCGATAACTTC	SspI	436	263,173
VC	F57F5	3.6	F:ATCAATCACATGATGCCGT R:TTTCAGCTAGACCTCCCATG	Hpy188III	578	326,252
VD	F57G8	10.0	F:GGCGGAAAGCAATTTCTATC R:AGCTGCAACCAACTGCTC	DraI	528	272,256
VE	F48F5.2	25.0	F:GCTTTGGAGACATTGAGCCGTG R:ATGCTCTTCACATTTTCCTGG	Hpy188III	439	258,181

Table 2.8: Primers used for the distinction of Hawaiian and Bristol sequences in *C. elegans* on several regions of Chromosome V.

The enzymes in each can recognise a specific base sequence on the DNA. The number of restriction sites available changes depending on SNP of the Hawaiian and the Bristol DNA. The restriction fragments generated in each genome are indicated and are in bp

2.3.17 DNA Gel electrophoresis

Agarose gel of 1-2% w/v were prepared in 1x TBE. Approximately 100 ml of 1-2% agarose gel were cast into the gel tank with 5 µl Ethidium Bromide. The gel was left to solidify. A 1kb or 100bp ladder from NEB or BIO-RAD was used depending on the desired DNA fragments in each case. 10 µl of ladder (premixed with 6x loading dye) were added to the first well. The appropriate amount of loading dye was added to each sample for a final dilution of 1/6. 10 µl from each reaction were then loaded on to the gel. Gels were run for approximately 45 minutes at 100V. Gels were viewed using the Chemidoc XRS System (Bio Rad) and were captured using a camera attached to it.

2.3.18 Detecting the ER redox state of nematodes using a 96-well plate reader

The PHERASTAR FS 96-well plate reader (BMG Labtech) was used to read the fluorescence of the transgenic strains. Approximately, 1000 larvae synchronised at the L4 stage on petri dishes. Animals were washed off NGM plates into a sterile 15ml tube. *C. elegans* were washed twice using S-basal. *C. elegans* were then prepared in a volume of 100 µl and added onto the 96-well plate. The plate was used using the plate reader with the settings as shown on table 2.8. The plate reader would excite the protein at 390nm and 460nm and receive emission spectra at 520nm. If a higher emission was obtained from the excitation of 390nm the protein was in an oxidised state, whereas if the emission from the 460nm excitation then more protein would be in the reduced state. For each strain carrying the roGFP ER3 marker, its equivalent parental non-fluorescent one was used as a blank control to subtract background fluorescence, using the Pherastar software (BMG Labtech). In the case of *unc-51 (e369)* mutant which could not retain synchrony when cultured from L1 arrest, the same procedure as above was followed, with the only difference being that a mixture of animals was obtained, the vast majority of which were at the L3 and L4 stages. Animals were cultured at 15°C throughout.

For comparisons at 25°C, synchronous L1 larvae were cultured at 15°C until they reached the L4 stage and were then shifted to 25°C for a further 12 hours culture prior to loading on the 96-well plate for the reading on the plate reader.

Well scan settings

No. of flashes per scan point: 50

Scan mode: matrix scan

Scan matrix dimension: 5 × 5

Scan width [mm]: 5

Optic settings

No.	Optic module	Excitation	Emission	Gain
1	FI 390 520	390	520	1200
2	FI 460 520	460	520	1200

Optic settings

Focal height [mm]: 4,2

General settings

Bottom optic used

Settling time [s]: 0,2
bidirectional, vertical left to right, top to

Reading direction: bottom

Target temperature [°C]: monitoring

Table 2.9: Settings used by the plate reader for the detection of the redox state of the roGFP marker in nematodes

2.3.19 Scoring *C. elegans* adult lifespan

C. elegans were cultured to adulthood in asynchronous cultures. 50 young adult were picked from each strain, before producing any eggs, and were transferred for each strain to a new plate. The plate was then put to the appropriate temperature for culturing (15°C or 25°C). The number of alive animals was counted every 24 hours until the number of alive *C. elegans* reached zero.

2.3.20 Scoring *C. elegans* viability under oxidative stress

Oxidative stress was induced using Hydrogen peroxide (H₂O₂). M9/ H₂O₂-containing solution was prepared, with a final concentration H₂O₂ ranging from 0-1mM. For this protocol. 40µl of buffer was added to each well of a 96-well plate. 5-8 nematodes were transferred to each well and viability was scored hourly. For each sample, a total of 12 wells was used. For each condition the experiment was repeated three times (Possik & Pause 2015).

2.3.21 Quantifying GFP expression under oxidative stress

Oxidative stress was by preparing a hydrogen peroxide solution as described on 3.8.2. Larvae were synchronised as described on 2.3.6. Approximately 100 Synchronised L1 larvae were transferred to NGM plates seeded with OP50. They were cultured until they REACHED the L4/early adult stage. *C. elegans* were washed off the plate with M9 buffer into an Eppendorf tube. All samples were washed 3 times in M9 buffer. Each sample was made up in 100µl of M9 buffer + 1mM H₂O₂ and transferred to a 24-well plate. An equivalent negative control for each sample was include were nematodes would remain in M9 buffer without the addition of H₂O₂.

C. elegans were left in the solution for 1 hour. Worm from each well were transferred to an 15ml Eppendorf tube, washed twice with M9 buffer. Sodium azide was added at a final concentration of 10mM. 30µl of each sample were

placed on a microscope slide. A cover slip was placed on the sample and the nematodes were observed under the microscope as described on section 2.3.7.

2.3.22 RNAi of *C. elegans* by bacterial feeding method

Single colony of the HT115 bacteria expressing the vector with the desired gene was picked from the plates and a 10ml L-broth with 100 µg/ml Ampicillin was inoculated. Cultures were grown overnight at 37°C with shaking. L-agar plates containing 100 µg/ml Ampicillin and 12.5 µg/ml Tetracycline. Bacteria were grown overnight at 37°C (Ahringer 2006). The list of RNAi cosmid clones used is shown on table 2.10.

Cosmid name	Gene
F35H10.4	<i>vha-5</i>
F49C12.13	<i>vha-17</i>
R12A1.2	<i>snt-5</i>
F10C1.2	<i>ifb-1</i>
Y110A2AL.8	<i>ptc-3</i>
W08F4.6	<i>mlt-8</i>
C09H10.3	<i>nuo-1</i>
M03F4.2	<i>act-4</i>
F42C5.10	<i>ifo-1</i>
C07A9.2	BUD31 homolog
K10B2.1	<i>lin-23</i>
F27C1.8	<i>dpy-5</i>
C44C1.4	<i>vps-45</i>
	RNAi empty vector

Table 2.10: List of RNAi bacterial strains used in this study.

Cosmid code and the corresponding gene name are shown.

2.3.22.1 Agar plates for *C. elegans* feeding of RNAi expressing bacterial strains

Larvae were synchronised as described on section 2.3.6 Synchronised L1 animals were placed on NGM plates +Amp +IPTG with the desired RNAi expressing strain spread on the plate. Larvae were left to grow to the desired stage.

2.3.23 Western blots

2.3.23.1 Preparation of *C. elegans* whole animal lysates for detection of the roGFP ER3 protein

C. elegans whole animal lysates were prepared for SDS-PAGE (section 2.3.1) and immunoblot analysis (sections 2.3.3 and 2.3.4) as follows. Nematodes were synchronised to the L4 stage. 20 animals were picked per lysate. Nematodes were left on to crawl on an unseeded late to get rid of excess OP50 bacteria. The animals were then transferred to a 1.5ml Eppendorf tube with 500µl of 20mM NEM/0.1% Tween. Samples were pelleted by centrifugation in the bench top microfuge for 3 minutes at 200rpm. Supernatant was then removed leaving 20µl of the buffer. 20µl of Novex Tricine SDS Sample Buffer (2x) were added. Samples were frozen on dry ice and were then transferred to -80°C for 30 minutes if they are to be used on the same day or can be stored for up to two weeks. Samples were heated at 95°C directly from -80°C followed by incubation at room temperature for 5 minutes. Each sample was split into two 20µl samples, and b-mercaptoethanol was added to 5% to one of the two split samples as a reducing agent. All samples (with and without reducing agent) were further boiled for an extra 5 minutes before loading.

2.3.23.2 SDS-polyacrylamide gel electrophoresis

Proteins were resolved according to their electrophoretic mobility using discontinuous sodium dodecyl sulphate polyacrylamide gel electrophoresis (SDS-PAGE) as described previously (Laemmli, 1970). Novex 10%, 12 well, Tricine Protein Gels, of 1.0mm of thickness were transferred to a XCell SureLock Mini-Cell Electrophoresis unit and submerged in 1x Novex Tricine SDS running buffer. 15µl of the non-reducing samples and 10µl of the reducing samples were loaded, with one well left empty between the non-reduced and reduced samples during the loading. The gels were transferred to an XCell SureLock Mini-Cell Electrophoresis unit and submerged in 1x Novex Tricine SDS running buffer. Gels were run at 125V for 1 hour 45 minutes. BioRad all blue precision plus protein standard was routinely included in the analysis. Resolved proteins contained within the gel were subjected to immunoblot analysis (described in sections).

2.3.23.3 Western blot transfer

For antibody staining, proteins were transferred to nitrocellulose membrane (BioTrace™, pore size 0.2µm). Protein samples were resolved by SDS-PAGE as described on 2.3.20.2. The membrane gel and filter papers were soaked in SDS-PAGE transfer buffer (25 mM Tris-HCl, 192 mM glycine, 20% (v/v) methanol). Membrane and gel were sandwiched between 2 sheets of filter paper and 4 transfer sponges, soaked in transfer buffer then housed in BioRad mini Protean III trans-blot system transfer cassettes. The cassette was immersed in transfer buffer and transfer was achieved by applying 100V for 1 hour.

2.3.23.4 Immunological detection of proteins

Following transfer, nitrocellulose membranes were stained with Ponceau S solution (0.1% (w/v) Ponceau S, 5% (v/v) acetic acid) to assess transfer efficiency. Membranes were blocked for 45 minutes in either 5% made up in

PBST (85 mM NaCl, 1.7 mM KCl, 5 mM Na₂HPO₄, 0.9 mM KH₂PO₄, 0.1% (v/v) Tween-20). Primary antibody was diluted 1/1000 in 5% PBST and applied to membranes overnight at 4°C with rotation. Membranes were then washed three times for 10 minutes in PBST. The secondary antibody was applied for one hour at room temperature with rotation. Membranes were washed a further three times, twice in PBST and blots were visualised using infra-red imaging (LICOR). Secondary antibodies were labelled with infrared dye (LI-COR Biosciences Ltd). To minimise bleaching of the image signal when using the LICOR system secondary antibodies and subsequent wash steps were all completed under dark conditions.

2.3.24 Immunolocalisation of *C. elegans* proteins

C. elegans embryos, larvae or adults of similar developmental age were washed off a petri dish with an excess of M9 buffer and were collected in a 1.5ml Eppendorf tube. The animals were washed 5 times in M9 buffer and the once with RFB (Section 2.1) +2% formaldehyde. Finally, 1ml of RFB +2% formaldehyde was added in the tube. Tubes were placed to freeze in a dry-ice/ethanol bath. They were subsequently transferred to ice/ice water bath for 3.5 hours with an occasional inversion. After incubation in the ice bath, samples were washed once in TTB and were subsequently put in TTB +1% b-mercaptoethanol at 37°C with gentle agitation for 1 hour. Samples were washed once with B03 buffer. To pellet the nematode at this stage mild centrifugation was used (800rpm), followed by addition of B03 buffer/10mM DTT at 37°C with gentle agitation for 15 minutes. Samples were washed once again in B03 buffer and were then incubated in B03 buffer/0.3% (v/v) H₂O₂ at room temperature with gentle agitation for 15 minutes. Nematodes were washed again in B03 buffer and were spun down to pellet them, and were put in PBS-T with 0.02% sodium azide. At this stage, the samples could be stored overnight at 4°C or at -20°C for longer storage. Supernatant was removed and 100µl of PBS-T 1% milk was added, and animals were incubated for 1 hour at 4°C for blocking. Supernatant was removed and samples were incubated in PBS-T 1% milk plus the primary antibody for 4 hours at room temperature or overnight at 4°C. *C. elegans* were then washed three times, for 20 minutes at each wash, in PBS-T. The animals were incubated in 100µl of secondary antibody in

PBS-T 1% milk at 4°C overnight. Samples were washed once again three times in PBS-T. Supernatant as removed. 100µl of mounting solution (50% (v/v) glycerol in PBS) were added in the tube. 30µl of the solution were placed on a polylysine coated slide and an 18 mm x 18 mm coverslip was gently lowered over the sample with a scalpel blade to prevent the formation of air bubbles. Excess mounting solution was carefully removed from around the coverslip edge. Specimens were visualised using a Zeiss Axioskop 2 MOT microscope equipped with a HBO100 illuminator (Carl Zeiss, Germany). Images were captured and processed for presentation as described in section 2.3.7.

2.4 Graphs and statistical analysis

Calculations were performed using the Microsoft Excel 2016 software (Microsoft), Graphs and statistical analysis were done using the Graphpad Prism 7 software (Graphpad).

Chapter 3: Phenotypic characterisation and comparison of *vps-45* (*tm246*) and *unc-51* (*e369*) mutants and identification of a functional relationship between autophagy and the endosomal trafficking pathway in *C. elegans* molting.

3.1 Overview and aims

In this chapter, the main aim is to analyse the developmental phenotypes of the IA757 strain, genotype, *vps-45* (*tm246*), assess similarities and differences with the CB369 strain, genotype *unc-51* (*e369*), to identify and assess any functional overlaps between endosomal trafficking and autophagy. Phenotypic analysis of the mutant was performed using Normaski microscopy and immunolocalization of the DPY-7 cuticle collagen utilising the DPY7-5a monoclonal antibody (McMahon et al. 2003). The IA757 strain carries a deletion at the *vps-45* gene, of 1178bp in length extending from the promoter to the fourth exon and hence can be considered a null allele. Thus, animals homozygotic for the deletion are not able to produce a functional VPS-45 protein. The original paper describing the mutation, (Gengyo-Ando et al. 2007) shows defects in trafficking proteins during embryonic development. More specifically, in the IA757 strain oocytes have been shown to be unable to properly uptake yolk proteins as demonstrated by a vitellogenin::EGFP reporter. Furthermore, defective endocytosis was also observed in the pseudocoelom. Both phenotypes were only observed at the developmentally non-permissive temperature of 25°C, however it is not specified on whether the protein trafficking defects are persistent and to what degree in the permissive temperature of 15°C. Moreover, it was reported that the mutant demonstrates developmental defects when cultured at 25°C but was reported to develop relatively normally when grown at 15°C. Animals grown at the non-permissive temperature arrested their development at various stages, mostly though at the L1 stage. Additionally, they were often found encased in their old cuticle, suggesting defects during the ecdysis stage of moulting. Both phenotypes were absent from animals cultured at 15°C. Furthermore, animals showed an inverse correlation of body length with increasing temperature. Finally, an enlarged gut lumen was observed for the IA757 strain independent of the culturing temperature (Gengyo-Ando et al. 2007). Given that this is a deletion allele

and presumed genetic null, the reasons behind its temperature sensitive behaviour are not explained. Presumably for whatever reason, the key biological process to which functional VPS-45 protein contribute can work relatively effectively without VPS-45 at lower permissive temperatures but not at the higher and non-permissive one.

During moulting a substantial amount of protein is secreted which forms the new cuticle. The expression of the cuticular collagens is subject to spatial and temporal regulations. These genes are expressed in the hypodermis and only at specific developmental time points, once in the embryo prior to hatching and four more times at the end of each larval stage before the moult. As such the hypodermis goes through an oscillation of highly secretory and non-secretory phases in accordance to the expression of the cuticular genes [(Fränd et al. 2005), reviewed in (Johnstone 2000)]. During this highly secretory phase the seam cells of the hypodermis acquire a highly granular appearance. This granularity is a result of the accumulation of densely accumulated Golgi bodies, from which vesicles bud off and move to the cell surface where the components of the cuticle are deposited. These Golgi bodies are rapidly removed during lethargus and before the animals go through ecdysis (Singh & Sulston 1978). It is possible that endocytic pathway and autophagy play key roles in moulting, collagen biogenesis and maybe the mechanisms responsible for this rapid turnover of the Golgi bodies at the end of each moult. Development and autophagy in *C. elegans* have been linked in the past (Sato et al. 2014). However, autophagy has not previously been investigated in relation to the moulting process itself.

An example of how an autophagic defect can affect *C. elegans* development, involves the implication of the UNC-51 kinase. UNC-51 is part of the complex which initiates autophagy through the formation of the phagophore. *unc-51 (e369)* mutants which show reduced autophagy exhibits a dumpy body phenotype (dpy) and an uncoordinated movement phenotype (unc). The uncoordinated phenotype is a result of defective axon development (Ogura, Wicky, Magnenat, Tobler, Mori, Müller, et al. 1994) whereas the smaller size of the animals has been attributed to smaller cell size (Aladzcity et al. 2007). Despite that however, many *C. elegans* genes with a dpy mutant phenotype are known to encode components of the cuticle or enzymes associated with collagen/cuticle assembly (Johnstone, 2000; McMahon et al., 2003). Thus, based on this aspect of the *unc-51 (e369)* phenotype and the fact that a substantial number of the *unc-51* alleles also exhibit this phenotype (http://www.wormbase.org/species/c_elegans/gene/WBGene00006786#0c-9ga4-10), it is possible that cuticle synthesis and/or moulting is affected by the reduced levels of autophagy caused by the *unc-51 (e369)* mutation. Thus, although *unc-51* mutants

are able to moult, they do have the *dpy* phenotype associated with cuticle synthesis defects so it can be assumed that *unc-51* and by extension autophagy, is also involved in the moulting process.

Furthermore, since VPS-45 plays such an important role in the endocytic pathway by facilitating the accurate and appropriate fusion of vesicles with the membrane of appropriate target organelles, it is possible that loss of VPS-45 function might result in an excess of aberrant vesicles/organelles which are the result of inaccurate and inappropriate membrane fusion events. Hence, in order for the cell to survive under such conditions, it might require the aid of autophagy for the degradation of these aberrant structures. Furthermore, in the case of highly secretory cells, such as the seam cells and the hypodermis, the loss of VPS-45 could apply an extra burden to these cells if vesicle targeting was less accurate than when VPS-45 function is present in the wild type, and as a result produced aberrant structures that need to be degraded through autophagy.

It can therefore be hypothesized, that the *vps-45 C. elegans* mutant might have a greater requirement for autophagy than the wild type in order to survive, with autophagy being required to recycle aberrant vesicles and secretory components which were miss-targeted as a result of defective vesicle fusion. Finally, Tlg2 which is the binding partner of Vps45 and is stabilized by an interaction with VPS45 as shown in yeast (Bryant & James 2001). Tlg2 has been previously shown to regulate autophagy (Abeliovich et al. 1999; Ohashi & Munro 2010; Nair et al. 2011) thus potentially also implicating *vps-45* in the regulation of autophagy, via the stabilisation of Tgl2. As a result, it is interesting to assess if any similarities between the phenotypes exhibited by the two mutants exist and to test for genetic interactions such as synthetic lethality. Additionally, it is possible that any identification of previously unknown moulting defects in the *unc-51 (e369)* mutant that would be similar to the *vps-45* mutant could indicate a functional relationship between the two genes and processes.

As such this study, along with the IA757 strain, the CB369 strain which carries the *unc-51 (e369)* mutations and has reduced levels of autophagy, was studied. Each of the strains was observed to identify any delays in the completion of the moult and/or the life cycle compared to the wild type strain.

Furthermore, a double mutant was constructed to further investigate the possible involvement of the two processes in the development of the nematode. Phenotypic characterisation of the double mutant could help assess the type and levels of genetic

interaction between the two genes and as such provide additional information regarding their role in the larval and embryonic development of the animal.

3.2 The *vps-45 (tm246)* endosomal trafficking mutant at 25°C exhibiting defects in moulting.

Animals homozygotic for the *vps-45 (tm246)* allele (IA757), were cultured at the non-permissive temperature of 25°C in order to replicate the previously described moulting defects. When *C. elegans* were grown at the non-permissive temperature (25°C), many demonstrated cuticular defects thought to be associated with moulting defects. Larvae often got stuck in the cuticle (Figure 3.1 A-C). It appears that animals have a problem completing the moult, and more specifically during the ecdysis process as they are often found encased in the old cuticle. In the occasion where larvae were able to complete the moult a subset of nematodes was found to have parts of the old cuticle still attached to its body, around the head restricting part of the pharynx, suggesting an incomplete ecdysis (Figure 3.1 D,E). These phenotypes are consistent with other moulting defects observed in *C. elegans*, for example those associated with growth under low cholesterol conditions; an exogenous source of cholesterol is a requirement for the moult and proper development in *C. elegans* (Yochem et al. 1999; Hieb & Rothstein 1968; Kuervers et al. 2003; Frand et al. 2005).

3.3 The *vps-45 (tm246)* and *unc-51 (e369)* mutant strains exhibit embryonic lethality during development

As previously discussed (Section 3.1) the *vps-45 (tm246)* mutant (IA757), shows defective protein trafficking of yolk components by the oocytes. In cultures for the *vps-45 (tm246)* strain unhatched eggs were often encountered. It can be speculated that such a defect could potentially result in defects during embryonic development and potentially embryonic lethality. Furthermore, *unc-51 (e369)* mutant (CB369) has been previously shown to produce dead embryos (Erdélyi et al. 2011). In this case, I was interested in investigating the embryonic lethality of the *vps-45 (tm246)* mutant, as well as compare it to that of *unc-51 (e369)* in a temperature dependent manner.

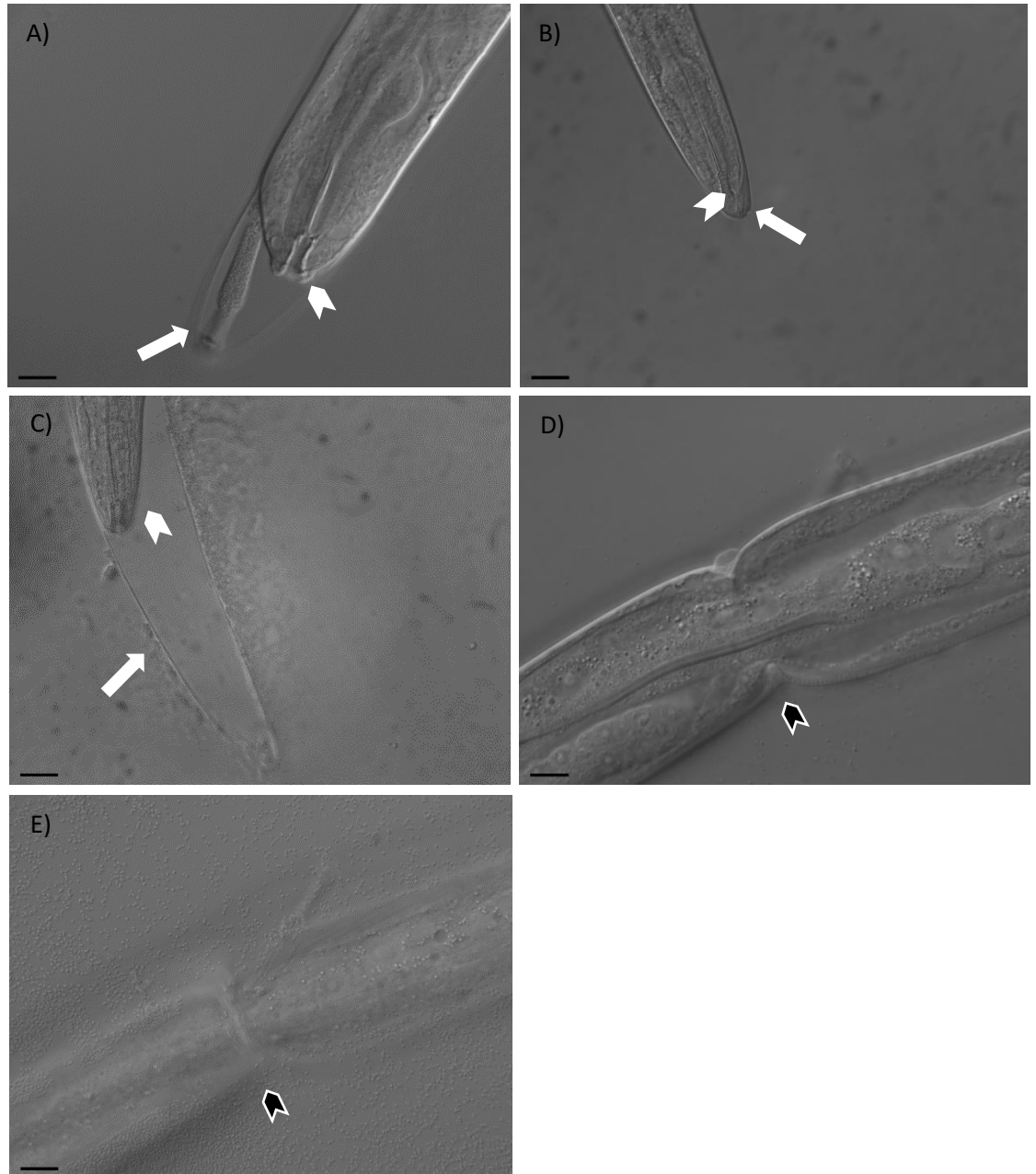


Figure 3.1: DIC microscopy, moult arrest of IA757 animals when cultured at 25°C.

A-C) IA757 animals at various stages stuck in the old cuticle (arrows), with the head of the animal slightly retracted (white arrowheads). **D-E)** Different focal points of moulted animals with old cuticle restricting its body post moult (black arrowheads). Scale bars represent 5 μm .

As such, the embryonic lethality for each of the mutants was scored, in both the permissive (15°C) and non-permissive temperatures (25°C) for the *vps-45 (tm246)* moulting death phenotype. The *vps-45 (tm246)* mutant exhibited higher embryonic lethality than both wild type and *unc-51 (e369)* mutant at 15°C. However, a substantial number of the wild type N2 embryos also died at this temperature and this frequency was similar to the frequency observed for the *unc-51 (e369)* mutant. As mentioned above the embryonic lethality for the *unc-51 (e369)* animals has been previously reported however the culturing temperature was not reported (Erdélyi et al. 2011). Certainly, here we found no difference between the rates of embryonic death at 15°C between the wild type N2 and *unc-51* mutant strain and hence conclude that the loss of *unc-51* function at this temperature does not contribute to a higher frequency of embryonic lethality than in the wild type.

The average embryonic lethality of the *vps-45 (tm246)* mutant was almost triple (30.5%) of that shown by the wild type and *unc-51(e369)* mutants (9.7% and 10.7% respectively) (Figure 3.2 A). Additionally, it should be noted that lower embryonic lethality was observed for the wild type and *unc-51(e369)* mutant when they were cultured at 25°C. This suggest that the lower temperature of 15°C is not an optimal temperature for *C. elegans* embryonic development. The *vps-45 (tm246)* mutant on the other hand maintained the same levels of embryonic lethality in both temperatures. More specifically the wild type strain only showed an average embryonic death of only 2.05% and the *vps-45* and *unc-51* mutants exhibited an embryonic death of 30% and 6.7% respectively (Figure 3.2 B). This suggest that along with the moulting death the *vps-45* mutant at the non-permissive temperature exhibits problems during its embryonic development as well. In contrast to the moulting death phenotype however, this lethality extends to the permissive temperature of 15°C. Additionally, *unc-51 (e369)* also showed higher embryonic lethality than the wild type at 25°C however not to the same extent as the *vps-45 (tm246)* strain.

3.4 The autophagy defective *unc-51 (e369)* mutant strain does not die by moulting when cultured at 25°C

The *vps-45 (tm246)* and *unc-51 (e369)* mutants were tested for arrest during the molt and subsequently death at 25°C. Embryos from each of the strains were acquired by subjecting worms to standard bleach treatment and harvesting the eggs in S-Basal to produce synchronous L1 larvae (Chapter 2, section 2.3.6). 50-60 synchronous L1 larvae for each

strain were seeded on NGM plates and were left to grow over a period of 120 hours at 25°C. Three plates were prepared for each strain. For the wild type strain 98.33% of the animals survived on average. Similarly, the *unc-51* exhibited an average survival of 98.5% after 5 days of development for L1 arrest. By contrast, for the *vps-45* mutants, only 14.17% of the original inoculate was still alive (Figure 3.3). In all cases, the larvae had developed to the adult stage.

Thus, under the condition used the *unc-51* mutants did not display larval lethality or any lethality attributable to moulting defects with survival indistinguishable from wild type. Thus, while loss of VPS-45 function which reduces the fidelity of vesicle trafficking and causes defects in endosomal recycling results in lethality associated with moulting in *C. elegans* at elevated culture temperatures (25°C), impairment of autophagy caused by the *unc-51* (369) allele does not.

3.5 The *unc-51(e369)* V; *vps-45(tm246)* X double homozygotic mutant exhibits a synthetic effect

Although the *unc-51(e369)* mutation does not mimic the moulting defect caused by the *vps-45* (*tm246*) null allele, the possibility of a genetic interaction between these two genes was further investigated by construction of the double mutant carrying both mutant alleles. For the cross, initially 10 wild type males were crossed with a single homozygotic *unc-51* (*e369*) hermaphrodite (CB369). The *unc-51(e369)* allele is recessive to wild type and hence outcrossed F1 males are phenotypically wild type. A successful cross was assessed by the ratio of male/hermaphrodite worms in the progeny, (if the ratio was close to 50% the cross was considered successful) as well as the phenotype of the progeny. After a successful cross, outcrossed progeny were heterozygotic for the *unc-51(e369)* allele which is recessive to wild type, and hence easily identified. From this F1 generation, 20 males were isolated and transferred to a plate with a single *vps-45* (*tm246*) homozygotic hermaphrodite (IA757) for mating. The resulting progeny of this cross produced two genotypes *unc-51(e369)/+ V*; *vps-45(tm246)/+ X* and *+/+ V*; *vps-45(tm246)/+ X*.

For construction of the double homozygote it is the former of these two genotypes that was required. Hence virgin F2 hermaphrodites were selected and were clonally transferred to fresh NGM petri dishes and were left to produce progeny for 24 hours before being removed from the plates.

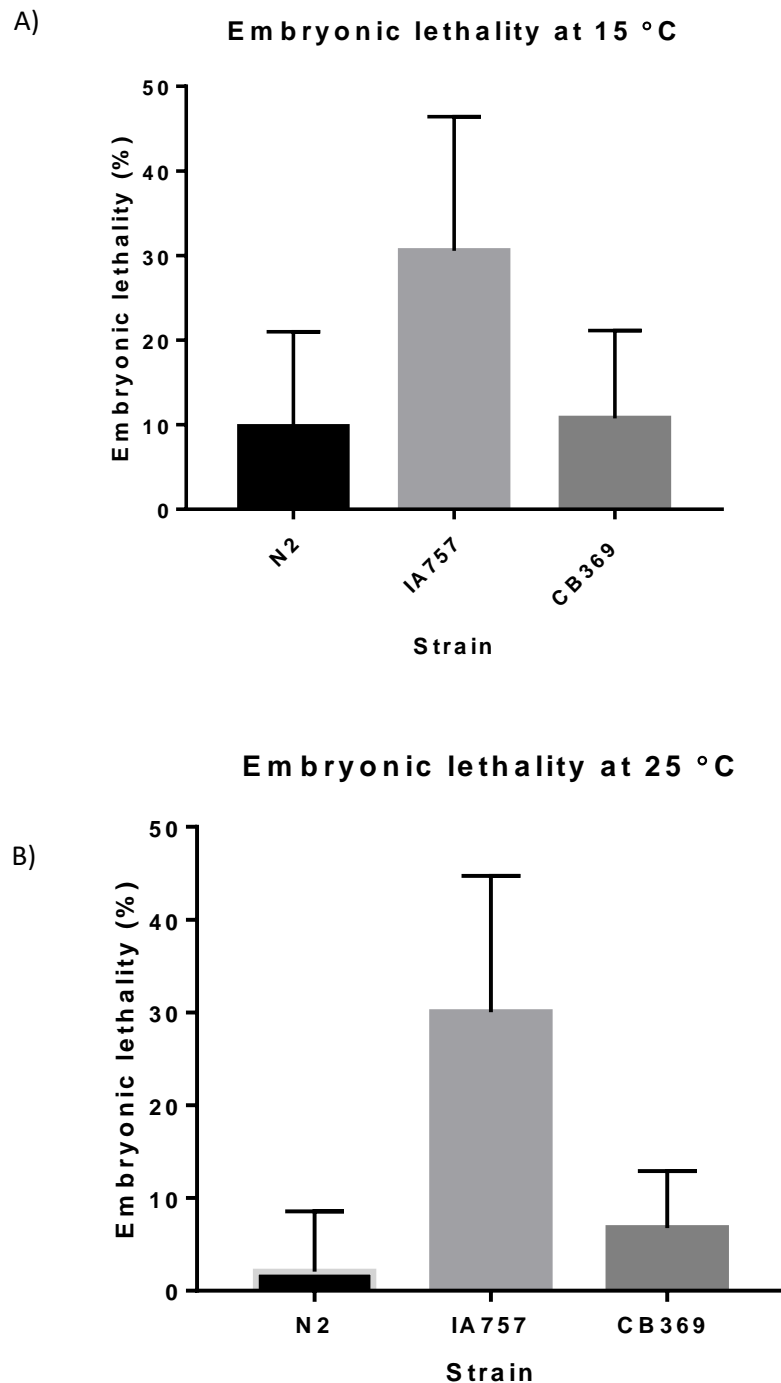


Figure 3.2: Progeny of young adult *C. elegans* which were hatched 48h hours after egg laying as a percentage of total number of eggs laid. A) Average embryonic lethality (\pm SD) of the progeny of single animals cultured at 15°C. N2 (n=10), IA757 (n=11), CB369 (n= 10). Tukey's multiple comparisons test. N2 vs. IA757, $p = 0.0030$. N2 vs. CB369, $p = 0.9834$. IA757 vs. CB369, $p = 0.0047$. B) Average embryonic lethality (\pm SD) of *C. elegans* cultured at 25°C. N2 (n=10), IA757 (n= 10), CB369 (n= 11). Tukey's multiple comparisons test. N2 vs. IA757, $p < 0.0001$. N2 vs. CB369, $p = 0.5255$. IA757 vs. CB369, $p < 0.0001$.

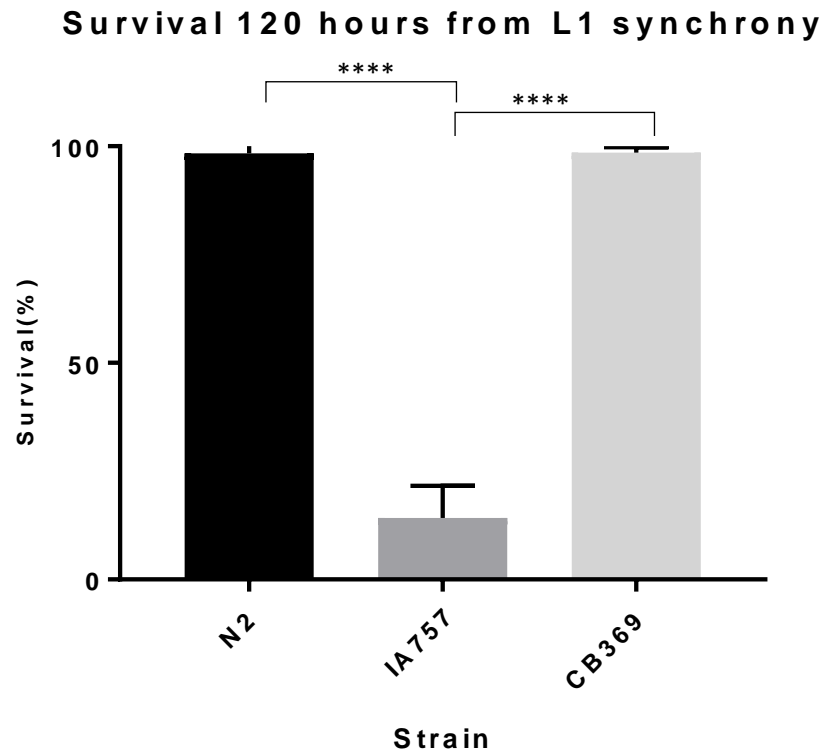


Figure 3.3: Assessment of the molting death of the *vps-45 (tm246)* mutant at 25°C.

Plates inoculated with 50-60 L1 larvae for each strain. Alive *C. elegans* were scored after 120 hours of development. Experiments were done in triplicates for each of the N2, IA757 and CB369 strains. Average survival (%) \pm SD is shown. Tukey's multiple comparison test: N2 vs IA757 $p < 0.0001$. IA757 vs CB369 $p < 0.001$.

The F3 broods of these cloned F2 parents were scored for the segregation of homozygotes for *unc-51(e369)* as indicated by ~25% with the unc phenotype. This identified broods derived from F2 parents of the required double heterozygotic genotype *unc-51(e369)/+ V; vps-45(tm246)/+ X*.

Unc F3 progeny were cloned to fresh NGM plates and left to lay eggs. At this stage, these F3 *unc-51(e369)* animals are a mix of 25% +/+, 50% *vps-45(tm246)/+* and 25% *vps-45(tm246)/vps-45(tm246)* on chromosome X. After egg laying, the F3 Unc parents were removed and the resulting progeny was left to develop at the permissive temperature (15°C) in order to avoid losing any homozygotic *vps-45(tm246)* animals. At this stage F4 animals which exhibited a new phenotype (different from either parental strain), namely Unc and very much smaller dumpy body compared to the parental CB369 strain, were identified in a proportion of the cultures.

At 15°C (the permissive temperature for the *vps-45* moulting death), the newly isolated mutant animals exhibited a very severe dumpy phenotype with a smaller overall body size compared to the *unc-51 (e369)* mutant and a wrinkled cuticle near the head (Figure 3.5). However, the rest of the cuticular structures, such as alae and the annular furrows appeared to be forming normally (Figure 3.5). The double mutants also exhibited an uncoordinated phenotype which appeared to be more severe to that observed in *unc-51 (e369)* animals. The homozygotic double mutant was much less mobile than the *unc-51 (e369)* mutant, since after several days of culturing each position on the petri dish was mostly unchanged as observed by the trail left on the bacterial lawn.

It was considered most likely that this new phenotype was the *unc-51(e369) V; vps-45(tm246) X* double mutant. However, on first attempt it was impossible to generate a brood from these animals as they died before reproducing. To confirm the genotype very small unc animals were picked for single worm PCR to verify that they carried both *unc-51 (e369)* and *vps-45 (tm246)* alleles in a homozygotic state (Figure 3.4). Animals which exhibited a normal size unc phenotype were also subjected to single worm PCR to identify how the heterozygotic state of the *vps-45 (tm246)* allele could potentially be affecting the phenotype of the animals in an *unc-51 (e369)* homozygotic background.

The DNA from these animals was initially amplified for the detection of the *unc-51 (e369)* allele. Animals carrying the mutant *unc-51* allele produced a 381bp amplified fragment on the gels after digestion with PvuII (section 2.3.15.4) whereas the wild type animals produced two bands of 330bp and 51bp (Figure 3.4A). As demonstrated on Figure 3.4A, all samples (1-3) produced a single 381bp band after amplification verifying that the animals were homozygotic for the *unc-51 (e369)* allele, as already expected due to the Unc phenotype. The same samples were then tested via PCR for the *vps-45 (tm246)* allele. DNA from wild type animals produced a 629bp band whereas for *vps-45* mutants animals produced a 480bp band (Figure 3.4B).

Animals which were heterozygotic for the *vps-45 (tm246)* allele produced both bands (Figure 3.4B). Of the three previously identified *unc-51 (369)* homozygotic samples, sample 1, which exhibited a phenotype similar to the parental *unc-51 (e369)* mutant was heterozygotic for the *vps-45 (tm246)* allele whereas samples 2,3, which exhibited the very small Dpy body and Unc phenotype, were homozygotic (Figure 3.4B). As a result, sample 1 had the *unc-51(e369)/unc-51 (e369) V; vps-45(tm246)/+* X and samples 2 and 3 had the *unc-51 (e369) V; vps-45(tm246) X* genotype. The former can normally reach adulthood and develop to a phenotype indistinguishable from the *unc-51 (e369)* mutant, suggesting that a single copy of the mutant *vps-45 (tm246)* allele does not affect body size of the *unc-*

51 (e369) mutant. These same animals, routinely produced ~ 25% of the *unc-51(e369)* V; *vps-45(tm246)* X double mutant (Section 3.6) and were given the strain name IA900. A pool of IA900 animals was isolated from the F3 generation produced from the original cross to maintain production the double mutant. The genotype of that mutant was verified by PCR for both genes as previously and by phenotype for the *unc-51 (e369)* allele, since it exhibited the dumpy body and the uncoordinated phenotypes.

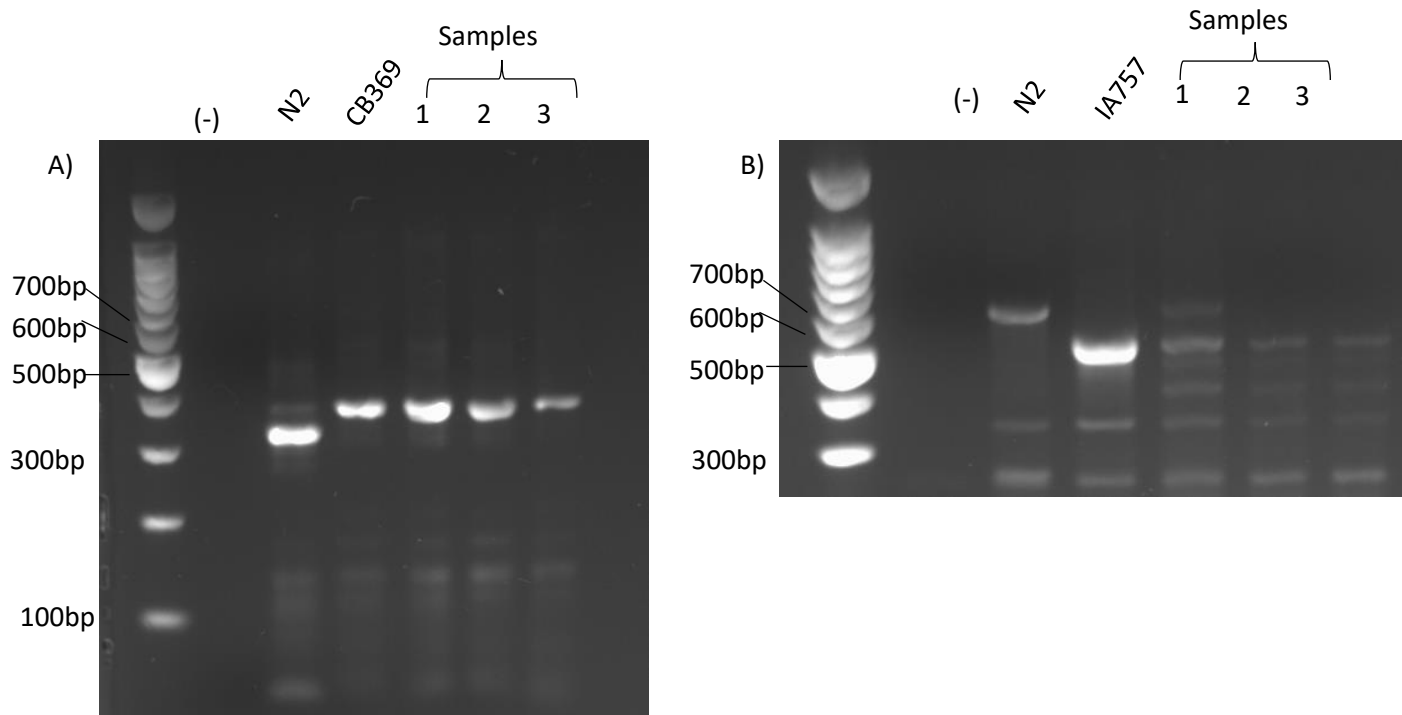


Figure 3.4: PCR samples run on 2% agarose gels for the detection of *unc-51 (369)* and *vps-45 (tm246)* alleles.

A) Detection of the *unc-51 (e369)* allele. PCR samples were digested with the restriction enzyme PvuII. Wild type fragments (N2) 51,330bp, CB369 fragments, 381bp. **B)** Detection of the *vps-45(tm246)* allele. Wild type band (N2) 629bp, IA757 band. 480bp. Samples 1,2,3 in both gels respond to the same animal lysates for each allele. Sample 1 is homozygotic for the *unc-51 (e369)* allele, and heterozygotic for the *vps-45 (tm246)* allele. Samples 2,3 are homozygotic for both the *unc-51 (e369)* and *vps-45 (tm246)* allele.

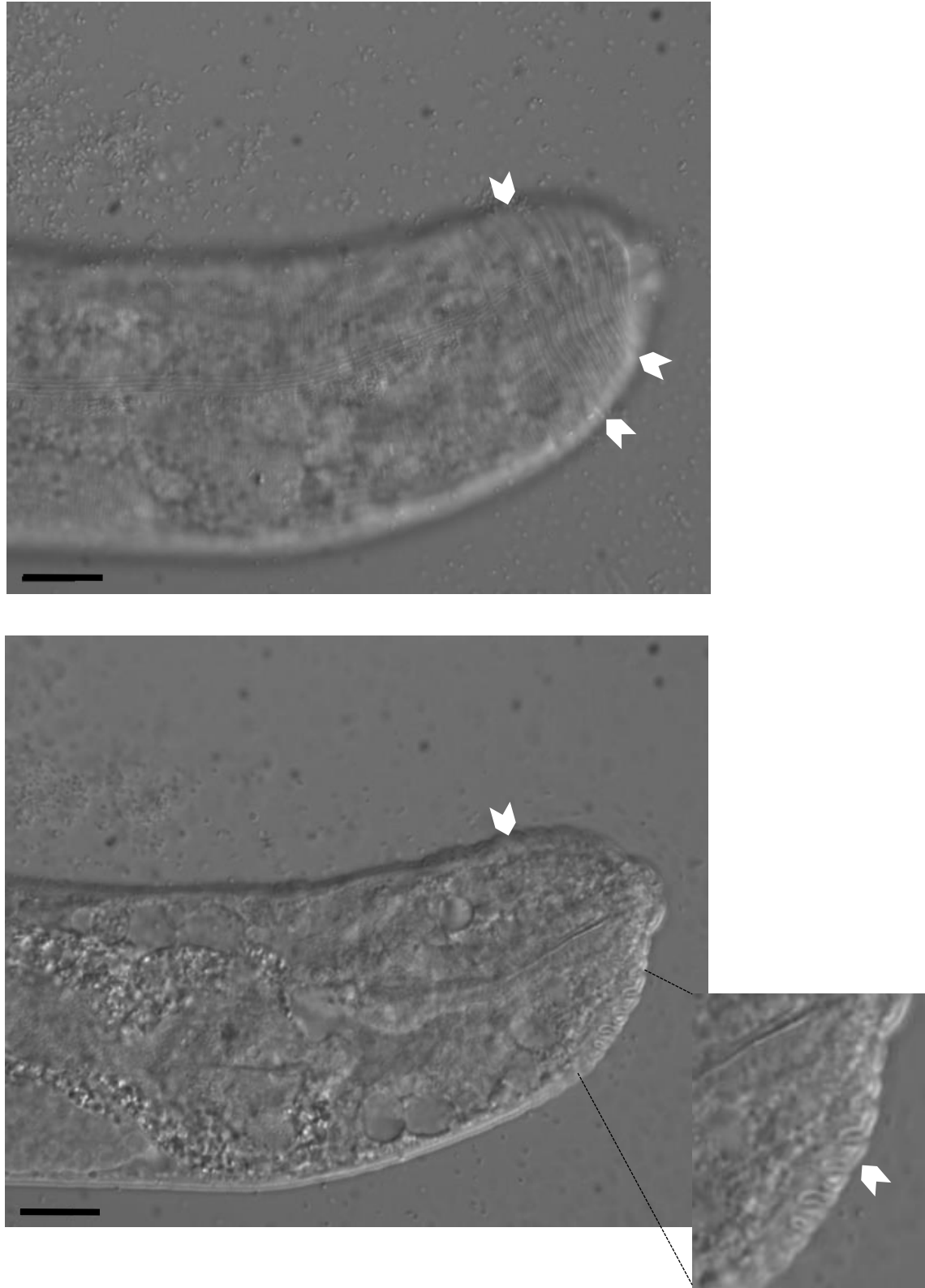


Figure 3.5: Cuticular defects of the *vps-45 (tm246) unc-51(e369)* double homozygous hermaphrodite. Different focal point of head from adult hermaphrodite. Arrow heads point to the wrinkles on its cuticle. Scale bars represent 100 μ m

3.6 Genetic analysis of the *unc-51(e369) vps-45(tm246)* double homozygotic mutant

The percentage segregation of the double mutant and its Mendelian pattern of inheritance was tested. The IA900 animals were no different from the *unc-51* mutant in terms of body size and movement when observed from a stereo- dissecting microscope. A single IA900 parent verified for its genotype by PCR was left to egg lay. Every 24 hours the eggs were clonally transferred to new NGM plates and were left to develop. Developing larvae were scored on whether they showed the dumpy body and uncoordinated movement phenotypes of the *unc-51* mutant or the completely paralyzed very small body phenotype of the *unc-51(e369) vps-45(tm246)* double mutant.

Commonly, IA900 progeny were identified that arrested in early larval developmental stages and then died (Figure 3.6). The early larval death was observed at 60% of the double homozygotic progeny (Table 3.2). The stage of the larvae was verified by observing the shape of the developing germ lines. This phenotype of early larval death had not been previously observed for either of the two single mutants cultured at 15°C. Moreover, these animals took longer to develop than the rest of the progeny of the parental strain. As such these were also classified as double mutants. Eggs that did not hatch were accounted for in each case. The progeny of the animals which did not have the double mutant phenotype was also scored and were classified as heterozygotic for the *vps-45 (tm246)* allele, and hence same as the IA900 strain or homozygotic for the wild type *vps-45*, therefore being the same as the CB369 strain based on their own progeny (Figure 3.6, Table 3.2). The progeny of all IA900 adults observed is summarised on Table 3.1. Overall the double mutants account for approximately 27% of the total progeny consistent with the expected Mendelian frequency of segregation. Additionally, the average embryonic lethality from an IA900 adult was 13.12% at 15°C (Table 3.1), a small but overall insignificant increase compared to the individual embryonic lethality previously exhibited by each of the individual mutants (section 3.2).

This would suggest there is no additive effect from each of the individual mutations, *unc-51 (e369)* and *vps-45 (tm246)*, regarding embryonic lethality. As a result, it was considered that the same frequency of embryonic death should exist in the progeny of IA900 mutant for any of the allelic combinations of the *unc-51 (e369)* and *vps-45 (tm246)* mutant alleles. As a result, only the alive progeny was analysed to assess at what percentage the double mutants segregate in the progeny.

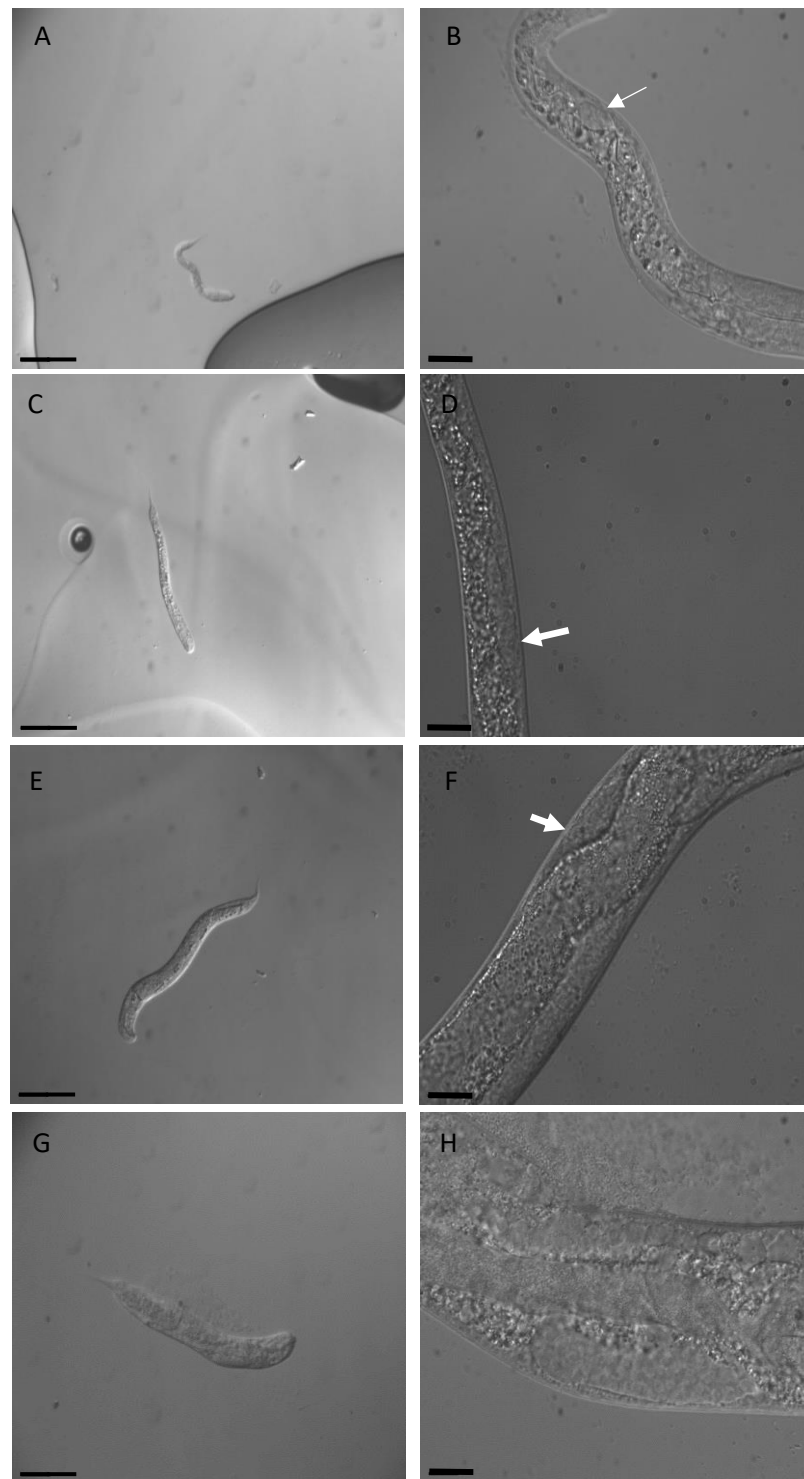


Figure 3.6: DIC microscopy of *unc-51 V; (e369) vps-45 (tm246) X* double homozygotic animals at various larval stages.

10x (A, C, E, G), and 63x (B, D, F, H) lenses. Scale bars represent 100 μ m and 10 μ m in each case respectively. A-F) Animals died by larval arrest at various stages white arrows point at the germline of each animal. G-H) Adult hermaphrodite, with an underdeveloped germline for its age (white arrow).

By Mendelian rules of segregation, 25% of the progeny would have an *unc-51 (e369)* genotype with uncoordinated and dumpy phenotype, 50% would have an *unc-51 (e369)* homozygotic *vps-45 (tm246)* heterozygotic genotype (IA900) with a Dpy and Unc (DpyUnc) phenotype and 25% would have the *unc-51 (e369) V; vps-45 (tm246) X* genotype with a very severe Dpy and Unc phenotype with a very small body size. Therefore a 3:1 ratio of the very small dumpy and severe uncoordinated double mutant phenotypes would be expected. A χ^2 test showed that the observed values are significantly different from the expected values of the Mendelian model of segregation with a p value of 0.1 (Table 3.1).

Progeny classification of IA900 parent	Parent 1	Parent 2	Parent 3	Parent 4	Parent 5	Parent 6	Total observed	Expected values
DpyUnc animals	8	9	6	8	6	8	45	48.75
Double mutant	4	5	3	3	2	3	20	16.25
Dead embryos	2	1	2	2	1	2	10	-
Total progeny	14	15	11	13	9	13	75	-
Total progeny excluding dead embryos	12	14	9	11	8	11	65	65
							Average Dead embryos	
Dead embryos (%)	14.28571429	6.666666667	18.18181818	15.38461538	11.11111111	15.38461538	13.5024235	

Table 3.1: Table of progeny from five IA900 parents.

Genotype of the parents was deduced from their progeny. Progeny was classified as DpyUnc animals, based on phenotype resembling the *unc-51 (e369)* mutant including both CB369 and IA900 animals. Double mutant for the *vps-45 (tm246) unc-51 (e369)* homozygote based on dead larvae, severe dumpy adults and dead embryos for the unhatched eggs. The observed and expected total values based on mendelian segregation are shown, excluding the dead embryos class. $\chi^2 = 1.153846154$, suggesting no great deviation of the observed values from the expected ones at $p=0.1$ and $df=1$. Percentage of dead embryos for each individual progeny is shown along with the average percentage.

Double mutant progeny classification	Original Parent	F1 Parent 1	F1 Parent 2	F1 Parent 3	F1 Parent 4	F1 Parent 5	Total
Arrested dead larvae	2	2	4	1	1	2	12
Double mutant adult	1	2	1	2	2	0	8
Total	3	4	5	3	3	2	20
Lethality (%)	66.66666667	50	80	33.33333333	33.33333333	100	60

Table 3.2: Table of showing the number of double mutant progeny dying during larval development.

Animals exhibiting the double mutant phenotype were classified according to their ability to reach adulthood (Double mutant adult) or die during larval development (Double mutant larvae).

3.7 Size comparison of the *vps-45 (tm246)*, *unc-51 (e369)* and *unc-51 (e369) V; vps-45 (tm246) X double mutant*

The *unc-51 (369) vps-45 (tm246)* was measured for the length of its body and was compared to the individual single mutants that produced it. The double mutant had a much smaller body size when compared to the single homozygotic mutants from which it originated as well as the wild type. For the wild type and the single mutant 10 adult hermaphrodites were measured. For the double mutant, due to the difficulty in acquiring viable adults only two animals were measured. Only a small number of the double mutant was observed with DIC microscopy and pictures could be acquired. Only a small number of the double mutant animals could survive and develop to adulthood and from those a substantial number ruptured while handling the nematodes with the platinum wire pick or after addition of S-basal buffer on the slides potentially suggesting defective cuticle structure. Most animals (~60%) in the case of the double mutant were found dead in earlier stages of development (Table 3.2). Adult wild type *C. elegans* cultured at 15°C has an average length of 1211µm. The *vps-45 (tm246)* and *unc-51 (e369)* animals have an average length of 1048µm and 819µm respectively. By contrast, the *unc-51 (369) vps-45 (tm246)* double mutant had a size of 330µm (Figure 3.6). Going over the data one can argue, that a more than additive effect is present in the double mutant in regard to the length of the animals.

More specifically the *vps-45 (tm246)* mutant has an average size of 1048µm, which is ~86.5% of the wild type length (1211 µm). The *unc-51 (e369)* mutant has an average length of 819 µm which corresponds to 67.6% of the original length. If the two genes had an additive effect towards the length of the double mutant, then the animals would have a size of 58.5% of the wild type length (67.6% of 86.5%). As a result, the expected length of these mutants would be 708.5 µm. However, the observed size of the *unc-51 (e369) V; vps-45 (tm246) X double mutant* is 330 µm which translates to approximately 27.2% of the wild type length (Figure 3.7). That is almost twice as severe as the expected phenotype, suggesting a more than additive effect with respect to body length. However, as most animals of this genotype died during larval development and most adults ruptured during transfer to slides, the actual phenotype of the double mutant is much more severe than this size of two intact adults suggests. Also, it proved impossible to breed from this genotype, so the true genetic interaction is one of synthetic lethality.

The interaction between the two gene can be classified as negative epistasis, the extreme case of which would be synthetic lethality. This aggravating interaction suggest that the two genes are operating in different pathways but also exhibit some compensating function, possibly in the post embryonic development of the animals (St Onge et al. 2007).

3.8 Phenotypic analysis of internal and cuticular structures of *vps-45 (tm246)*, *unc-51 (e369)* and *unc-51 (e369) V; vps-45 (tm246) X* mutants

To further identify differences between the double and the single mutants in terms of both the cuticle structure as well as the internal organs Nomarski microscopy was employed. The three strains wild type (N2), *vps-45 (tm246)* mutant (IA757) and *unc-51 (e369)* mutant (CB369) all showed normal development of the buccal cavity, whereas the *unc-51(e369) V; vps-45 (tm246) X* double mutant shows a collapsed pattern of the buccal cavity structure, which appears to be, which appears to be due to the shorter body size of the animals (Figure 3.8). The animals could feed and pharyngeal pumping was observed along with shuttle movement of the mouth. However, the animal did not exhibit any other movement beyond that.

Additionally, closer observation of the intestine showed that *vps-45 (tm246)* and *unc-51 (e369)* both have an enlarged intestinal lumen compared to the wild type strain. The enlarged lumen could be a result of incomplete digestion due to defective secretion of digestive enzymes or due to other structural problems with the intestinal cells, like enlarged cells. As a result, it is no surprise that, in the case of the double mutant an enhanced phenotype is observed severe as the intestinal lumen seems to be enlarged along with high amounts of undigested bacteria inside (Figure 3.9).

Structures of the cuticle where more closely observed in order to identify any defects on the surface of the cuticle that would indicate problematic formation of the structure in *vps-45 (tm246)* and *unc-51 (e369)* and the double mutant. In all cases the adult alae were observed and it was demonstrated that they can normally form despite defects in protein trafficking, autophagy or both. In the case of the double mutant the annular furrows are easily visible on the cuticle suggesting that in general even the double mutant exhibits normal major structural features of the cuticle when it is able to survive the early larval death, as observed by light microscopy (Figure 3.10).

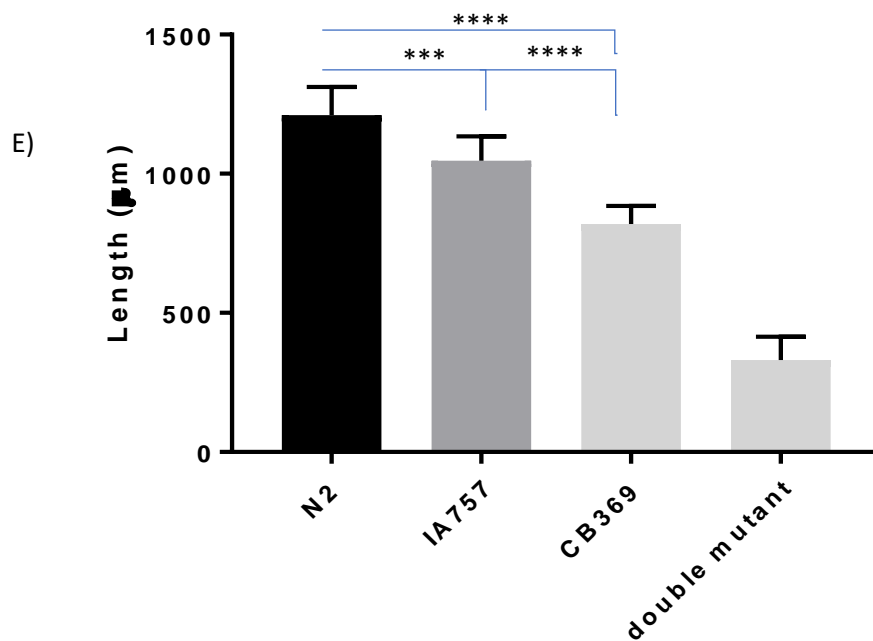
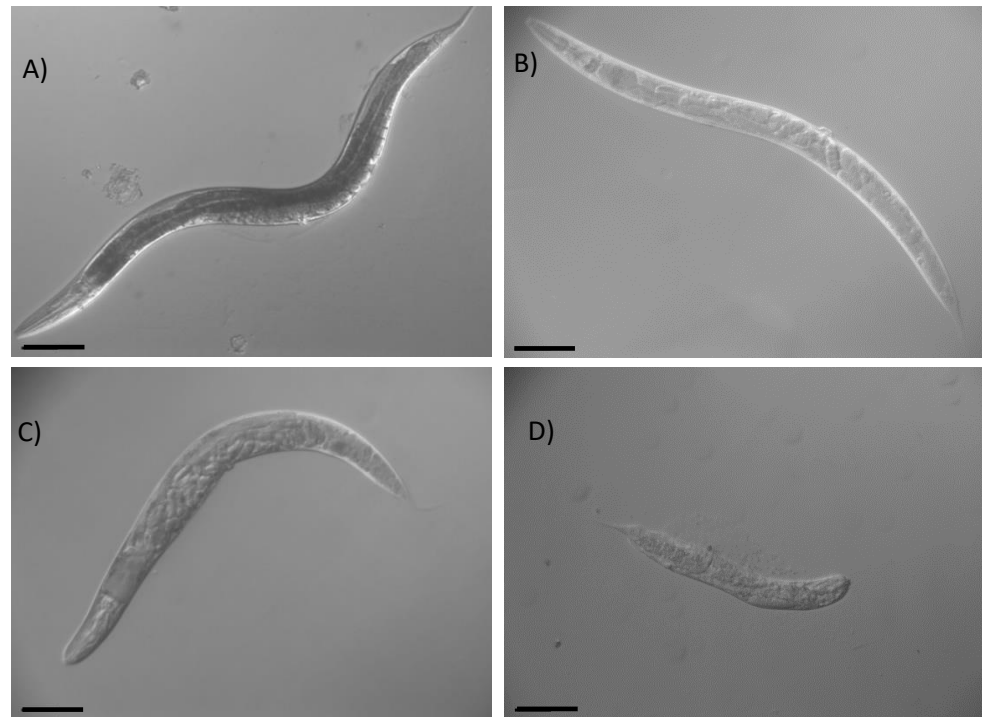


Figure 3.7: Length comparison of wild type, IA757, CB369 and *unc-51 (e369) V; vps-45 (tm246) X* double mutant.

A-D) DIC images of adult N2, IA757, CB369 and the synthetic double mutant *vps-45 (tm246) unc-51 (e369)*. Scale bars represent 100µm. E) Average length (+SD) of each strain at the adult stage when cultured at 15°C. N2 (n=10), IA757 (n=11), CB369 (n=11), double mutant (n=2). Tukey's multiple comparisons test: N2 vs IA757, $p=0.0004$. N2 vs CB369 $P<0.0001$. IA757 vs CB369 $p<0.001$.

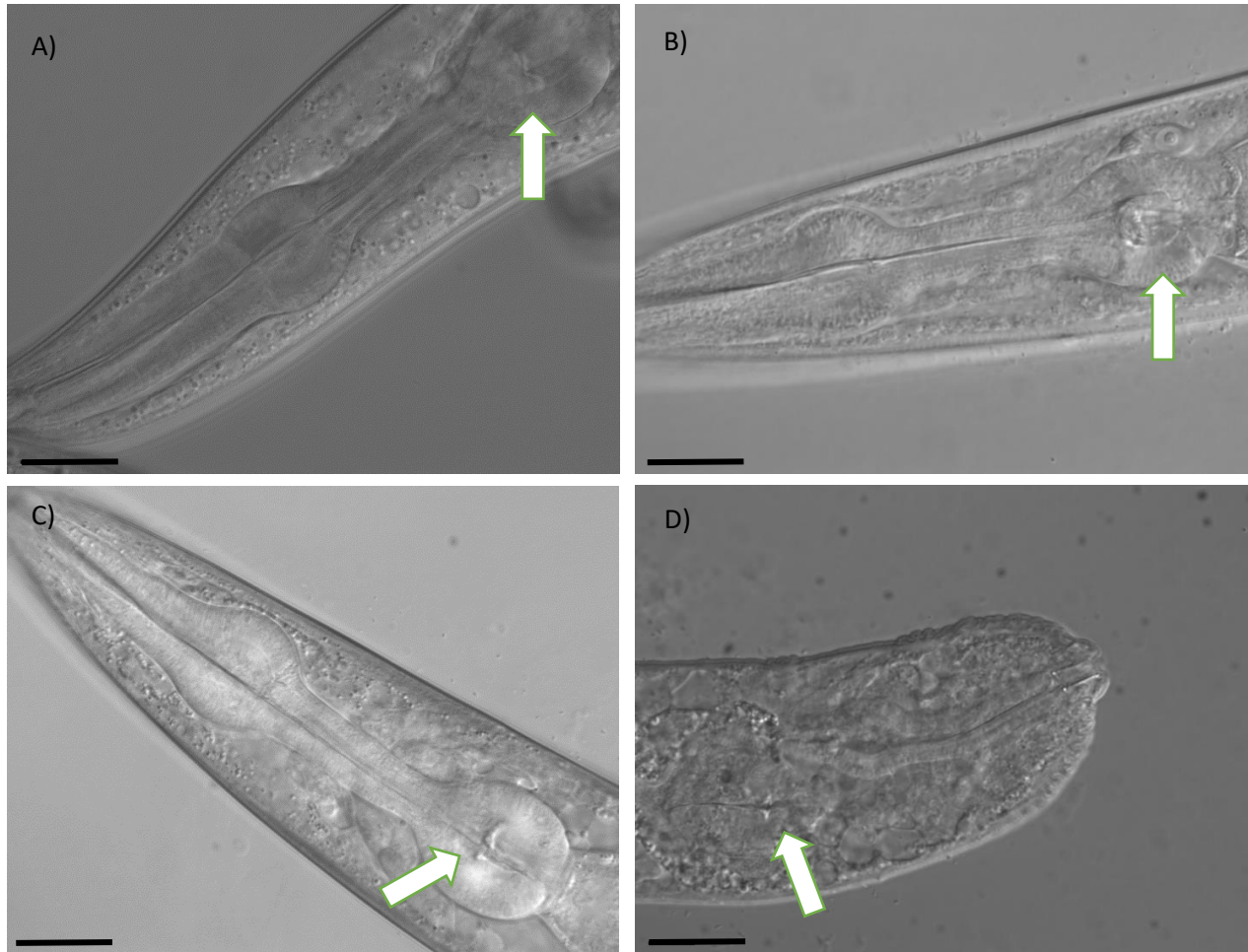


Figure 3.8: DIC microscopy, of the pharynx of adults cultured at 15°C.

A) N2 B) IA757 C) CB369 D) *vps-45 (tm246) unc-51(e369)* double mutant. White arrows point to the pharyngeal bulb. It is severely mislocalised in the *vps-45 (tm246) unc-51(e369)* double mutant. Scale bar represent 100µm

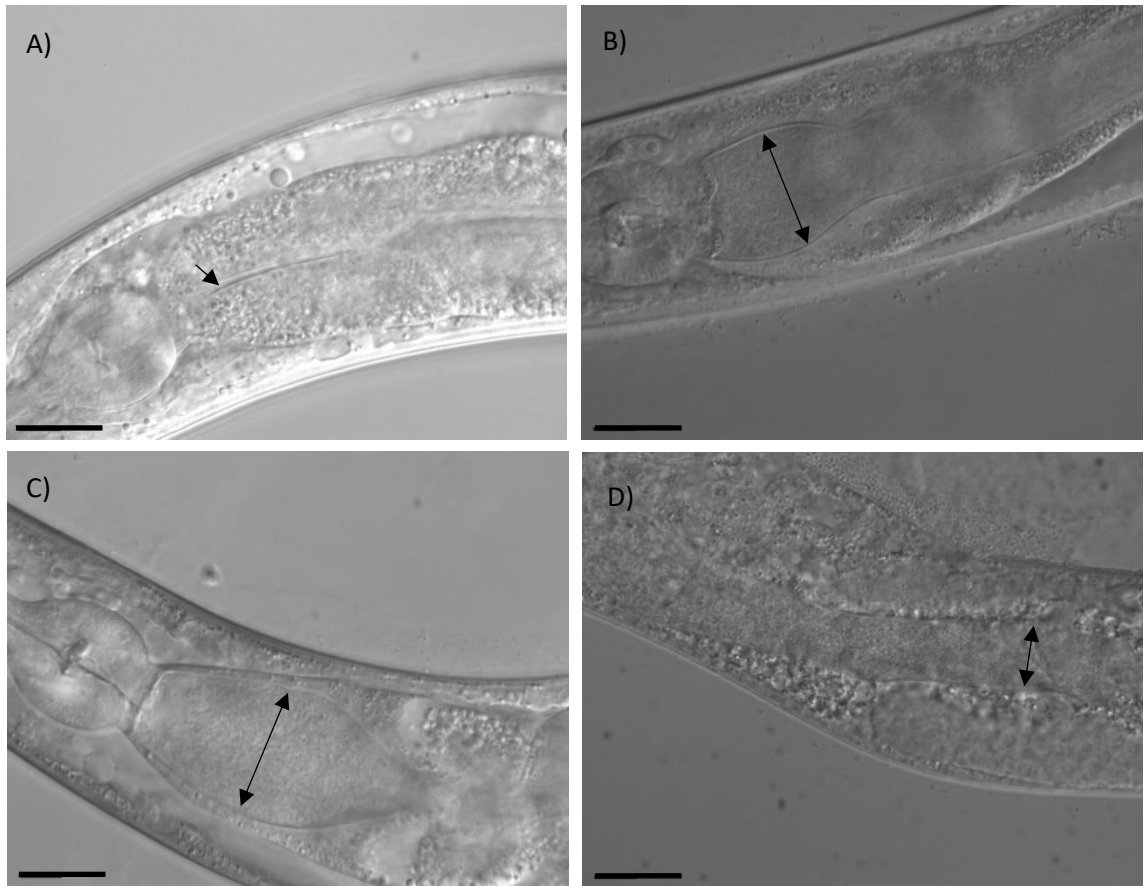


Figure 3.9: DIC microscopy, of intestine of adult animals cultured at 15°C.

Double headed arrows show borders of the intestinal lumen. A) N2- normal development of the intestine.

B) IA757- enlarged intestinal lumen. C) CB369- enlarged intestinal lumen D) *unc-51(e369) vps-45(tm246)*

double mutant, collapsed intestinal lumen.

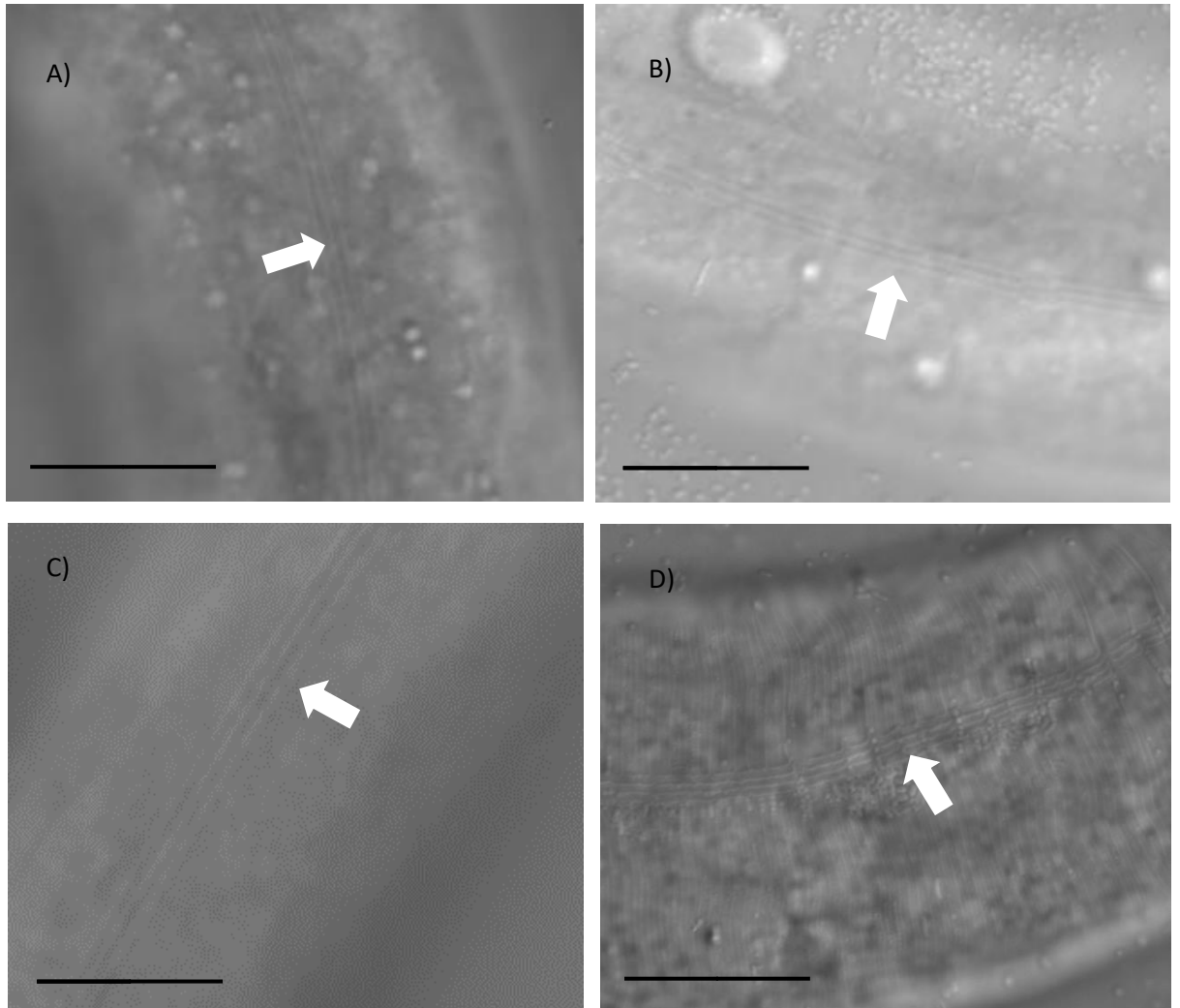


Figure 3.10: DIC microscopy, of adult cuticular alae (white arrows).

C. elegans were cultured at 15°C. Normal pattern of the alae for all strains. A) N2 B) IA757 C) CB369 D) *unc-51(e369) vps-45(tm246)*. Scale bars represent 10µm.

Immunolocalisation was employed in order to better visualise the annular furrows during normal development as well as during the moulting death of the *vps-45 (tm246)* mutant. The cuticular component which was stained was the DPY-7 collagen, since the antibodies were readily available in our lab. DPY-7 is one of the cuticular collagens and it localizes in the annuli. An anti-DPY-7 primary antibody was used which can bind to the cuticular collagen DPY-7. The DPY-7 protein is detected within the cuticle in circumferential bands or stripes which are continuous except over the lateral sides of the animal when the alae are present. These stripes correspond to the evenly spaced indentations or furrows that define the annuli of the cuticle. A IgG conjugated fluorophore secondary antibody was used to visualise the structures under UV light. In all cases when the strains were cultured at the permissive temperature (15°C) (Figure 3.11) the furrows were normally formed as part of the cuticle. No antibody staining could be performed for the *unc-51 (e369) V; vps-45 (tm246) X* double mutant due to the low number of animals being produced at each generation from the IA900 strain however the annular furrows were previously visualised with DIC microscopy and appear to be forming normally (Figure 3.5).

For the *vps-45 (tm246)* mutant strain the staining was repeated at the non-permissive temperature (25°C), to identify any potential defects in the formation of the cuticle during the moulting arrest. After treatment with the antibodies, animals which were unable to complete the moult and were encased in their cuticle or showed other cuticular defects, such as incomplete cuticle shedding were identified and observed (Figure 3.12). It appears that the moulting death is not a result of a defective cuticular structure as it appears to have properly formed annular furrows similar to the wild type. The new cuticle appeared to be forming in a normal way underneath the old one, with the new annular furrows mirroring the structure of the old ones. This potentially suggest that both *vps-45* and *unc-51* are not explicitly necessary for the cuticle to be deposited and structured properly and are required for the shedding and completion of the moulting process. Thus, the *vps-45 (tm246)* temperature sensitive death is most likely a result of problems caused during the later stages of the moult, namely the ecdysis, after the deposition and formation the new cuticle has been completed.

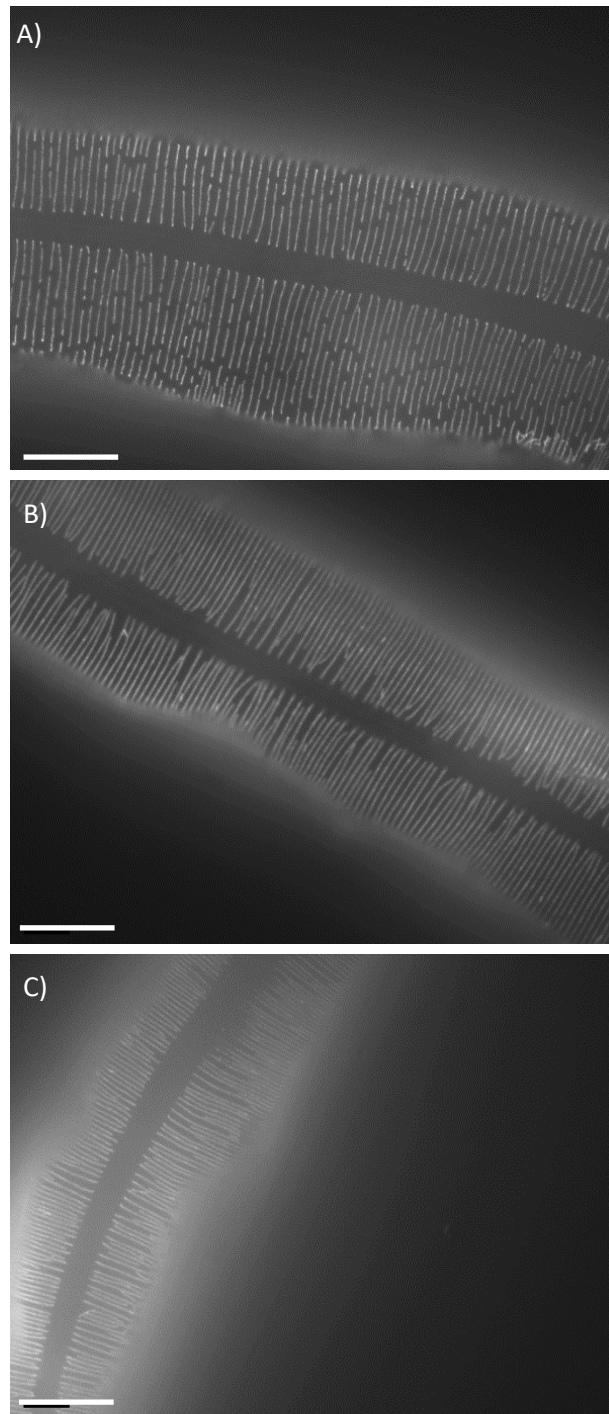


Figure 3.11: Immunolocalisation of *C. elegans* DPY-7 cuticular collagen.

Mouse monoclonal primary antibody, Alexa Fluor 488 Fluorophore conjugated whole IgG from goat 1:200 secondary antibody. 63x magnification. No difference between strains in the pattern of the annular furrows. A) N2 ,B) IA757, C) CB369 respectively.

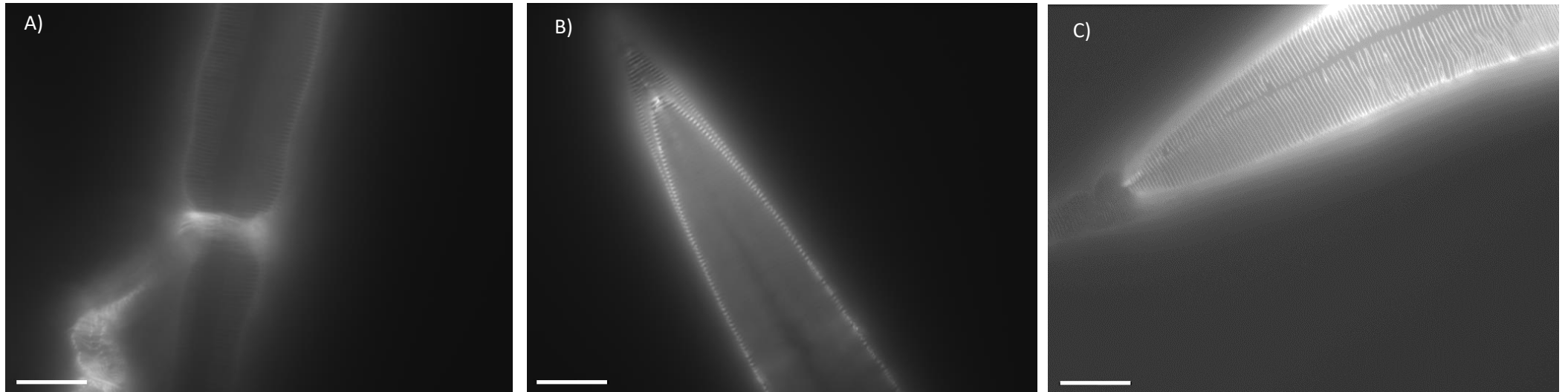


Figure 3.12: Immunolocalisation of DPY-7 cuticular collagen, in *vps-45 (tm246)* mutants during moulting arrest when cultured at 25°C. Alexa Fluor 488 Fluorophore conjugated whole IgG from goat 1:200 secondary antibody. 63x Magnification. A) Old cuticle partially shed, parts of it constricting the worm body. B,C) Larvae encased in the old cuticle at the end of the moult. Both the old and new cuticle annular furrows are visible.

3.9 Characterisation of the moult and intermoult periods on *vps-45 (tm246)* and *unc-51 (e369)* mutants

To further investigate this idea of defective exit of the mutant animals from the moult as a cause of death for the *vps-45 (tm246)* mutant (IA757), L1 larvae were observed throughout the duration of their moult to the L2 stage along with the *unc-51 (e369)* mutant (CB369) and wild type (N2) strains for comparison. Moulting for the wild type strain at 15°C started at 22 hours from seeding the plates with L1 arrested animals. At this point the number of larvae on each plate that were in lethargus was counted for each of the strains.

Characteristic trait for the lethargic state was the lack of movement and more importantly the stopping of the pharyngeal pumping (Singh & Sulston 1978). The stopping of the pharyngeal pumping was proven very useful in the case of the *unc-51 (e369)* mutant which exhibited an uncoordinated movement phenotype which made it difficult to assess whether larvae were in a lethargic state (lack of movement) or not. The experiment was repeated three times. Data showed that both the *vps-45 (tm246)* and *unc-51 (e369)* mutants had a delayed entry into the moult of roughly 2 hours when compared to the wild type. The first lethargic animals for these two strains were observed 1-2 hours later than the wild type strain (Figure 3.14A). The *vps-45 (tm246)* population appeared to remain in the lethargic state for longer than the wild type in general and required approximately 11-12 hours to exit the moulting state completely compared to approximately 10 hours for the wild type strain. Additionally, it appears that on average the same number of animals were in lethargus at the same time at the peak of the moult, (Figure 3.13 A) at approximately 60% of the total population for both *vps-45 (tm246)* and wild type animals. Thus, suggesting that the *vps-45 (tm246)* mutant requires longer to complete the moult. The *unc-51 (e369)* mutant population generally required longer than wild type to exit the moult. However, with a much smaller number of larvae being in a lethargic state at the peak of the moult (40%). Consequently, individual animals were most likely not taking longer to moult as was the case with the *vps-45 (tm246)* mutant, but different larvae were starting the moulting process at different time points (Figure 3.13 A).

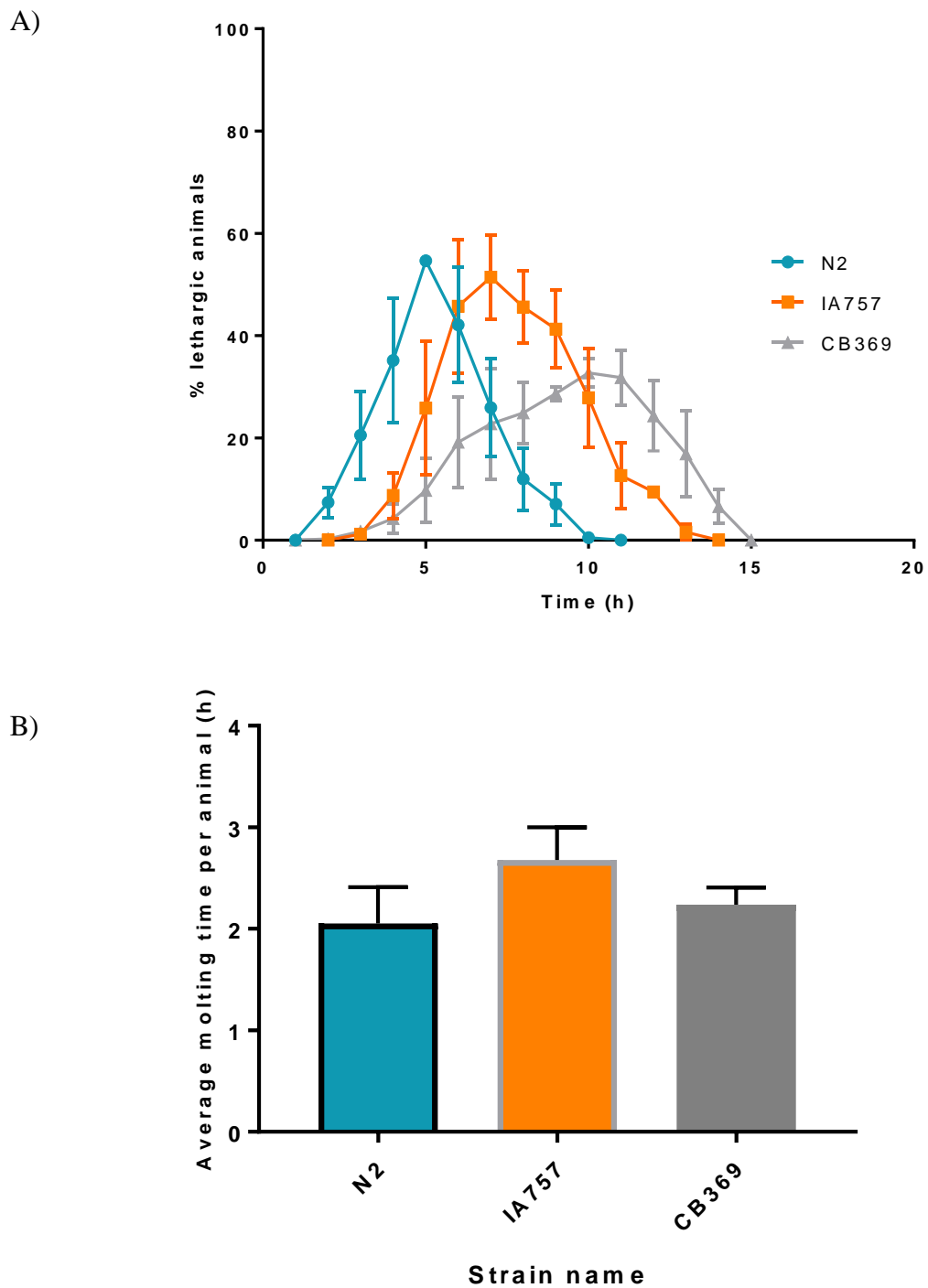


Figure 3.13: Molting profiles of N2, IA757, CB369 strains during the L1-L2 moult at 15°C. A)

Percentage of moulting animals at hourly intervals (\pm SD) for the duration of the moult. Average of three

experiments for each strain. **B)** Average time required for each strain go through the moult as the product of

the calculation of the average area under the curve (\pm SD) for each moulting graphs obtained from the

triplicate experiments of each strain tested. Tukey's multiple comparisons test. N2 vs. IA757, $p=0.0901$.

N2 vs. CB369, $p=0.7311$. IA757 vs. CB369, $p=0.2407$.

Both the *vps-45 (tm246)* and *unc-51 (e369)* populations start moulting later compared to wild type (1 hour later), and take longer to complete the moult, at 14 hours and 15 hours respectively when compared to 10 hours of the wild type strain (Figure 3.14). Additionally, the synchrony of the animals moulting was expressed as a measure of the breadth of the curve and the height of its peak. If synchrony through the moult was perfect, the population would move from 0% lethargic to 100% lethargic instantaneously and stay at that state until the end of the moult at which point it would reach 0% again in perfect synchrony. Such a perfectly synchronous population would produce a rectangular graph. A high and narrow peak indicates a better synchrony (though still imperfect) whereas a low and broader peak indicates a less synchronised moulting population. Therefore, the area under the curve can act as product which expresses the measure of the total time taken by the population (or average for each animal) to get through lethargus. If the area under the curve is greater in one case than another, then in that case the animals should be taking longer to go through the moult. The area under the curve was measured for each of the individual experiments for each of the strains (Appendix 1) and the average area was plotted for each (Figure 3.13B). Despite no significant differences the data once again suggest that *vps-45 (tm246)* does stay in lethargus longer (2.67 hours) than the wild type and *unc-51 (e369)*, both of which seem to require approximately the same amount of time to go through the moult (2.05 and 2.24 hours respectively) (Figure 3.13B).

To verify this, individual animals were observed under the microscope from their entry into lethargus (stop of movement and pharyngeal pumping) until the moment they exit lethargus (onset of movement and the start of ecdysis). Results demonstrated that wild type and *unc-51 (e369)* animals require approximately 6 hours to complete the moult whereas *vps-45 (tm246)* animals requires approximately 8 hours to go through the same process (Figure 3.14).

Since the differences in moulting between all three strains were established a new question arose regarding how the animals behave in the intermoult periods. Observing through these periods was difficult due to the variability between each of the strains compared to the wild type strain, and especially for *unc-51 (e369)* mutants which exhibits severe asynchrony at later larval stages. However, the behaviour of each of the strains during the intermoult stages could be inferred by how fast each of the animals can reach adulthood from L1 arrest, as well as how synchronous or asynchronous animals are when they reach that stage.

It has been previously shown that wild type *C. elegans* requires approximately 60 hours to reach adulthood from hatch at 16°C, 44 hours at 20°C and 30 hours at 25°C. A similar inverse correlation between time and temperature is also observed for the intermolt periods (Byerly et al. 1976). As a result, in agreement to this all the mutants in this study required longer to reach the adult stage at the lower temperature of 15°C.

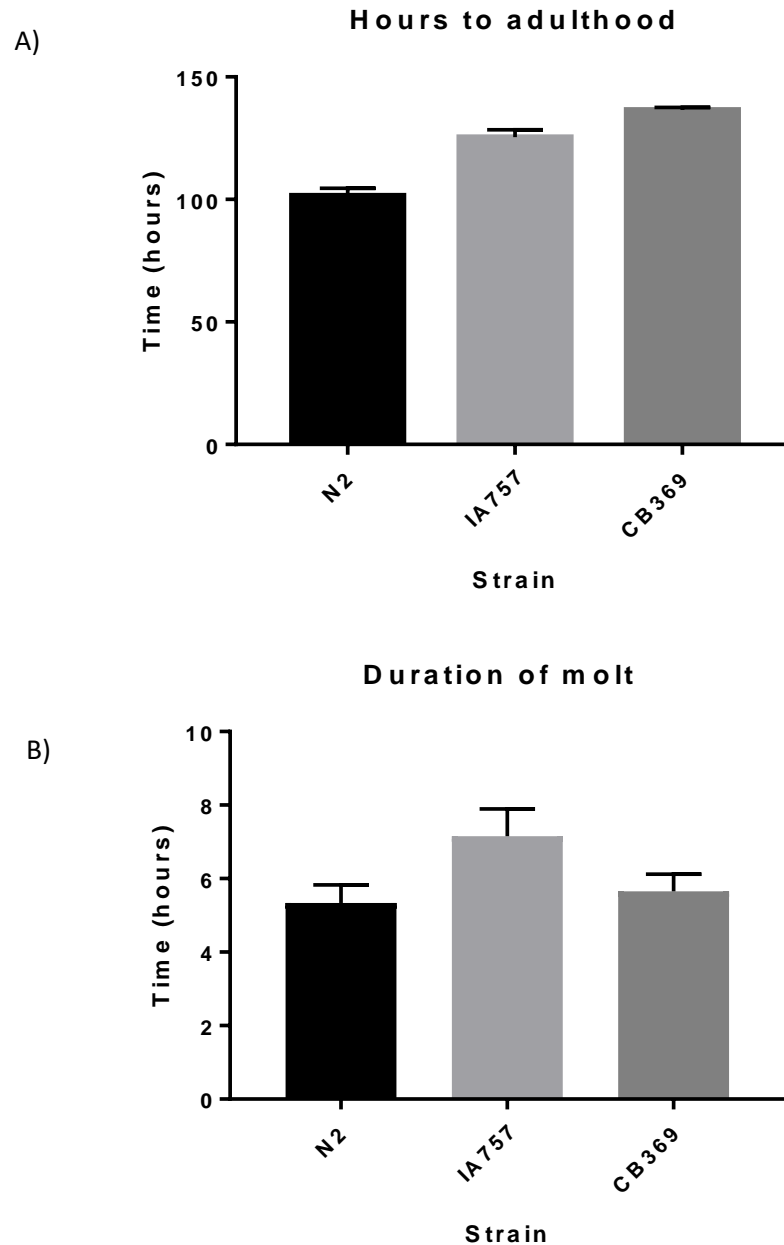


Figure 3.14 Duration of molt and development time to adulthood for N2, IA757 and CB369 strains.

A) Average development time (\pm SD) for >50% the population to reach adult stage for N2 (n=5), IA757 (n=4), CB369 (n=4) *C. elegans* when cultured at 15°C. Tukey's multiple comparison test N2 vs IA757, $P < 0.0001$. N2 vs CB369, $P < 0.0001$. IA757 vs CB369, $P = 0.002$. **B)** Average time (\pm SD) for the completion of molt at the L1-L2 when cultured at 15°C, N2 (n=12), IA757 (n=10), CB369 (n=10). Tukey's multiple comparison test N2 vs IA757, $P < 0.0001$. N2 vs CB369, $P = 0.4188$. IA757 vs CB369, $P < 0.0001$.

The wild type, could reach the adult stage after approximately 100 hours of development when cultured at 15°C whereas *vps-45 (tm246)* and *unc-51 (e369)* mutants require 125 and 136 hours respectively to reach the same developmental stage in 50% of their total population. The condition of 50% of the animals to have reached the adult stage was introduced due to the asynchrony observed for the *unc-51 (e369)* mutant. The developmental stage for all larvae was scored for all strains after 72 hours of development from L1 arrest. While the wild type strain had already reached the L4 stage by that time, the *vps-45 (tm246)* strain was one stage behind at the L3 stage. On the other hand, for the *unc-51* mutant a mixed population was obtained. Most the animals, were at the L2 stage (65%) and the rest at the L3 (20%) and at the L4 stage (15%) (Figure 3.15, Appendix 3).

The above data collectively present some interesting conclusions. Firstly, *vps-45* mutants appear to remain in lethargus for longer than the wild type strain, potentially due to a delayed exit from the moult. It can be speculated that this delayed exit from the moult is what causes the moulting death at the non-permissive temperature. The loss of a functional VPS-45 could potentially result in ineffective and less accurate vesicle targeting than in the wild type, resulting in the requirement for autophagy for the removal of these aberrant membranes. As previously described (section 3.1) autophagy is possibly also required for the removal of the membranes forming the Golgi bodies in the hypodermis during the moult. As such it is possible that the increased requirement of autophagy for the clearance of the extra material originating from defective endosomal fusions, causes a delayed removal of these Golgi bodies in the *vps-45(tm246)* mutant background hence resulting in the delayed exit from the moult. In this case, the population in general remains in synchrony (Figure 3.15). Furthermore, under the assumption that each moult stage take the same amount of time throughout *C. elegans* development, as it is demonstrated by the temporal expression of moulting related genes during the moult (Johnstone & Barry 1996), it is easy to infer that in the case of the *vps-45* mutant the intermoult period also last longer than wild type. These animals require 2 extra hours to proceed through each moult, which means that they require 8 extra hours to go through all moulting stages and reach the adult stage at 108 hours. However, it does so at 126 hours, requiring an extra 18 hours which are most likely a result of prolonged intermoult periods. On the other hand, the *unc-51 (e369)* mutant although it can complete the moult in the same amount of time as the wild type strain, it exhibits asynchrony at the onset of the moult after larvae where synchronised and

a similar effect was observed in later developmental stages. Along with the asynchrony a great delay in development was observed when compared to the wild type strain. The above could suggest that the *vps-45 (tm246)* undergoes a lengthier moulting process and has longer intermoult periods whereas the *unc-51 (e369)* mutant, potentially only exhibits the prolonged intermoult period phenotypes, taking longer to enter the next moult after it has recovered from the previous one. Furthermore, the asynchrony suggests variable entry into the next moult. This can potentially be attributed to the very limited capacity of the *unc-51* mutant to initiate and carry out autophagy.

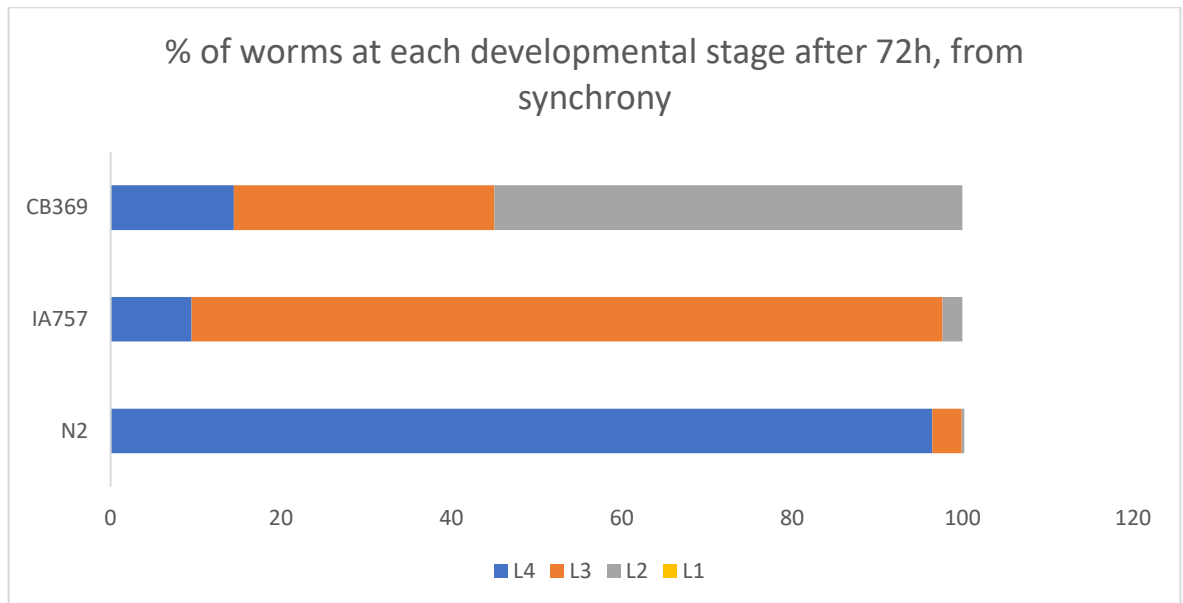


Figure 3.15: Developmental stage of N2, IA757, CB369 animals in cultures after 72h of development, from L1 arrest at 15°C.

IA757 and CB369 appear to be at the L3 and L4 stage for the majority of the population. N2 strain is at the L4 stage. IA757 and CB369 lose synchrony during development. Average of three experiments for each strain.

3.10 Determination of lifespan for *vps-45 (tm246)* and *unc-51 (e369)* mutants

This difference in the moulting entry as well as the duration of the moult for *vps-45 (tm246)* and *unc-51 (e369)* mutants raised the question about how the two mutants compare after they have completed all larval moults and reached adulthood. As a result, their lifespan was compared. Young adult *C. elegans* for each strains were transferred to NGM plates and

were cultured at the permissive and non-permissive temperatures. At 15°C the wild type population exhibited a median survival of 17 and reached 100% lethality on day 36. The *vps-45* and the *unc-51* mutants exhibited a median survival of 6 and 5 days respectively. Both had no more surviving animals after 17 days. The adult lifespan of the *unc-51(e369) V; vps-45 (tm246) X* double mutant was not assessed due to the limited number of animals available.

At 25°C the wild type had a much reduced lifespan compared to 15°C, which agrees with previously published data suggesting that a colder environment increases *C. elegans* longevity (Zhang et al. 2015). In the case of the wild type the median survival was 6 days and no animals were alive after 13 days. Both of the mutants tested followed this pattern of having a longer lifespan at the lower temperature (Figure 3.16). The *vps-45 (tm246)* mutant had a reduced lifespan compared to both other strains, as opposed to the data described above where the *unc-51 (e369)* and *vps-45 (tm246)* had a similar lifespan. The *vps-45* mutant had a median survival of 3 days and no more animals were alive after 7 days. The *unc-51* mutant had a median survival of 5 days and had no more surviving animals after 11 days. This suggests that *vps-45 (tm246)* animals exhibit defects in the non-permissive temperature extend beyond the molt and larval development defects (Figure 3.16).

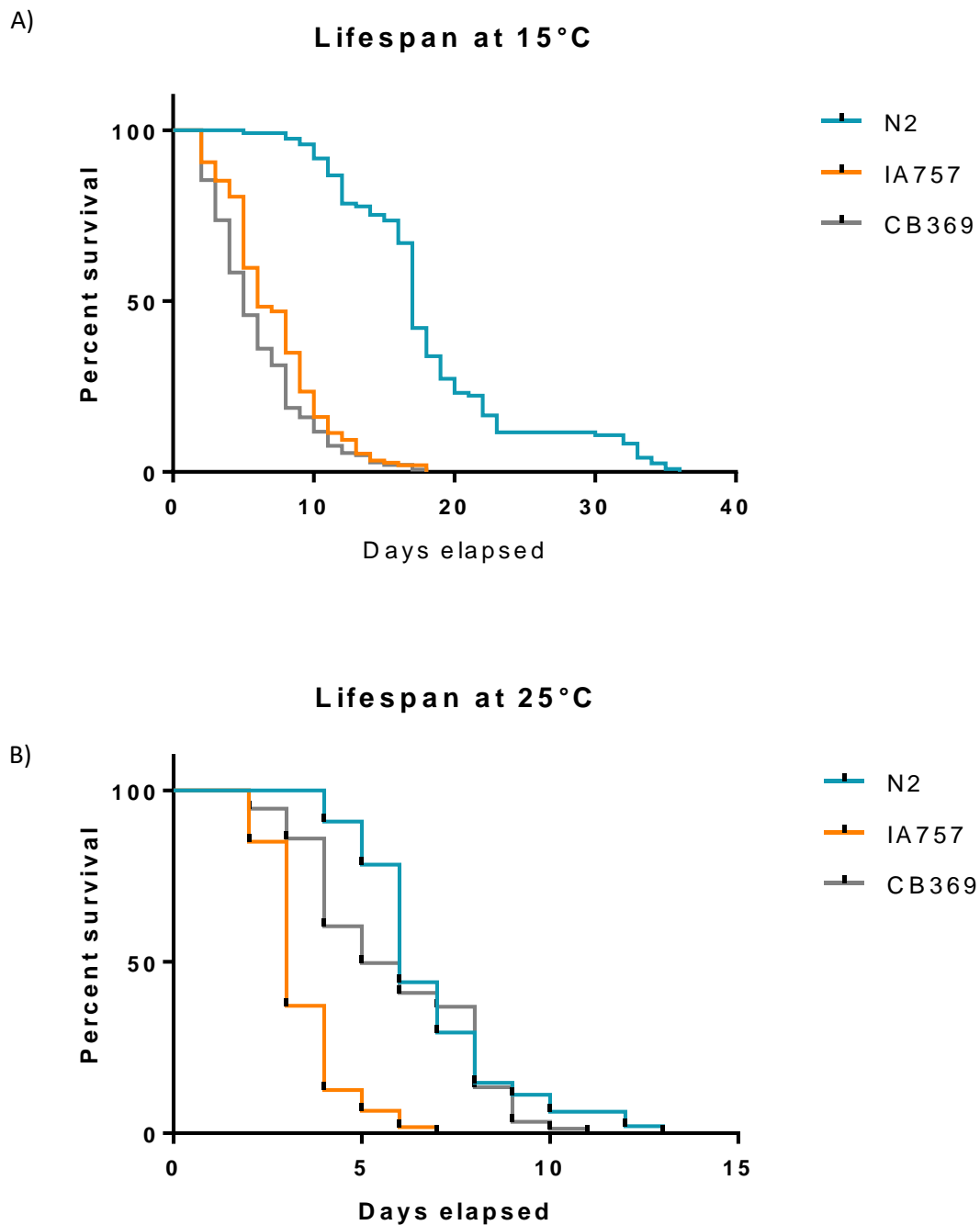


Figure 3.16 Lifespan of adult N2, IA757 and CB369 *C. elegans* at 15°C and 25°C. 3 populations of 50 young adults were observed for each of the strain. **A)** Survival of adult *C. elegans* at 15°C. Log rank test for comparison of the curves. N2 vs IA757, $p < 0.0001$. N2 vs CB369, $p < 0.0001$. IA757 vs CB369, $p < 0.0001$ **B)** Survival of adult *C. elegans* at 25°C. Log rank test for comparison of the curves. N2 vs IA757, $p < 0.0001$. N2 vs CB369, $p = 0.008$. IA757 vs CB369, $p < 0.0001$. P values < 0.017 are considered significant as determined by the Bonferroni method for threshold determination.

3.11 Chapter summary

In this chapter, the phenotypes of the *vps-45(tm246)* mutants (IA757) and *unc-51(e369)* mutant (CB369) strains were identified and compared in terms of size, embryonic lethality, internal organ structures, longevity and cuticle structures. The initial data by Gengyo-Ando et al., which suggested that there is a defect in Yolk protein accumulation in addition to my data demonstrating embryonic lethality could suggest that incomplete protein trafficking of the yolk proteins is responsible for the reduced viability of embryos during early development in *vps-45* mutants (Gengyo-Ando et al. 2007). Furthermore, it appears that there is almost no lethality for the *unc-51 (e369)* mutant after the hatch at 25°C (98.33% survival), unlike the *vps-45 (tm246)* mutant, which exhibited a very high lethality at the non-permissive temperature (14.17% survival), as a result of moulting arrest (Figure 3.3). Part of the reason for the lethality in both embryonic and post embryonic lethality for the *vps-45* mutant could be due to the fact that *C. elegans* also need to secrete their first cuticle prior to hatching as well as at each of the subsequent moults. A subset of embryos dies during that period. Since this is the first time a cuticle is being synthesized there would be no previous cuticle, or parts of it, to be removed and as such if autophagy plays a role in that process it wouldn't be required during that stage.

A *unc-51 (e369)* V; *vps-45 (tm246)* X double homozygotic mutant was constructed and a synthetic lethal phenotype was identified. In order to keep generating the synthetically lethal double mutant which could not be cultured, a *vps-45 (tm246)* heterozygotic, *unc-51 (e369)* homozygotic mutant (strain IA900), was utilised and the double mutant was isolated each time from its progeny. The newly identified synthetic lethal mutant was characterised and compared to the single mutants. Data demonstrated that IA900 animals segregated close to 25% progeny which were very sick exhibiting severe morphological defects, or they died at earlier larval stages before reaching adulthood (approximately 60% lethality) even at the permissive temperature of 15°C (Tables 3.1, 3.2).

The general morphology of the cuticle in all mutants was identified to be similar to the wild type cuticle. As a result, it was assumed that any differences should exist in the moulting process itself. As a result, both, *vps-45* and *unc-51* mutants were characterised in terms of the moulting process and their overall development in order to identify traits that would establish a connection between autophagy and the moulting defects exhibited by the *vps-45 (tm246)* mutant. It was demonstrated that both mutants show differences in terms of

development compared to wild type. In short, *vps-45 (tm246)* animals required longer to complete the moult, a defect which extended a delay in the overall development of the mutants. On the other hand, *unc-51 (e369)* animals required the same amount of time to moult as the wild type strain, however the overall population took longer to moult, and had increased asynchrony in its population after a few days of development. Suggesting, that there could be a delay in the development in the intermoult periods. For both mutants, the reason for the delay in development could be attributed to the clearance of the membranes at the end of each moult in the hypodermis (Singh & Sulston 1978), in each case however for different reason. The *vps-45 (tm246)* mutant required longer to complete the moult possibly as a result of increased requirements for autophagy to clear a greater number of cellular material from the inefficient vesicle fusion along with the Golgi bodies that are formed in the hypodermis at the moult. The *unc-51 (e369)* mutant on the other hand by default exhibits much lower levels of autophagy (Ogura, Wicky, Magnenat, Tobler, Mori, Müller, et al. 1994) and as such would take longer to exit the last stage of the moult because at the last stage of the moult it would take longer to start the ecdysis because of the delayed removal of the Golgi bodies. This claim could be further enforced by the fact that the double mutant exhibited a synthetic lethality. Finally, both mutants exhibited a shorter lifespan compared to the wild type, possibly due to an increased oxidised state of the cells because of the accumulation of cellular material because of the endocytic and autophagy defects in each mutant respectively or maybe other aspects of general fitness.

Chapter 4: The role of autophagy and protein trafficking during embryonic development and moulting

4.1 Overview and aims

As analysed on Chapter 3 the *unc-51 (e369) V*; *vps-45 (tm246) X* double homozygotic mutant animals exhibit a synthetic lethality. The double homozygous mutants were derived by selfing of hermaphrodites of the strain IA900 which is a non-balanced heterozygote for *unc-51 (e369)/+ V* and homozygotic for *vps-45 (tm246) X*. The double homozygotic progeny were paralyzed and with a much smaller body size when compared to CB369 animals. Almost all of these animals display a larval lethality and a very small proportion reach adult but do not produce broods. The homozygotic strain cannot be maintained (Sections 3.3 and 3.6).

Considering that each mutation by itself produces under certain conditions viable animals, the synthetic lethality might indicate some interaction between the two processes within which these genes function during the development of the organism. Since both CB369 and IA757 exhibit cuticle synthesis and/or moulting defects (dumpy body and moulting death respectively), it can be theorised that both processes (VPS-45 mediated endosomal recycling and UNC-51 induced autophagy) are important but not on their own essential for cuticle biogenesis and/or moulting. However, that the organism cannot survive when both are lost simultaneously possibly indicates a level of interaction between these two discrete functions.

Autophagy is a catabolic process in which lysosomes degrade intracytoplasmic contents transported in double-membraned autophagosomes. Autophagosomes are formed by the elongation and fusion of phagophores, which can be derived from pre-autophagosomal structures coming from the plasma membrane and other sites like the endoplasmic reticulum and mitochondria (Lamb et al. 2013; Biazik et al. 2015). One of the first events in autophagy is the formation of the phagophore, a double membrane that encloses cellular components during macroautophagy [(Abeliovich et al. 2000; Biazik et al. 2015), reviewed in (Mizushima 2007; Meléndez & Levine 2009)]. Formation of the phagophore is initiated

by the activity of the ATG1 kinase (orthologues ULK1 in mammals and UNC-51 in *C. elegans*) (Meléndez et al. 2003; J. Kim et al. 2011).

Therefore, UNC-51 is essential for the initiation of autophagy in *C. elegans*. The LC3/Atg8 protein is commonly used as an autophagy marker for the detection of autophagosomes involved in the expansion of the autophagosome membrane [reviewed in (Suzuki & Ohsumi 2007)]. The phosphatidyl-ethanolamine (PE)-conjugated form of this protein is recruited to the maturing autophagosome during the elongation process and is attached by the PE to both the inner and outer membranes of the formed autophagosome. This process occurs downstream of and is regulated by the activation of the ATG1/UNC-51 kinase. The PE conjugated form of LC3/Atg-8 bound to the outer membrane of the maturing autophagosome is released by removal of the conjugated PE whereas the LC3/Atg-8 bound to the inner membrane remains as part of the autophagosomes during the fusion with the lysosome where it is degraded along with the autophagosome and its components marking the end of the autophagic process.(Huang et al. 2000; Tanida et al. 2005). As a result, it is a useful marker for the detection of the autophagosomes and the quantification of the levels of autophagy. *C. elegans* has two orthologues of LC3/ Atg8, namely LGG-1 and LGG-2 (Meléndez et al. 2003) and a LGG-1::GFP fusion has been used as a marker for autophagy in *C. elegans* (Meléndez et al. 2003; Aladzcity et al. 2007). The protein is expressed in a number of tissues in a diffuse pattern under normal conditions. Upon occasions where autophagy is required the expression levels of the proteins rise and distinct punctate structures are formed, corresponding to the autophagosomes carrying LGG-1 on their membranes (Meléndez et al. 2003; Aladzcity et al. 2007).

Furthermore, it has been previously reported that autophagy is observed in the seam cells of the *C. elegans* during its development (Aladzcity et al. 2007). Autophagy has been shown to play an important role in the early developmental stages as well as the subsequent developmental stages such as the dauer larva. More specifically mutation in the autophagy gene *bec-1* causes early embryonic death as well as larval arrest (Meléndez et al. 2003). Additionally, a number of autophagy genes including *unc-51* and *bec-1* have been implicated with normal dauer morphogenesis as well as the regulation of normal cell size and subsequently body size in *C. elegans* (Meléndez et al. 2003; Aladzcity et al. 2007). Furthermore, the seam cells are known to play an important role in the development of the animal as well as cuticle biogenesis and the formation of the cuticular structures such as the alae as discussed previously (Section 1.1.6). It is therefore possible that during the moult where the seam cells are extremely active in secretion of collagen and other

components of the cuticle, that autophagy might play a role. To investigate the potential involvement of autophagy in the seam cells during and after moulting, an LGG-1::GFP fusion protein was used to identify the patterns of the autophagic process in seam cells through moulting in the *vps-45 (tm246)* and *unc-51 (e369)* mutant backgrounds and identify any deviation from normal patterns. In order to achieve this, a transgenic strain DA2123 was employed which carries an LGG-1::GFP transgene in an integrated array together with the *rol-6 (su1006)* marker which causes a roller (*rol*) phenotype. This marker was utilised for easier selection during the crosses to introduce the GFP marker in the *vps-45(tm246)* and *unc-51(e369)* mutant backgrounds. The higher accumulation of the marker in a diffuse cytoplasmic pattern within cells of certain tissues or at specific developmental stages could be the results of an increased requirement for autophagy and thus might potentially help identify specific tissues where increased autophagy is required. On activation of autophagy the diffuse cellular localised LGG-1::GFP forms discrete puncta believed to be formed autophagosomes (Meléndez et al. 2003; Aladzcity et al. 2007). This activation is believed to require the function of the Atg1/UNC-51 kinase. The subsequent disappearance of the marker after a developmental process is completed, in this case moulting, would suggest that a period of raised rate of autophagy has terminated.

To verify that an observed elevated expression of the LGG-1 marker was indeed in the seam cells an epithelial junction GFP marker AJM-1::GFP, was utilised. AJM-1 localizes in the periphery of the of the seam cells and controls the integrity of a distinct apical subdomain of epithelial junctions in *C. elegans* (Köppen et al. 2001).

4.2 Introduction of the LGG-1::GFP and AJM-1::GFP markers in *unc-51 (e369)* and *vps-45 (tm246)* backgrounds

To introduce the LGG-1::GFP autophagy marker in the mutant backgrounds of interest, IA757 and CB369 respectively, were crossed with the DA2123 strain which carries expressing the LGG-1::GFP transgene. For the construction of the IA888 strain, genotype *adIs2122 [lgg-1p::GFP::lgg-1 rol-6(su1006)]; vps-45 (tm246) X*], 10 DA2123 LGG-1::GFP males were crossed with a single IA757 hermaphrodite. The success of the cross was assessed by the ratio of males to hermaphrodites as well as the presence of GFP expression in the F1 hermaphrodites. The F1 hermaphrodites were transferred clonally to new plates and were left to egg lay. The F2 worms were transferred clonally and left to lay

eggs for 12 hours. The F2 parents were then lysed for single worm PCR genotyping of *vps-45* and the F3 broods that were derived from homozygotic *vps-45 (tm246)* parents were kept.

In order to check the zygosity of the LGG-1::GFP transgene (*adIs2122*) the F3 broods were observed under the microscope and scored for 100% GFP expression. The strain IA888 thus selected is homozygotic for both the *vps-45 (tm246)* allele and the integrated *adIs2122* transgene. The strain was further checked again for LGG-1::GFP homozygosity by the phenotype of its progeny, in which case 100% of the progeny demonstrated the roller phenotype confirming the genotype.

A similar approach was followed for the creation of the IA897 transgenic strain, genotype *adIs2122 [lgg-1p::GFP::lgg-1 rol-6(su1006)]; unc-51 (e369) V*]. In this case however the UNC phenotype was followed and the same approach with the GFP phenotype of the progeny was used.

Finally for the construction of the of the IA903 double marker strain, genotype *adIs2122 [lgg-1p::GFP::lgg-1 rol-6(su1006)]; jclIs1 [ajm-1::GFP unc-29(+)] IV* , 10 SU93, genotype *jclIs1 [ajm-1::GFP unc-29(+)] IV* , males were crossed with a single DA2123 hermaphrodite, genotype *adIs2122 [lgg-1p::GFP::lgg-1 rol-6(su1006)]*. A ~50% ratio of males to hermaphrodites indicated a successful cross. F1 hermaphrodites were transferred clonally to fresh NGM plates and were left to reproduce. Animals which exhibited the roller phenotype were selected and were once again clonally transferred. F2 adult animals were left to egg lay and their progeny was collected as eggs and observed with fluorescent microscopy. In the case were 100% of the eggs was expressing both markers the parent and its progeny were kept as the new double marker IA903 strain.

4.3 LGG-1 accumulates in the seam cells during moulting

LGG-1 localisation was observed and compared in the DA2123, IA888 and IA897 strains specifically focusing on changes between moulting and non-moulting periods of development in the three strains. As discussed in detail below, it was observed that LGG-1::GFP fluorescence increases to high levels in the seam cells (relative to the rest of the anatomy), and that this accumulation is very dynamic between inter-moult, lethargus and

moulting/post-moult periods. This observation raises the question of a developmentally regulated involvement of autophagy in cuticle biogenesis or moulting. Seam cells in *C. elegans* are localized in the hypodermis, they exhibit stem cell-like features as they have the ability to continue to divide and give rise to new cells capable of differentiating at each larval moult [(Sulston & Horvitz 1977; Singh & Sulston 1978) reviewed in (Brabin & Woollard 2012)]. Furthermore, larval development during the periods of cuticle synthesis prior to each moult, in periods of development described as lethargus the seam cells are highly secretory as evident by the formation of a large amount of Golgi bodies and they appear to be responsible for the secretion of significant quantities cuticular components (Sulston & Horvitz 1977; Singh & Sulston 1978). Synthesis of cuticular components is not restricted specifically to the seam cells of the hypodermis, but in the various hypodermal syncytia also, however high levels of expression of the LGG-1::GFP was observed specifically within the seam cells and not in the remainder of the hypodermis or in other tissues.

As discussed above, LGG-1 and its mammalian orthologue LC3 have been used in multiple studies of autophagy. LGG-1/LC3 is believed to in part drive the maturation process and LGG-1/LC3- PE proteins bound to the internal part of the autophagosome membrane remain there during the fusion with the lysosome making it an excellent marker for the appearance and disappearance of autophagosomes. With the LGG-1::GFP marker, the generally uniform diffuse cytoplasmic localisation changes and distinct GFP puncta are observed under conditions where autophagy is believed to be actively induced, these puncta representing autophagosomes (Aladzcity et al. 2007; Meléndez et al. 2003).

In a preliminary study of the behaviour of the LGG-1::GFP during moulting in seam cells, synchronised L1 larvae in liquid cultures were obtained and were seeded on NGM plates as previously described in material methods (section 2.3.6). All strains were cultured on the NGM petri dishes until they started moulting at which point they were transferred onto slides to be observed under the high magnification microscope (section 2.3.9). Images were acquired at several points during the moult, from the onset of lethargus until beyond ecdysis (Figure 4.1).

The normal wild type pattern of expression of the LGG-1::GFP marker was observed in the DA2123 strain. An intense accumulation of the LGG-1::GFP in a diffuse localisation throughout the seam cells was observed at the onset of lethargus at 27 hours post L1 larval arrest (Figure 4.1). By contrast there is no visible accumulation of LGG-1::GFP before the onset of lethargus at 24 hours post L1 arrest (Figure 4.1) or even prior to that. The

fluorescence microscopy used here could not rule out a possible low level of expression of this marker in other tissues or at other developmental times. However, the seam cell expression during lethargus is very evident and clearly different from anything in the rest of the animal's anatomy.)

At ~30 hours post L1 arrest towards the end of the L1 lethargus the seam cells undergo a cell division (Figure 4.1) and at this time the appearance of the LGG-1::GFP localisation changed. Whereas earlier in lethargus it is evenly and diffusely distributed throughout the seam cells, at the end of lethargus when the seam cells can be observed to divide, discrete foci of LGG-1::GFP become apparent. These foci have previously been proposed to be autophagosomes. Finally, after 31 hours when the seam cells have divided and the nematodes have finished the moult and shed their cuticle the LGG-1::GFP is not visible in the seam cells anymore (Figure 4.1).

Thus the LGG-1::GFP marker is developmentally regulated in at least two distinct ways in *C. elegans* development; firstly via changes to its abundance and secondly by its conversion from a diffuse probably cytoplasmic pattern of localisation into discrete foci. It accumulates in a homogenous diffuse manner throughout seam cells during the period of lethargus; this probably represents the unmodified inactive version of the protein. Late in lethargus when the seam cells divide, it then forms discrete puncta within seam cells, believed to represent active autophagosomes. Finally, shortly after completion of the moult the LGG-1::GFP accumulation in seam cells is lost. This is consistent with the completion of an active period of autophagy specifically in seam cells at the end of a moulting cycle. This in turn is consistent with the possible involvement of autophagy in some aspect of cuticle synthesis/moulting. One possible function could be the removal of secretory apparatus at the end of cuticle synthesis. Cuticle synthesis and moulting in *C. elegans* is an example of developmentally regulated protein secretion from the seam cells and other components of the hypodermis. In the intermoult periods there are relatively low numbers of Golgi bodies and membranous structures associated with protein secretion in the seam cells. At the onset of lethargus there is a radical change with extensive accumulation of Golgi and vesicles which after moulting is complete rapidly disappear (Sulston & Horvitz 1977; Singh & Sulston 1978). Thus, seam cells switch between secretory and non-secretory phases between each period of lethargus and subsequent inter-moult. Possibly autophagy has a role in removing secretory apparatus at the end of each moult returning the cells to their non-secretory phase.

This experiment was repeated with the IA903 strain, which carried both LGG-1::GFP and AJM-1::GFP to verify that the accumulated LGG-1::GFP is indeed localised in the seam cells. The pattern was similar to the DA2123 strain. Lethargus started at 25-26 hours of development after inoculation of the synchronised L1 larvae. At 24 hours before the onset of lethargus the seam cells show no expression of the LGG-1::GFP marker. At 26 hours and the onset of lethargus and the moult, the seam cells are expressing the LGG-1::GFP marker and diffuse GFP is clearly visible in the seam cells. The AJM-1::GFP marker is clearly visible as it surrounds the seam cells (Figure 4.2).

A similar experiment was conducted using the IA888 and IA897 strains in order to identify any potential difference in the autophagic process during the moult in *vps-45 (tm246)* and *unc-51 (e369)* mutant backgrounds respectively.

For the *vps-45 (tm246)* mutant (IA888) a similar absence of LGG-1 accumulation was observed prior to the onset of lethargus shown at 25 hours of development from L1 arrest (Figure 4.3). Lethargus started at 29 hours of development (slightly delayed relative to the wild type) and the LGG-1::GFP marker was observed to accumulate in seam cells at the onset of lethargus as it did for the wild type strain (Figure 4.3). Once again, a similar punctate pattern was observed to develop during the seam cell division, which took place at 35 hours of development post L1 arrest in this strain, compared to 30 hours in the wild type. Finally, no seam cell expression of the LGG-1::GFP marker was observed after the end of the moult at 36-37 hours (Figure 4.3). These results suggest that a loss of *vps-45* function does not affect the autophagy process in seam cells as assessed with the LGG-1::GFP marker. Although the moulting period is extended in the mutant *vps-45* background taking on average 8 hours to complete compared to 4 hours in the wild type, the behaviour of the LGG-1::GFP displays approximately the same relationships to the stage of lethargus as in the wild type. The loss of *vps-45* function delays completion of moulting, the timing of the seam cell division and the alterations to the accumulation of LGG-1::GFP in a similar manner and extent. Coordination of these processes is therefore retained.

In the case of the *unc-51 (e369)* mutant (IA897) strain where, no LGG-1::GFP accumulation is observed in the seam cells of the animals before the onset of lethargus. Lethargus started at 29 hours at which point LGG-1 has accumulated in the seam cells (Figure 4.4) in a similar pattern of accumulation to the two other strains. For the *unc-51* mutant the seam cell division was observed at ~31 hours post L1 arrest at which point the LGG-1::GFP appears predominantly diffuse and with fewer visible punctate foci of GFP by comparison to the two other strains. At 34 hours at which point the moulting has

completed and the pharyngeal pumping has started, diffuse localisation of LGG-1::GFP remains visible although less intense than in the previous time points of 29 and 31 hours (Figure 4.4). Thus while in the wild type the LGG-1::GFP accumulation is lost by one hour after the seam cell division (and moulting is complete), in the *unc-51* mutant moulting takes approximately three hours post seam cell division to complete and the LGG-1::GFP although reduced in abundance after 3 hours, is still detectable. Thus LGG-1::GFP in the *unc-51* mutant background is retained longer after seam cell division than in the wild type.

Additionally, in the *unc-51* mutant there is also a more visible GFP fluorescence in several other tissues of the body of the animal than is seen for either the wild type (DA2123) or the *vps-45* mutant (IA888). Thus loss of Atg1/UNC-51 function appears to extend the period of accumulation of LGG-1::GFP in the seam cells associated with moulting and cause a general increase in various other tissues, although not to the same levels of normal accumulation in seam cells during the moult.

Collectively it appears that in all three strains, the seam cells follow the same basic pattern of inducing expression and accumulation of the LGG-1::GFP autophagy marker during the moult, and loss of its accumulation at the end of the moulting process. Although the general pattern is similar, there are specific differences. In the case of the *unc-51* mutant there is a delay to the loss of LGG-1::GFP accumulation within seam cells after moulting is completed; loss takes approximately 1 hour in the wild type and approximately 3 hours in the *unc-51* mutant as presented in more detail below (section 4.4).

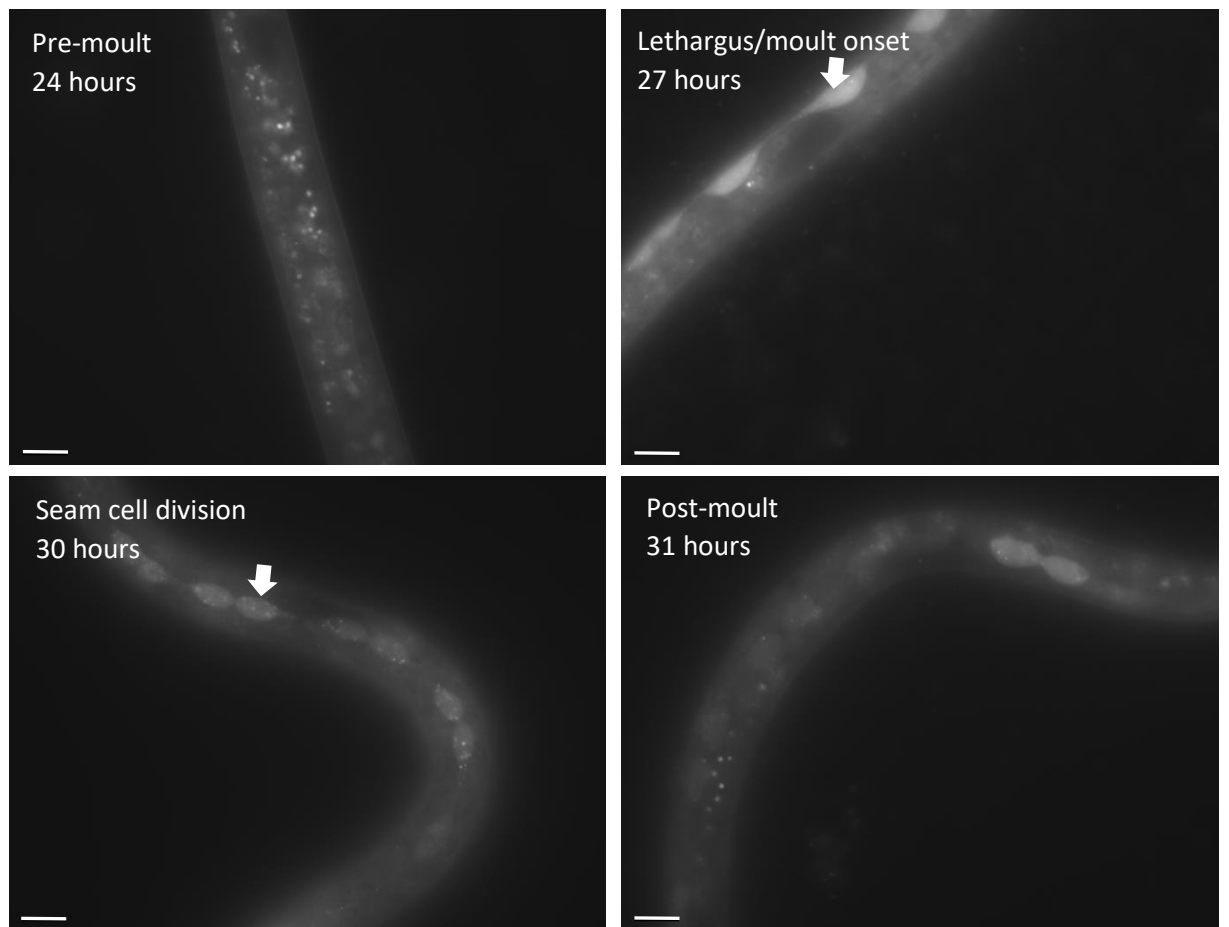


Figure 4.1: UV microscopy DA2123 L1 larvae before (24 hours), during (27 and 30 hours) and after (31 hours) of the L1-L2 moult. 63x

magnification, 200ms exposure. Arrows show the LGG-1::GFP marker being expressed in the seam cells during the moult. Small foci of GFP can be observed in the seam cells after the accumulation of GFP. Size bars represent 5 μ m.

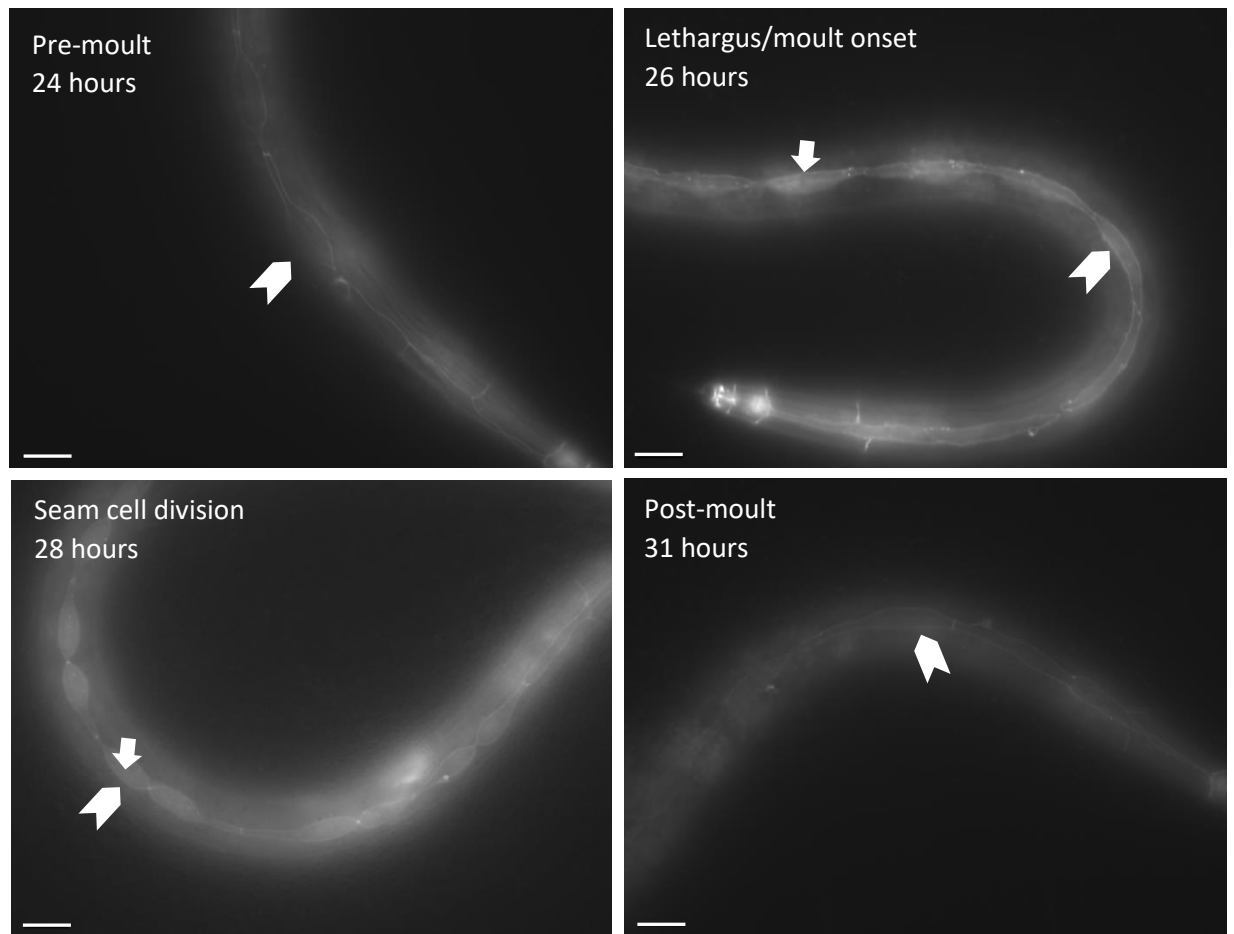


Figure 4.2: UV microscopy of IA903 animals before (24 hours), during (26 and 28 hours) and after (31 hours) the L1-L2 moult. 63x magnification, 200ms exposure. Arrow heads show the epithelial junctions marked by the AJM-1::GFP marker surrounding the seam cells. Arrows show the LGG-1::GFP marker being expressed in the seam cells during the moult. Size bars represent 5 μm.

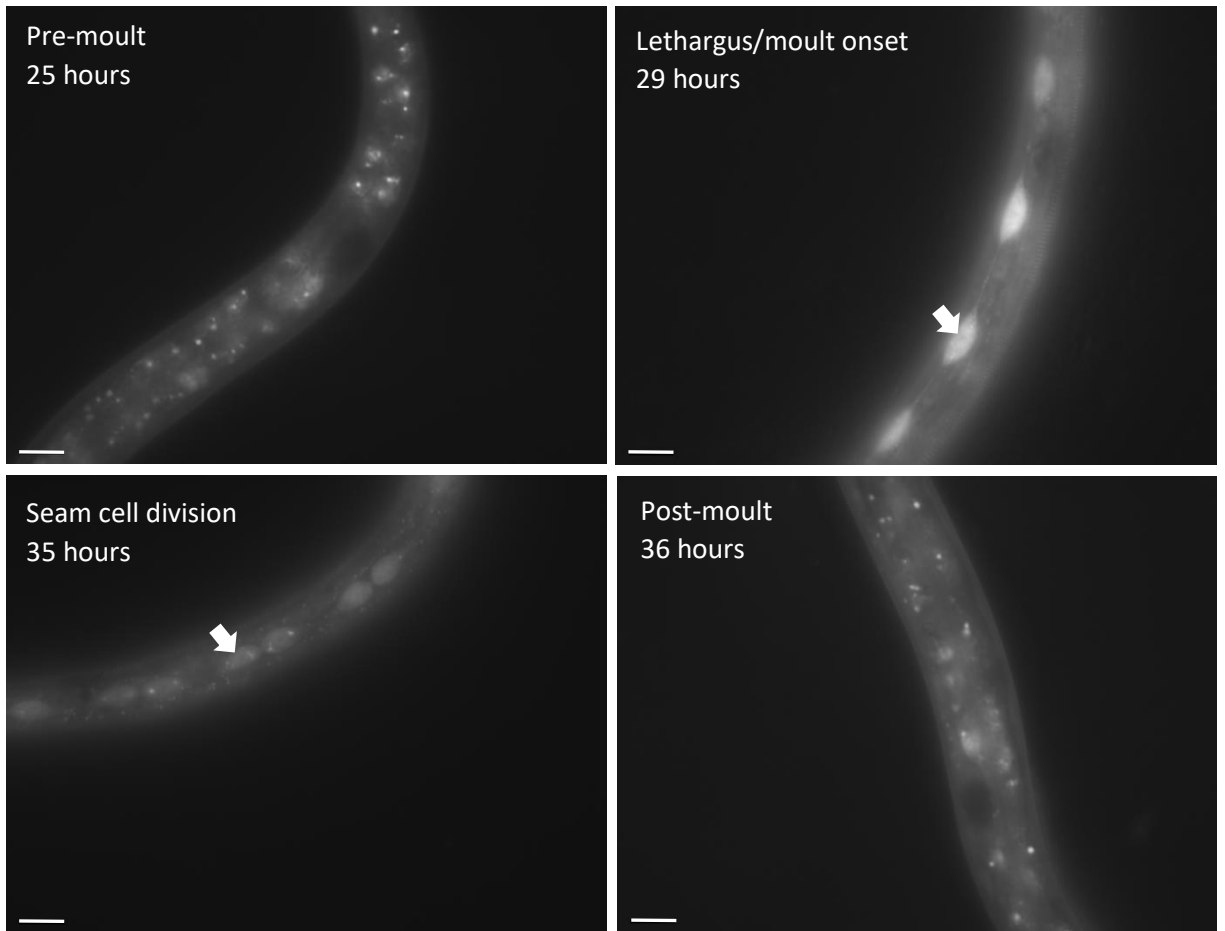


Figure 4.3: UV microscopy of IA888 larvae before (25 hours), during (29 and 35 hours) and after (36 hours) of the L1-L2 moult.

63x magnification, 200ms exposure. Arrows show the LGG-1::GFP marker being expressed in the seam cells during the moult. Small foci of GFP can be observed in the seam cells after the accumulation of GFP.

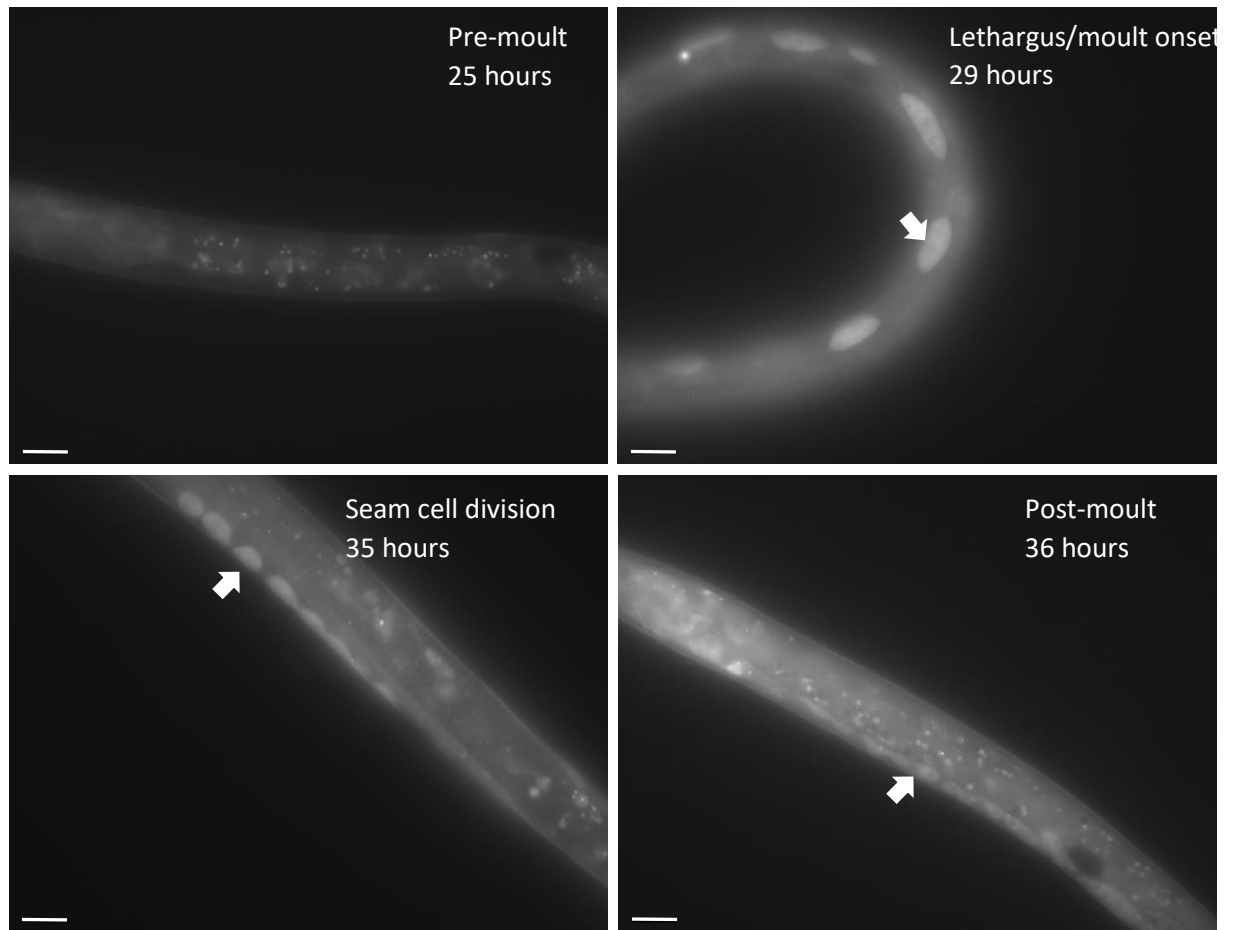


Figure 4.4: UV microscopy of IA897 L1 larvae before (25 hours), during (29 and 31 hours) and after (34 hours) of the L1-L2 moult.

63x magnification, 200ms exposure. Arrows show the LGG-1::GFP marker being expressed in the seam cells during the moult.

4.4 Assessment of the retention of the LGG-1 autophagy marker in the seam cells in *vps-45 (tm246)* and *unc-51 (e369)* mutants

In the previous section the expression of the LGG-1::GFP autophagy marker in the seam cells was observed in the wild type, the *vps-45 (tm246)* and *unc-51 (e369)* backgrounds during the moult, and differences in the timing of patterns of accumulation were identified (Section 4.3). These are documented in more detail in this section. Differences in the retention time of LGG-1 protein in the seam cells of the IA897 and IA888 strains and the wild type strain post moult, could potentially indicate differences in the autophagic process, as well as establish a link between VPS-45 and its role in the process if that exists. To accurately measure this, ten larvae from each strain were put on a single slide each after being synchronised from the L1 arrest. A 0.5µl of OP50 bacteria was added provide food for the animals. The slides were kept in a box with moist tissue in order to animals from dehydrating. It should be noted that sodium azide was not added in the agar pad of the slides in order to keep the worms active so they could go through the moulting process. Each slide was observed hourly from the onset of the moult to its end and the time at which the LGG-1 first started being expressed in the seam cells was noted. The visible marker for the ending of the moult was the division of the seam cells near the end of the L1-L2 moult. Slides were observed until LGG-1 was no longer visible in the seam cells.

On average lethargus started at 25.3 hours for the wild type strain, 27.8 hours for IA888, genotype, *adIs2122; vps-45 (tm246)* X and 27.6 hours for the IA897, genotype *adIs2122; unc-51 (e369)* V. LGG-1 had accumulated in the seam cells in less than an hour from the onset of lethargus for the wild type strain, at about 1 hour of lethargus for the IA888 and approximately two hours after lethargus for the IA897. The lethargus process lasted approximately 4 hours for the wild type strain, from 25.3 to 29.1 hours on average for the 10 animals observed. For IA888 it lasted for approximately 7 hours, from 27.8-35 hours and for IA897 it lasted for approximately 5 hours, from 27.6 to 32.3 hours which generally agrees with our data from Chapter 3 regarding the moulting profile of the mutants.

At the end of the moult, at the seam cell division and exit from lethargus, the LGG-1::GFP marker was visible in the seam cells for approximately an hour in DA2123 and IA888, at 29.1 to 30.4 hours and 35 to 36 hours respectively. By contrast, for the IA897 strain, the LGG-1::GFP was visible in the seam cells for approximately 3 hours, from 32.3 to 34.8

hours, after the end of seam cells division and the exit from lethargus (Figure 4.5, Table 4.1).

From these results, the evidence suggests that VPS-45 function although required for the completion of the moult process at a wild type rate, is not required for the normal coupling of the regulation of LGG-1::GFP accumulation within the seam cells to the process of lethargus, seam cell division and moulting. By contrast, ATG1/UNC-51 clearly does influence the normal loss of LGG-1::GFP that occurs at the end of the moult as in the *unc-51* mutant the marker accumulation persists after the moult for at least three times longer than in the wild type, 3 hours compared to 1 hour. This result is consistent with the possibility that the rate of activation of the autophagy process in seam cells by ATG1/UNC-51 kinase positively regulates the rate of removal of LGG-1::GFP from seam cells at the end of the moult. It is known for LC3 the mammalian orthologue of LGG-1, that PE-LC1 in the autophagosome is destroyed by a cycle of autophagy. Thus, it is possible that autophagy itself plays a role in the timely removal of LGG-1 at the end of the moult.

A)

Strain	Sample	Lethargus (h)	LGG-1 ON (h)	Seam cells division (END OF MOULT) (h)	LGG-1 OFF (h)
DA2123	1	24	25	29	30
	2	24	25	28	30
	3	26	26	29	30
	4	25	26	28	29
	5	24	25	29	30
	6	25	26	29	30
	7	25	26	29	30
	8	27	28	30	32
	9	27	28	30	32
	10	26	26	30	31
	Average time (h)	25.3	26.1	29.1	30.4

B)

Strain	Sample	Lethargus (h)	LGG-1 ON (h)	Seam cells division (END OF MOULT) (h)	LGG-1 OFF (h)
IA888	1	27	29	35	36
	2	28	29	35	36
	3	28	29	34	35
	4	28	29	35	36
	5	27	30	35	36
	6	28	29	35	36
	7	28	29	35	36
	8	28	29	35	36
	9	28	29	35	36
	10	28	29	36	37
	Average time (h)	27.8	29.1	35	36

C)

Strain	Sample	Lethargus (h)	LGG-1 ON (h)	Seam cells division (END OF MOULT) (h)	LGG-1 OFF (h)
IA897	1	27	30	31	34
	2	28	30	32	35
	3	26	29	31	35
	4	28	30	31	34
	5	26	29	32	34
	6	27	30	32	35
	7	28	30	32	34
	8	27	30	33	35
	9	29	31	33	34
	10	30	34	36	38
	Average time (h)	27.6	30.3	32.3	34.8

Table 4.1: Analytical tables of the onset of LGG-1 expression during the moult for individual *C. elegans* for each strain.

Four time points were scored for each worm, Onset of lethargus (Lethargus), first observation of LGG-1::GFP in the seam cells (LGG-1 ON), Seam cell division (END OF MOLT) and the stopping of LGG-1::GFP expression from the seam cells (LGG-1 OFF). A) DA2123 B) IA888 C) IA897.

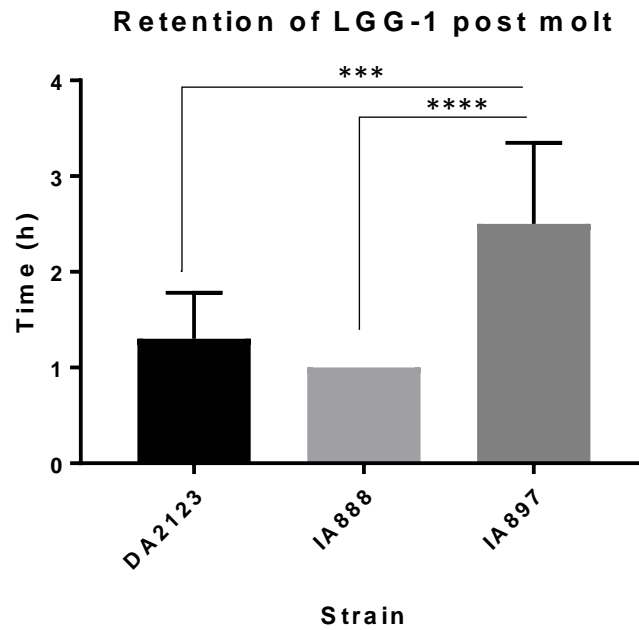


Figure 4.5: Average time of retention of LGG-1 in the seam cells after the end of the molt.

All strains were cultured at 15°C. Average time \pm SD is shown for each strain. DA2123 (n=10), IA888 (n=10), IA897 (n=10). Tukey's multiple comparisons test: DA2123 vs IA888 P= 0.47. DA2123 vs IA897, P= 0.0002. IA888 vs IA897 P<0.001.

4.5 Assessment of the autophagy levels in the seam cells of wild type, *vps-45 (tm246)* mutant and *unc-51 (e369)* mutant *C. elegans*

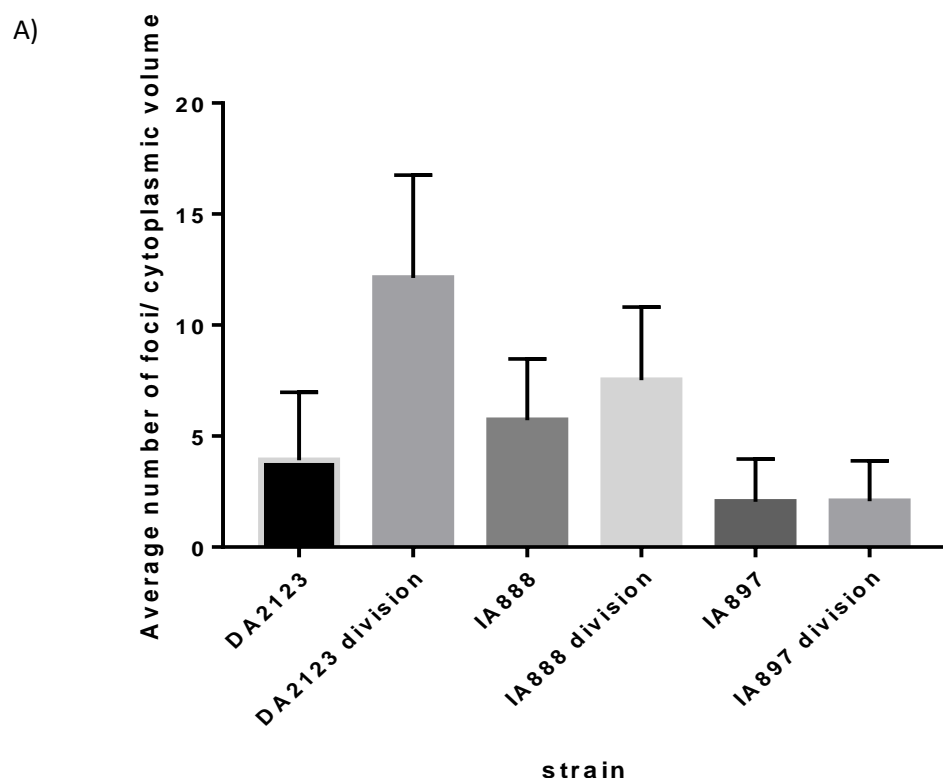
As discussed in the introduction to this chapter, active involvement of LC3/LGG-1 in an autophagy cycle involves its accumulation on the membranes of the developing phagosome and subsequent formed autophagosome. In this form, it appears as intense foci of fluorescence when coupled to GFP. Data previously presented in Section 4.3 suggest that in the wild type during the seam cell division near the end of the moult for each animal more foci are present in the seam cells suggesting a higher level of autophagy at that time. Therefore, the formation of discrete GFP fluorescent foci in seam cells was observed in the DA2123, IA888 and IA897 strains for evidence of active autophagy in these cells during lethargus/moulting. Larvae were observed at the L1-L2 moult. Foci form in all seam cells in the wild type strain however not all of the seam cells divide at the same time. In order to determine more accurately when relative to the division the foci are formed and accumulate the same seam cell was selected and documented for each animal. That was the first ventral seam cell (V1). The foci were counted in the cells at two stages; in lethargus before and during V1 seam cell division. During the division, the forming daughter cells were considered as a single dividing cell sharing the same cytoplasm and foci/autophagosomes.

The average number of foci during the division in the wild type strain DA2123 was 12.1 foci per cell compared to 3.9 foci per cell before the division, exhibiting a 3-fold increase during the division. By contrast, the IA888 strain, genotype *adIs2122; vps-45 (tm246)* X, exhibited higher numbers of foci than the wild type before the seam cells division with an average number of 5.7 foci per cell (Figure 4.6). A modest increase in the foci at the seam cell division of IA888 animals was observed which however, was lower compared to the number in the dividing wild type seam cells with an average number of 7.5 foci per seam cell. For the IA897 strain, genotype *adIs2122; unc-51 (e369)* V, the number of foci remained low and very similar both prior and during the division of the seam cells as opposed to IA888 and DA2123 strain with an average number of 2 foci both before and during the division of the seam cells (Figure 4.6). (As discussed below it is possible that a proportion of GFP foci represent artefactual aggregation of GFP and not autophagosomes.)

The data indicate that in the DA2123 strain, LGG-1::GFP accumulation is induced in the seam cells as *C. elegans* enter lethargus, at the beginning of the moult. However, a limited

number of punctate GFP foci are formed at this point suggesting a lower rate of autophagy compared to during seam cell division. As the larvae approach the end of the moult the seam cells divide and at this time a significant increase in the numbers of LGG-1::GFP foci was observed, consistent with an increase in the numbers of autophagosomes. This coincides with the completion of a period of secretion and cuticle synthesis. An obvious possibility is that autophagy is required for the clearance of secretory apparatus formed for the secretion of the cuticle as previously discussed, and the return of these cells to the inter-moult non-secretory phase (Chapter 3).

In the case of IA888 strain, which carries the *vps-45* (*tm246*) mutation, key differences are observed in that pattern. A higher number of LGG-1::GFP foci were observed in the seam cells at earlier stages of lethargus prior to the seam cell division than in the wild type. The level of increase at the division was slightly less than observed in the wild type. This is consistent with possibly a more continuous and elevated level of autophagy throughout the cuticle synthesis process in lethargus when VPS-45 is absent. VPS-45 plays an important role in the fidelity of correct vesicle targeting and fusion within the endosomal system (Cowles et al. 1994; Piper et al. 1994; Carr & Rizo 2010; Dulubova et al. 2002). One consequence of the loss of VPS-45 function is an increase in the rate of aberrant and inappropriate membrane fusions resulting in perturbed delivery of cargo and thus the accumulation of aberrant membranes producing ER stress (P. Stepensky et al. 2013) which might also induce autophagy.



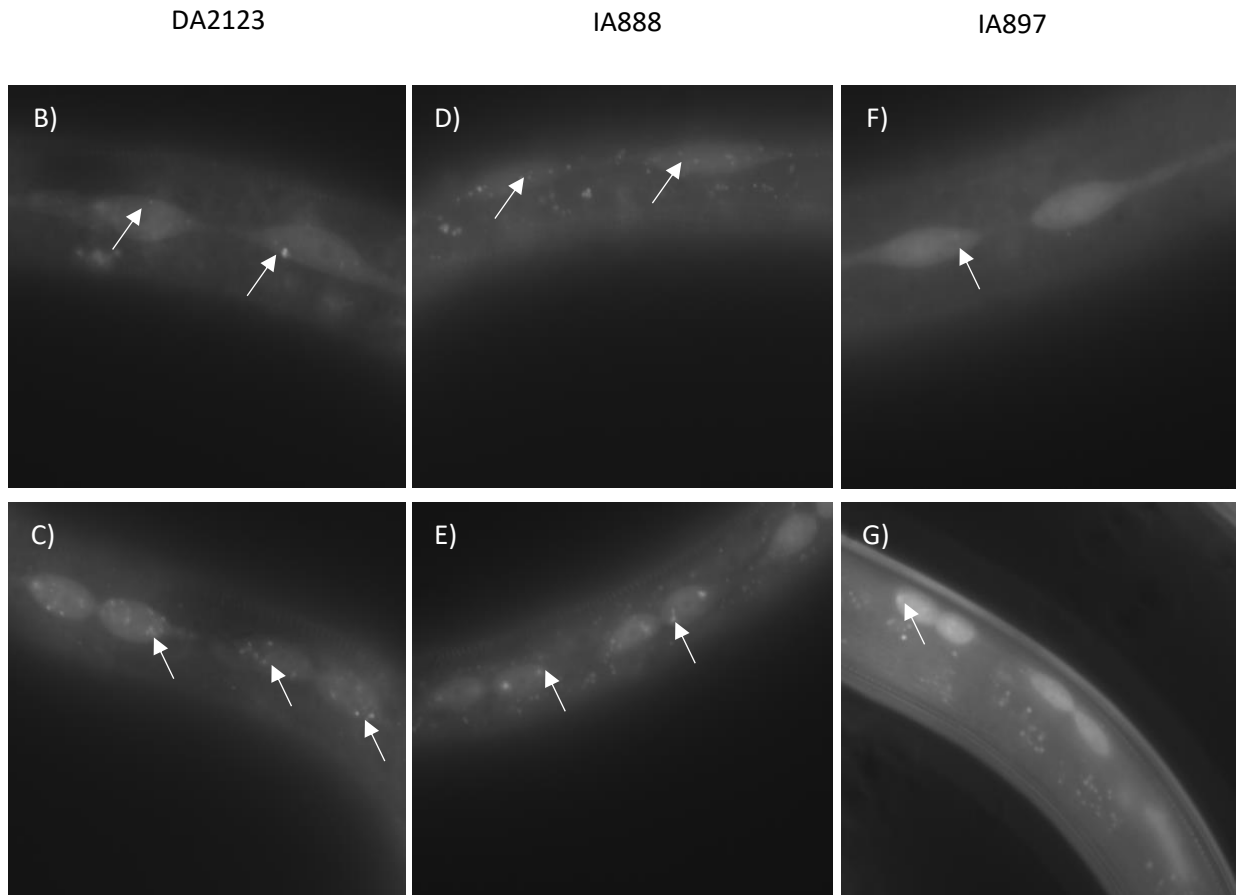


Figure 4.6: Level of autophagy in the seam cells in DA2123, IA888 and IA897 animals.

A) Average number of autophagic foci per cell/dividing cell (\pm SD) DA2123, IA888 and IA897 L1-L2 molting animals. DA2123 (n=37), DA2123 division (n=25), IA888 (n=71), IA888 division (n=33), IA897 (n=43), IA897 division (n=27) DA2123 vs DA2123 division, $P < 0.0001$. DA2123 vs IA888, $P = 0.0321$. DA2123 vs IA888 division, $P < 0.0001$. DA2123 vs IA897 $P = 0.0531$, DA2123 division vs IA897 $P = 0.1315$, DA2123 division vs IA888 $P < 0.0001$, DA2123 division vs IA888 division $P < 0.0001$, DA2123 division vs IA897 division $P < 0.0001$, IA888 vs IA888 division $P = 0.0449$, IA888 vs IA897 $P < 0.001$, IA888 vs IA897 division $P < 0.001$, IA888 division vs IA897 $P < 0.001$, IA888 division vs IA897 division $P < 0.001$, IA897 vs IA897 division $P > 0.9999$. **B-G)** Representative images (UV) of V1 seam cells of L1-L2 molting animals before and during the division. White arrows point to the autophagy foci of LGG-1::GFP.

As presented in Chapter 3 (Section 3.9) the *C. elegans vps-45* mutant takes longer to proceed through cuticle synthesis/lethargus than the wild type and thus the process is working less quickly than in the wild type. Here evidence is presented for a higher level of autophagy in seam cells during the earlier stages of lethargus (as opposed to just at the end of lethargus when seam cells divide) in the *vps-45 (tm246)* mutant (Figure 4.6). Data are consistent with a higher level of autophagy throughout lethargus when VPS-45 is absent, rather than a rapid induction at the end of lethargus. One possibility is that elevated rates of autophagy throughout lethargus occurs to remove membrane organelles that have had inappropriate vesicle fusions during cuticle synthesis and this may also be the reason for the increased time taken to complete cuticle synthesis/lethargus. It is not clear why the level of increase in LGG-1::GFP autophagic foci going from early lethargus and into the seam cell division at the end of moulting is less in the *vps-45* mutant than the wild type.

In interpreting these data, the possibility that some of the visible “foci” of fluorescence are in fact artefactual aggregates of GFP and not autophagosomes should be considered. Previous studies have shown that mouse embryonic fibroblast (MEF) cells transiently overexpressing the autophagy marker GFP::LC3, (LC3 being the mammalian homologue of LGG-1), form artefactual GFP aggregates especially when autophagy was compromised. These aggregates cannot be discerned from real autophagosomes by fluorescent microscopy (Kuma et al. 2007). Since the Atg1/UNC-51 kinase is central to induction of autophagy, the difference in behaviours of the wild type and the *unc-51* mutant strains is most compelling. While the *unc-51* mutant had an average of 2 foci before seam cell division and during seam cell division, the wild type had 3.9 versus 12.1 respectively. The dynamic change in number of foci from before seam cell division to during division in wild type is consistent with an active induction of autophagy (and not GFP artefact). That this induction is totally absent in the *unc-51* mutant is the strongest evidence that this a real measure of a developmentally regulated increase in autophagy towards the end of lethargus at the time of seam cell division. That there is no increase in the number of foci in the *unc-51* mutant (on average 2 foci before seam cell division and during seam cell division), suggests that the induction in wild type is entirely dependent on Atg1/UNC-51 function and that the *unc-51 (e369)* allele is with respect to this function either a null allele or is of too limited function to detect by this assay. It is therefore possible that the small number of foci visible in the *unc-51 (e369)* mutant are in fact GFP artefacts. By contrast, the increase in foci from lethargus pre-seam cell division to during seam cell division that is *unc-51* dependant most likely is a measure of a genuine increase in autophagy. Interestingly, while the *vps-45 (tm246)* mutant takes approximately twice as

long as wild type to progress through moulting as the wild type (~8 hours for *vps-45* (*tm246*) mutant compared to ~4 hours for the wild type), the difference is much less for the *unc-51* (*e369*) mutant which takes on average 4.7 hours (Table 4.7). Thus, although the evidence presented here, demonstrating a developmental induction of autophagy at the end of a moulting cycle in seam cells, is consistent with autophagy functioning within cells involved in cuticle synthesis and moulting at the end of a moult cycle, loss of VPS-45 function has a far greater impact than loss of Atg1/UNC-51 on the length of time taken to complete lethargus and moulting. Therefore, as the *unc-51* (*e369*) mutant takes significantly longer to develop from the L1 larva through the four larval stages to the adult than wild type, this is not the result of moulting taking longer and thus can only be the result of the intermoult phases taking longer (Section 3.9). It is therefore possible that failure to induce autophagy at the end of the moult does not seem to affect the completion of the moult but it does seem to cause difficulties in the subsequent intermoult stage and that protein trafficking plays an important role in the moulting process itself.

4.6 LGG-1 is expressed in the seam cells in *C. elegans* embryos at the 3 fold stage and is retained for longer in the *unc-51* (*e369*) mutant post-hatch

In the previous sections the behaviours of the LGG-1::GFP autophagy marker was studied in seam cells during the L1 larval stage lethargus and subsequent moult to L2 larval stage. In *C. elegans* cuticle synthesis occurs five times during development, once in the embryo prior to hatch and then at the end of each larval stage during lethargus prior to completion of the associated moult. The *vps-45* and *unc-51* mutant strains rapidly lost synchrony after the first moult (L1 to L2), and this made study of the timing of LGG-1::GFP accumulation at later moults problematic. However, the stages of embryonic elongation (Sulston et al. 1983) and the timing of hatching facilitate observations relative to developmental time in embryos and into early L1 larval development and the behaviour of LGG-1::GFP was studied during and after the period of first cuticle synthesis which occurs in the embryo and is followed by subsequent hatching.

Embryos from each of the LGG-1::GFP expressing transgenic strains were selected at the later stages of embryonic development during elongation and were observed under the fluorescent microscope. For all strains, eggs were observed and LGG-1::GFP fluorescence recorded at the comma, two-fold and three-fold stages of embryonic elongation and during

hatching. Eggs were randomly picked and were documented and observed at the appropriate developmental stage. For observations during hatching, embryos were picked at the 3-fold stage and were observed until hatching occurred at which point their images were taken. These observations cover the period of cuticle secretion and synthesis during embryogenesis, analogous to the cuticle synthesis that occurs subsequently at the end of each larval stage during lethargus. In L1 development, the seam cells undergo their first post embryonic division at approximately 5 hours after hatch (Shemer & Podbilewicz 2000; Podbilewicz & White 1994). For observations of the post-hatch LGG-1::GFP behaviour, this seam cell division was observed and used as a developmental time marker. This provides a consistent time point after completion of embryonic cuticle synthesis and before the L1 to L2 lethargus when the second period of cuticle synthesis occurs.

The accumulation of LGG-1::GFP in embryos in the wild type background was observed using the DA2123. It is evident that fluorescence is generally diffuse in the comma and two-fold stage, and is very clearly expressed in the seam cells at the three-fold stage (Figures 4.7). The IA903 strain, genotype *adIs2122 [lgg-1p::GFP::lgg-1 rol-6(su1006)]; jcls1 [ajm-1::GFP unc-29(+)] IV*, was utilised once more to verify that LGG-1::GFP was indeed being expressed at higher levels in the seam cells (Figure 4.8). It is interesting and consistent with the previous data for the L1 to L2 moult that the LGG-1 accumulates in the seam cells during periods of cuticle synthesis, and not simply during post-embryonic moulting. Furthermore, right at the point of hatch the LGG-1::GFP marker can no longer be seen in the seam cells suggesting that after the L1 larval cuticle has been synthesised in the embryo, that the autophagy marker is rapidly degraded and that a cycle of autophagy associated with secretion of this cuticle has completed (Figure 4.7H and Figure 4.8K, L).

A similar pattern was observed during the embryonic development of the *vps-45* mutant IA888 strain. LGG-1 appears to be expressed in many tissues during the coma and two-fold stages of development, and it appears to be accumulating to higher levels in the seam cells once the embryo reaches the three-fold stage (Figure 4.9). It also appears that embryos from this mutant have higher levels of GFP overall in all stages. The GFP fluorescence is rapidly lost, once again, at the moment of hatching (Figure 4.9H).

Finally, in the case of the IA897 strain the overall levels of fluorescence were much higher than the other two strains. In this case to properly visualise the seam cell expression the exposure time was reduced by half from 200ms to 100ms. In a similar way to the previous strains, LGG-1::GFP accumulated to its highest levels in the three-fold stage. However, in

addition to the seam cell expression there is a general GFP fluorescence in other cells throughout much of the anatomy of the animal visible easily from the comma stage (and earlier, not shown). These cells were not formally identified but probably include other cells of the hypodermis (Figure 4.10). Additionally, after the eggs hatched the LGG-1::GFP did not quickly disappear but persisted for a time. Seam cells were clearly visible as the worm was exiting the egg shell, and the LGG-1::GFP marker could also be detected throughout the body of the animal (Figure 4.10H).

The results clearly indicate the accumulation of the LGG-1::GFP autophagy marker in the hypodermal seam cells at the three-fold stage in all strains. LGG-1::GFP is no longer detectable in the fluorescence microscopy used after the embryos hatch in both the wild type strain and *vps-45 (tm246)* mutant but is retained for longer in the *unc-51 (e369)* mutant strain post hatch. This is similar to its post-moult retention in larvae (section 4.4). Thus the activity of the Atg-1/UNC-51 kinase is required for the normal loss of the LGG-1::GFP autophagy marker immediately after cuticle synthesis (in the egg prior to hatch and after synthesis of the L2 cuticle at the L1 to L2 moult). These results are consistent with the hypothesis that cycles of autophagy degrade the autophagy marker LGG-1::GFP, and most likely normal LGG-1 also, at these developmental times. This strongly implicates a developmental cycle of autophagy being involved in converting the highly secretory seam cells during cuticle synthetic phases to their quiescent non-secretory forms in between cuticle synthesis phases.

Furthermore, it appears that *vps-45 (tm246)* and *unc-51 (e369)* mutants exhibit higher levels of expression than the wild type strain with the later one exhibiting the highest expression, something which is further investigated below (Section 4.8).

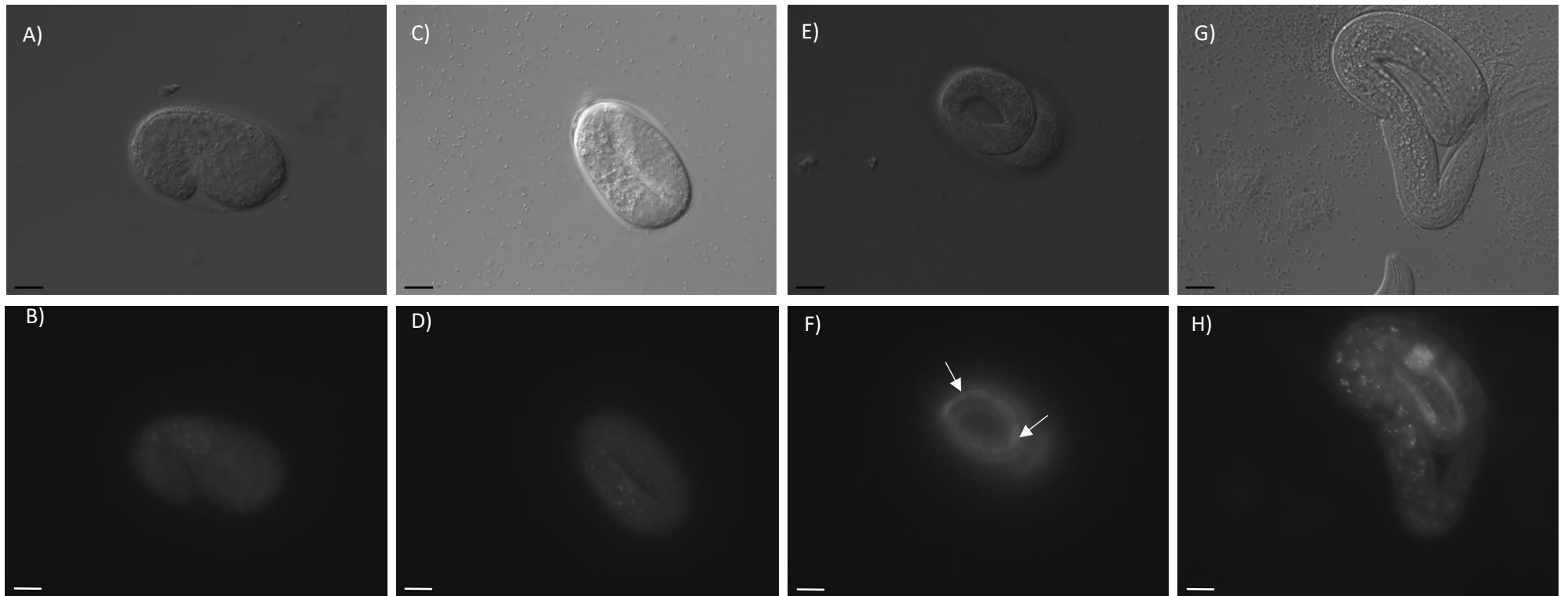


Figure 4.7: Representative images of DIC and UV (200ms) images of coma stage, two-fold and three-fold stage embryos along with hatching embryos of DA2123[*adIs2122 [lgg-1p::GFP::lgg-1 rol-6(su1006)]*] strain. 63x magnification. White arrows point to the seam cells. Scale bars represent 5 μm.

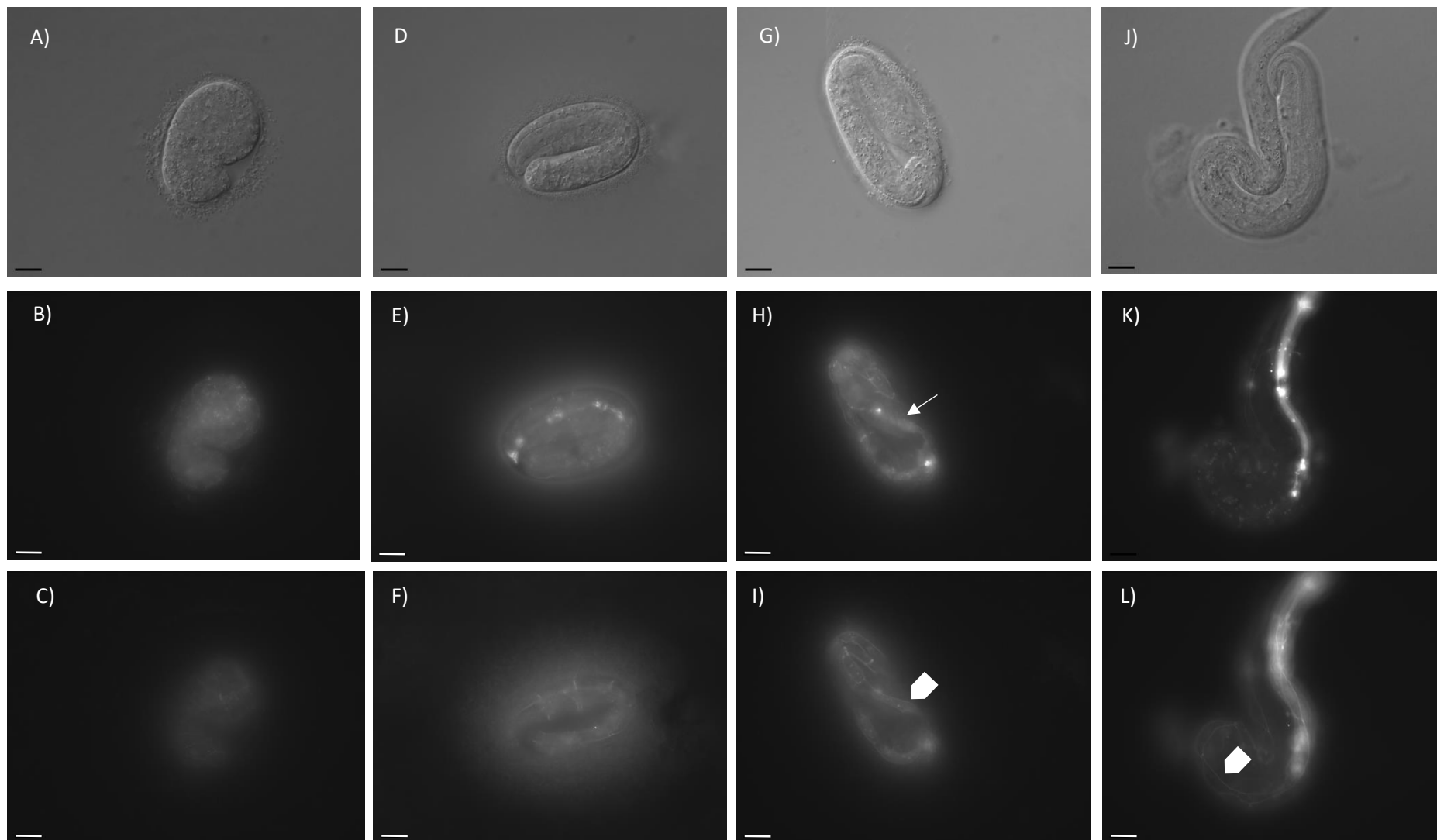


Figure 4.8: Representative images of DIC and UV (200ms) images of coma stage, two-fold and three-fold stage embryos along with hatching embryos of wild type IA903 [*adIs2122 [lgg-1p::GFP::lgg-1 rol-6(su1006)]; jclIs1 [ajm-1::GFP unc-29(+ rol-6(su1006)] IV*] strain. 63x magnification. Two focal points are shown. One focusing on the LGG-1::GFP marker (B,E,H,K) and one on the junctions visualised by the AJM-1::GFP marker (C,F,I,L). White arrows point to the AJM-1::GFP localising at the periphery of the seam cells. Arrow heads point to the LGG-1::GFP expressed in the cytoplasm of seam cells. Scale bars represent 5 μ m

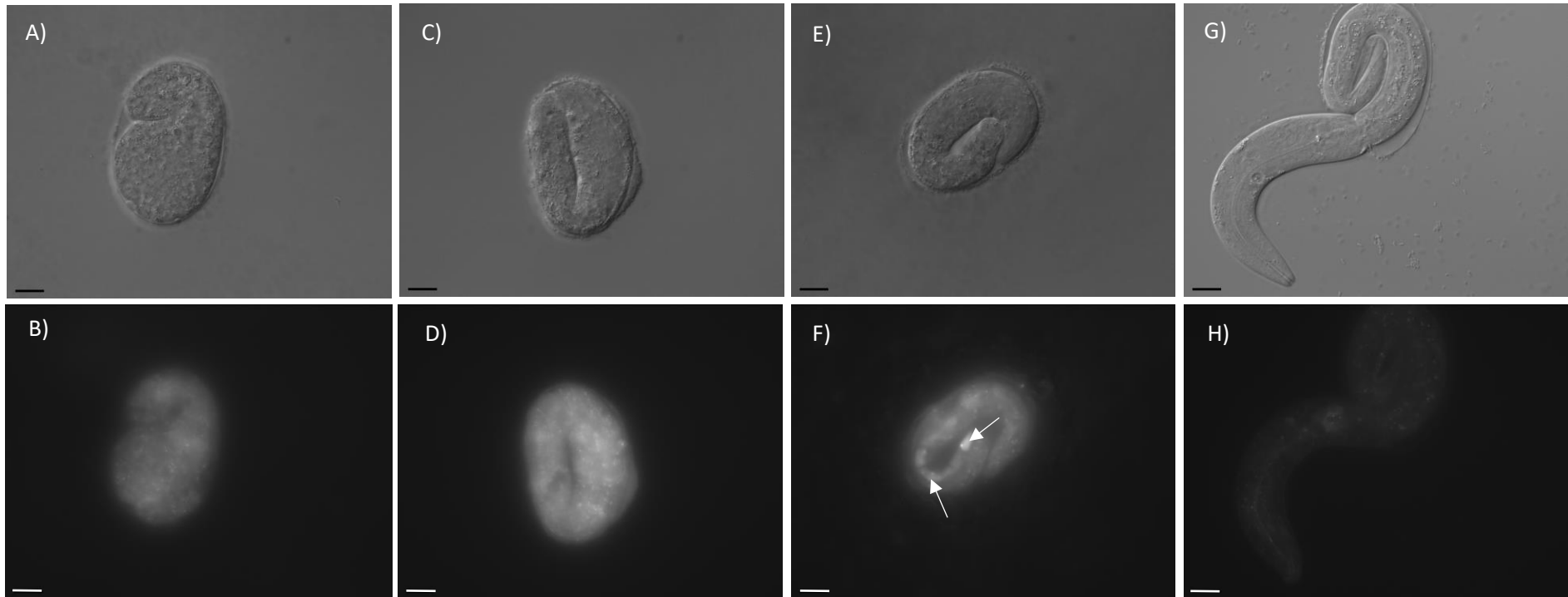


Figure 4.9: Representative images of DIC and UV (200ms) images of coma stage, two-fold and three-fold stage embryos along with hatching embryos of IA888 [*adIs2122 [lgg-1p::GFP::lgg-1 rol-6(su1006)]; vps-45 (tm246) X*] strain. 63x magnification. White arrows point to the seam cells. Scale bars represent 5µm.

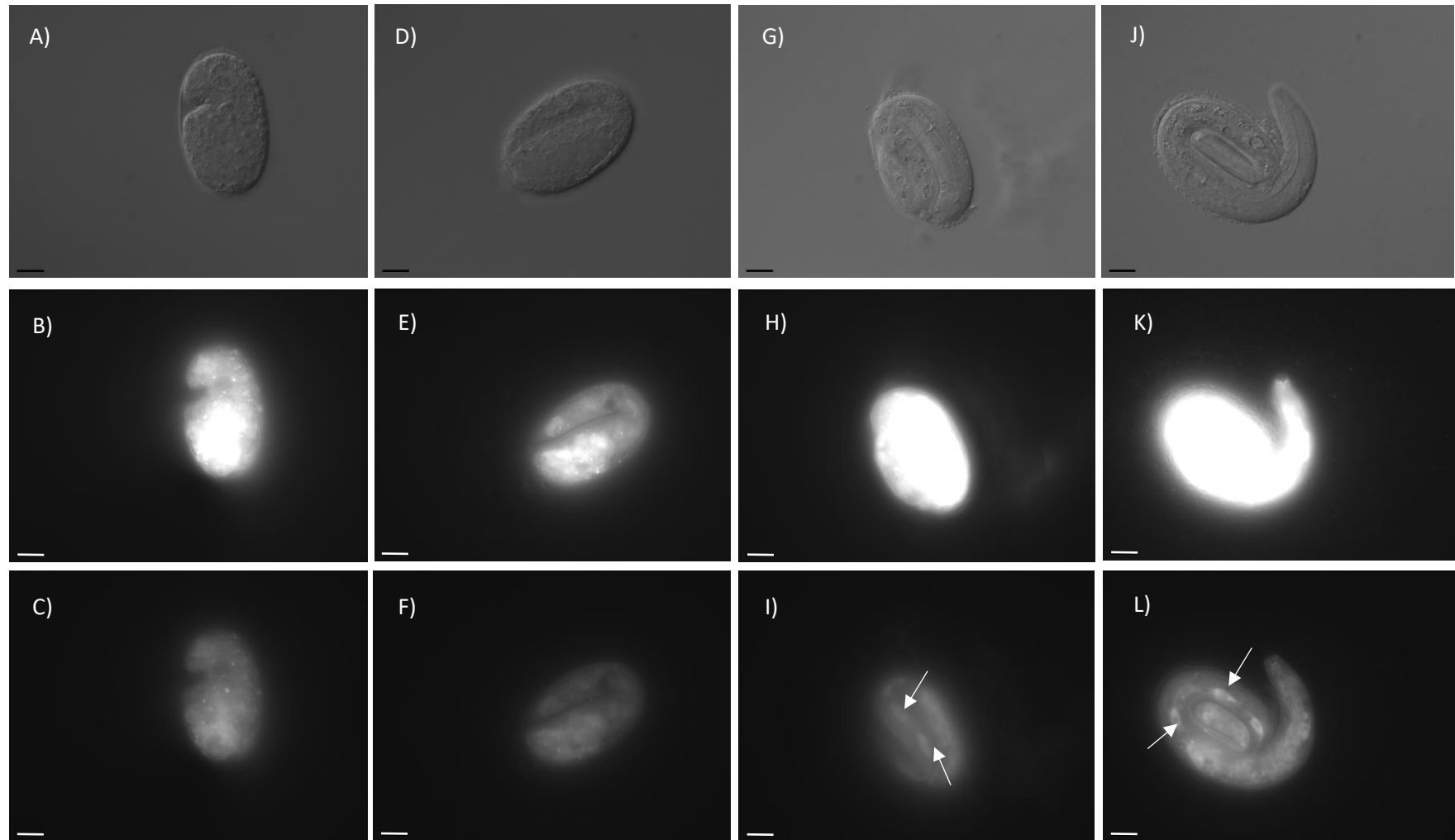


Figure 4.10: Representative images of DIC and UV (200ms & 100ms exposure) images of coma stage, two-fold and three-fold stage embryos along with hatching embryos of **IA897** [*adIs2122* [*lgg-1p::GFP::lgg-1 rol-6(su1006)*]; *unc-51* (*e369*) V] strain. 63x magnification. White arrows point to the seam cells. Scale bars represent 5 μ m.

4.7 LGG-1 expression in the seam cells and seam cell division are two distinct processes

In order to verify that autophagy in the seam cells is not induced as a result of the cell division and is associated with moult and the secretion of the cuticle, newly hatched L1 larvae were observed before the moult at the first seam cell division post hatch. DA2123, genotype *adIs2122 [lgg-1p::GFP::lgg-1 rol-6(su1006)]*, SU93, genotype *jcIs1 [ajm-1::GFP unc-29(+) rol-6(su1006)] IV* and IA903, genotype *adIs2122 [lgg-1p::GFP::lgg-1 rol-6(su1006)]; jcIs1 [ajm-1::GFP unc-29(+) rol-6(su1006)] IV*, embryos were picked at the three-fold stage, and were observed under the microscope until they hatched. Newly hatched animals were transferred clonally on NGM plates and five hours later were observed under the microscope. At this point the seam cells are undergoing their first division post hatch (Podbilewicz & White 1994; Shemer & Podbilewicz 2000). It was easy to visualise the dividing seam cells utilising the AJM-1::GFP marker. In all cases the LGG-1::GFP protein was never observed in the seam cells either in the DA2123 strain or the double marker IA903 strain. Consequently, the seam cell division and the LGG-1 accumulation during the *C. elegans* moult are two distinct processes (Figure 4.11).

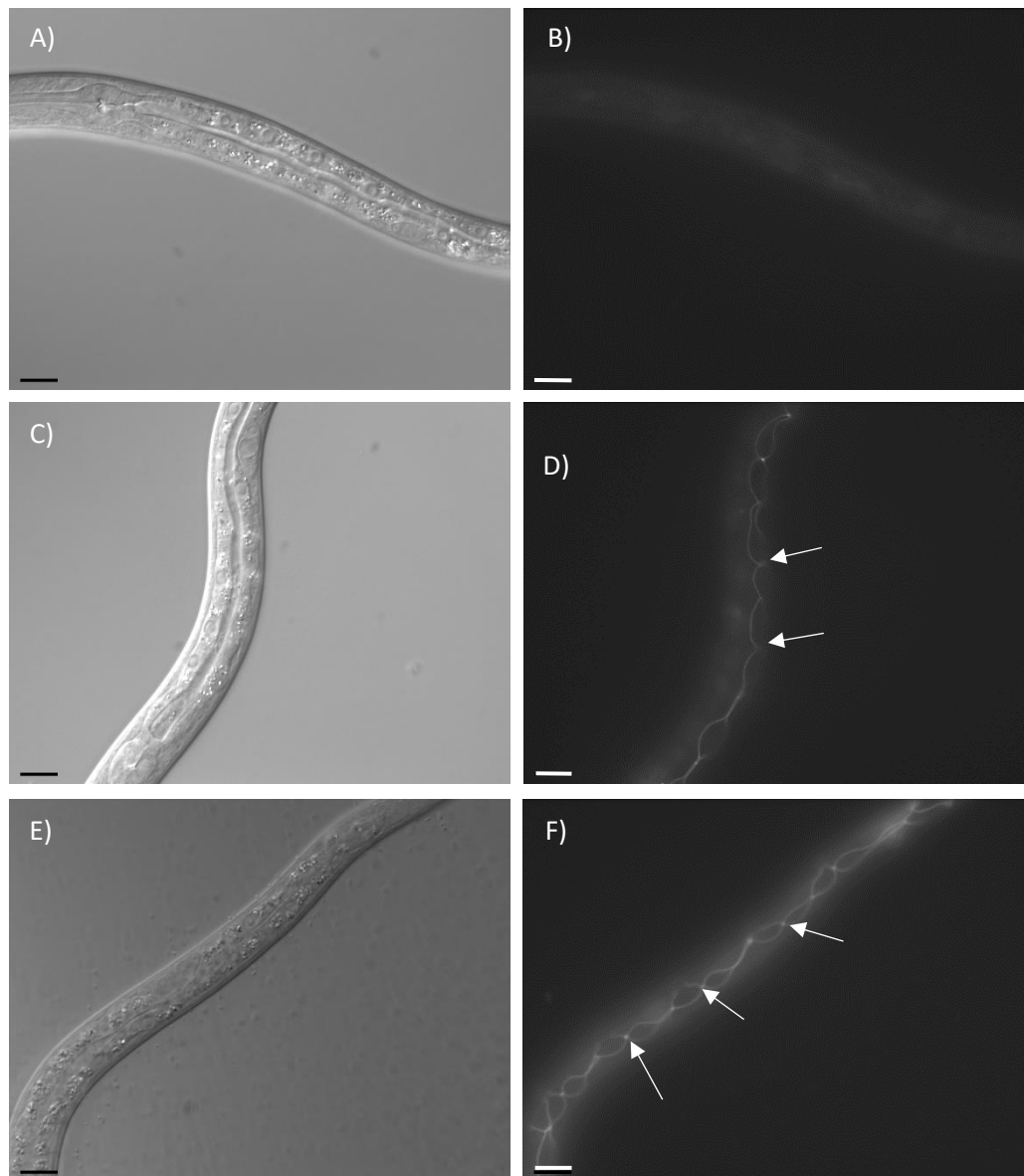


Figure 4.11: DIC and UV images of L1 larvae seam cells, 5 hours post hatching.

White arrow point to the dividing seam cells. A-B) DA2123 [*adIs2122 [lgg-1p::GFP::lgg-1 rol-6(su1006)]*] strain C-D) SU93 [*jcIs1 [ajm-1::GFP unc-29(+)] rol-6(su1006) IV*] strain E-F) IA903 [*adIs2122 [lgg-1p::GFP::lgg-1 rol-6(su1006)]; jcIs1 [ajm-1::GFP unc-29(+)] rol-6(su1006) IV*] strain. Scale bars represent 5 μm .

4.8 *vps-45 (tm246)* and *unc-51 (e369)* mutant embryos demonstrate higher levels of LGG-1 marker at the 3-fold stage

Due to the difference observed in the intensity of the LGG-1::GFP in the *unc-51 (e369)* and *vps-45 (tm246)* mutants in the previous experiments (section 4.6) as well as the differences in autophagy in moulting larvae (section 4.5) the total fluorescence of 10 embryos at the three-fold stage was quantified for the DA2123, IA888 and IA897 strains in order to quantify this visible difference in the corresponding mutant background. The method used to measure the total fluorescence was the one described in section 2.3.10 of Materials and Methods. The same exposure of 200ms was used when acquiring the pictures for all mutants. The *vps-45 (tm246)* mutant embryos showed slightly increased levels of LGG-1 fluorescence compared to the wild type. The difference was small but significant, with the wild type exhibiting an average fluorescence of 4.19×10^{10} and the *vps-45* mutant an average total fluorescence of 6.68×10^{10} . The *unc-51 (e369)* had a much higher total fluorescence of 2.23×10^{11} (Figure 4.12).

This method of quantification is simply a measure of total brightness of fluorescence per embryo measured, and hence will reflect a relative measure of abundance of LGG-1::GFP in each animal tested. It is not a count of LGG-1::GFP foci and hence not a measure of what is believed to be LGG-1 in its active state associated with autophagosomes. For technical reasons, it was not possible to accurately count foci in the embryos where 3-fold animals move constantly.

Therefore this measure will be influenced both by the amount of LGG-1::GFP synthesised in each animal versus its rate of decay/turnover. It is possible to speculate that in the case of loss of *vps-45* function where endosomal trafficking is believed to result in mistargeting of vesicles, that this might cause an increase in autophagy that is entirely independent of the proposed developmentally regulated one associated with the end of lethargus/moulting.

Despite not being able to count individual foci of GFP in the seam cells, and hence formation of autophagosomes it is easy to speculate that once again *vps-45 (tm246)* exhibits this increased fluorescence as a result of the increased demands for autophagy. By contrast, in the case of the *unc-51 (e369)* mutant the increase in LGG-1::GFP may be a result of the lack of turnover of LGG-1 by autophagy, as autophagy cannot be activated in the absence of the Atg1/UNC-51 kinase.

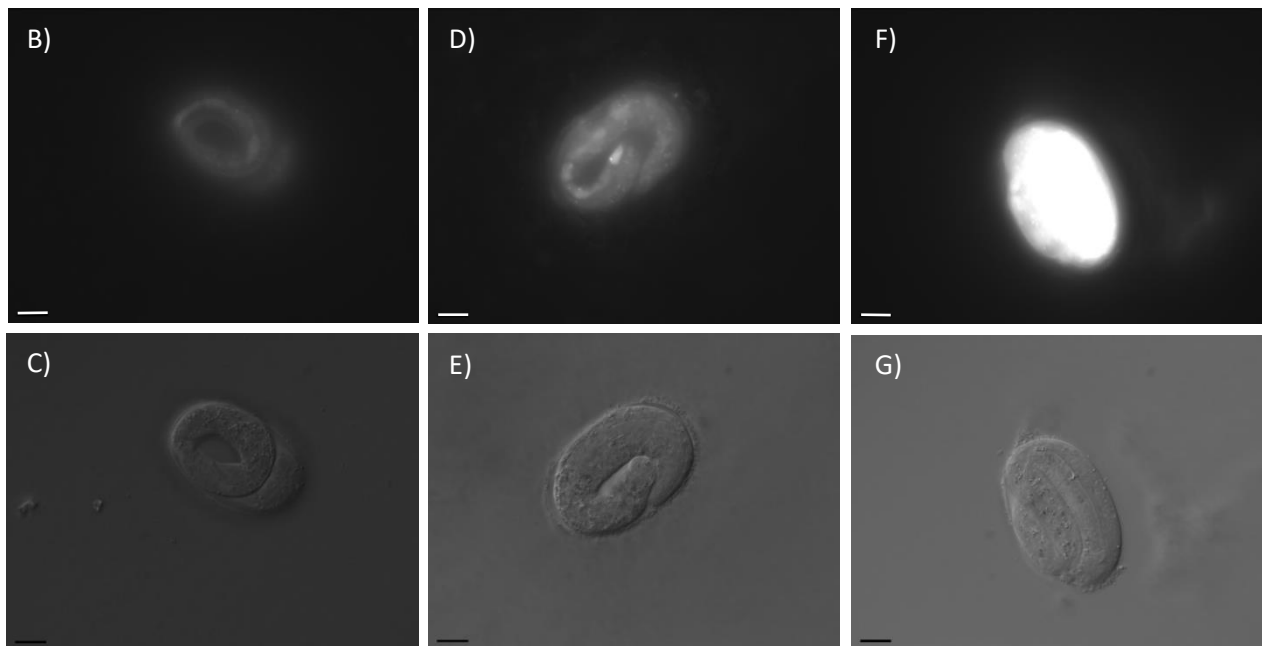
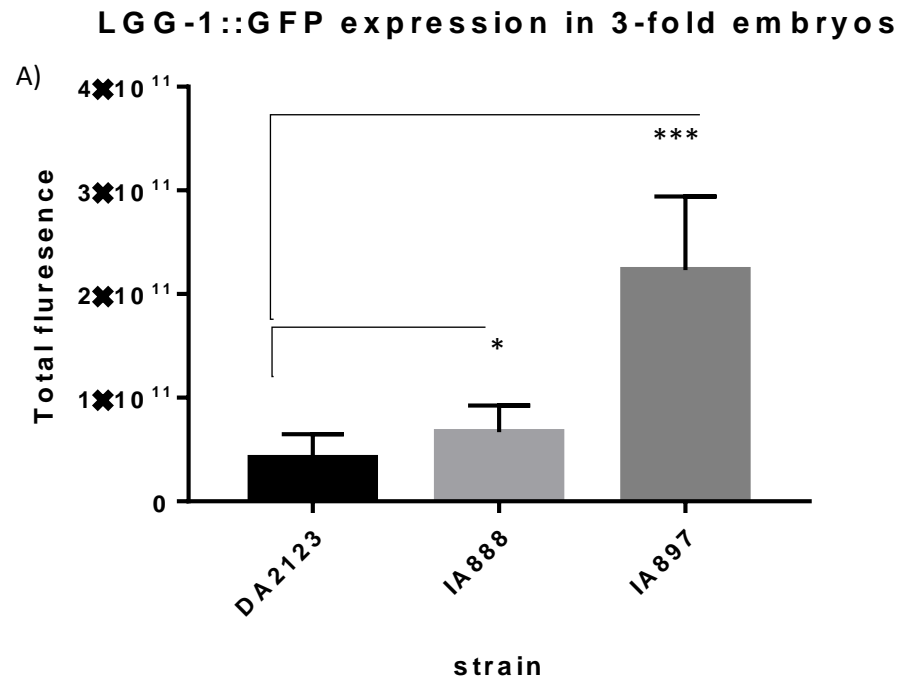


Figure 4.12: Total levels of LGG-1::GFP in 3 fold DA2123, IA888 and IA897 embryos

A) Average total fluorescence (\pm SD) in DA2123 [*adIs2122 [lgg-1p::GFP::lgg-1 rol-6(su1006)]*], IA888 [*adIs2122 [lgg-1p::GFP::lgg-1 rol-6(su1006)]; vps-45(tm246) X*] and IA897 [*adIs2122 [lgg-1p::GFP::lgg-1 rol-6(su1006)]; unc-51(e369) V*] three-fold stage LGG-1::GFP :transgenic embryos. DA2123 (n=27), IA888 (n=31), IA897 (n=16). Tukey's multiple comparisons test: DA2123 vs IA888 $P=0.0474$. DA2123 vs IA897, $P<0.001$. IA888 vs IA897 $P<0.001$. **B-C**) Representative images (UV, DIC) of

DA2123 three-fold stage embryos 63x, 200ms. **D-E**) Representative images (UV, DIC) of IA888 three-fold stage embryos 63x, 200ms. **F-G**) Representative images (UV, DIC) of IA897 three-fold stage embryos 63x, 200ms. Scale bar represent 100µm.

4.9 *vps-45 (tm246)* and *unc-51 (e369)* mutants exhibit higher levels of expression of the LGG-1 protein outside of the moult

To assess the levels of LGG-1::GFP in animals carrying the *vps-45 (tm246)* and *unc-51 (369)* mutant alleles outside of the lethargus/cuticle synthesis phases, the total body fluorescence of adult animals was measured (described in section 2.3.10) in the adult stage when all cuticle synthetic phases have terminated. Thus it is expected that any fluorescence will come from the LGG-1::GFP marker not associated with moulting and cuticle synthesis.

Measurements indicate that there is higher fluorescence in the *vps-45* and the *unc-51* mutants compared to the wild type. The *vps-45 (tm246)* mutant (IA888) had an average total fluorescence per area of 19.98 compared to 18.77 of the wild type (DA2123), a small but significant difference. The *unc-51 (e369)* mutant (IA897) on the other hand showed much higher levels of fluorescence at 37.57 (Figure 4.13).

The data presented above suggest that the *vps-45* and *unc-51* mutants express LGG-1 at higher levels compared to the wild type strain across a variety of tissues in their bodies after cessation of the repeating moulting cycles. Therefore, any expression of the LGG-1 marker and possibility autophagy, is not a result of the moulting process in this case. However, as previously discussed higher levels of LGG-1 do not necessarily indicate higher levels of autophagy (section 4.5). Therefore, it is possible that *vps-45 (tm246)* mutant exhibits higher levels of the LGG-1 protein (compared to the wild type) due to the higher requirements for autophagy to clear the aberrant membranes that are accumulating due to the defective endosomal trafficking which result in the accumulation of aberrant proteins that require the autophagic mechanism to clear them. The *unc-51 (e369)* mutant on the other hand, has high levels of diffuse protein which should correspond to the non-PE conjugated form of the protein that does not take part in the formation of the autophagosomes. It is therefore easy to conclude that there is a very low utilisation of the LGG-1 protein which does not get incorporated into autophagosomes and consequently, does not get degraded. This non-degraded LGG-1 remains in a diffuse state in several

tissues of the animals. Therefore, in the case of the LGG-1::GFP marker, it results in higher body fluorescence in the autophagy defective *unc-51* mutants. This is further supported by the results previously presented for *unc-51 (e369)* embryos (section 4.9) and the very reduced number of GFP foci in the seam cells of the same mutants during the molt (section 4.5).

A)

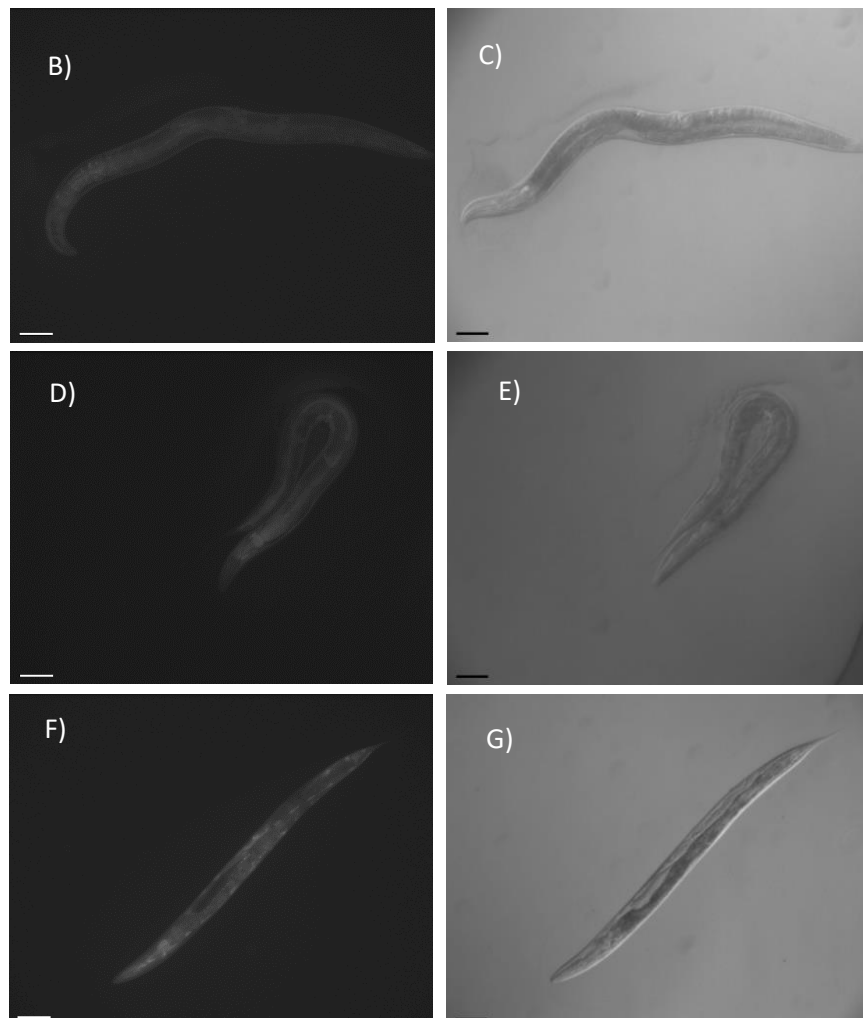
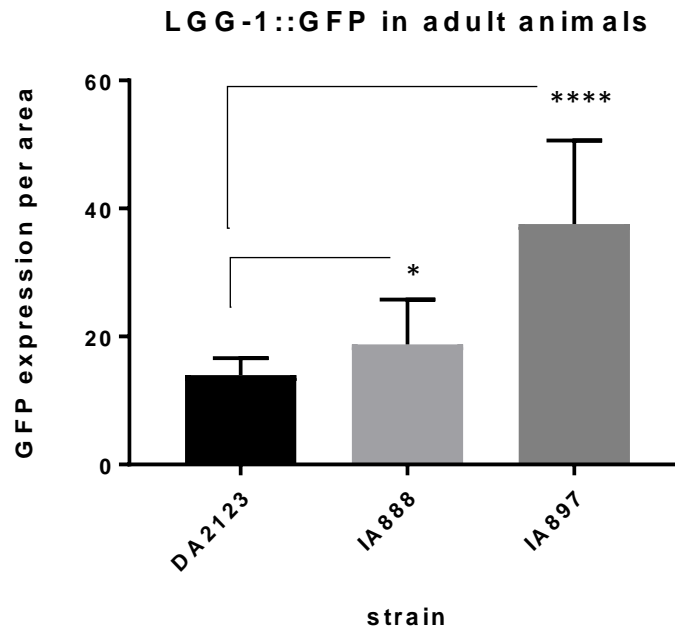


Figure 4.13: Overall levels of LGG-1::GFP in N2, IA888 and IA897 adult *C. elegans*.

A) Average GFP expression per area of animal body (\pm SD) in young. DA2123 (n=38), IA888 (n=45) and IA897 (n=47) animals. Tukey's multiple comparisons test: DA2123 vs IA888 $P=0.0434$. DA2123 vs IA897, $P<0.001$. IA888 vs IA897 $P<0.001$. **B-C)** Representative images (UV, DIC) of DA2123 adult worm 63x, 200ms. **D-E)** Representative images (UV, DIC) of IA888 adult worm 63x, 200ms. **F-G)** Representative images (UV, DIC) of IA897 adult worm 63x, 200ms. Scale bar represent 100 μ m (Previous page).

4.10 Chapter summary

In this chapter, a period of developmentally regulated autophagy associated with molting was identified in *C.elegans*. An increased expression of the LGG-1::GFP marker was identified in the seam cells, which are associated with the secretion of cuticular structures, during the moult (Section 4.3) and at the late stages of embryogenesis at the first secretion of the cuticle (Section 4.6). Autophagy appeared to be taking place near the end of the moult, supporting the idea for its requirement for the removal excessive membranes and secretory structures at the end of the highly secretory phase of the cells involved in the secretion of cuticular components (Singh & Sulston 1978). This was further supported by the fact that the Atg1/UNC-51 kinase is required for the developmental upregulation of autophagy in the seam cells at the later stages of the moult.

Interestingly, the *unc-51* mutant take 36 hours longer than wild type to proceed through four larval stages (Section 3.9) and associated moults to reach adult than the wild type. However, the moults only take at the most 1 hour longer than the wild type strain (Section 3.9, 4.3, 4.4), and hence most of that increase must be a result of the inter-moults lasting longer. This might fit with secretion of the new cuticle at each lethargus working almost normally, however a failure to clear out the secretory organelles etc. at the end of each secretory moult is perhaps hindering passage through the next non-secretory intermoult phase.

On the other hand, it was demonstrated *vps-45* (*tm246*) mutants which are defective for endosomal trafficking do not exhibit defects in the onset of autophagy during the moulting process. However, higher levels of autophagy were observed in these mutants (Section 4.4), suggesting that autophagy acts as the homeostatic mechanism for the clearance of aberrant membranes resulting from defective membrane fusions in the endosomal system. Furthermore, it was shown that *vps-45* mutants require approximately 8 hours to go

through the moult compared to approximately 4 hours for the wild type strain (Section 4.4), and according to previous data longer intermoult periods as well, however not to the same extent as the *unc-51 (e369)* mutants (Section 3.9) providing evidence for the requirement of the endosomal system predominantly for the regulation of moulting duration and secondly for the intermoult periods. Thus, although both the *vps-45* and *unc-51* mutants extend time taken for *C. elegans* to progress through larval development, loss of *vps-45* function primarily extends lethargus while loss of *unc-51* function primarily extends inter-moult periods.

Chapter 5: Investigating oxidative imbalances and resistance to oxidative stress in *unc-51 (e369)* and *vps-45 (tm246)* mutants

5.1 Overview and aims

Fibroblasts, bone marrow and neutrophils from patients carrying the homozygous T224N mutation in human VPS45 exhibit accelerated rates of apoptosis (Stepensky et al., 2013; Vilboux et al., 2013). The low cellular levels of human Vps45 bearing the T224N mutation (Vilboux et al., 2013) may directly result in perturbed delivery of protein cargo from the TGN to the endosomal pathway. Stepensky and colleagues (P Stepensky et al. 2013) suggested that, similar to the ELANE and G6PC3 variants of congenital neutropenia (Grenda et al. 2007; Boztug et al. 2009), Vps45 T224N may induce a block in the earlier secretory pathway, which in turn may lead to overwhelming endoplasmic reticulum (ER) stress and subsequent apoptosis. Hydrogen peroxide (H₂O₂) has previously been shown to induce ER stress and subsequent apoptosis in *S.cerevisiae* as a direct result of reactive oxygen species (ROS) accumulation (Madeo et al. 1999). Yeast cells harboring the analogous mutation in Vps45 (T238N) also exhibit increased apoptosis after exposure to H₂O₂ (Cowan 2014).

This potentially identifies a previously uncharacterised phenotype of Vps45, which is consistent with the apoptotic phenotype observed in neutrophil and fibroblast cells of patients affected by the Vps45 T224N variant of congenital neutropenia (P Stepensky et al. 2013; Vilboux et al. 2013). This apoptotic phenotype is not directly associated with the vacuolar protein sorting phenotype previously described for *vps* mutants (Cowles et al. 1994; Piper et al. 1994), it may however be a result of ER stress and by extension oxidative stress, as a result of aberrant vesicles accumulating as a result of defective membrane fusions (P. Stepensky et al. 2013). The mechanism by which Vps45 deficient mammalian cells and yeast expressing Vps45 T238N give rise to increased H₂O₂ sensitivity remains unclear, however it could be a result of the above mentioned oxidative stress. To obtain a better understanding of this increased sensitivity to oxidative stress in *vps-45* deficient cells and the underlying mechanism, *C. elegans* was employed as a multicellular system to study how *vps-45 (tm246)* mutant animals lacking a functional Vps45 protein react to oxidative stress. In this study a redox sensitive ER marker and three

well established oxidative stress GFP markers were used. Because of the genetic interaction (synthetic lethality) presented previously in Chapter 3 describing the *unc-51 (e369) V; vps-45 (tm246) X* double mutant, the *unc-51(369)* single mutant was also assessed for oxidative stress sensitivity and redox imbalances in the ER. Although the exact reason for synthetic lethality has not been identified, if loss of Vps45 causes defects in vesicle trafficking with aberrant targeting of vesicles from the TGN to the endosomal pathway, the synthetic lethality when ATG1/UNC-51 is also mutated could suggest that autophagy plays a critical role in viability of Vps45 mutant cells. It may be essential to remove and recycle components of the TGN, endosomes or ER where an excessive build-up of the wrong cargo has occurred in Vps45 mutants. Indeed, it is possible that autophagy plays a homeostatic role in the TGN/secretory system even in wild type cells. If so, loss of autophagy, particularly in highly secretory cells like neutrophils and *C. elegans* seam cells during cuticle synthesis, could potentially result in similar ER stresses and by extension oxidative stress, to that theorised to exist in neutrophil cells and previously suggested in *S. cerevisiae* (Cowan 2014) under loss of Vps45 function.

The synthetic lethality effect observed by the double mutant could potentially indicate the involvement of both *vps-45* and *unc-51* in the same broad cellular process and maintenance of a healthy secretory/TGN membranous network system would be an obvious possibility. Consistent with this suggestion, loss of Tlg2 function, which is the binding partner of Vps45, has previously been implicated with autophagy and more specifically in the recruitment of ATG9 to the PAS in yeast (Noda et al. 2000; Ohashi & Munro 2010; Nair et al. 2011).

Potential imbalances in the ER of the *vps-45 (tm246)* mutant, most likely towards an oxidised state could possibly address the sensitivity of *S. cerevisiae* to H₂O₂ derived oxidative stress (Cowan, 2014) and enforce the idea that neutrophil cells with a defective VPS-45 protein undergo apoptosis as a result of oxidative stress. Additionally, identification of similar oxidative sensitivity and/or imbalances in the *unc-51 (e369)* mutant could explain in part the synthetic lethality and developmental arrest of the double mutant as a result of an additive sensitivity. Finally, previously presented data (Section 3.9) indicate that both mutants exhibited a shorter lifespan compared to wild type strain, also possibly resulting from an oxidised state in the cells of the mutants.

5.2 The roGFP ER3 marker and its introduction in the *vps-45 (tm246)* and *unc-51 (e369)* mutant backgrounds

Previous work in our lab showed that yeast Vps45 mutants are more sensitive to oxidative stress (Cowan, 2014). An existing collaboration within our College was researching oxidative stress within the ER in *C. elegans* using a redox-sensitive GFP (roGFP) that was targeted to the ER. It was decided to make use of a reduction-oxidation sensitive green fluorescent protein marker (roGFP) to test for ER redox imbalance in both the *vps-45* and *unc-51* mutant *C. elegans*.

A roGFP marker is a redox sensitive biosensor which has two cysteine residues into the beta barrel structure of the GFP. This cysteine residues can form a reversible disulphide bridge, depending on the oxidation state, which alters the conformation of the protein and by extension alters the emission spectra of the protein (Hanson et al. 2004; Lohman & Remington 2008). The ratio of the emissions from these excitations at 390nm and 460nm (390:460) determines whether the environment is oxidising (higher ratio) or reducing (lower ratio) (van Lith et al., 2011).

In this study a variant of this marker, roGFP ER3 was used, provided by Prof. Tony Page (University of Glasgow). The marker was adapted by Dr. A. Winter (University of Glasgow). It was based on the sensors developed by Hanson et al. and Lohman et al. for expression in the ER, along with the appropriate folding mutations and was derived from a synthetic gene designed with *C. elegans* optimised codons. It is expressed in a pAW2 vector under the control of the *pdi-2* gene promoter (Figure 5.1) and it was shown that the presence of the sensor does not induce ER stress (A. Winter, personal communication).

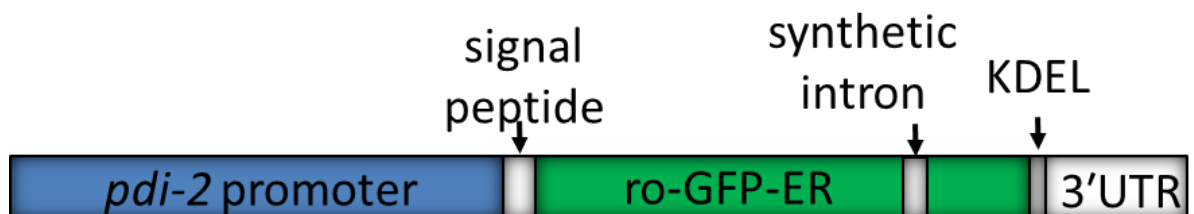


Figure 5.1: The roGFP ER3 marker

Schematic depicting the roGFP-ER3 construct for its expression in *C. elegans* (provided by Dr. Alan Winter).

The initial step for this investigation involved the introduction of the roGFP ER3 marker into the *vps-45* (*tm246*) and *unc-51* (*e369*) *C. elegans* mutants. The typical process of constructing double mutants was followed. TP198, genotype *kaIs6* [*pADW0083* (*pdi-2prom::roGFP-ER3::phy-1* + *unc-119(+)*)], male animals were crossed with hermaphrodites carrying the desired mutant allele, either with IA757, genotype *vps-45* (*tm246*), or CB369, genotype *unc-51* (*e369*). The ratio of hermaphrodites and male animals indicated if the crossing was successful. Heterozygotic hermaphrodites from the F1 generation, which carried the roGFP ER3 marker as observed under UV light, were clonally transferred into plates and left to egg lay. For *vps-45* (*tm246*) mutants, heterozygosity was verified via PCR using the same primers and method described previously on Chapter 3. For the *unc-51* (*e369*) heterozygosity in the F1 generation was verified via the presence of GFP positive animals, which were not Dpy Unc. The Dpy Unc phenotype is only present in homozygotic *unc-51* (*e369*) animals since the mutation is recessive.

Hermaphrodite F2 offsprings for each cross were then clonally transferred into new plates and left to breed. For the *vps-45* (*tm246*) mutants the F2 parents were lysed and homozygosity for the *vps-45* (*tm246*) allele was assessed through PCR. This was also confirmed in subsequent generations by 100% molting death phenotype at 25°C. The lines were further tested for homozygosity of the roGFP ER3 marker. Only lines which originated from parents which produced 100% GFP positive offspring were kept, confirming homozygosity.

For the *unc-51* (*e369*) mutant, F2 parents which displayed the *unc-51*(*e369*) DpyUnc phenotype and were GFP positive were selected. Homozygosity for the roGFP ER3 marker was assessed as described above.

As such two new strains were constructed, IA881, genotype *kaIs6* [*pADW0083* (*pdi-2prom::roGFP-ER3::phy-1* *unc-119(+)*)];*vps-45* (*tm246*) X and IA880, genotype *kaIs6* [*pADW0083* (*pdi-2prom::roGFP-ER3::phy-1* *unc-119(+)*)];*unc-51* (*e369*) V.

In all cases in order to verify the presence and expression of the roGFP ER3 marker protein, in the strains whole worms-lysates were prepared for SDS-page as described in the materials and methods section 2.3.22.1. Non-reducing and reducing samples were prepared from each lysate for each strain (TP198, IA880, IA881) as well as for the GFP negative N2 wild type strain. In all cases under the reducing conditions only the reduced state of the protein was detected at approximately 30kDa. By contrast in the non-reducing conditions two bands were detected at ~30kDa for the reduced form (no disulphide bond formation)

and around 27kDa for the oxidised form (disulphide bond formation). Thus, the redox sensor was expressed and was functional as a sensor in *C. elegans* in the wild type strain and in the two mutant backgrounds (Figure 5.2).

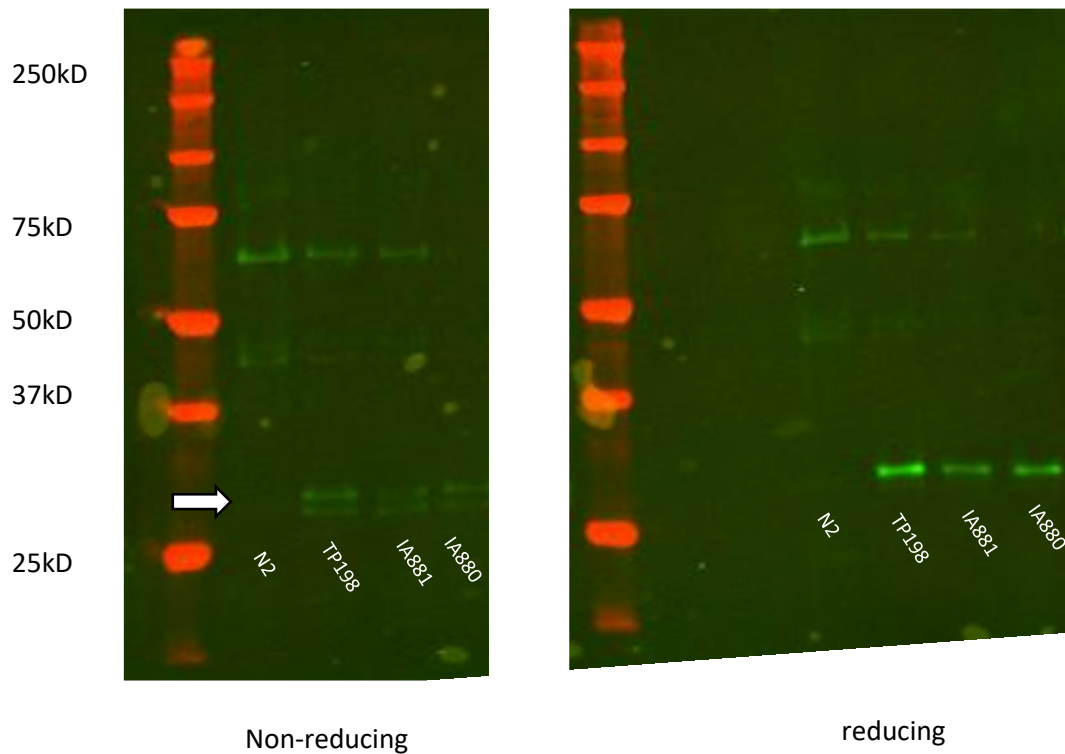


Figure 5.2: Western blot of roGFP ER3 protein resolved on a 10% tricine gel.

The roGFP can be detected in all transgenic strains (TP198, IA881, IA880) and not on the wild type strain (N2 just above 25kDa). Both versions of the marker can be detected in the non-reduced samples, at non-reduced (two bands) and reduced (single band) forms shown.

5.3 The roGFP ER3 marker can detect changes in ER redox state in *C. elegans*

The roGFP ER3 marker was employed in order to investigate the oxidation state of the ER in *vps-45* (*tm246*) and *unc-51* (*e369*) mutant backgrounds by measuring the fluorescence of the different states of the marker in the animals on a plate reader. Animals, were synchronised to the L4 stage on petri dishes and were then added on each well and measured as previously described on section 2.3.6.3 and 2.3.18. The corresponding GFP negative strains were used for normalisation purposes, more specifically the N2, IA757 and

CB369 strains. The value obtained from the GFP negative animals was subtracted in each case from the corresponding animals expressing the roGFP ER3 marker.

To verify that the marker can detect redox changes in the ER of *C. elegans* cells a positive control experiment was carried out using RNAi of the *ero-1* gene. ERO-1 is an oxidoreductase involved in the formation and isomerisation of disulphide bonds in the ER. As such disruption of the *ero-1* gene can inhibit the formation of disulphide bonds, resulting in a more reducing environment within the ER (Pollard et al. 1998; Harding et al. 2003). For this experiment, the wild type roGFP ER3 marker strain TP198 was used. Two cultures were prepared, a standard culture without RNAi and one delivering RNAi of the *ero-1* gene by the bacterial feeding method as described in materials and methods (section 2.3.6). The plate reader would produce a 390nm:460nm emission ratio. Emission from the 390nm excitation corresponded to the oxidised state of the protein, whereas emission from the 490nm excitation corresponded to the reduced state of the protein (Section 2.3.18). The TP198 strain fed on OP50 *E. coli* had a 390:460 emissions ratio of 0.74 compared with 1.05 for the same strain fed on the RNAi *E. coli* strain HT115 carrying the empty RNAi vector. *C. elegans* fed HT115 *E. Coli* instead of the OP50 strain have been shown to have altered metabolism, including faster development and higher consumption of oxygen (Xiao et al. 2015). The exact reason for this difference in measured redox state in the ER is not known, but it might relate to such differences.

That growth on OP50 results in a different measured ER redox state than growth on the RNAi *E.coli* strain HT115, means that growth on OP50 cannot be used as a control in these experiments. The empty vector HT115 data was therefore used as a control for the RNAi experiments. Animals fed with the *ero-1* RNAi exhibited a ratio of 0.55 compared to 0.74 for the empty vector HT115 fed animals, approximately a 35% reduction (Figure 5.3).

The reduction obtained when the *C. elegans* were fed with *ero-1* RNAi expressing HT115 when compared to the empty vector proves that the method is working. Thus, successful use of this redox marker was verified and the results constitute a positive control for the later experiments.

Experiments to test the ER oxidation environment of *vps-45* and *unc-51* mutants, were performed and compared to the wild type strain. For the TP198 and IA881 strains L4 animals were added on each well and measured. In the case of the IA880 strain, obtaining synchronous cultures at the L4 stage was not possible, since the mutant grows asynchronously (Section 3.9) and thus a mixture of animals of different developmental

stages was obtained, the vast majority of which were at the L3 or L4 stages. In the first set of experiments, all strains were cultured at 15°C. The choice of this temperature was based on it being the permissive temperature for culture of the *vps-45* (*tm246*) mutant and identical conditions for all strains being tested was desired. A slightly more reduced condition was observed in the *vps-45* mutant in strain IA881 relative to the parental roGFP ER3 marker strain TP198 with average ratios of 1.11 for TP198 and 0.91 for IA881, however this is not significant ($p=0.2$). A greater difference was measured in the *unc-51* mutant strain IA880 with a ratio of 0.72. In this case the difference with TP198 has greater significance ($p=0.009$). Thus, it is probable that the ER in the *unc-51* mutant has a significantly more reduced state than in the wild type when animals are cultured at 15°C.

All the strains were further tested after a period of culture at 25°C which is the non-permissive temperature for the *vps-45* (*tm246*) moulting death phenotype. There is relatively little measured difference in the behaviour of the wild type strain TP198 at 25°C with a ratio of 0.96 compared to 1.11 at 15°C (Figure 5.5 A and B). However, both mutant strains show a shift towards a more oxidised state at the higher temperature. With 25°C culture, the *vps-45* mutant strain IA881 has a 390nm:460nm ratio of 1.37 compared to 0.91 at 15°C (Figure 5.4 A and B). With 25°C culture, the *unc-51* mutant strain IA880 has a ratio of 0.99 compared to 0.72. when cultured at 15°C (Figure 5.3 A and B).

Overall, it appears that the *vps-45* mutant exhibits an ER environment similar to the wild type at the permissive temperature for the moulting death phenotype, whereas the *unc-51* mutant has a reduced environment under the same culturing conditions. By contrast when the temperature was shifted to 25°C, the *vps-45* mutants exhibited an oxidised environment in the ER compared to the wild type. The *unc-51* mutant exhibited a similar ER redox state to the wild type at 25°C, but there is a shift in an oxidising direction relative to when it is grown at the lower temperature of 15°C. Thus, while redox state of the wild type strain is not substantially influenced by temperature going from 15°C to 25°C culture, both the *vps-45* and *unc-51* mutants altered in the direction of increased oxidation at the higher temperature relative to their state at the lower culture temperatures.

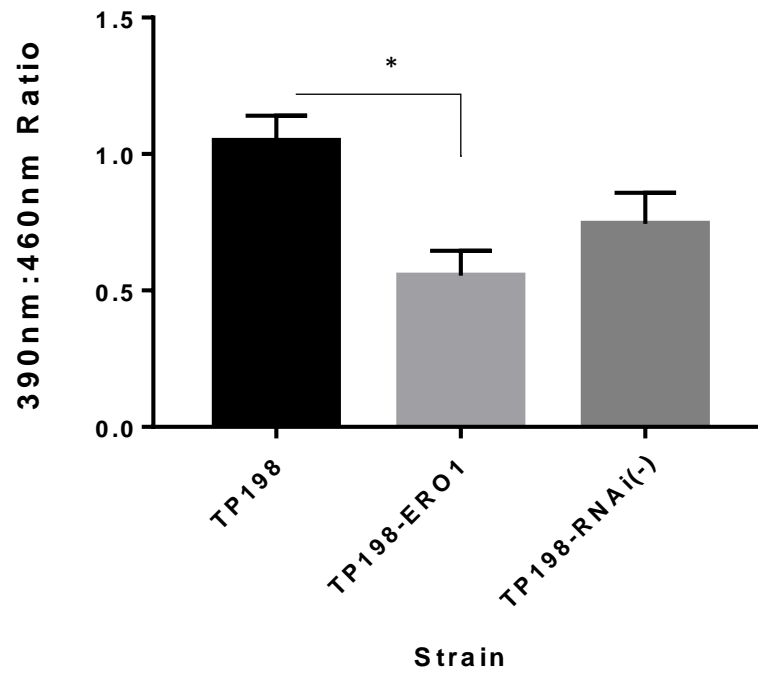
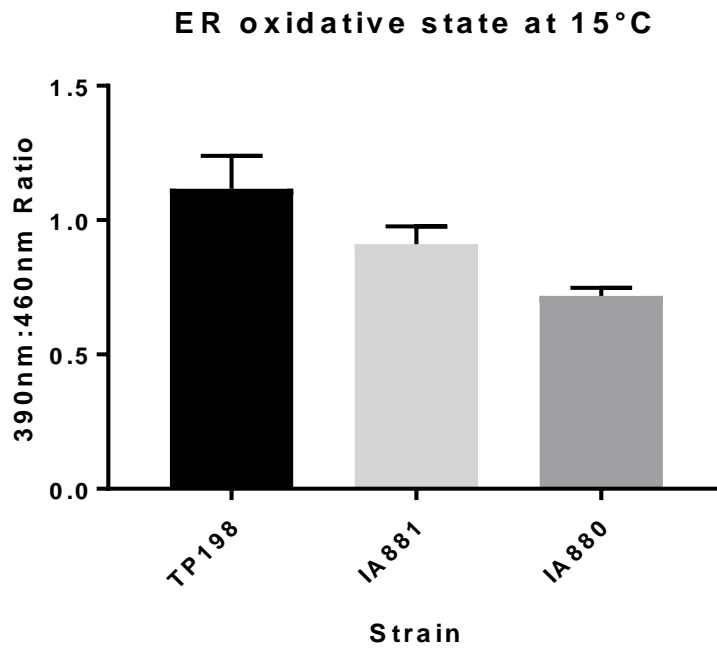


Figure 5.3: Test of roGFP ER3 oxidation state in *C. elegans* .

390:460 ratios (\pm SEM) for the wild type roGFP ER3 expressing strain, TP198 (n=3), the wild type roGFP ER3 expressing strain under the effect of *ero-1* RNAi, TP198 ERO1 (n=3) and the wild type roGFP ER3 expressing strain under the effect of the empty vector RNAi TP198-RNAi (-), (n=3). Lower ratios represent a more reduced state in the ER. Tukey's multiple comparisons test. TP198 vs TP198 ERO1 p=0.0248, TP198 vs TP198 RNAi (-), p=0.29. TP198 ERO1 vs TP198 RNAi (-), p=0.83.

A)



B)

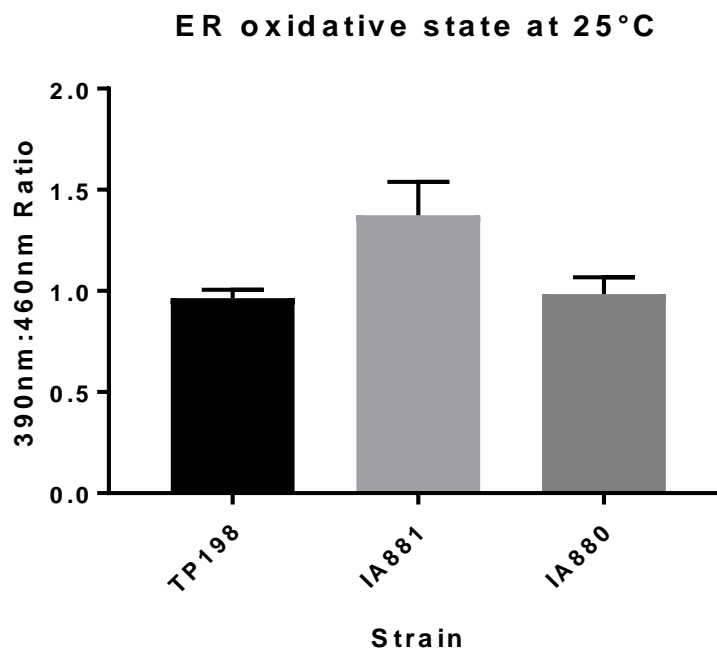


Figure 5.4: roGFP ER3oxidation state in TP198, IA881 and IA880 strains.

390nm:460nm ratios (\pm SEM) for TP198, IA881 and IA880. Lower ratios represent a more reduced state in the ER. **A)** *C. elegans* cultured at 15°C, TP198 (n=9), IA881 (n=10) and IA880 (n=8). Tukey's multiple comparisons test. TP198 vs IA881 p=0.2, TP198 vs IA880 p=0.009, TP198 vs IA880 p=0.26 **B)** *C. elegans* cultured at 15°C and then stressed at 25°C for 12 hours, TP198 (n=6), IA881 (n=4) and IA880 (n=3). Tukey's multiple comparisons test. TP198 vs IA881 p=0.02, TP198 vs IA880 p=0.98, TP198 vs IA880 p=0.07. Comparison with p values >0.05 are considered significant.

5.4 Assessing the survival of *vps-45 (tm246)* and *unc-51 (e369)* mutants under oxidative stress

The results in the previous section indicated that both the *vps-45 (tm246)* and *unc-51 (e369)* mutants under certain conditions of temperature culture behaved differently than wild type in measured ER redox state. As a next step, the sensitivity of the *vps-45 (tm246)* and *unc-51 (e369)* mutants to oxidative stress by exposure to hydrogen peroxide was assessed. Strains were treated with H₂O₂ and their viability was scored at 25°C.

Initially, a range of concentrations from 0mM to 5mM and an exposure period of 4 hours were tested on wild type early adults to identify at which concentration H₂O₂ stress should be carried out. The number of alive animals was scored hourly.

A very small number of animals died at 0mM of H₂O₂ concentration and at 4 hours 98.4% of the original inoculate was still alive. Very similar lethality was observed at 0.1mM, 0.5mM and 1mM with approximately 80% of the animals surviving after 4 hours. More specifically, at 0.1mM 79.2% of the original inoculate was still alive, at 0.5mM 81.7% and finally at 1mM 77.8%. At 5mM higher lethality was observed with only 35% of the animals surviving after 4 hours of exposure (Figure 5.5).

Based on the results obtained for the wild type strain N2, the 5mM and 1mM concentrations were chosen to be tested on the mutant strains; 5mM gave over 50% death with wild type and 1mM approximately 20%, representing “strong” and “mild” stress respectively.

With 1mM H₂O₂, the *vps-45* mutant (IA757) exhibits similar sensitivity to oxidative stress to the wild type strain (Figure 5.6A). More specifically the median survival for both strains was 2 hours, and a very similar percentage of surviving animals from each population after the 4-hour mark, a 33.3% for the wild type strain, and 30.7% for the IA757 strain. With exposure to 5mM H₂O₂ the *vps-45* mutant IA757 strain demonstrated the same median survival to wild type at 3 hours, however the percentage of surviving animals after 4 hours of exposure was lower for IA757, at 8.2% percent of the total population compared to 15.8% for the wild type strain (Figure 5.6B). However, this strain also exhibited some death in the assay without addition of H₂O₂ with 7.9% and 7% dying after 4 hours in the 1mM and 5mM experiments. Therefore, not all of the additional death in the *vps-45* mutant

at 4 hours exposure can be attributed to the H_2O_2 and it is concluded that no evidence was found indicating an increased sensitivity to H_2O_2 for the *vps-45* mutant.

By contrast, the *unc-51* mutant strain did display sensitivity to exposure to H_2O_2 in this assay. With 1mM H_2O_2 the *unc-51* mutant CB369 strain exhibited a much lower survival with a median of 1 hour and only 11.1% of the total population surviving after 4 hours. With 5mM H_2O_2 1.4% of the total population survived to the end of the 4 hour period (Figure 5.6).

Survival of wild type *C.elegans* under H_2O_2

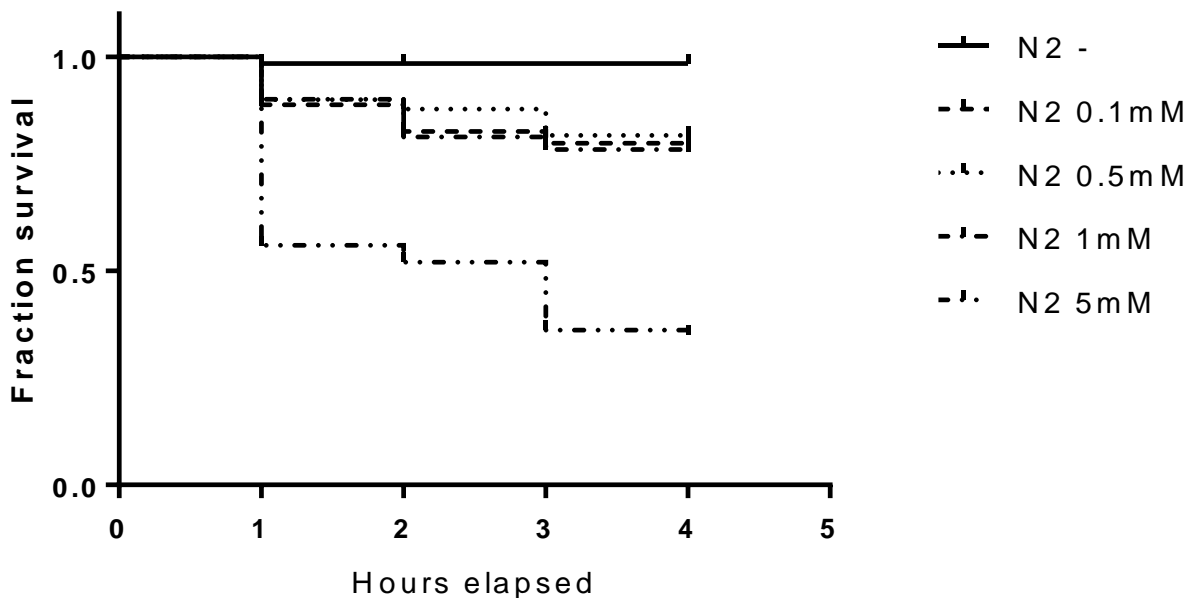


Figure 5.5: Survival fractions of wild type *C. elegans* over 4 hour time period under the influence of 0, 0.1, 0.5, 1 and 5mM hydrogen peroxide.

Survival was scored hourly. N2 -, n=181. N2 0.1mM, n= 180. N2 0.5mM, n=180. N2 1mM, n=171. N2 5mM, n=201. Log rank test for comparison of the curve. N2 vs N2 0.1mM, $p < 0.0001$. N2 vs N2 0.5mM, $p < 0.0001$. N2 vs N2 1mM, $p < 0.0001$. N2 vs N2 5mM, $p < 0.0001$. N2 0.1mM vs N2 0.5mM, $p = 0.5224$. N2 0.1mM vs N2 1mM, $p = 0.22$. N2 0.1mM vs N2 5mM, $p < 0.0001$. N2 0.1mM vs N2 0.5mM, $p = 0.055$. N2 0.5mM vs N2 5mM, $p < 0.0001$. P values < 0.006 are considered significant as determined by the Bonferroni method for significance threshold determination

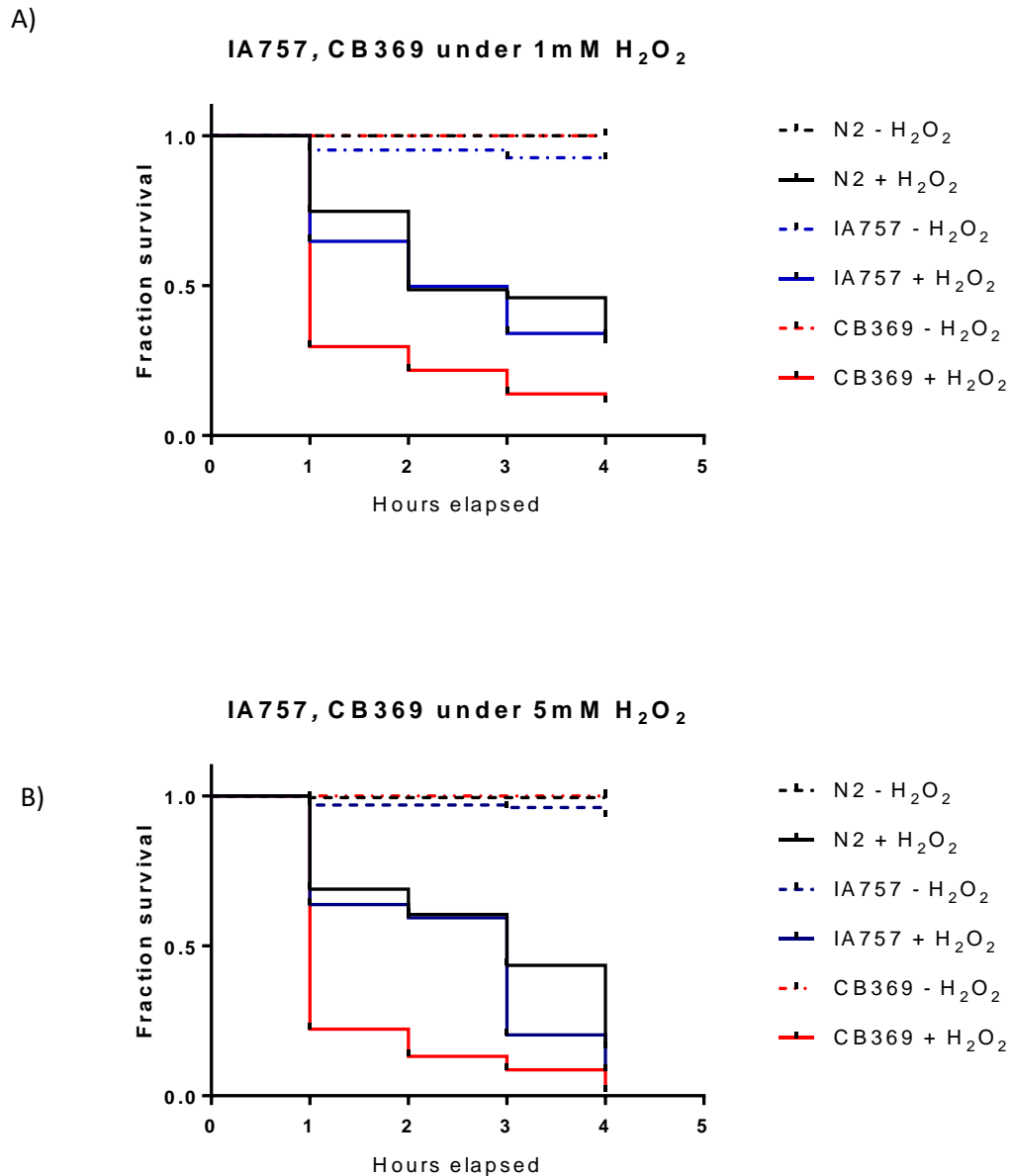


Figure 5.6: Survival fractions of N2, IA757 and CB369 *C. elegans* over a 4 hour time period under the influence of 1mM and 5mM hydrogen peroxide

A) Animals were incubated with 1mM H₂O₂ (+) or without H₂O₂ (-) for 4 hours. Survival was scored hourly. N2 - n= 188. N2 +, n=232. IA757, n= 189. IA757 +, n= 179. CB369, n= 206. CB369 +, n= 225. Log-rank test for comparison of the curves N2- vs N2+, p<0.0001. IA757 - vs IA757 +, p<0.0001. CB369- vs CB369 +, p<0.0001. N2- vs IA757-, p=0.0016. N2- vs CB369-, p>0.9999. IA757- vs CB369-, p<0.001. N2+ vs IA757+, p <0.0001. N2+ vs CB369+, p <0.0001. IA757+ vs CB369+, p <0.0001. **B)** Animals were incubated with 5mM H₂O₂ (+) or without H₂O₂ (-). Survival was scored hourly. N2 - n= 130, N2 +, n=181, IA757, n= 189, IA757 +, n= 182, CB369, n= 206, CB369+, n= 221. Log-rank test for comparison of the curves N2- vs N2+, p<0.0001. IA757 - vs IA757 +, p<0.0001. CB369- vs CB369 +, p<0.0001. N2- vs IA757-, p=0.0017. N2- vs CB369-, p= 0.286. IA757- vs CB369-, p<0.001. N2+ vs IA757+, p = 0.0066. N2+ vs CB369+, p <0.0001. IA757+ vs CB369+, p <0.0001. P values <0.006 are considered significant as determined by the Bonferroni method for significance threshold determination.

5.5 Assessing the oxidative response of *vps-45 (tm246)* and *unc-51 (e369)* mutants under oxidative stress

To assess if there is any difference in as the magnitude of the response to oxidative stress by the *vps-45 (tm246)* and *unc-51 (e369)* mutants, a set of GFP reporters were utilised. The reporter genes that were used are GCS-1::GFP, GST-4::GFP and finally SOD-3::GFP. The corresponding strains carrying the transgenes were: LD1171, genotype *ldIs3 [gcs-1p::GFP rol-6(su1006)]*, CL2166 with genotype *dvIs19 [(pAF15)gst-4p::GFP::NLS] III* and finally CF1553 with genotype *muIs84 [(pAD76) sod-3p::GFP rol-6(su1006)]*.

Gamma-glutamylcysteine synthetase (GCS) catalyse the first step in the biosynthesis of glutathione (GSH). *gcs-1* is the *C. elegans* orthologue of GCS, and the production of GSH result in the inactivation of hydrogen peroxide (H₂O₂) through the action of glutathione peroxidase, and the production of glutathione disulphide (GSSG) and water (H₂O) (Schulz et al. 2000).

GST-4 on the other hand, is part of the glutathione-s-transferase group of enzymes, or GSTs. GSTs can metabolize xenobiotics; superoxide anion and hydrogens peroxide among others. GSTs can conjugate reduced GSH with other toxic compounds. GST genes are upregulated in response to oxidative stress such as increased exposure to H₂O₂ or paraquat (Hayes et al. 2005; Nebert & Vasiliou 2004; Hoeven et al. 2011).

Finally, there is the superoxide dismutase (SOD) family of enzymes. SOD enzymes are responsible for the conversion of superoxide species to hydrogen peroxide which in turn is converted to water by catalases (Fridovich 1995). Superoxide dismutase-3 (SOD-3) in particular, is a manganese superoxide dismutase. Data have supported a role in maintaining oxidative balance in the extracellular matrix and in the nucleus (Oury et al. 1996; Ookawara et al. 2002). It is theorised, that its function promotes normal lifespan in worms, however its loss has not been shown to reduce longevity (Samuelson et al. 2007). Activity of *sod-3* is affected via *daf-2* signalling, which is homologous to *igf1* (insulin growth factor-1) and regulates longevity in *C. elegans* (Finch & Ruvkun 2001) and mediates metabolism and expression of free radical detoxification enzymes across multiple organisms (Honda & Honda 1999; Finch & Ruvkun 2001; Garofalo 2002; Holzenberger et al. 2003). Decreased *daf-2* signalling causes dephosphorylation and subsequently nuclear

localisation of DAF-16 transcription factor (Lee et al. 2001). Two DAF-16 binding sites are contained on the *sod-3* gene. Decrease in insulin/IGF-1 signalling results in *daf-16* upregulation of *sod-3*. Many of the genes involved in the lysosomal vesicular trafficking are also necessary extension of *C. elegans* lifespan as a result of decrease in insulin/IGF-1 signalling. Furthermore, the same genes are involved in the induction of *sod-3*. More specifically all five subunits of the ESCRT complex (CD4.4, C27F2.5, F1741.8, Y654.3 and T27F7.1) an essential component of the endosomal system (Samuelson et al. 2007). Additionally, data have also suggested that *sod-3* can also be regulated via the NRF2 pathway in breast cancer cells and consequently it is possible that in *C. elegans* it is regulated by SKN-1 similar to Phase II enzymes such as GST-4 and GCS-1 (An & Blackwell 2003; Singh & Bhat 2012; Blackwell et al. 2015).

All 3 of the reporter gene were tagged with GFP. The reporters were introduced to the IA757 and CB369 strains by crossing the GFP carrying strains LD1171, genotype *ldIs3* [*gcs-1p::GFP rol-6(su1006)*], CL2116, genotype *dvIs19* [(*pAF15*)*gst-4p::GFP::NLS*] III, and DA2123, genotype *muIs84* [(*pAD76*) *sod-3p::GFP rol-6(su1006)*] with the *unc-51* (*e369*) and *vps-45* (*tm246*) mutants as previously described for the roGFP ER3 marker (section 5.2). Thus, the following strains were created.

- IA887, genotype *muIs84* [(*pAD76*) *sod-3p::GFP rol-6(su1006)*]; *vps-45* (*tm246*) X
- IA896, genotype *muIs84* [(*pAD76*) *sod-3p::GFP rol-6(su1006)*]; *unc-51* (*e369*) V]
- IA890, genotype *dvIs19* [(*pAF15*) *gst-4p::GFP::NLS*] III; *vps-45* (*tm246*) X
- IA899, genotype *dvIs19* [(*pAF15*) *gst-4p::GFP::NLS*] III; *unc-51* (*e369*) V
- IA889, genotype *ldIs3* [*gcs-1p::GFP rol-6(su1006)*]; *vps-45* (*tm246*) X
- IA898 strain, genotype *ldIs3* [*gcs-1p::GFP rol-6(su1006)*]; *unc-51* (*e369*) V

L4 synchronised larvae were exposed to 1mM of hydrogen peroxide for 1 hour. They were subsequently washed with S-basal prior to mounting on a glass slide with sodium azide to anesthetize them. Pictures were acquired through the fluorescent microscope with 200ms exposure times in all cases. This permitted a direct comparison of intensities of fluorescence between different strains and conditions tested. Whole animal fluorescence was quantified using the ImageJ software.

The SOD-3::GFP marker in the wild type background (strain CF1553) is expressed at a higher measured level when treated with 1mM hydrogen peroxide for 1 hour than in the 0mM hydrogen peroxide control, 8.14 compared to 6.68 (Figure 5.7B). A representative

image is given (Figure 5.7A). As can be seen in the image, most of the GFP fluorescence is in the head and tail of the animal. When treated with H₂O₂, GFP fluorescence can be observed in the rest of the body, however the bulk of expression still remains in the head and tail of the animal (Figure 5.7A).

Expression of the SOD-3::GFP marker in the *vps-45 (tm246)* background (strain IA887) in the absence of hydrogen peroxide is higher than in the wild type background, 8.24 compared to 6.68 and is similar to the induced level of wild type expression when treated with 1mM hydrogen peroxide for 1 hour (8.14) as stated above (Figure 5.7B). With treatment with 1mM hydrogen peroxide the average measured expression increases further at 10.34, however this increase is not significant due to the variability between different animals (Figure 5.7B). However, although the quantified average fluorescence is variable, the physical pattern of expression in the anatomy of the animals is altered in that GFP expression visibly and reproducibly extends more throughout the body of animals than in untreated (Figure 5.7A). Thus, although the measured numerical increase in GFP fluorescence is not significant in the samples sizes tested, expression is visible in more tissues/cells.

In the *unc-51 (e369)* background the SOD-3::GFP marker (IA896) was expressed at a higher measured level in the absence of hydrogen peroxide at 11.55, compared to the wild type (CF1553) as well as the *vps-45 (tm246)* mutant (IA887). With treatment with hydrogen peroxide a significant increase in the fluorescence was observed, at 16.22 (Figure 5.7B). Expression of GFP was observed mostly in the head and tail, and upon treatment considerable expression was observed in the intestine of the animals (Figure 5.7A)

The GST-4::GFP marker, in the wild type background (CL2116), GFP was visible at low levels in the intestine (Figure 5.8A) with a measured fluoresce of 5.19 (Figure 5.8A). Upon treatment, fluorescence was further induced in the intestine of the animals (Figure 5.8A) with a measured value of 8.05 (Figure 5.8B).

In the *vps-45 (tm246)* mutant background (IA890), in untreated animals, expression of GST-4::GFP was observed in the intestine (Figure 5.8A) at similar levels to the wild type with a measured value of 4.67 (Figure 5.8B). After treatment with H₂O₂ the same pattern of increased fluorescence in the intestine was observed as in the case of the CL2116 strain with a measured value of 6.40.

For the *unc-51 (e369)* mutant background (IA899), GFP fluorescence was once again localised in the intestine at low levels when untreated (Figure 5.8A) and a value, similar to the wild type and *vps-45 (tm246)* backgrounds, was obtained at 4.42 (Figure 5.8B). H₂O₂ GFP expression was increased in the intestine in H₂O₂ treated animals (Figure 5.8A) with a value of 8.05 (Figure 5.8B). Overall, minor differences were observed between the strains which were not significant, suggesting that the *gst-4* dependent oxidative response is not affected by the *vps-45 (tm246)* or the *unc-51 (e369)* mutant backgrounds.

The final marker to be tested was GCS-1::GFP. In the wild type background (LD1171) almost no GFP was expressed when animals were cultured without H₂O₂ (Figure 5.9A) and the obtained measured value was 1.35 (Figure 5.9B). This value was most likely a result of background fluorescence in this case. When animals were treated with 1mM H₂O₂, expression of the marker was observed in the intestine of the animals (Figure 5.9A) and the measured value was 2.57.

A similar pattern was observed in the *vps-45 (tm246)* (IA889) background. In the case of the *vps-45 (tm246)* (IA889) mutants without H₂O₂ treatment, no GFP expression was observed (Figure 5.9A) and the basal fluorescence value was 1.23 (Figure 5.9B). When the mutants were treated with H₂O₂ GFP was observed in the intestine and average GFP fluorescence per area of 3.16 was measured.

Finally, in the *unc-51 (e369)* mutant background (IA898) low levels of GFP were observed at the pharynx (Figure 5.9A) and the measured value was 1.98. A significant increase in the expression of GFP in the intestine was observed in the animals treated with H₂O₂ (Figure 5.9A) which was reflected the average GFP expression per area value, at 7.54 (Figure 5.9B), suggesting an increased susceptibility of this strain to oxidative stress. Overall all data suggest that there is no difference on how *vps-45 (tm246)* mutants react to H₂O₂ derived oxidative stress compared to the wild type strain. On the other hand *unc-51 (e369)* mutants show a stronger response compared to the same stress in the wild type, especially in the case of the GCS-1::GFP marker. GCS-1 is part of the phase II detoxification response and its expression is directly controlled from the *skn-1* gene. SKN-1 activity is directly controlled by the presence of reactive oxygen species (Schulz et al. 2000). On the other hand, SOD-3 is regulated by *daf-16* which respond to nutrient starvation in *C. elegans* and has been associated with aging and longevity (Honda & Honda 1999). As such it is possible that the marker is not exclusively responding to oxidative stress. Additionally, SOD-3 mainly acts in converting ROS to H₂O₂ and as such

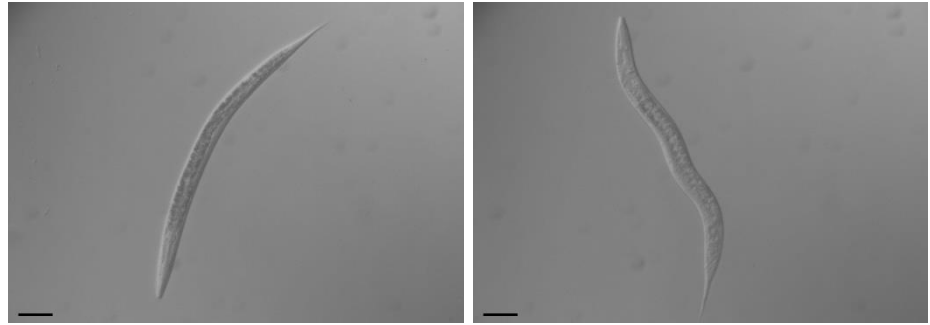
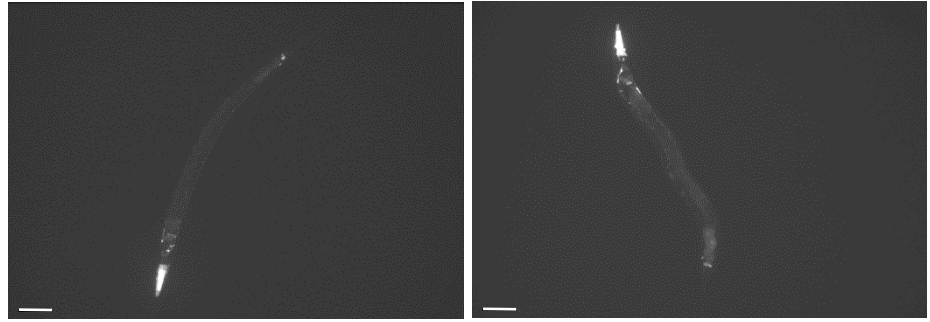
by increasing the supply of H₂O₂ did not increase ROS production in worms and subsequently not enough to elicit a greater response from the marker (Fridovich 1995). Lastly GST-4 expression is controlled by GCS-1 so it is acting at a different stage of the redox pathway, primarily reacting to the exposure of H₂O₂ and it is regulated by SKN-1 (Hoeven et al. 2011; Hayes et al. 2005; Nebert & Vasiliou 2004).

A) H₂O₂ 1mM

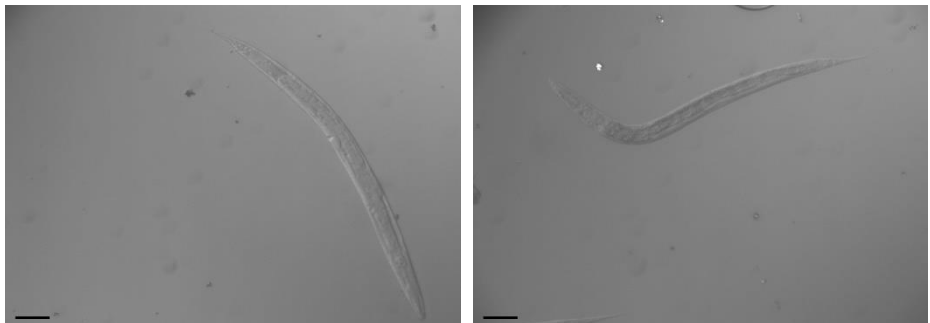
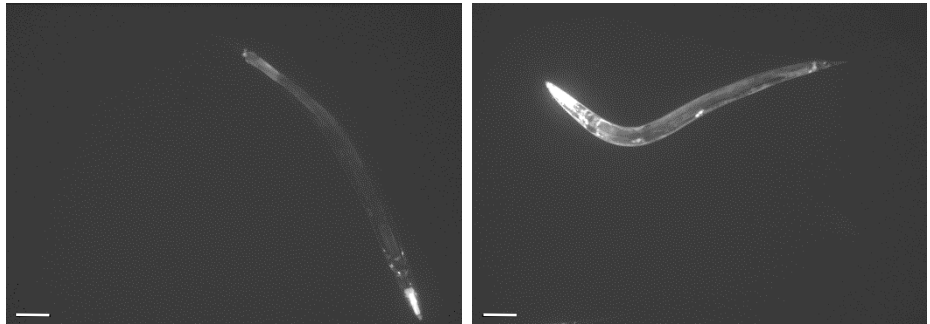
-

+

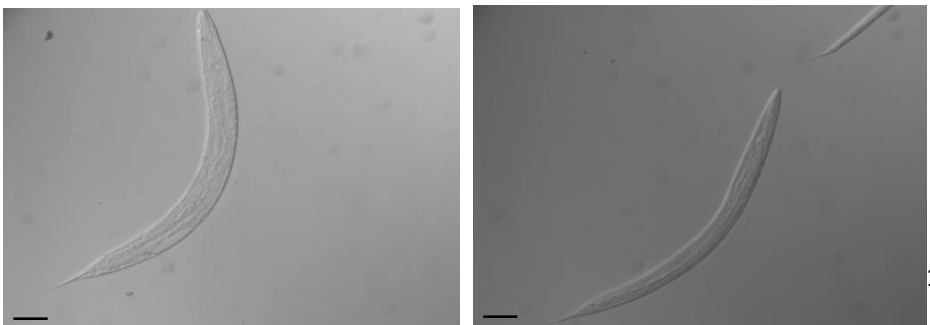
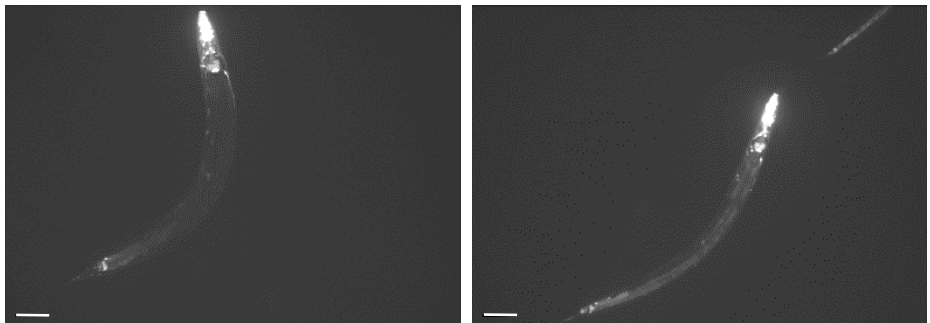
CF1553



IA887



IA896



B)

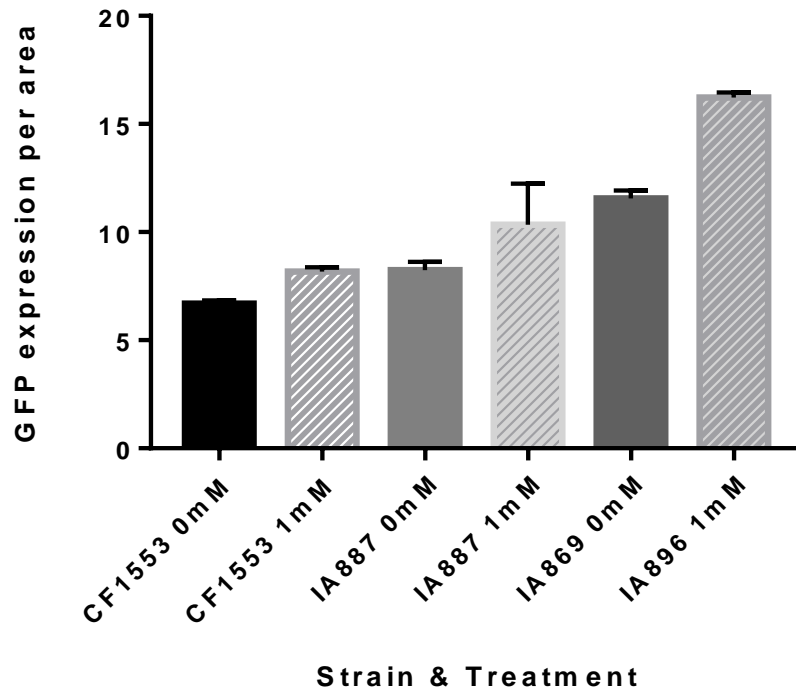


Figure 5.7: Assessment of oxidative response in CF1553, IA887 and IA896 strains using the SOD-3::GFP marker.

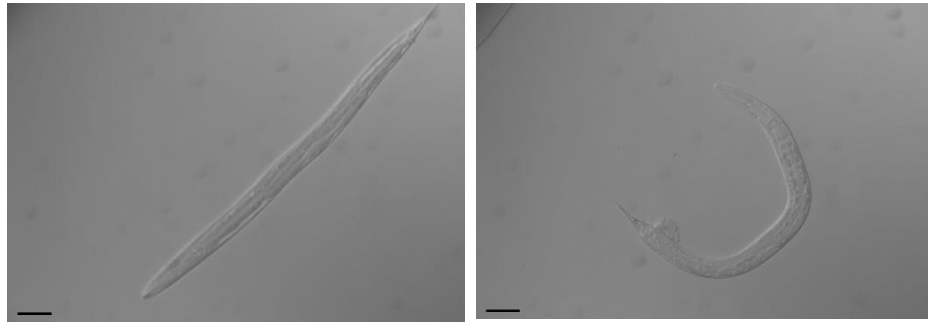
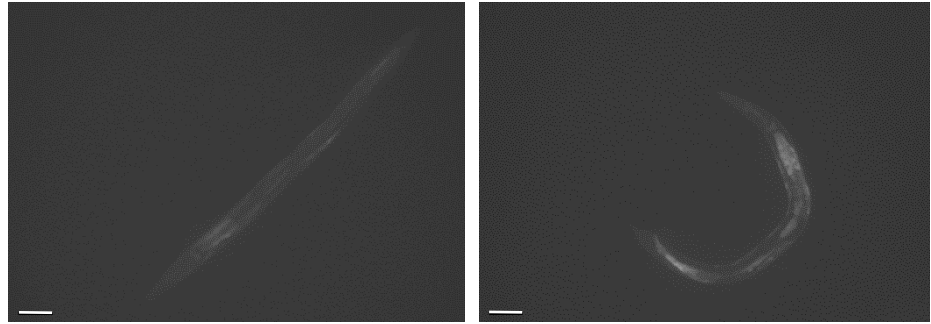
A) Representative pictures of treated (+) and untreated (-) CF1553[(*pAD76*) *sod-3p::GFP rol-6(su1006)*], IA887 *mul84* [(*pAD76*) *sod-3p::GFP rol-6(su1006)*]; *vps-45 (tm246)* X and IA896 *mul84* [(*pAD76*) *sod-3p::GFP rol-6(su1006)*]; *unc-51 (e369)* V] *C. elegans* treated with 1mM hydrogen peroxide over a period of 1 hour. **B)** Average total body fluorescence (integrated density/area) for treated and untreated CF1553, IA887 and IA896 animals with 1mM hydrogen peroxide over a period of 1 hour. For each experiment 30 individual animals were measured. 3 experiments carried for each strain at each condition (Average fluorescence \pm SD). Tukey's multiple comparisons test. CF1553 0mM vs. CF1553 1mM, $p = 0.2945$. CF1553 0mM vs. IA887 0mM, $p = 0.2525$. CF1553 0mM vs. IA887 1mM, $p = 0.0015$. CF1553 0mM vs. IA896 0mM, $p = 0.0001$. CF1553 0mM vs. IA896 1mM, $p < 0.0001$. CF1553 1mM vs. IA887 0 mM, $p > 0.9999$. CF1553 1mM vs. IA887 1mM, $p = 0.0578$. CF1553 1mM vs. IA896 0 mM, $p = 0.0028$. CF1553 1mM vs. IA896 1 mM. $p < 0.0001$. IA887 0mM vs. IA887 1 mM, $p = 0.0694$. IA887 0mM vs. IA896 0mM, $p = 0.0034$. IA887 0mM vs. IA896 1mM, $p < 0.0001$. IA887 1mM vs. IA896 0 mM, $p = 0.4955$. IA887 1mM vs. IA896 1 mM, $p < 0.0001$. IA896 0mM vs. IA896 1mM $p = 0.0002$.

A) H₂O₂ 1mM

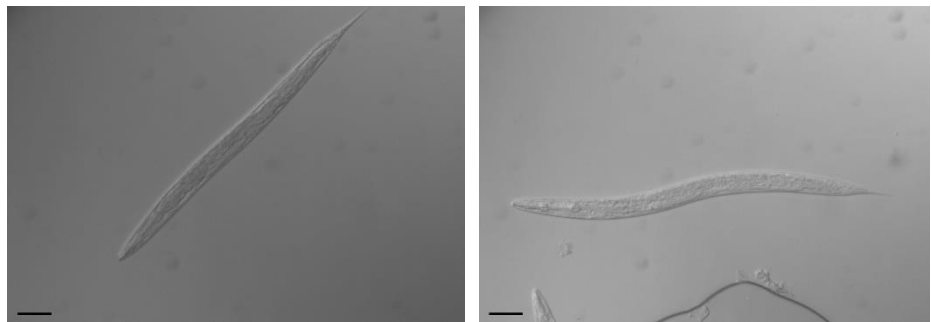
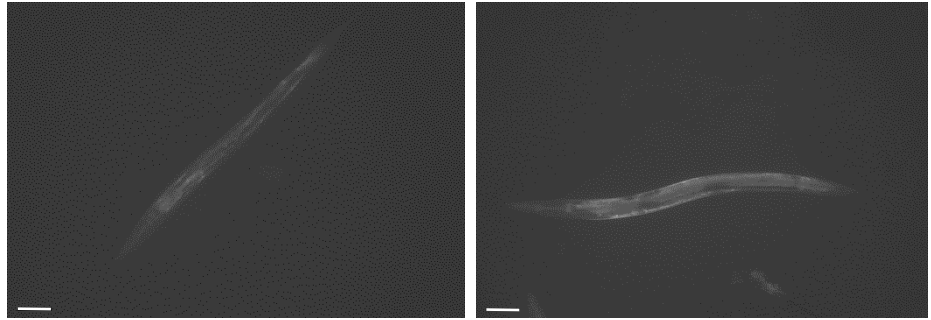
-

+

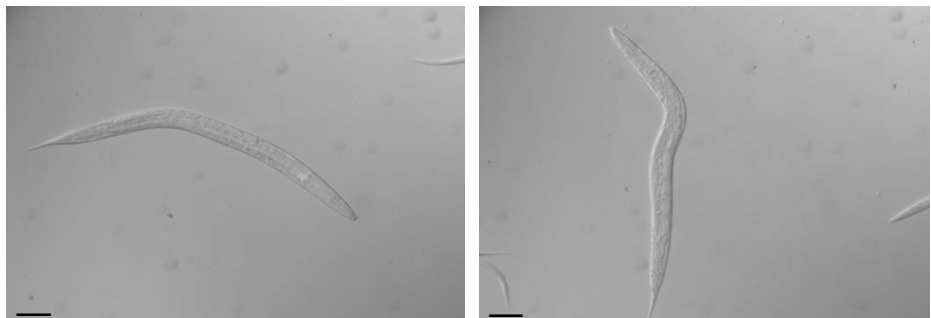
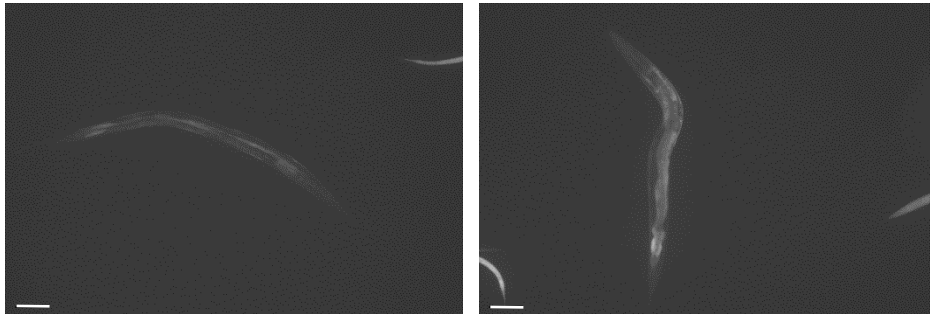
CI2116



IA890



IA899



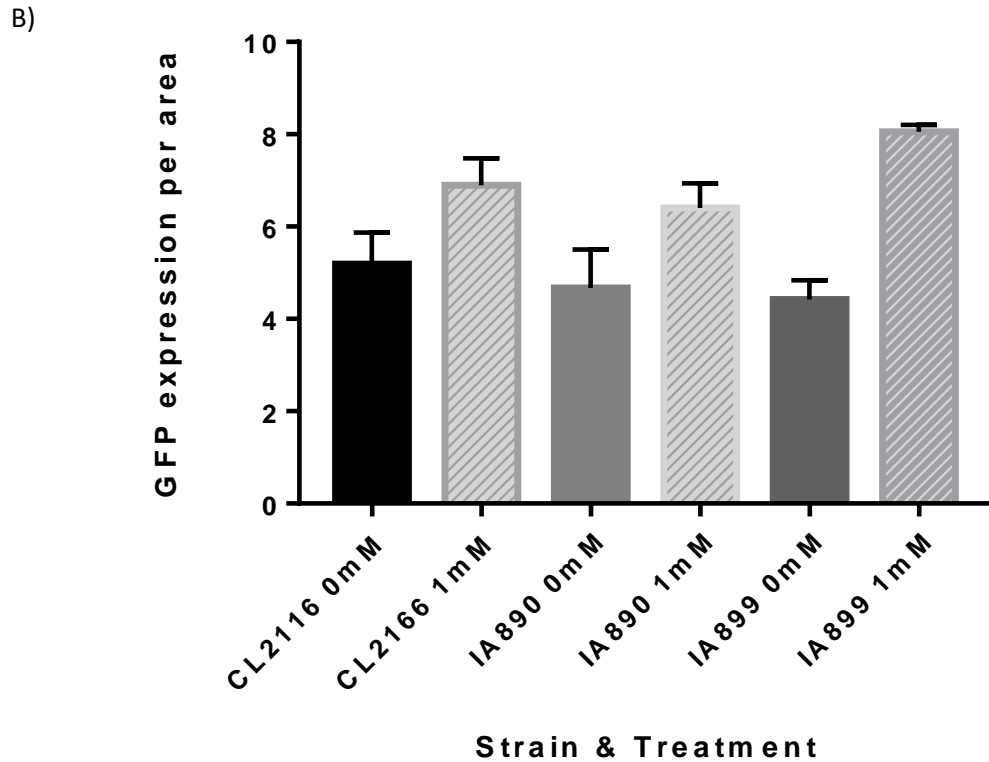


Figure 5.8: Assessment of oxidative response in wild type, *vps-45* (*tm246*) and *unc-51* (*e369*) strains using the GST-4::GFP marker.

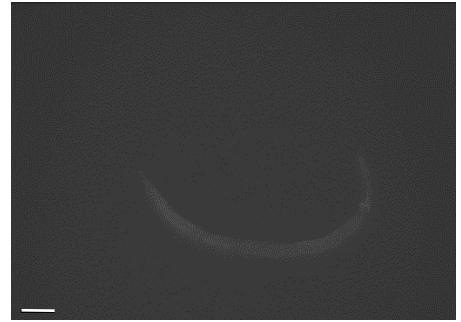
A) Representative pictures of treated (+) and untreated (-) CL2116 *dvIs19* [(*pAF15*) *gst-4p*::GFP::NLS] III, IA890 *dvIs19* [(*pAF15*) *gst-4p*::GFP::NLS] III; *vps-45* (*tm246*) X and IA899 *dvIs19* [(*pAF15*) *gst-4p*::GFP::NLS] III; *unc-51* (*e369*) V *C. elegans* treated with 1mM hydrogen peroxide over a period of 1 hour. B) Average total body fluorescence (integrated density/area) for treated and untreated CL2116, IA890 and IA899 animals with 1mM hydrogen peroxide over a period of 1 hour. For each experiment 30 individual animals were measured. 3 experiments carried for each strain for each condition. (Average fluorescence +SD). Tukey's multiple comparisons test. CL2116 0mM vs. CL2166 1mM, $p = 0.0322$. CL2116 0mM vs. IA890 0 mM, $p = 0.8697$. CL2116 0mM vs. IA890 1mM, $p = 0.1759$. CL2116 0mM vs. IA899 0mM, $p = 0.5958$. CL2116 0mM vs. IA899 1mM, $p = 0.0006$. CL2166 1mM vs. IA890 0mM, $p = 0.0050$. CL2166 1mM vs. IA890 1mM, $p = 0.8950$. CL2166 1mM vs. IA899 0mM, $p = 0.0022$. CL2166 1mM vs. IA899 1mM, $p = 0.2135$. IA890 0mM vs. IA890 1 mM, $p = 0.0288$. IA890 0mM vs. IA899 0mM, $p = 0.9940$. IA890 0mM vs. IA899 1mM, $p = 0.0001$. IA890 1mM vs. IA899 0mM, $p = 0.0119$. IA890 1mM vs. IA899 1mM, $p = 0.0400$. IA899 CB369 0mM vs. IA899 1 mM, $p < 0.0001$

A) H_2O_2 1mM

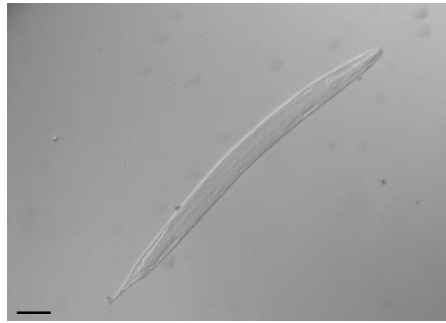
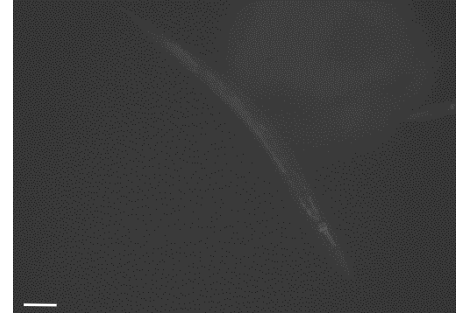
-

+

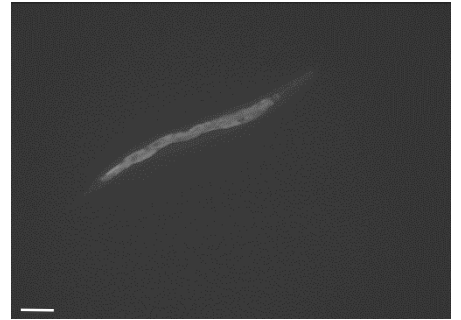
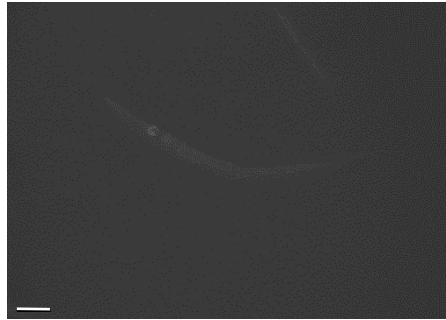
LD1171



IA889



IA898



B)

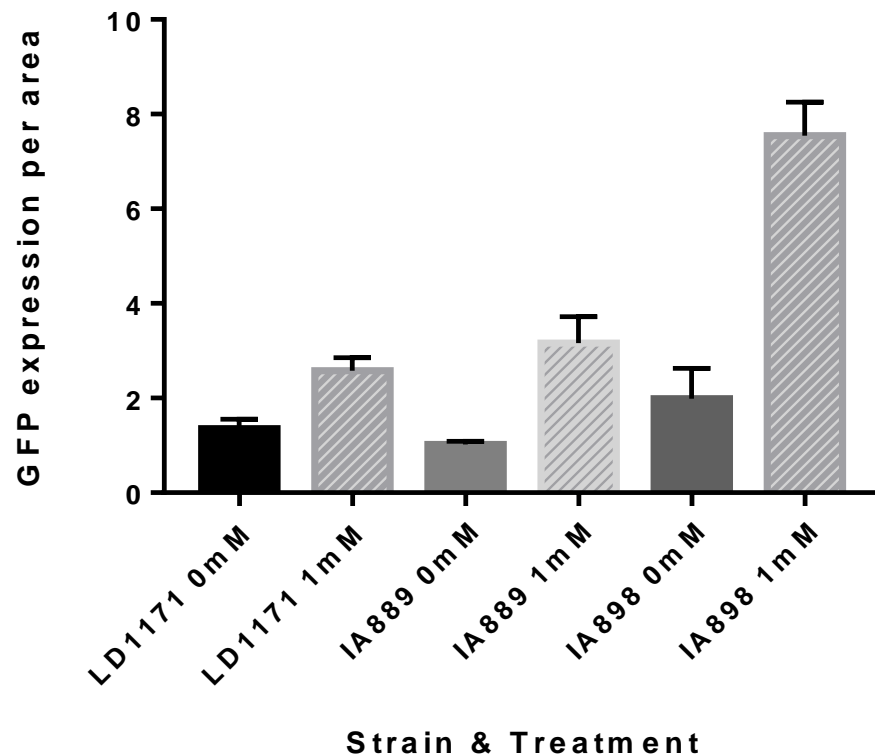


Figure 5.9: Assessment of oxidative response in wild type, *vps-45* (*tm246*) and *unc-51* (*e369*) strains using the GCS-1::GFP marker

A) Representative pictures of treated (+) and untreated (-) LD1171 *ldIs3* [*gcs-1p::GFP rol-6(su1006)*], IA889 *ldIs3* [*gcs-1p::GFP rol-6(su1006)*]; *vps-45* (*tm246*) X and IA898 *ldIs3* [*gcs-1p::GFP rol-6(su1006)*]; *unc-51* (*e369*) V *C. elegans* treated with 1mM hydrogen peroxide over a period of 1 hour. **B)** Average total body fluorescence (integrated density/area) for treated and untreated LD1171, IA889 and IA898 animals with 1mM hydrogen peroxide over a period of 1 hour. For each experiment 30 individual animals were measured. 3 experiments carried for each strain at each condition. (Average fluorescence +SD). Tukey's multiple comparisons test. LD1171 0mM vs. LD1171 1mM, $p = 0.0692$. LD1171 0mM vs. IA889 0mM, $p = 0.9505$. LD1171 0mM vs. IA889 1mM, $p = 0.0054$. LD1171 0mM vs. IA898 0mM, $p = 0.5889$. LD1171 0mM vs. IA898 1mM, $p < 0.0001$. LD1171 1mM vs. IA889 0mM, $p = 0.0165$. LD1171 1mM vs. IA889 1mM, $p = 0.6591$. LD1171 1mM vs. IA898 0mM, $p = 0.6589$. LD1171 1mM vs. IA898 1mM, $p < 0.0001$. IA889 0mM vs. IA889 1mM, $p = 0.0014$. IA889 0mM vs. IA898 0mM, $p = 0.1993$. IA889 0mM vs. IA898 1mM, $p < 0.0001$. IA889 1mM vs. IA898 0mM, $p = 0.0847$. IA889 1mM vs. IA898 1mM, $p < 0.0001$. IA898 0mM vs. IA898 1mM, $p < 0.0001$.

5.6 Chapter summary

In this chapter, the *vps-45 (tm246)* and *unc-51 (e369)* mutants were characterised in terms of their oxidative sensitivity. Initially an ER redox sensor was employed to identify any potential redox imbalances in the ER of *vps-45 (tm246)* or *unc-51 (e369)* mutant *C. elegans*. It was verified that the sensor was functional in *C. elegans* by using western blots and RNAi for the *ero-1* gene and reading the samples the 96-well plate reader. The experiments for the strains were then conducted in both the permissive (15°C) and non-permissive temperatures (25°C) for the *vps-45 (tm246)* moulting death. It was demonstrated that the *unc-51 (e369)* mutant had a more reduced environment in its ER at 15°C. The same mutant, appeared to have a similar ER environment to the wild type at 25°C suggesting that the elevated temperature caused an oxidation in the ER of the mutant. On the other hand, the *vps-45 (tm246)* mutant had a similar ER environment at 15°C to the wild type but a much more oxidised environment at 25°C. Coming in agreement with data previously acquired for yeast (Cowan, 2014) as well as the theory that impairment of *vps-45* could potentially be causing ER stress, similar to ELA2 mutations (Grenda et al. 2007) and this could be resulting to apoptosis of neutrophils in neutropenia patients carrying the T224N mutation on the human Vps45 gene (Vilboux et al. 2013). Furthermore, the reduced ER environment exhibited by the *unc-51* mutant can act as an indication that the synthetic lethal phenotype exhibited by the *unc-51 (e369) V; vps-45 (tm246) X* (Section 3.3) mutant is not a result of an additive effect in oxidative stress.

To further investigate these results a killing assay was performed on both mutants using hydrogen peroxide at concentrations of 1mM and 5mM. It was observed in both concentrations that the *unc-51 (e369)* mutant was the most sensitive to the oxidising agent. The *vps-45 (tm246)* mutant also exhibited a higher sensitivity to oxidative stress when compared to the wild type at the higher concentration. This comes in agreement with the previous results which indicated that the *vps-45* mutant was more sensitive to H₂O₂ mediated killing possibly, as a result of its oxidised environment in the ER. The fact that the *unc-51* mutant is more sensitive to hydrogen peroxide mediate killing than the *vps-45* mutant, despite its reduce environment in the ER, can potentially be explained due to the reduced autophagy exhibited by this mutant, which is likely to be acting as a homeostatic mechanism.

Three GFP tagged oxidative stress markers were used, and their induction in each mutant was measured via microscopy and quantification of the worm's total body fluorescence to examine this. Overall in all three cases the wild type strain and the *vps-45 (tm246)* showed similar levels of induction between the non-stressed and stressed states across all three markers. On the other hand, the *unc-51 (e369)* mutant exhibited a higher fluorescence with the two of the three markers, namely the SOD-3 and GCS-1 and not the GST-4. Furthermore, an increased sensitivity of the *unc-51 (e369)* to oxidative stress both in terms of survival and in terms of the anti-oxidant response was identified.

Thus, by all assays used, the *unc-51* mutant exhibited a reduced environment in its ER and appeared to be more sensitive to oxidative stress, with the SOD-3 and GCS-1, GFP markers being expressed at higher levels when stressed with H₂O₂ the GST-4 marker showing no difference from the wild type or *vps-45* mutants. On the other hand, the *vps-45* mutant exhibited a oxidised environment in its ER and milder sensitivity to oxidative stress compared to the *unc-51* mutant, however still greater compared to the wild type. A slight increase in of the GFP markers was generally observed, however not significantly higher to the wild type strain.

Chapter 6: Characterisation and identification of the *vps-45 (tm246)* moulting death suppressor

6.1 Overview and aims

An EMS (ethylmethasulphonate) mutagenesis screen which was previously done in our lab, identified multiple independent suppressed lines for the 25°C moulting death of the *vps-45 (tm246)* mutant. The original *vps-45 (tm246)* mutation is an extensive deletion and as a result is considered to be a non-revertible genetic null allele. Therefore, the suppressor has to be extragenic. The original *vps-45 (tm246)* mutants are viable at 15°C and die by moulting arrest at 25°C. These newly acquired suppressed mutants grow and develop relatively normally at 25°C despite lacking the Vps45 protein. One of the suppressed lines (IA773) was selected for work described here, the objective being to characterise the extent of the suppression across a collection of phenotypes that were observed in the *vps-45 (tm246)* mutant strain. Additionally, whole genome sequencing was employed in order to attempt to identify the mutated gene in strain IA773 responsible for the suppressed phenotype.

6.2 Characterization of the *svp (ij117) vps-45 (tm246)* suppressed mutant

For the reasons discussed above the suppressor of the *vps-45 (tm246)* allele must be extragenic. This unknown suppressor was named *svp (ij117)* (suppressor of *vps-45*). This was done under the assumption that only a single suppressor allele was present in the suppressed strain.

The phenotypic characterisation of the original *vps-45 (tm246)* strain IA757, and the comparisons with the phenotypes of the wild type strain N2, is all presented in Chapter 3. Here an extension of that study is presented with the phenotypic characterisation of the suppressed IA773 strain, genotype *svp (ij117) vps-45(tm246)*. Furthermore, a new strain IA882 where the *vps-45 (tm246)* allele was twice backcrossed with the CB4856 Hawaiian wild type strain was utilised in the comparisons where appropriate. Only the data from IA773 and IA882 is new and the comparisons are with the data presented for the other strains in Chapter 3; experiments were not repeated here for the other strains.

6.3 *svp (ij117)* suppresses the *vps-45 (tm246)* moulting death at 25°C

To assess how the *svp (ij117)* allele affects the embryonic lethality previously demonstrated by the *vps-45 (tm246)* mutant (section 3.3), IA773 and IA882 L1 arrested animals were inoculated in NGM plates and were left to grow at the non-permissive temperature. 50-60 L1 larvae were used for each strain and each experiment was done in triplicate. After 120 hours of culturing, the number of surviving adults was scored for each strain, as a measure of the animals that did not die through moulting. Data clearly shows that a large majority (78.3%) of animals survives for IA773 whereas very few animals (10%) were alive after 120 hours of culturing for IA882 (Figure 6.1). More specifically, as previously described in section 3.4 for the wild type strain N2, 98.3% of the larvae were able to survive and reach adulthood and for the IA757 strains percentage of animals which survived through moulting was 14.2% and (Figure 6.1 and Chapter 3). Two conclusions can be drawn from this data. First, it is evident that the *svp (ij117)* suppressor greatly improves the survival of the animals carrying the *vps-45 (tm246)* allele with considerable suppression of the moulting death, however the survival is still slightly lower when compared to the wild type strain. Second, it is suggested that the presence of Hawaiian genome does not affect the survival of *vps-45 (tm246)* animals as IA882 larvae exhibit a very similar larval lethality to the original the IA757 strain. It should be noted that the % of the genome that is Hawaiian in the IA882 strain is not known however it is the result of a two-time backcross with CB4856 and the presence of Hawaiian DNA was verified across chromosomes I, IV and V (Figure 6.9).

6.4 The suppressor does not change the body size of *vps-45 (tm246)* mutants

The length of mature adult IA773 animals was measured to assess if the suppressor reverses the small body phenotype exhibited by the *vps-45 (tm246)* mutant. Animals were cultured at the permissive temperature of 15° C where the IA757 strain can survive to adulthood and display the smaller body size phenotype. The average size measured here for the suppressed strain IA773 was 1047µm (Figure 6.2). This compares with the previous measurements for the non-suppressed IA757 strain of 1048µm and 1211µm for the wild type N2 strain (Chapter 3, and Figure 6.2). Thus, the IA773 strain does not exhibit any suppression for the shorter body length associated with the *vps-45(tm246)* allele in the

IA757 strain with the two of them exhibiting almost the same length. As a result, it is evident that the suppressor mutation does not reverse the identified smaller body size phenotype of *vps-45(tm246)* (section 3.5).

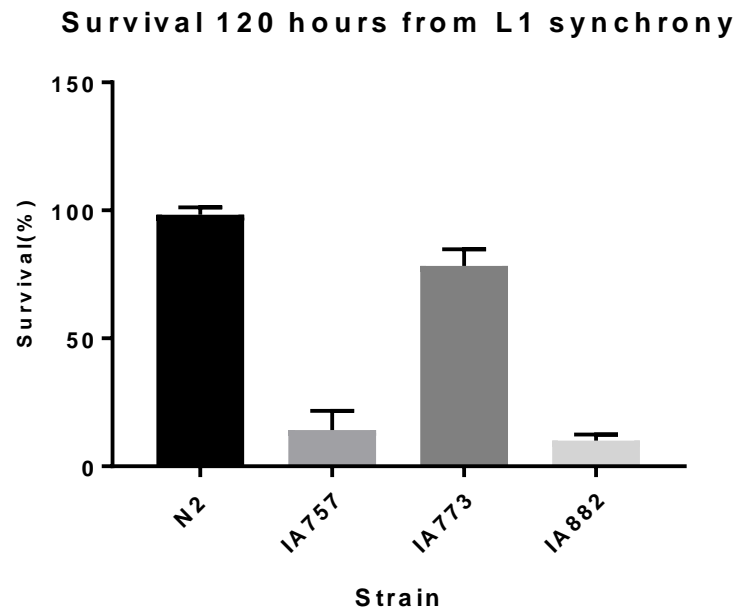


Figure 6.1: Assessment of the molting death of the suppressed *vps-45 (tm246)* mutant at 25°C.

Plates inoculated with 50-60 L1 larvae for each strain. Alive *C. elegans* were scored after 120 hours of development. Experiments were done in triplicates for each of the N2, IA757, IA773 and IA882 strains. Average survival (%)± SD is shown for each mutant Tukey's multiple comparisons test: N2 vs IA757, $p < 0.0001$. N2 vs IA773 $p = 0.074$. IA757 vs IA773, $p < 0.0001$. N2 vs IA882, $p < 0.0001$. IA757 vs IA882, $p = 0.77$. IA773 vs IA882, $p < 0.0001$.

6.5 The *svp (ij117)* suppressor allele does not suppress embryonic lethality

As previously discussed, the IA757 strain, exhibits defective protein trafficking of yolk components by the oocytes and it was shown on a previous chapter that such mutants exhibit high rates of embryonic lethality when grown at both the permissive and non-permissive temperatures (section 3.4). Previous data showed that, at 15°C the wild type strain exhibited an embryonic lethality of 11.07% compared to 30.6% for the IA757 strain (section 3.4). The IA773 strain on the other hand showed an average embryonic lethality of 26.6%, reduced but not to a significant degree, compared to IA757. Thus, suggesting a mild, however not significant suppression of the mutant phenotype by the *svp (ij117)* allele (Figure 6.3A).

At 25°C, a similar pattern was observed. The suppressed strain in this case demonstrated an embryonic lethality of 21.61% (Figure 6.3B). The wild type strain had previously exhibited an embryonic lethality of 2.05% and IA757 an embryonic lethality of 30.04%. Once again, a reduced embryonic lethality is exhibited by the suppressed strain compared to the original mutant at the same temperature, however still an insignificant change. Although at both temperatures tested there was a small decrease in the numbers of embryos dying, the numbers were not significant. Therefore, it is unclear if there is any real suppression regarding the embryonic lethal phenotype.

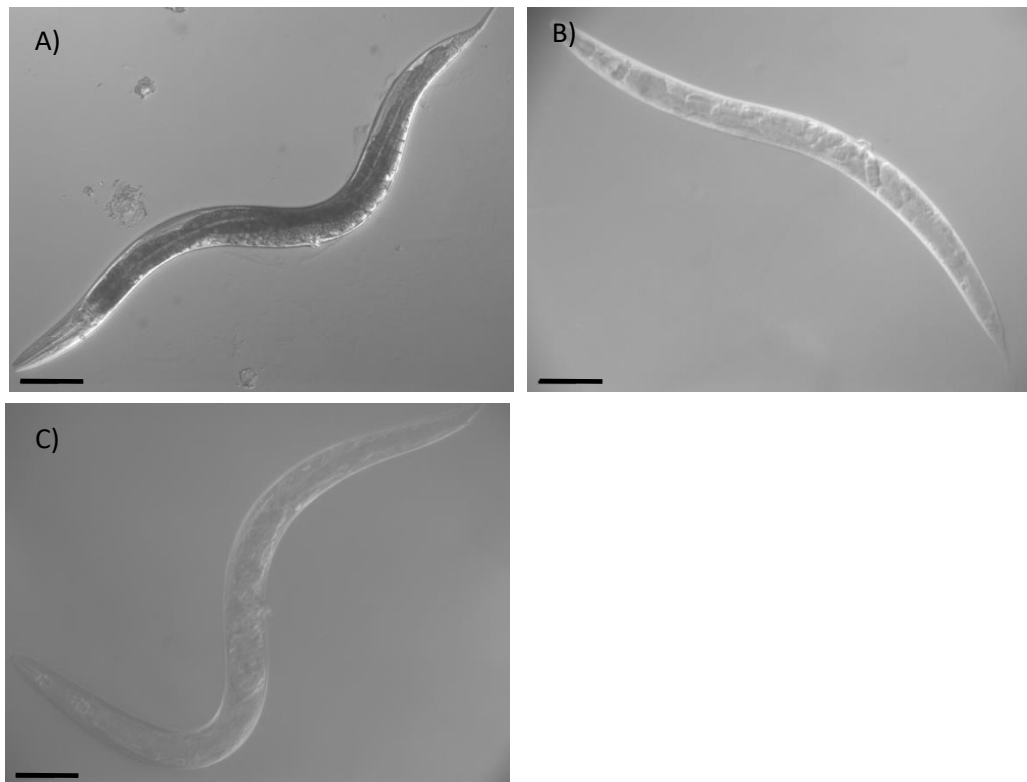


Figure 6.2: Length measurement of the suppressed *vps-45 (tm246)* mutant.

A-C) DIC images of adult wild type N2, IA757, IA773 animals. Scale bars represent 100 μm. **D)** Average length (\pm SD) of each strain at the adult stage when cultured at 15°C. N2 (n=10), IA757 (n=11), IA773 (n=9). Tukey's multiple comparisons test: N2 vs IA757, $P=0.0003$. N2 vs IA773 $P<0.0001$. IA757 vs IA773 $P=0.0003$.

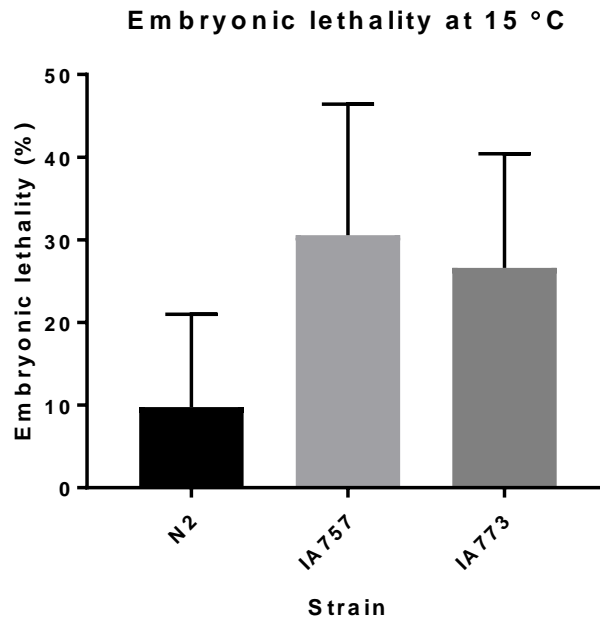
6.6 Characterisation of the moult and intermoult periods on the IA773 strain

As presented in Chapter 3, the *vps-45(tm246)* null mutant strain IA757 takes longer to moult than wild type and the intermoult periods are also longer, resulting in the strain taking significantly longer to reach adulthood from L1 arrest, than the N2 wild type strain (~25 hours longer). To assess the impact of the *svp (ij117)* suppressor, these phenotypes were measured in the IA773 strain.

Synchronised IA773 L1 larvae were seeded at the same time on NGM plates, were left to grow until the moulting process started and the duration of the moult was measured (section 3.9). IA773 animals exhibit a delayed entry into the moult in the same way the IA757 strain did. The first lethargic larvae for the wild type strain were observed at 22 hours of culturing from synchrony and two hours later for the IA757 and IA773 strains. Both the IA757 and IA773 populations appeared to remain in the lethargic state for longer than the wild type. On average the populations for both IA757, and IA773 required approximately 14 hours to exit the moulting state completely compared to 10 hours for the wild type (Figure 6.4 A). Additionally, it appears that more larvae were in lethargus at the same time at the peak of the moult for the IA773 population, as indicated by the higher peaks of the curves, at approximately 70% of the population as compared to 60% for the N2 and IA757 strains (Figure 6.4 A).

As previously described on Chapter 3 (section 3.9) the high peaks in the moulting graphs suggest high synchrony whereas low peaks suggest less synchrony in the population. Additionally, the area under the curve was measured for each of the individual experiments for each of the strains (Appendix 2) and the average area was plotted for each (Figure 6.4B) as a measure of the average time each of the animals stays in lethargus (section 3.8). No significant difference was demonstrated between IA773 and IA757 on that aspect. However, IA773 did significantly differ compared to the wild type strain. Overall it is suggested that both the suppressed (IA773) and non-suppressed (IA757) *vps-45* mutants stay in lethargus for longer than the wild type with 3 and 2.67 hours respectively as opposed to 2.05 for the wild type (Figure 6.4B).

A)



B)

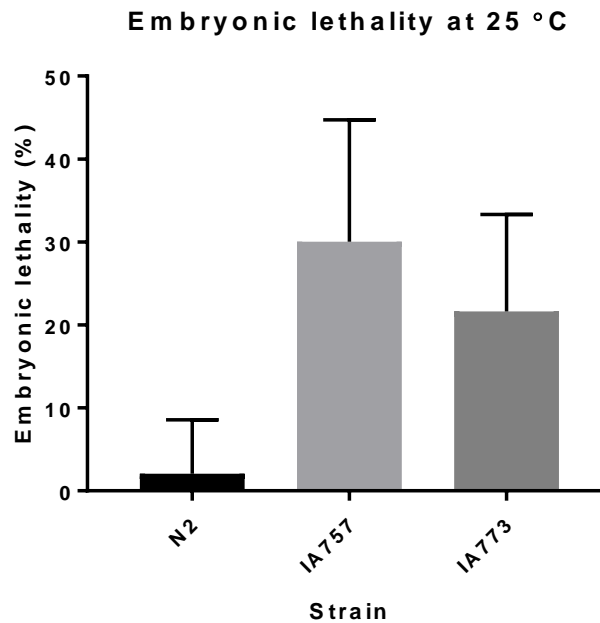


Figure 6.3: Embryonic lethality assessment of the IA773 strain.

A) Average embryonic lethality (\pm SD) of the progeny of single animals cultured at 15°C N2 (n=10), IA757 (n=10), IA773 (n= 8). Tukey's multiple comparisons test. N2 vs. IA757, $p = 0.0064$. N2 vs. IA773, $p = 0.0408$. IA757 vs. IA773, $p = 0.8180$. **B)** Average embryonic lethality (\pm SD) of *C. elegans* cultured at 25°C. N2 (n=10), IA757 (n= 10), IA773 (n= 10). Tukey's multiple comparisons test. N2 vs. IA757, $p < 0.0001$. N2 vs. IA773, $p = 0.0020$. IA757 vs. IA773, $p = 0.2453$

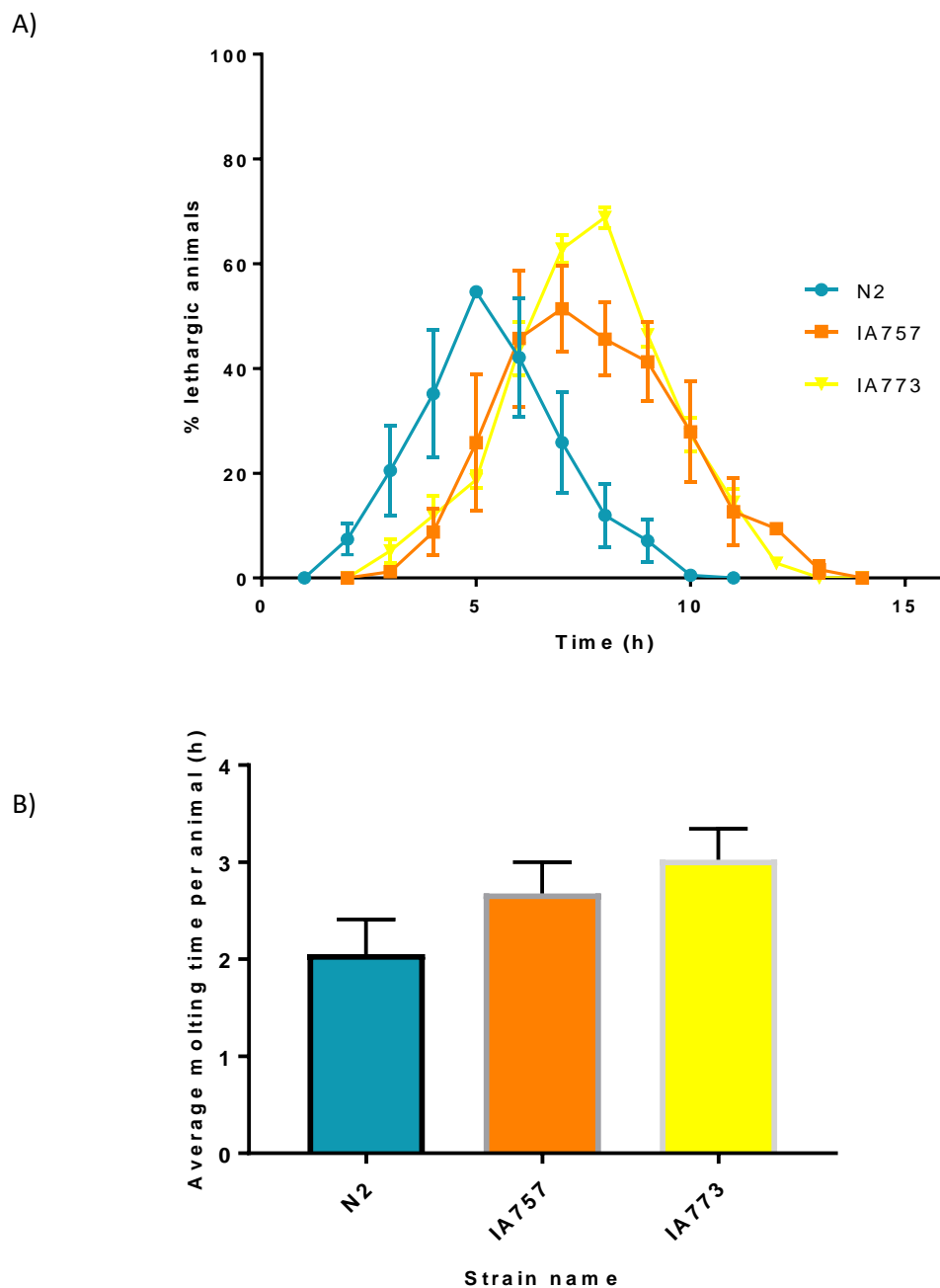


Figure 6.4: Molting profiles of wild type N2, IA757, IA773 during the L1-L2 moult at 15°C.

A) Percentage of molting animals (\pm SD) at hourly intervals for the duration of the moult for each of strain populations. Average of three experiments for each strain. B) Average time required for each strain go through the moult as the product of the calculation of the average area under the curve (\pm SD) for each molting graphs obtained from the triplicate experiments of each strain tested. Tukey's multiple comparisons test. N2 vs. IA757, $p=0.1327$. N2 vs. IA773, $p=0.0272$. IA757 vs. IA773, $p=0.4554$.

In order to, verify and accurately measure this prolonged lethargic state for the IA773 strain the moult duration of individual larvae was scored. Larvae were seeded on NGM plates after L1 arrest. 10 animals were individually observed as they entered the L1-L2 moults. The duration of the moult was scored as it was previously done with the N2 and IA757 strains (section 3.9). Individual animals were observed under the microscope, at hourly intervals, from the moment they entered lethargus (stop of movement and pharyngeal pumping) until the moment they exit lethargus (onset of movement and start of ecdysis). The results indicate that the IA773 strains required 7.63 to progress through the moult whereas previously acquired data (section 3.9) showed that the wild type and IA757 strains required 5.3 and 7.15 hours respectively. Overall an apparent small increase in the moulting time of the IA773 strain compared to the IA757 strain which however is not significant (Figure 6.5B). Therefore, the *svp* (ij117) suppressor does not change these aspects of moulting behaviour exhibited by the IA757 strain.

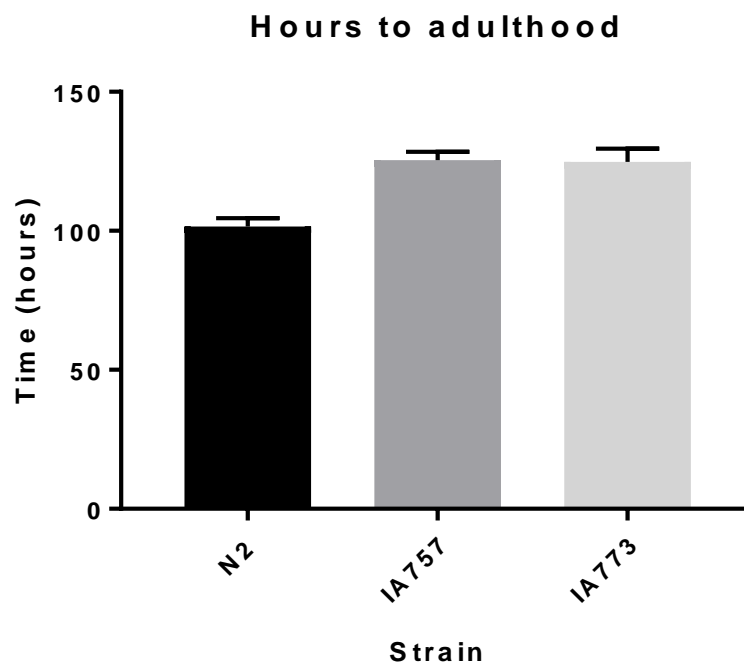
The duration of development from L1 arrested larvae to adult was tested next, in the IA773 strain. Populations of L1 arrested animals were left to feed until they reached the adult stage at 15°C. IA773 animals require longer to reach the adult stage compared to the wild type strain, which was the same as the time required for IA757 to reach the same stage. In previous experiments (Section 3.9) it was shown that the wild type, was able to reach the adult stage after approximately 100 hours of development when cultured at 15°C whereas IA757 require 125 hours to reach the same stage. In this case, the IA773 required 125 hours as well to reach adult (Figure 6.5 A). Considering that IA773 requires ~ 2,5 hours longer for the L1 to L2 moult compared to the N2 wild type (Figure 6.5B) this suggests that an additional 10 hours are required to go through each of the larval moults until adulthood assuming that each moult requires the same time to be completed as indicated by the expression of moulting genes (Johnstone & Barry 1996). Since an extra 15 hours appear to be required there is strong indication, that the IA773 strain also has longer intermoult stages compared to the wild type, in the same way IA757 does as already discussed (Section 3.9).

Finally, IA773 was also tested for levels of asynchrony during larval development. Arrested L1 larvae were seeded on NGM plates and were left to feed for 72 hours. No differences were observed in terms of how synchronous the populations were as far as the developmental stage is concerned. The majority of the IA773 population, approximately 94.7 % on average, was able to reach the L3 stage after 72 hours of development and a

small proportion, approximately 5.2% was at the L4 stage (Figure 6.6). Data previously acquired for the N2 and IA757 strains demonstrated that, the wild type strain had already reached the L4 stage by 72 hours of development with 96.4% of the population being at that stage and 3.6% being at the L3 stage. Furthermore, the IA757 population had delayed development with 88.1% of the population being at the L3 stage and 9.5% being at the L4 stage. Overall, the IA773 strains were one stage behind at the L3 stage after 72 hours of development similar to the IA757 strain, with negligible asynchrony in the populations of the animals (Appendix 3).

This was similar to the data presented for IA757 in Chapter 3, where 88% of the population was at the L3 larval stage, ~9.2% at the L4 stage and ~2% at the L2 stage (Figure 6.6). In both cases, most animals are at the L3 stage. As a result, there is a delay in development from L1 larva to adult, but the absence of multiple developmental stages present at any one time during culture suggests that there is not a great loss of synchrony and that the *svp (ij117)* suppressor did not affect the development speed and synchrony of the *vps-45* mutant animals.

A)



B)

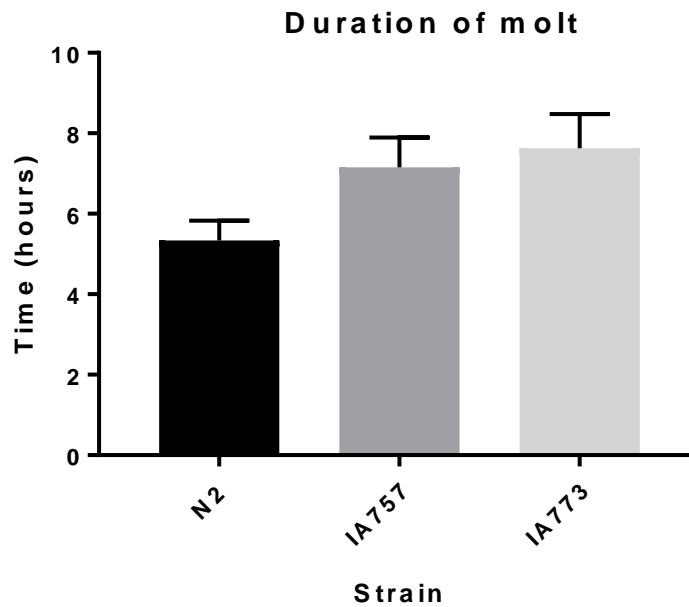


Figure 6.5: Moulting duration and development time characterisation of the IA773 strain.

A) Average development time (\pm SD) for >50% the population to reach adult stage from L1 arrest, for wild type N2 (n=5), *vps-45* (*tm246*) strain (IA757) (n=5), *svp* (*ij117*) strain (IA773) (n=5) when cultured at 15°C. Tukey's multiple comparison test N2 vs IA757, $P < 0.0001$. N2 vs IA773, $P < 0.0001$. IA757 vs IA773, $P = 0.9643$.

B) Average time (\pm SD) for the completion of molt at the L1-L2 when cultured at 15°C, N2 (n=12), IA757 (n=10), IA773 (n=12). Tukey's multiple comparison test N2 vs IA757, $P < 0.0001$. N2 vs IA773, $P < 0.0001$. IA757 vs IA773, $P = 0.2795$. Average time \pm SD

6.7 Determination of lifespan for the IA773 strain

As previously presented on Chapter 3 the IA757 strain has a shorter lifespan compared to the wild type strain at both the permissive and non-permissive temperature for the *vps-45* (*tm246*) moulting death. To assess how the *svp* (*ij117*) suppressor affects the longevity of the *vps-45* mutants the IA773 adult *C. elegans* were cultured at the 15°C and 25°C and the survival of the population was scored over time.

The IA773 population exhibited a median survival of 8 days and an overall survival of 17 days when cultured at 15°C (Figure 6.7A). This is significantly lower to the previously demonstrated median survival of 17 days and an overall survival of 36 days for the N2 strain (Section 3.10, Figure 6.7A). It is also very similar to the data already obtained for the IA757 strain, which demonstrated a median survival of 6 days and complete death of all the animals after 18 days.

At the non-permissive temperature of 25 °C the median survival for the IA773 strain was 4 days and it reached 0% survival after 12 days (Figure 6.7B). This was lower compared to the data obtained for the N2 wild type strain which had a median survival of 6 days. However, the overall survival for the wild type strain was 13 days (Section 3.10, Figure 6.7B,) which is similar to that demonstrated by the IA773 strain. On the other hand, the median survival of IA757 strain was 3 days. All animals were dead after 7 days for the same strain (Section 3.10, Figure 6.7B).

As such, in both cases the suppressed IA773 had a 25% increase in their median survival compared to their non-suppressed counterparts, which however resulted in an increased population lifespan only in the case of the 25°C cultures. Overall one can argue that the adult lifespan of the suppressed *vps-45* (*tm246*) mutant is higher than that of the non-suppressed one at 25°C and that the suppressed strain exhibits a better overall fitness in both 15°C and 25°C as opposed to the non-suppressed one as a result of the increased median survival.

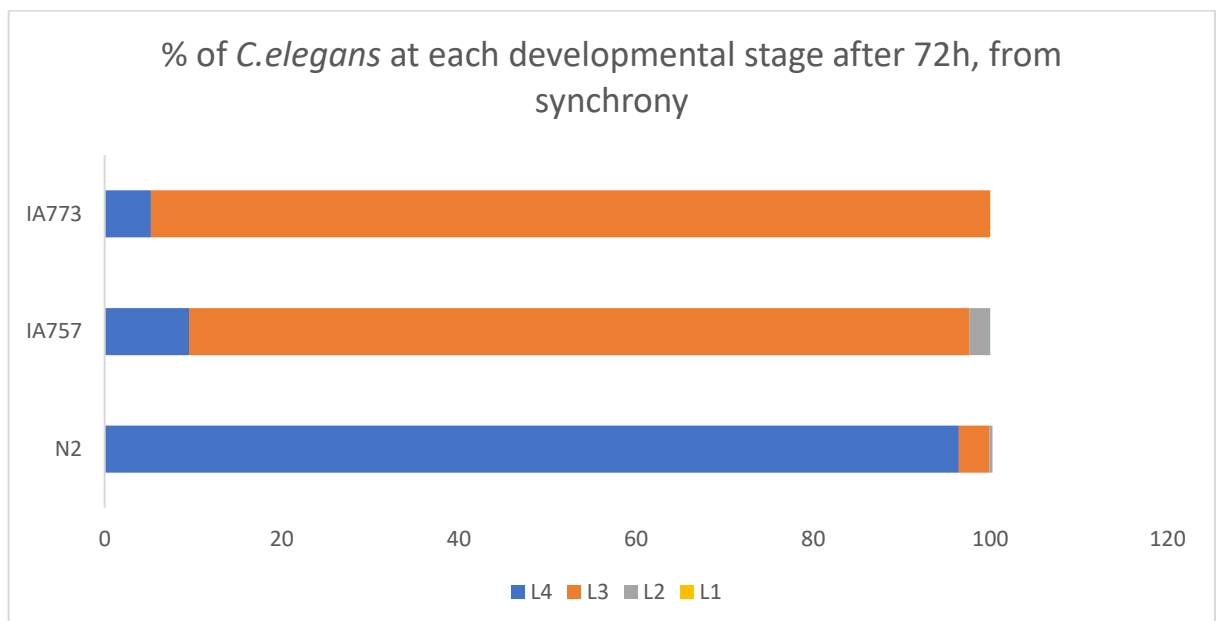


Figure 6.6: Developmental stage of N2, IA757, IA773 strains after 72h of development, from L1 arrest, at 15°C

IA757 and IA773 appear to be at the L3 and L4 stage for the majority of the population. N2 strains is at the L4 stage. Average of three experiments for each strain.

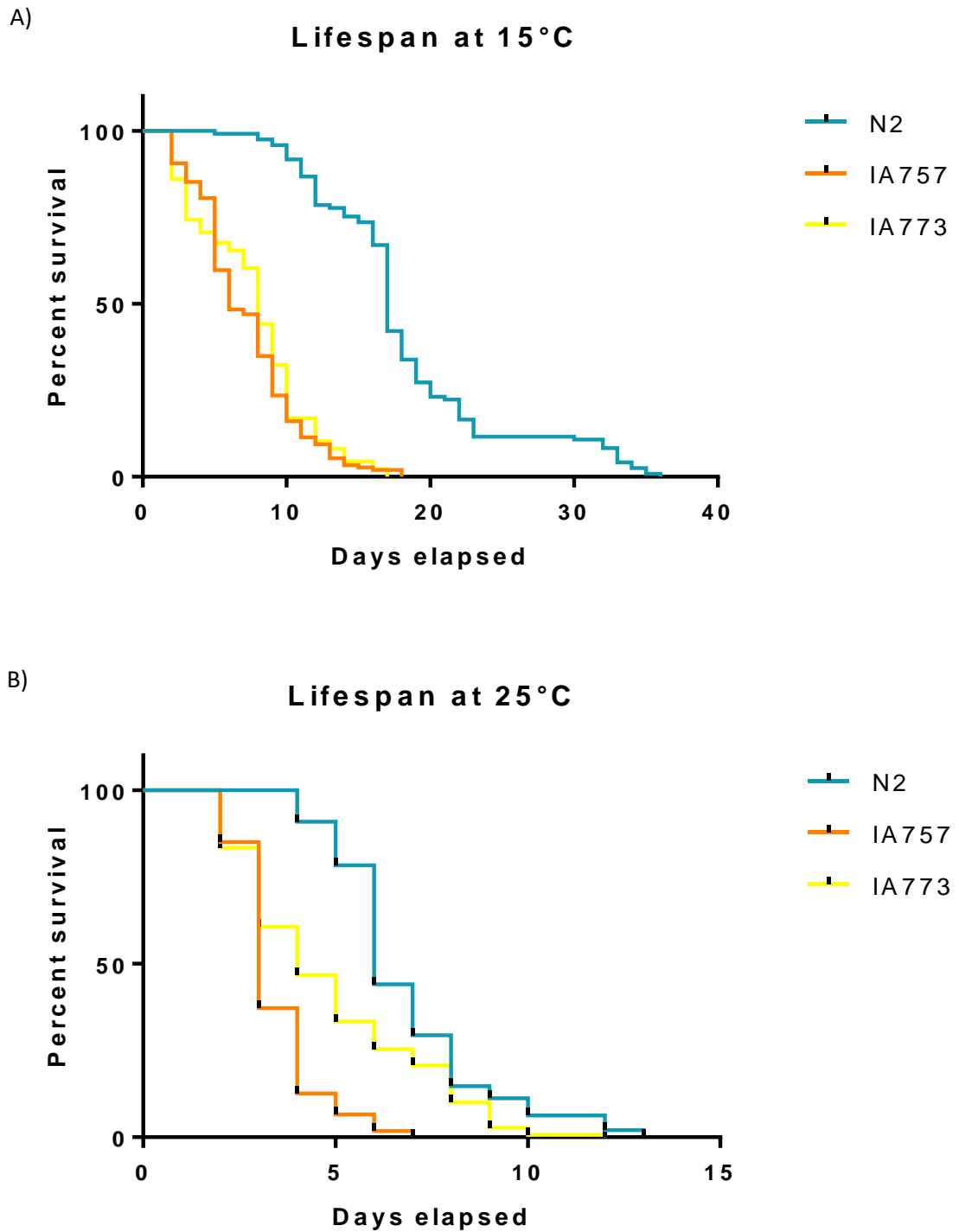


Figure 6.7: Life span of N2, IA757, IA773 *C. elegans* at 15°C and 25°C. 3 populations of 50 young adults were observed for each of the strains. **A)** Survival of adult *C. elegans* at 15°C. Log rank test for comparison of the curves. N2 vs IA757, $p < 0.0001$. N2 vs IA773, $p < 0.0001$. IA757 vs IA773, $p = 0.32$ **B)** Survival of adult *C. elegans* at 25°C. Log rank test for comparison of the curves. N2 vs IA757, $p < 0.0001$. N2 vs CB369, $p < 0.0001$. IA757 vs IA773, $p < 0.0001$. P values < 0.017 are considered significant as determined by the Bonferroni method for threshold determination.

6.8 The *svp (ij117)* suppressor follows a recessive and autosomal inheritance pattern

To test the genetic behaviour of the suppressor, the inheritance pattern of the *svp (ij117)* allele was investigated through a cross with wild type N2 males. The *vps-45* gene is on the X chromosome and the location of the suppressor *svp (ij117)* is unknown. *C. elegans* males have only one X chromosome and are diploid for autosomes. Outcrossed F1 males from this cross would have a single *vps-45 (tm246)* X chromosome inherited from their mother and for autosomes they would carry one from each parent. Outcrossed F1 hermaphrodites would carry a copy of all chromosome from each parent and thus would be *vps-45 (tm246) / +* on the X chromosome. For this experiment, there are in principle two possible outcomes for males:

- Outcome 1 - outcrossed male animals suppressed for the larval arrest at 25 °C.
- Outcome 2 - outcrossed male animals not suppressed for the larval arrest at 25 °C.

Outcome 1 would indicate one of two possibilities; either the suppressor is dominant if it is autosomal (heterozygotic state of the allele in these males) or that it is X-linked and as a result segregates together with *vps-45 (tm246)* in the hemizygotic state.

Outcome 2 would indicate that the suppressor is not X-linked and that it is autosomal recessive. In this case, the autosomal heterozygotic *svp (ij117)* would not be able to suppress the 25°C larval arrest caused by the hemizygotic *vps-45 (tm246)*.

To assess which of these possible outcomes holds true, the procedure described below, was followed:

- 10 wild type males were crossed with a single IA773 hermaphrodite. 15 crosses were prepared and as a result 15 F1 populations were generated.
- The F1 brood of each hermaphrodite was divided approximately equally between two plates
- For each brood, 1 plate was cultured at 15°C and the other at 25°C.
- The proportion of males to hermaphrodite F1 progeny for each mated hermaphrodite at each temperature were compared.
- If the frequency of males generated (as surviving adults) was much lower at 25°C versus 15°C, then it was concluded that the males are dying at 25°C but hermaphrodites were not.
- If the frequency of males generated (as surviving adults) is the same at 25°C versus 15°C, then F1 males were surviving at 25°C

The data demonstrated that F1 progeny from the same parent, only contained similar numbers of surviving males and with hermaphrodites when cultured at the permissive 15°C. By contrast at 25°C very small numbers of males survived by comparison to hermaphrodites. Thus, a high proportion of the males relative to hermaphrodites were not surviving to adulthood at the non-permissive temperature. (Table 6.1).

As discussed above, this suggests that the *svp (ij117)* allele which causes the suppression of the *vps-45 (tm246)* moulting death and larval arrest, follows a recessive and autosomal pattern of inheritance. The *vps-45* gene is an X-linked gene. Male *C. elegans* have only one X-chromosome and the single maternally-derived copy of the mutant *vps-45 (tm246)* allele results in the moulting death phenotype at 25°C in these animals. In the case of the outcrossed F1 generation all hermaphrodites should be heterozygotic for both the *vps-45 (tm246)* allele and the suppressor *svp (ij117)* allele. If the *svp (ij117)* allele was dominant or X-linked the male animals should be able to survive at the non-permissive temperature (Table 6.1), which is not the case.

IA773xN2 F1 15°C

A)

Parent	Progeny (24h)	XX adult Progeny	XO adult Progeny	XO%
i	38	20	18	47.36842
ii	48	30	18	37.5
iii	41	34	7	17.07317
iv	16	10	6	37.5
v	35	21	14	40
vi	60	32	28	46.66667
vii	61	40	21	34.42623
viii	53	28	25	47.16981
ix	42	27	15	35.71429
x	48	30	18	37.5
xi	50	40	10	20
xii	50	24	26	52
xiii	20	14	6	30
xiv	45	30	15	33.33333
Average				36.87514

B)

IA773xN2 F1 25°C

Parent	Progeny (24h)	XX adult Progeny	XO adult Progeny	XO%
i	30	19	0	0
ii	40	25	3	7.5
iii	35	19	1	2.857143
iv	15	10	1	6.666667
v	35	23	0	0
vi	60	36	2	3.333333
vii	60	40	5	8.333333
viii	50	28	1	2
ix	35	23	1	2.857143
x	42	18	2	4.761905
xi	55	27	0	0
xii	37	23	2	5.405405
xiii	22	12	0	0
xiv	43	19	2	4.651163
Average				3.454721

Table 6.1: Inheritance pattern of the *svp (ij117)* suppressor allele

A) Table showing the progeny of *svp (ij117)*, (IA773) hermaphrodites crossed with wild type (N2) males after 24 hours of egg laying, 15 crosses were set up. Egg laying was done at 15°C. **B)** Table of progeny for each of the crosses originating from Table A selected to grow at 15°C. Hatched eggs after 24 hours and surviving progeny after 72 hours are shown. **C)** Table of progeny for each of the crosses originating from Table A selected to grow at 25°C. Hatched eggs after 24 hours and surviving progeny after 72 hours are shown.

6.9 Introduction of the *vps-45* (tm246) deletion allele and *svp* (*ij117*)

suppressor, into 'Hawaiian' genetic background for whole genome sequencing analysis

In order to identify the suppressor for the temperature sensitive molting death of the *vps-45* null mutant a combination of traditional SNP mapping and next generation sequencing was employed as previously described in the introduction (section 1.1.8). As already mentioned this method has already been utilized in *C. elegans* (Doitsidou et al. 2010b). It has already been shown that the Hawaiian genome does not appear to suppress the *vps-45* (*tm246*) molting arrest phenotype, a critical factor for the use of this method (Section 6.1). As a result, the Hawaiian genome could be used as the reference genome for the mapping and 40 independent homozygotic lines for both the *svp* (*ij117*) suppressor and the *vps-45* (*tm246*) null mutant created in the Hawaiian genetic background.

The Hawaiian *C. elegans* strain is wild type but has multiple polymorphisms on all chromosomes, which make its genome distinct from the N2 Bristol strain which was used for the creation of the IA757 strain and as a result was also the genetic background of its EMS isolated suppressor. As such, when the two are crossed their F1 progeny will have one set of "Bristol chromosomes" and one set of "Hawaiian chromosomes".

Recombination can occur between chromosome pairs. Recombination will be possible across the entire *C. elegans* genome, but by selecting for homozygosity for the *vps-45* (*tm246*) mutation and its suppressor, genomic regions containing these genes and closely linked sequences must remain Bristol. On the other hand, unlinked DNA sequence will tend towards a 50% Bristol and 50% Hawaiian ratio (Figure 1.5).

The 40 independent lines used for sequencing are generated from 40 independent F2 animals homozygotic for the *vps-45* (*tm246*) allele and its suppressor. Homozygosity for *vps-45* (*tm246*) was verified via PCR and for the suppressor by survival at 25°C. To achieve this IA773 hermaphrodites were crossed with CB4856 (wild type Hawaiian) males. F1 hermaphrodites were picked and individually left to egg lay a F2 brood. After egg laying, the F1 parents were lysed and PCR was carried out with their DNA to test for the presence of both the wild-type and mutant *vps-45* (*tm246*) alleles (thus ensuring that the F1 animals selected were outcrossed and not the result of IA773 self-progeny. PCR verified that the hermaphrodites were indeed outcrossed since they were heterozygotic for

the *vps-45* (*tm246*) null allele as previously discussed in Chapter 3, section 3.4 (Figure 6.8).

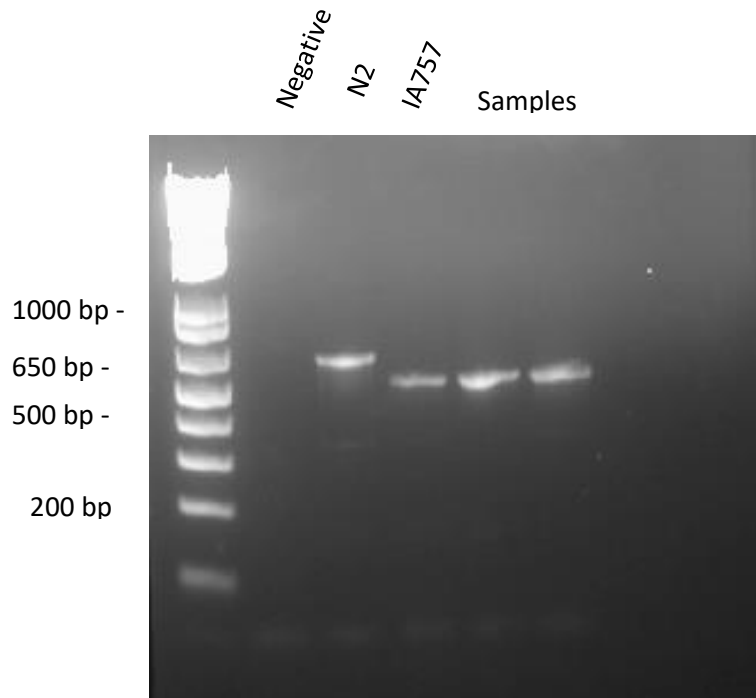


Figure 6.8: Representative gel for detection of *vps-45* (*tm246*) allele.

Primers used are described in materials and methods. 629bp band corresponds to the wild type allele for the wild type *vps-45* and 480bp to the TM246 null *vps-45* allele.

To increase the possibility of getting that double homozygotic strain selection was done in two stages. Initially worms were cultured at 15°C at which stage all IA757 animals will be able to survive, with or without the suppressor. Single hermaphrodites from each F2 plate were then transferred to new plates and left to generate a brood by selfing.

Multiworm lysates that were prepared from those broods and were genotyped using PCR, and those homozygotic for the *vps-45* (*tm246*) were transferred at 25°C to grow. At this stage, only animals also homozygotic for the suppressor should be able to survive, thus having the double homozygotic lines, which will be carrying Hawaiian wild type DNA.

All lines were further tested to establish that they were carrying Hawaiian DNA in addition to the *vps-45 (tm246)* mutation and its suppressor. Three sets of primers were used for this purpose (Bazan & Hillers 2011). One set amplifies a sequence at Chromosome I in both Bristol (N2) and Hawaiian (CB4856) wild type strains, which produces a band of 594bp. A second primer set amplifies a sequence on Chromosome IV, which produces a band of 852bp. Finally, the third set can amplify a sequence of 528bp for Chromosome V. In each case, the amplified band contains a SNP between Hawaiian and Bristol DNA at an enzyme restriction site. Depending on the sequence only the Bristol or the Hawaiian sequence can be digested on each case producing two distinct fragments (Figure 6.9). All lines produced were checked for the presence of Hawaiian DNA across all three chromosomes. All 40 suppressed lines for the moulting death at the non-permissive temperature were lysed and their DNA was purified and mixed in a single solution in equal amounts (Appendices 4-7) and were sent for Illumina sequencing.

6.10 Next generation sequencing analysis of the *svp (ij117) vps-45 (tm246)* suppressed mutants in Hawaiian background

Analysis of the result obtained by the next generation sequencing process was conducted by the University of Glasgow Polyomics department using a Modified Cloudmap pipeline on the Galaxy platform (Minevich et al. 2012). The reads were aligned to the reference genome using bowtie2 (Langmead et al. 2009). Duplicate aligning reads were marked using Picard MarkDuplicates from SAMtools (Li et al. 2009). Reads around indels were realigned to eliminate false SNPs around the indels, using GATK (Genome Analysis Toolkit) Realigner Target Creator and Indel Realigner. Variants were then called using GATK Unified Genotyper (DePristo et al. 2011). The variant sites were filtered for read depth coverage of greater than 3 reads. The variant recombination frequencies were plotted using the custom CloudMap module, CloudMap: Hawaiian

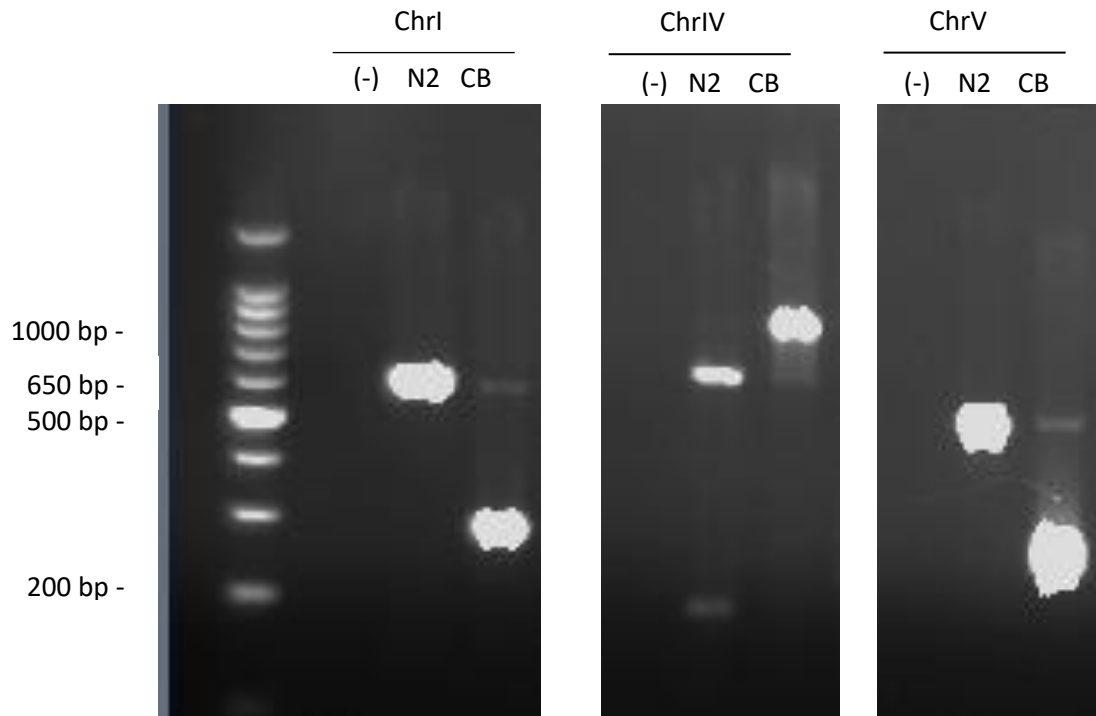


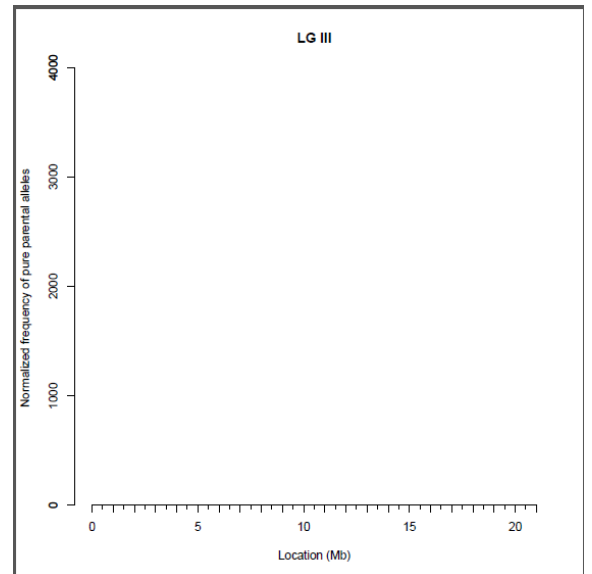
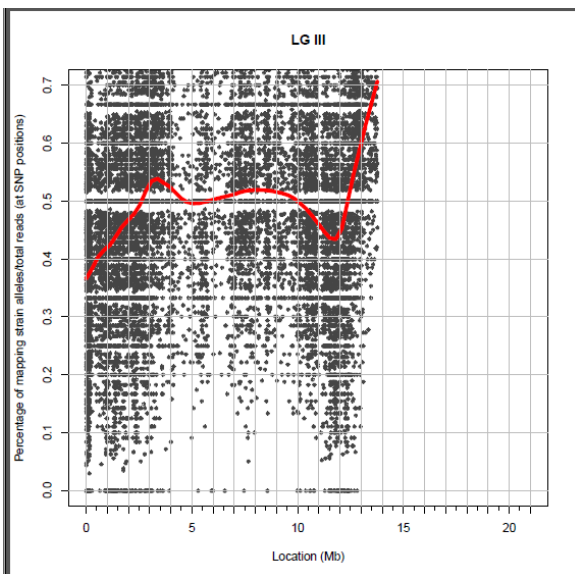
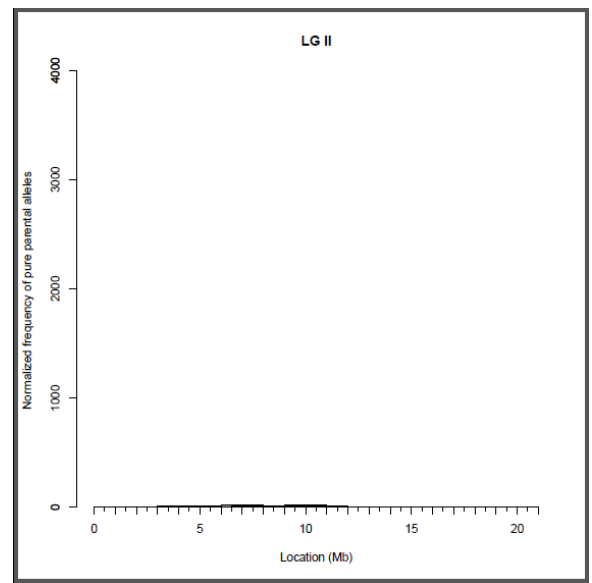
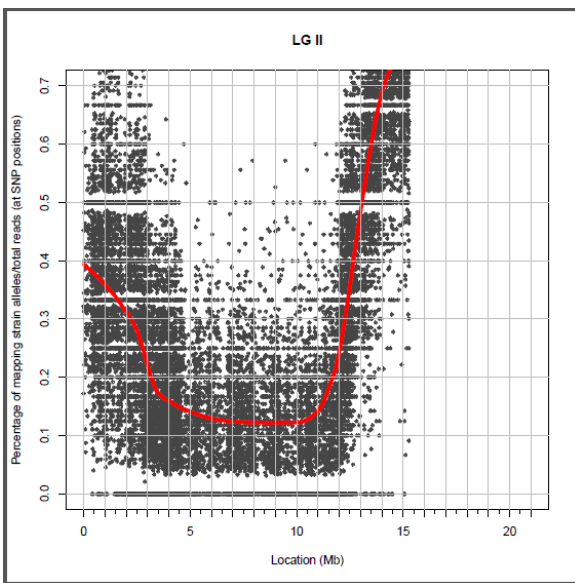
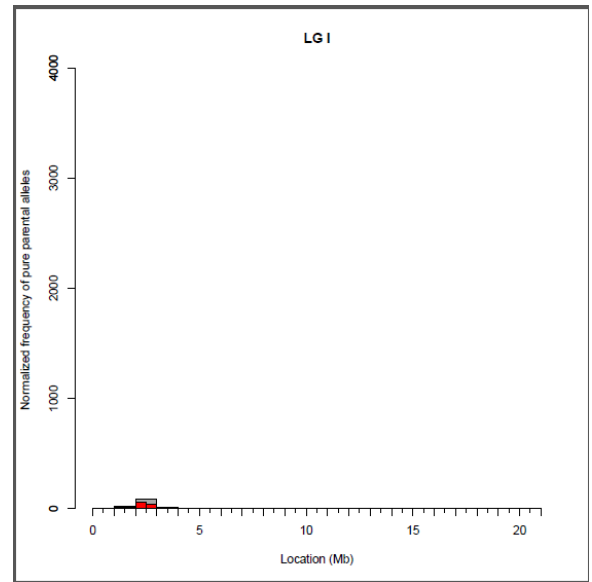
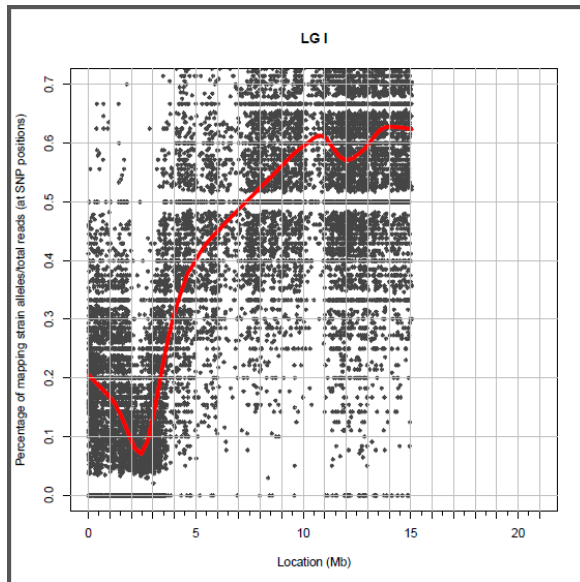
Figure 6.9: Representative PCR for the detection of “Hawaiian” and “Bristol” DNA.

Sequences are amplified for each. The presence or absence of the Hawaiian SNP allows the appropriate enzyme to cut the sequence in each case. Fragment sizes and enzymes used are detailed in sections 2.3.14 and 2.3.15.4.

Variant Mapping. Results were returned and are shown below. Two graphs were produced for each of the six chromosomes (LGI-V, LGX), a scatter graph and a frequency plot. The scatter graph represents the ratio of mapping strain nucleotides, in this case the Hawaiian strain over the mutant strain, in this case Bristol at all SNP positions. Chromosomes which contain regions of linkage, meaning the area where the mutation to be identified will be present will have regions where the frequency of mapping strain (Hawaiian wild type strain) reads will be equal or close to 0, and consequently the reference genome reads (Bristol wild type strain) will be approaching a frequency equal or close to 1. The corresponding plots for those regions will have data points lying on the X axis. To better visualise these regions where the frequency approaches zero on the scatter maps, a LOESS regression line is also produced (red line). Those data can then be normalised to produce frequency plots which show the regions of linked chromosomes where pure parental (mutant strain) alleles are concentrated (Minevich et al. 2012). On those plots 1Mb areas

for the 0 ratio SNP positions are coloured in grey and 0.5Mb areas in red. A strong linkage signal was observed at chromosome X. The frequency of the mapping strain reads at this point is zero and the LOESS regression line is adjacent on the x-axis of the graph. This signal corresponds to the *vps-45* deletion. This strong signal for the reference Bristol DNA demonstrated that the process had worked (Figure 6.10). Three more regions were observed where there was a signal pointing to parental allele representation in the genome. Those were on Chromosome I, II and V (Figure 6.10). The Chromosome I region was quickly disregarded. There is a common known incompatibility at this position arising from two genes (*zeel-1*, and *peel-1*) between Hawaiian and Bristol strain which often arises when using full genome sequencing for the identification of mutants, when using a mapping strain [reviewed in (Seidel et al. 2008)]. As a result, only two regions remained which showed a potential signal for the suppressor. However, the frequency of mapping strain reads, despite being low, wasn't close enough to zero to point to the location of a single allele (Figure 6.10).

A



B)

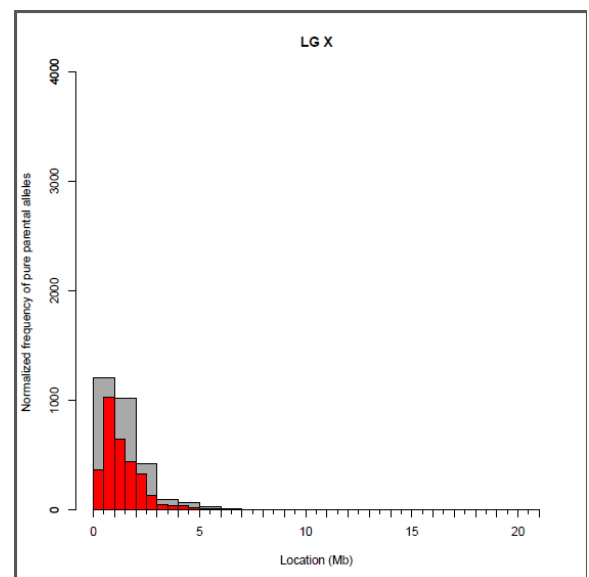
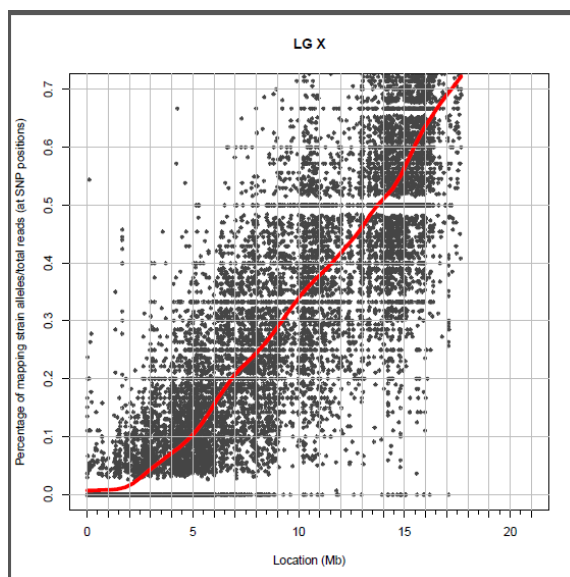
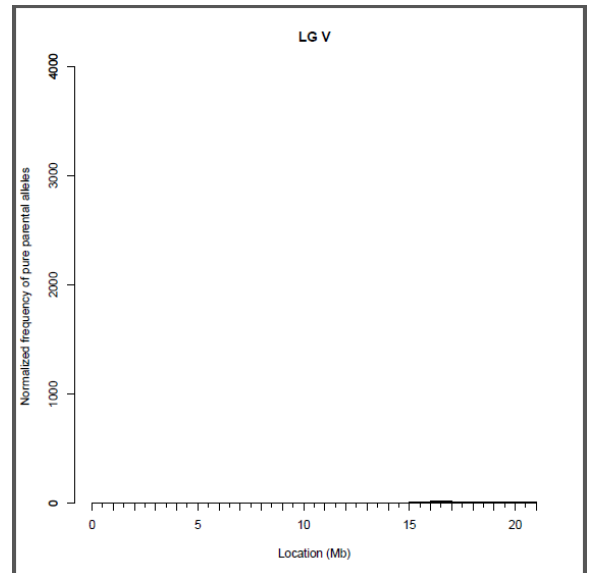
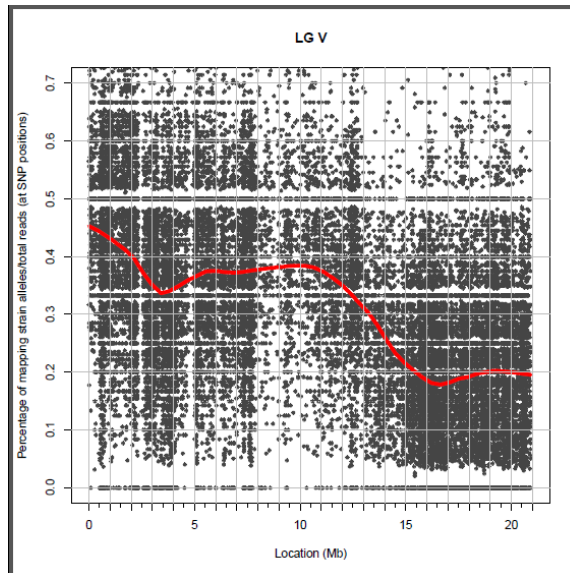
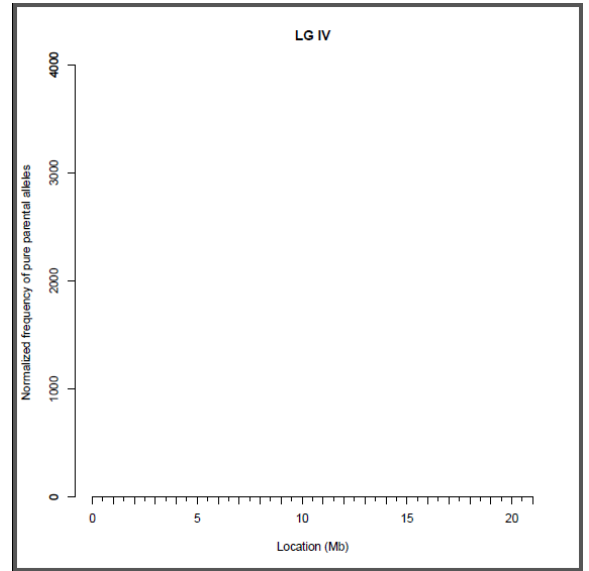
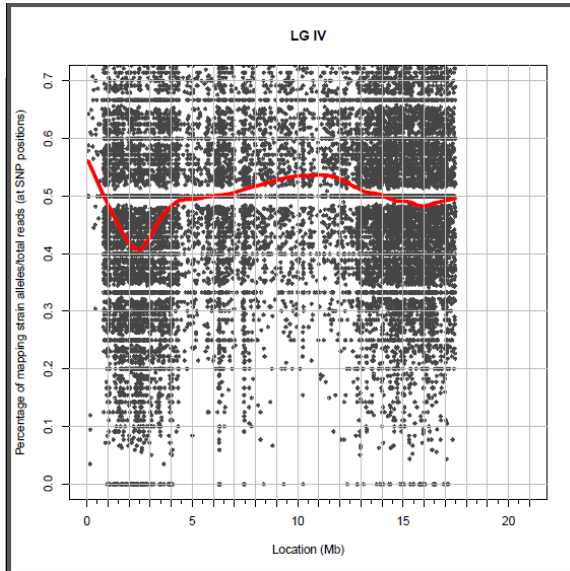


Figure 6.10: Cloudmap results as retrieved by the analysis of the full genome sequencing data obtained by the Galaxy software for the identification of the *svp* (*ij117*) suppressor allele.

Scatterplots for each SNP are shown for each chromosome on the right and accompanied by a frequency plot which displays the linked chromosomal regions where pure parental alleles (Bristol) are concentrated. **A)** SNP scatterplots for Chromosomes I (LG I), II (LG II and III (LGIII). **B)** SNP scatterplots for Chromosomes IV (LG IV), V (LG V) and X (LG X) (Previous page).

6.11 Identification of candidate suppressors for the *vps-45* (*tm246*) moulting arrest

Two regions stood out which showed a possible signal for a potential suppressor, a region on chromosome II and a region on chromosome V. However, the frequency of the mapping strain reads is not low enough to propose a definite single suppression region and especially in chromosome II too widespread not producing a single peak. Chromosome II however appeared to be the most likely region for the suppressor since it exhibited a lower frequency of Bristol/reference strain reads with 90% of the total reads being Bristol and approximately 10% being Hawaiian. (Figure 6.10). On the other hand, on chromosome V approximately 80% of the total reads was Bristol and only 20% was Hawaiian (Figure 6.10). Therefore, a stronger possible linkage to Bristol DNA is observed at chromosome II and thus it was selected for the attempted identification of candidate genes as suppressors.

To identify candidate suppressors, the DNA sequence of the region of chromosome II was compared against that of the wild type Bristol genome sequence, looking for DNA sequence changes that could alter gene function. These included nonsense and nonsynonymous changes within coding sequence, splice site mutations, deletions etc. (Minevich et al. 2012). In the chromosome II region of 5-10mb where a strong Bristol signal was indicated (Figure 6.11). In total 31 genes were identified with potentially functional sequence changes relative to the N2 wild type sequence as shown in table 6.2.

6.12 Testing of the candidate genes for suppression of the *vps-45 (tm246)* using RNAi

The candidate suppressor genes that were previously retrieved from the full genome sequencing (Table 6.2) were tested for the ability to suppress the *vps-45 (tm246)* moulting death phenotype using RNAi. This was done under the assumption that the mutations in these genes is a loss of function and as a quick method that would easily identify such an effect if it was present. Approximately, 100 L1 arrested larvae were cultured on plates seeded with the HT115 RNAi expressing bacterial strain. Bacteria carrying the empty vector were used for the culturing of the IA757, IA773 and N2 strains were used as the negative controls for the RNAi effect. The bacterial strains expressing each of the candidate suppressor genes to be silenced were fed to the IA757 strain as described on section 2.3.21. Five of those genes were not available in our RNAi library so they were not tested these were *ptc-2*, *pah-1*, *kin-6* and the unannotated regions Y110A2AM.1 and ZK945.7. The survival of each of the treated strains was assessed throughout development at 25°C. Larvae were observed over the period of development from the L1 stage to adulthood. Their survival was measured and compared to IA757, IA773 and the N2 strains. (Table 6.2, Figure 6.11).

None of those candidates that were tested was able to suppress the molting death at the non-permissive temperature, as in no case any of the RNAi affected animals exhibited a median survival higher than 96 hours which was also observed for the IA757 strain, genotype *vps-45 (tm246)*. None of the tested RNAi seemed to be preventing the *vps-45 (tm246)* 25°C moulting death and none of them came close to simulating the IA773 suppressed strain (Figure 6.11).

Cosmid	Gene name	map position	
W04H10.3	nhl-3	-15.59	← -17.9 T25D3
Y110A2AM.1		-9.38	← -14.5 R52 (B)
Y8A9A.2		-6.21	← -4 M03A1 (C)
F59A6.4		-2.6	
C27A2.6	dsh-2	-2.54	
C34F11.9	dsh-1	-1.93	
B0034.5		-0.77	
F21H12.4	ptc-2	-0.55	
K03H9.3		-0.3	
C56E6.1	abcx-1	-0.16	
T14B4.2		0.05	
F41G3.2		0.09	
C52E12.2	unc-104	0.21	
F43E2.4	haf-2	0.5	
R153.1	pde-4	0.51	
B0495.6		0.53	
B0495.5		0.53	
B0495.7		0.53	
B0495.10	cpna-5	0.54	
B0228.6		0.56	
M110.5	dab-1	0.75	
K08F8.4	pah-1	0.88	
W07A12.5	col-78	1.05	
ZK945.7		1.9	
ZK945.8		1.9	
C07E3.1	stip-1	2.44	
ZK673.9	clcc-143	2.65	
VM106R.1		3.13	
R06F6.2	vps-11	3.13	← 3.3 F37HB (D)
ZK20.2	kin-6	3.8	← 13.6 Y38F1 (E)
Y81G3A.3	gcn-2	14.1	← 20.9 Y51H1 (F)

Table 6.2: List of candidate suppressors retrieved from sequencing results for the *C. elegans* chromosome II.

Cosmid code and gene name are provided. Position of oligos that were used to check for lines that are not homozygous for Bristol DNA in the region, indicated as the 'Right side' and 'Left side' of the chromosome and the linkage region that was identified.

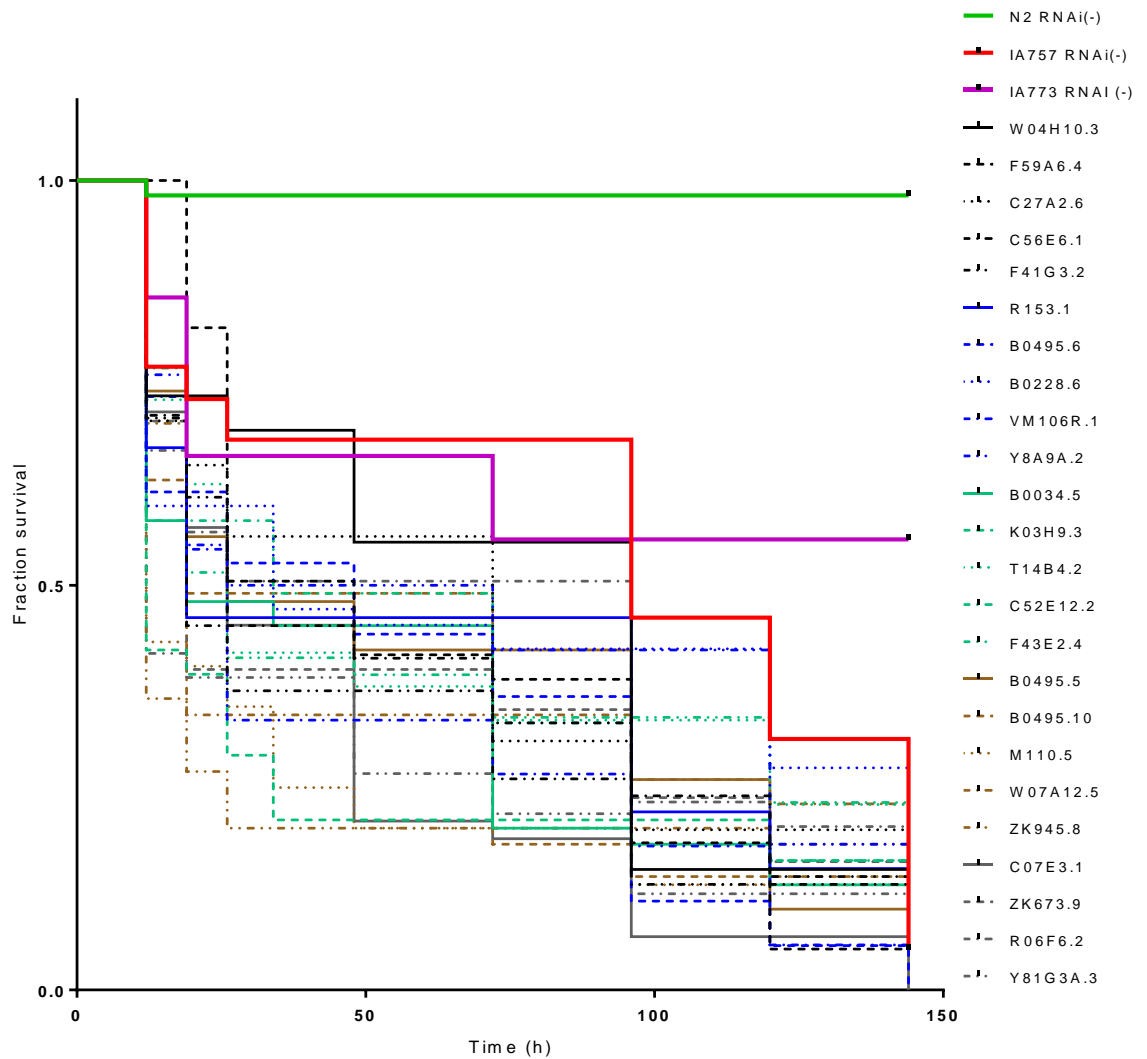


Figure 6.11: Survival fraction of animals under a period of 6 days, under the influence of RNAi for each of the candidate suppressor genes.

Animals were inoculated as synchronised L1 larvae onto the plates. Initial inoculate for each sample was 90-100 L1 larvae. All samples were cultured at 25°C. Median survivals: N2 RNAi(-) Undefined, IA757 RNAi(-) 96 hours, IA773 RNAi (-) Undefined, W04H10.3 96 hours, F59A6.4 48 hours, C27A2.6 72 hours, C56E6.1 19 hours, F41G3.2 26 hours, R153.1 19 hours, B0495.6 48 hours, B0228.6 34 hours, VM106R.1 26 hours, Y8A9A.2 49 hours, B0034.5 19 hours, K03H9.3 12 hours, T14B4.2 26 hours, C52E12.2 34 hours, F43E2.4 26 hours, B0495.5 26 hours, B0495.10 19 hours, M110.5 12 hours, W07A12.5 19 hours, ZK945.8 12 hours, C07E3.1 26 hours, ZK673.9 19 hours, R06F6.2 96 hours, Y81G3A.3 12 hours.

6.13 Identification of two different genetic subpopulations within the *vps-45*

(*tm246*) suppressed lines

Through the sequencing results presented above a possible linkage signal was identified on chromosome II for a high proportion of Bristol DNA sequence within the 40 backcrossed populations. However, that signal did not reach 100% representation of Bristol DNA as 10% of Hawaiian alleles was present. This contrasts with the clear signal on the X chromosome for the *vps-45(tm246)* allele (Figure 6.10).

Other possibilities were therefore considered. In handling the *vps-45(tm246)* mutant, it was observed that the strain frequently suppresses when cultured even although the (*tm246*) allele is an extensive deletion and hence not a revertible allele. Also, in the original EMS mutagenesis that generated the *svp (ij117)* suppressor, the rate of generation of suppressors was noted to be very high. Thus, the possibility that the IA773 strain is complex and carries more than one independent allele capable of acting as an extragenic suppressor of *vps-45(tm246)* was considered. Such a model could explain the genome sequence data described above.

To test this hypothesis, a method of SNP screening was employed to investigate each of the original 40 lines used to produce the pool of DNA used for sequence analysis. All 40 samples that were originally sent for sequencing were screened using PCR primers that can distinguish between Hawaiian and Bristol DNA at various positions on chromosome near the region of interest for the suppressor as detailed in section 2.3.15.5 section of Materials and methods. The primers chosen in this case corresponds to regions of the genome which are present at the two ends of the region with the candidate suppressor genes that were tested and hence the region from which the linkage signal for chromosome II originated (Table 6.2, Figure 6.12).

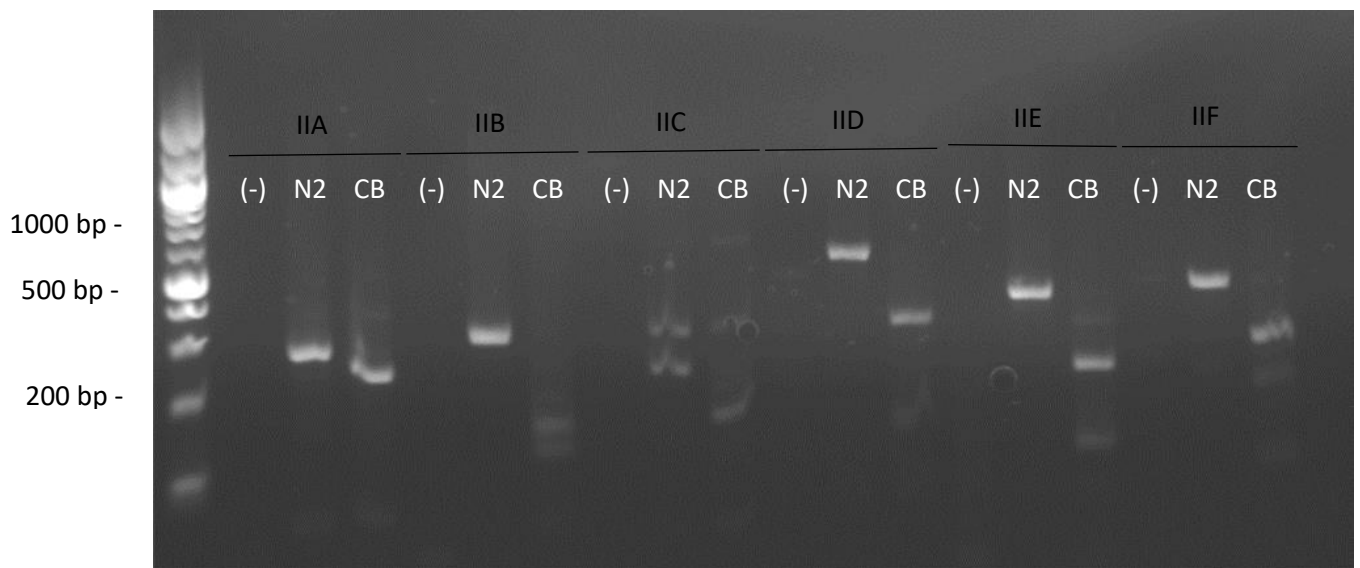


Figure 6.12: Detection of Hawaiian and Bristol SNPs across the *C. elegans* chromosome II.

Amplified sequences using the primer pairs described on sections 2.3.14 and 2.3.15.4. Each amplified fragment was digested with the appropriate restriction enzyme). After digestion Hawaiian DNA (CB) can be

	1	2	3	4	5	6	7	8	9	10	11	12	13	14	15	16	17	18	19	20	
A	B	B	H	B	B	B	B	H	B	B	B	H	B	H	B	H	B	B	B	B	B
B	B	B	H	B	B	B	B	H	B	B	B	H	B	H	B	H	B	B	B	B	B
C	B	B	B	B	B	B	B	B	B	B	B	B	B	B	B	B	B	B	B	B	B
D	B	B	H	B	B	B	B	B	B	B	B	B	H	B	B	B	B	H	B	B	H
E	B	H	B	H	B	B	B	H	B	B	H	B	B	B	B	H	B	H	B	H	B
F	H	H	B	B	H	B	H	B	H	B	H	B	H	B	B	B	H	B	H	B	H

	21	22	23	24	25	26	27	28	29	30	31	32	33	34	35	36	37	38	39	40	
A	B	H	H	B	B	H	B	H	B	H	B	B	H	B	H	B	H	H	B	H	B
B	B	H	H	B	B	B	B	B	H	H	B	B	H	B	H	B	H	H	H	B	H
C	B	B	H	B	B	B	B	B	H	B	B	B	B	B	H	B	B	H	B	H	B
D	B	H	B	H	B	B	H	B	H	B	B	B	B	B	H	B	B	H	B	H	B
E	B	H	B	H	B	H	B	H	B	H	B	H	B	B	H	B	H	B	H	B	H
F	B	H	B	H	B	H	B	H	B	H	B	H	B	B	H	B	H	B	H	B	H

Table 6.3: Visual representation of homozygosity of Bristol (red) or Hawaiian (green) sequences of each of the suppressed lines for Chromosome II.

Suppressed Hawaiian *vps-45* (*tm246*) mutant lines 23, 29, 35, 38 and 39 exhibit no homozygotic region for the Bristol alleles in any of the areas tested despite suggesting they could be carrying a different suppressor allele at a different chromosome.

Using the data obtained from the PCR amplification of DNA for each of the lines a table was constructed which allowed for the classification of each of the 40 lines as homozygotic for the Bristol SNP or homozygotic for the Hawaiian SNP or heterozygotic (Hawaiian and Bristol) for each. From the 40 samples, 35 were identified as homozygotic for the Bristol DNA at least in one of the positions tested for chromosome II SNP C (Table 6.3).

Interestingly, five of the lines that were sent for sequencing don't have a homozygotic region for Bristol DNA on chromosome II as detected by this low resolution SNP-mapping method (Table 6.3). These were lines 23, 29, 35, 38 and 39. Therefore the possibility that a suppressor does map to the chromosome II region identified, but not in these 5 lines was considered. However, all lines can survive at 25°C, so for this to be true there would have to be more than one suppressor allele in the strain IA773. Such a model could explain the poor resolution in the sequencing data for the suppressor allele but perfect mapping for the *vps-45* allele. As previously stated, a large number of suppressed lines were obtained from the original EMS mutagenesis (Section 6.1) and at a frequency that suggests either many genes can suppress or fewer but highly mutable. Also, the original IA757 strain frequently suppresses just by sub-culture without applying a mutagen. Therefore, perhaps having two suppressors in one isolate is not that unlikely. The other chromosomal location for a second suppressor could be on chromosome V where a weaker possible linkage signal was also observed (Figure 6.10).

6.14 A second linkage area on chromosome V suggest the existence of a second suppressor for the *vps-45 (tm246)* moulting arrest

To investigate the possibility of a second suppressor on chromosome V, all lines were screened in the linkage region for the identification of SNP of Bristol or Hawaiian DNA (Figure 6.13). The same five lines that had been previously identified for potentially not carrying a suppressor on chromosome II stood out once again. Results showed that all of them had a specific region which was exclusively Bristol on chromosome V snp D, for lines 23, 29, 35, 38, 39 (Table 6.4). This region coincides with the plateau of the LOESS regression line on the sequencing graph for chromosome V (Figure 6.10). This is consistent with the possibility that both the region on chromosome II and on chromosome V contain *vps-45(tm246)* suppressor alleles.

The identification of two regions with reduced mapping strain SNPs (in addition to the clear signal for *vps-45* itself) from the genome sequencing could indicate that there are two distinct genetic populations which are both suppressed. If that is the case, it is possible that despite both of these two populations (possibly 35 Chromosome II lines and 5 chromosome V lines) being suppressed for the moulting death at 25°C they might exhibit different levels of suppression as different genes would be involved and possibly exhibit other phenotypes, such as different growth patterns when cultured in the permissive temperature of 15°C.

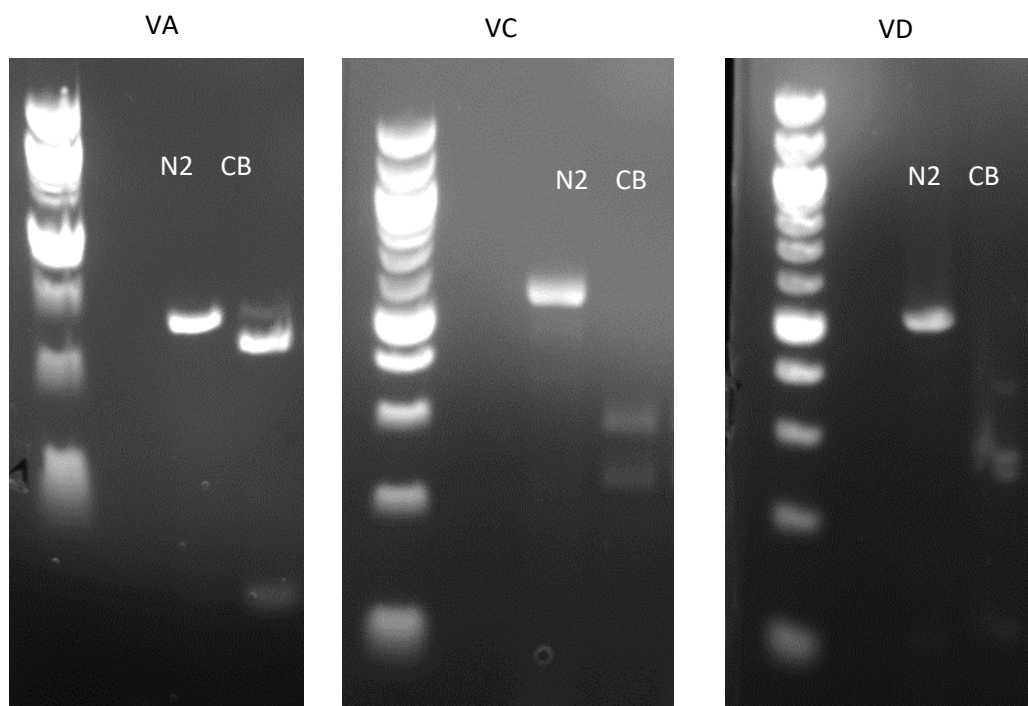


Figure 6.13: Detection of Hawaiian and Bristol SNPs across the *C. elegans* chromosome V

Each amplified fragment was digested with the appropriate restriction enzyme as described on sections 2.3.14 and 2.3.15.4 After digestion Hawaiian DNA (CB) can be distinguished from the Bristol one (N2).

	1	2	3	4	5	6	7	8	9	10	11	12	13	14	15	16	17	18	19	20
A	B B	B B	H H	B B	B B	B B	H H	H H	B B	B B	B H	B H	B H	B H	H H	H H	B H	B H	B B	B B
C	B B	B B	B B	B B	B B	B B	H H	B B	B B	H H	B B	B H	H H	B B	H H	H H	B B	H H	B B	B B
D	B H	B H	B B	B B	B H	B B	H H	B B	B H	H H	B B	B H	B H	B H	B H	B B	B H	H H	B B	B B

	21	22	23	24	25	26	27	28	29	30	31	32	33	34	35	36	37	38	39	40
A	B B	B H	H H	H H	B H	H H	B H	B H	H H	B H	B B	B B	H H	B H	H H	B H	B H	H H	H B	H H
C	B B	B H	H H	B H	H H	B B	B B	B B	H H	B B	B B	H H	B B	B H	B B	H H	B B	H H	B H	B B
D	B H	B H	B B	B B	H H	B B	B B	B B	B B	B B	B B	B H	B B	B B	B B	B H	B B	B B	B B	B B

Table 6.4: Visual representation of homozygosity of Bristol (red) or Hawaiian (green) sequences of each of the suppressed lines for chromosome V.

Suppressed Hawaiian *vps-45(tm246)* mutant lines 23, 29, 35, 38 and 39 exhibit exclusively Bristol DNA around the SNP D sequence

6.15 At least two phenotypic sub-populations exist within the 40 suppressed sequencing lines exhibiting different growth patterns

In order to assess if the two genetic sub-populations discussed above (chromosomes II and V possible suppressors) exhibit any phenotypic differences with one another, both were checked for differences in their growth pattern. Identifying different phenotypic subpopulations which fell into the same groups as the previously identified genetic ones enforces the idea that two suppressors exist rather than one.

As such, ten adults from each line were placed on a single plate and cultured at the non-permissive temperature of 25°C. The time it took for each suppressed line to starve was assessed. This was an indication of the overall growth speed of the whole population. This test provided potentially informative results. Firstly, the 5 lines that do not contain a detected homozygotic region for Bristol genome as detected by the SNP method, lines 23, 29, 35, 38, 39, all took longer to grow to starvation and all other individual lines. Secondly, they do not all behave quite the same; 23 and 29 appear to grow substantially slower than 35, 38 and 39. Finally, the other 35 lines all grow substantially faster than the parental suppressed line IA773 (Figure 6.14). This suggests a degree of genetic complexity to the suppression and possible multiple interacting loci. Potentially more than one loci are responsible for the suppression of the moulting death caused by the loss of Vps45 function. Also, the 35 'fast' growing lines that appear to be growing faster than the original isolate of the suppressor (IA773) could potentially indicate that the IA773 strain still carried mutations from the EMS screen which affect its fitness which were removed after the backcrosses with the Hawaiian wild type strain. Alternatively, regions of the Hawaiian genome could be enhancing the impact of EMS-induced suppressors from the Bristol genome.

New lysates were prepared only for the 35 "fast growing" lines and were mixed and cleaned appropriately in order to be sent for sequencing again in hopes of identifying one of the two potential alleles causing the suppression (Appendices 8-10).

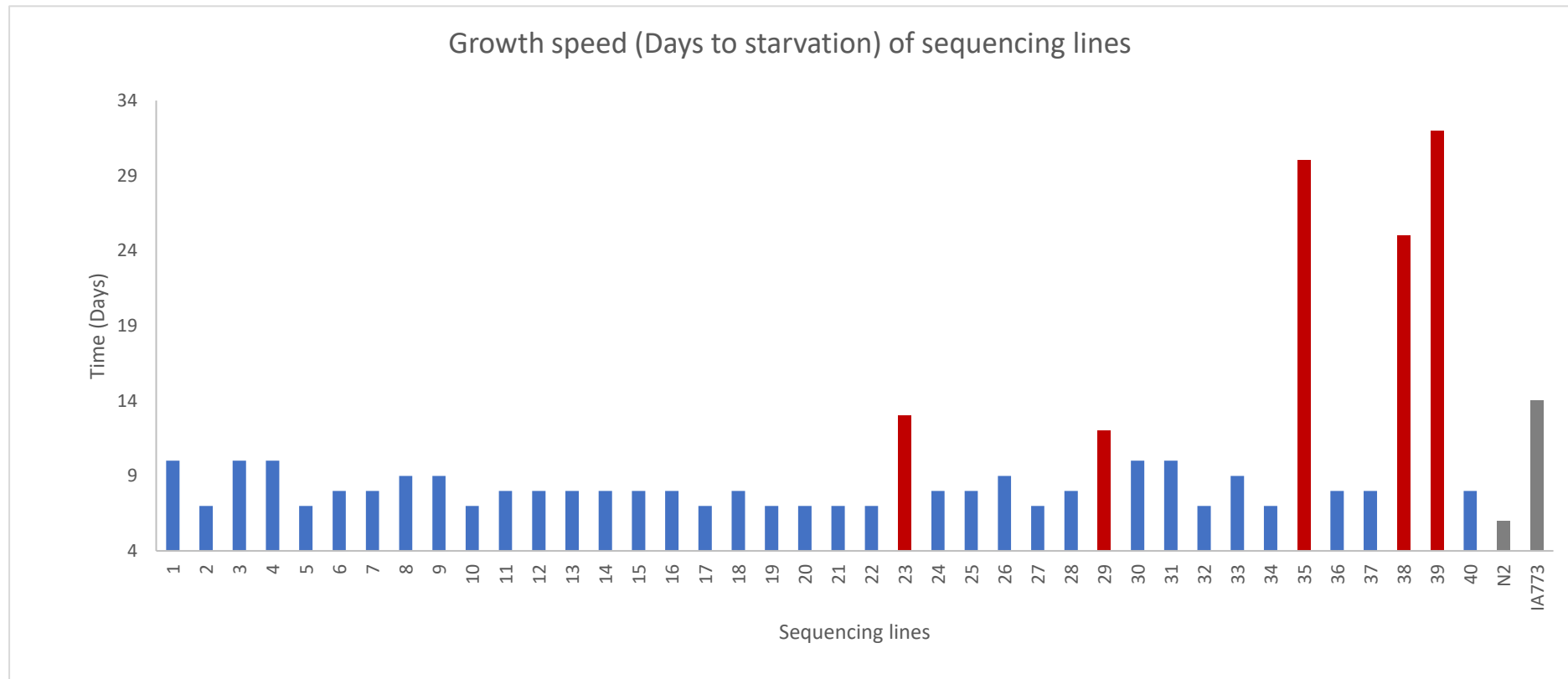


Figure 6.14: Two sub populations exhibiting different growth phenotypes within the Hawaiian *syp (ij117) vps-45 (tm246)* lines prepared for the sequencing experiment.

Fast growing lines are shown with blue. The five slow growing lines are, shown in red. The control lines wild type N2 and *syp (ij117)/IA773* are shown with the grey bars.

6.16 Chapter summary

In this chapter, the IA773 suppressed strain was phenotypically characterised by being compared to the original IA757 strain and to wild type N2. It was demonstrated that the *svp (ij117)* allele almost completely suppresses the 25°C moulting death and larval arrest in animals lacking the VPS45 protein. Furthermore, experiments showed that suppression by the *svp (ij117)* suppressor allele is almost exclusive to the temperature sensitive moulting death as the suppressor doesn't rescue the smaller body length phenotype originally observed for the IA757 strain, nor does it significantly alter the moulting profile, as both the original mutant and the suppressed strains require roughly 7-8 hours to go through a moult whereas the wild type strain requires 5- hours. Furthermore, IA773 animals exhibit a similar post-embryonic development time to the IA757 animals and both required approximately 130 hours to reach adulthood from arrested L1 larvae as opposed to the wild type strain which can achieve the same developmental stage at 100 hours.

The *svp (ij117)* suppressor, on the other hand, was able to mildly suppress the embryonic lethality exhibited by the *vps-45 (tm246)* homozygotic strain, however not to a degree that was comparable to the wild type strain in the permissive (15°C) and non-permissive temperatures (25°C). Finally, the IA773 strain exhibits a longer overall survival to IA757 at the permissive temperature and a higher median survival in both temperatures. Thus, the suppressor does improve the lifespan of animals lacking a functional *vps-45* gene and confers a significantly increased lifespan at the non-permissive culturing temperature. Overall, it was demonstrated that the suppressor mainly rescues the developmental arrest and moulting death phenotype observed when mutants are cultured at 25°C.

After the suppressor allele was phenotypically characterised, the pattern of inheritance for it was investigated. The suppressor behaved as being recessive and autosomal in the tests performed, and a strategy was elected to identify the gene responsible for the suppression through full genome sequencing. In order to do this the suppressor and the *vps-45* deletion mutant had to be introduced into wild type animals with Hawaiian DNA background. It was verified that the Hawaiian polymorphisms cannot suppress the *vps-45 (tm246)* molting death as worms which carried the deletion allele in Hawaiian background died after being continuously cultured at 25°C. Hence, the 40 individual lines were produced which

carried the *vps-45 (tm246)* allele and the suppressor in Hawaiian background, where lysed and their DNA was sent for full genome sequencing.

Data retrieved from the full genome sequencing however did not point to only one locus of suppression. Two areas of linkage for the suppressor were identified on chromosomes II and V. Using PCR to amplify those regions around the linkage hotspots on those chromosomes two subpopulations were identified within the 40 lines created for the whole genome sequencing experiment. 35 of those lines exhibit linkage for DNA of Bristol origin and hence for the suppressor on chromosome II, however 5 lines did not and only exhibited linkage in the chromosome V region of interest. Those two subpopulations were further phenotypically tested, the time for an original inoculate of 10 adults, to reach starvation was assessed. The five lines which exhibited linkage on chromosome V required overall longer to starve, thus suggesting that potentially a second suppressor is present on chromosome V. Overall the data strongly suggest the possibility of more than one locus which contributing to the suppression of the *vps-45 (tm246)* temperature sensitive molting death in strain IA773. This is consistent both with the various lines of mapping data (sequencing and SNP) and with the pattern of different growth rates at the non-permissive temperature for the 40 different lines used in the sequencing. Further mapping analysis is needed to resolve the level of complexity in this suppression of *vps-45(tm 246)*.

Chapter 7: Discussion

The primary focus of this work was to investigate the effect of the disruption of endosomal trafficking and autophagy in embryonic and post embryonic development of the nematode *C. elegans*.

C. elegans mutants lacking a functional *vps-45* gene, exhibit a temperature sensitive lethality where they are unable to shed their cuticle during ecdysis at the end of the molting and die. It should be noted at this point that the *vps-45* (*tm246*) mutant allele is a substantial deletion and therefore it must be considered a non-revertible mutation. Despite that, *vps-45* mutants were able to suppress the 25°C (non-permissive temperature) molting death phenotype after continuous culturing at the permissive temperature of 15°C at high frequency. This suppression of a non-revertible allele is unusual. Given the fact that the function of VPS-45 is the correct targeting and fusion of vesicles it is hard to imagine how suppression occurred and what spontaneous mutations might be able to suppress a non-revertible mutation. Furthermore, how and why the *vps-45* null mutants produce a temperature sensitive phenotype, is also of particular interest. It is possible to conclude that specificity for membrane fusion provided by VPS-45 vesicle targeting through the trans-Golgi network, and endosomal system are sufficiently functional at 15°C to permit survival, but somehow not at 25°C. Perhaps membrane trafficking at slower rates because of lower temperatures is sufficiently accurate, but not so at higher temperatures.

To identify how the suppression works, an EMS mutagenesis screen was carried out in our lab, prior to the start of this project. The screen was carried out in a relatively small sample of ~2000 genomes, from which at least 30 independent suppressors were obtained. This was viewed as a relatively high frequency which suggests most likely that multiple different genes can mutate to suppress the temperature sensitive lethality. Furthermore, by taking into account the frequent spontaneous mutations at the permissive culturing temperature as well as the high number of suppressors obtained by a relatively small EMS screen it is easy reasonable to conclude that there are multiple genes/mechanisms through which the suppression works.

One possibility is that the suppression could be working through activation of a stress pathway. The elevated function of such a pathway would allow for the survival of the *vps-45* mutants. Such pathways might involve the unfolded protein response or autophagy,

both of which could conceivably relieve potential cellular stresses caused by mistargeted or incompletely fused vesicles.

Early observations of molting in *C. elegans* have indicated the rapid disappearance of Golgi bodies and excessive membranes at the end of each molt. These were formed in the hypodermis of animals during the molt (Singh & Sulston 1978). It is reasonable to suggest that autophagy is the most likely mechanism responsible for this clearance of these structures at the end of the moult.

On the other hand, *C. elegans* lacking a functional VPS-45 protein exhibit a temperature sensitive moulting death phenotype, where they are unable to shed their cuticle and complete the moult (Gengyo-Ando et al. 2007). Therefore, a possible relation between the autophagy, the endocytic pathway and moulting could exist.

To answer the above questions, a suppressor for the *vps-45 C. elegans* temperature sensitive lethal phenotype was isolated and using next-generation sequencing and classic genetic approaches two possible chromosomal regions where potential suppressors might map were identified. Furthermore, *unc-51* and *vps-45 C. elegans* mutants defective for endosomal trafficking and autophagy respectively, were compared and phenotypically characterised during embryonic and post embryonic development (during the moult), with the aim of identifying any similarities or differences. In addition to this, a *unc-51 vps-45* double mutant was created and a synthetically lethal phenotype was identified possibly suggesting a functional relationship between the two genes. Furthermore, the process of autophagy was characterised in the hypodermal seam cells, which take part in the secretion of cuticular components during the moult, in both *unc-51* and *vps-45* mutants providing further proof for the involvement autophagy in this developmental process. Finally, the sensitivity of these mutant to oxidative stress as well as the redox state of the ER was assessed, in an attempt to identify cause for the previously identified apoptosis of neutrophil cells in humans carrying the T224N mutation on the Vps45 gene (P. Stepensky et al. 2013). It was demonstrated that *vps-45* and *unc-51* mutants exhibited an oxidised environment and higher sensitivity to oxidative stress, with the latter exhibiting the stronger phenotype.

7.1 Characterisation and identification of the *vps-45 (tm246)* molting death suppressor

The suppressed strain which was isolated from the EMS screen was subjected to several comparisons with the wild type strain in order to determine what other phenotypes apart from the moulting arrest at 25°C were suppressed or altered (Section 6.3). Overall, the suppressed strain was very similar to the original *vps-45 (tm246)* mutant strain. They showed a very similar body size (slightly smaller than wild type), similar levels of embryonic lethality, and moulting behaviour at the permissive temperature (Section 6.4, 6.5). The suppressed mutant exhibited a mild increase in its lifespan compared to the original mutant. This increase in the lifespan compared to the original mutant was temperature independent (Section 6.7). The fact that not all phenotypes were suppressed could indicate that loss of *vps-45* is involved in the animal causes various organismal defects, and that the allele responsible for the suppression is acting and compensating for the loss of *vps-45* only in a subset of them.

Full genome sequencing was utilised in an attempt to identify the suppressor. However, the sequencing data did not give a single chromosomal region of suppression but possibly two, and in both cases the signal was not very clean. However, the fact that in the sequencing data a very clean signal was obtained for the *vps-45 (tm246)* mutation itself indicates that the sequencing process and mapping by N2 versus Hawaiian SNPs worked well.

Furthermore, all 40 sequencing lines were homozygotic for the *vps-45 (tm246)* mutation and were able to easily grow at 25°C, so they were indeed carrying the suppressor mutation along with the *vps-45* mutant allele (Section 6.14). The lack of a second clean signal for a suppressor mutation, and the presence of two moderate signals could suggest the presence of two unlinked suppressors rather than one within the original suppressed strain (Section 6.10).

Further SNP mapping in the chromosome II locus, as well as the chromosome V locus, where the two moderate signals were located, identified two subpopulations within the original sequencing population lines. 5 of the 35 lines did not seem to be carrying the locus for the suppression identified on chromosome II. These 5 lines also appeared to give a signal in the possible chromosome V suppression locus (Section 6.13, 6.14). The two subpopulations were subjected to phenotypic screening and it was found that there is a difference in the development speed of the animals of the smaller chromosome V

subpopulation which grew slower, while still being suppressed for the molting death at the non-permissive temperature (6.14). The above further strengthen the possibility that two different suppressors are present. Furthermore, it is possible that the two suppressors might be interacting with each other and thus producing different levels of suppressions in strain that are carrying one or the other, or both, and in different combinations of homozygosity or heterozygosity.

This is indeed possible since in the original EMS screen a large number of suppressors were obtained and continuous culturing of the *vps-45 (tm246)* mutant strain (IA757) for prolonged time would spontaneously produce suppressed animals. This original large number of suppressed animals from the mutagenesis screen as well as the often-spontaneous suppression would suggest a number of potential suppressors for the moulting death and potentially other phenotypes caused by the loss of VPS-45. As previously suggested a possible way through which suppression might work could be through the upregulation of a stress pathway such as autophagy, which might remove the mistargeted or partially fused aberrant vesicles resulting from the loss of VPS-45. In this model, any mutation that caused an upregulation of autophagy might suppress the *vps-45 (tm246)* mutant.

A second possibility on how the suppression works could be through different SM proteins which can potentially take up the role of *vps-45* or other SNARE proteins apart from SYN-16/Tlg2. In the past VPS-45 has been proposed to act as a replacement for SM proteins VPS-33.1 and VPS-33.2 for the maturation of endosomes in *C. elegans* (Solinger & Spang 2014). It is interesting that VPS-33.2 is located on chromosome II which is the prime candidate for one of the suppressors based on the sequencing results (Section 6.10). As a result, it is not impossible that a mutation in the *vps-33.2* gene could alter its function to replace VPS-45. The nature of the potential second suppressor on chromosome V remains unknown (Section 6.10), as is its relationship with the first suppressor. It is possible that different interactions between the two suppressors could produce different levels of fitness in the animals. Concluding, a second round of sequencing with the two sub-population will help elucidate this and identify the allele or alleles that are responsible for the suppression.

7.2 Phenotypic characterisation of *unc-51 (e369)*, *vps-45 (tm246)* and *unc-51(e369) vps-45 (tm246)* synthetic lethal double mutant

The hypothesis formed in the section 7.1 suggest the upregulation of a stress pathway such as autophagy as the cause for the frequent suppression of the *vps-45* mutant temperature sensitive lethality. The autophagy defective mutant *unc-51 (e369)* and the *vps-45 (tm246)* mutant exhibit different phenotypes overall.

It was shown that both mutants do not exhibit any obvious phenotypic similarities in terms of body shape, with the *vps-45 (tm246)* mutant exhibiting a relatively normal body shape and movement, but with a slightly reduced body size. On the other hand, *unc-51 (e369)* mutant, exhibits uncoordinated movement phenotype (Unc) (Ogura *et al*, 1994) as well as a shorter and fatter body shape similar to that of a Dpy phenotype (Aladzcity *et al*. 2007). A number of mutant animals (*dpy-5*, *dpy-7*, *dpy-11*) have the Dpy phenotype as a result of cuticular defects rather than changes in cell size (Thein *et al*. 2003). It is possible that autophagy could be playing a role in moulting since autophagy defective mutants exhibit cuticular abnormalities. Further to this VPS45 in yeast, and its binding partner Tlg2/Syntaxin16 have been shown to play a role in the regulation of autophagy (Ohashi & Munro 2010; Nair & Klionsky 2011; Chen *et al*. 2014). Taking into consideration all of the above factors, it is reasonable to consider that autophagy could have some impact in moulting and development through its interaction with the endosomal system.

Therefore, both the *unc-51* and *vps-45* mutants were characterised phenotypically in terms of their development either as embryos for embryonic lethality or post embryonically for post embryonic development, cuticular, morphological or moulting defects. Wild type, *vps-45 (tm246)* and *unc-51 (e369)* animals which were cultured from the non-permissive temperature for *vps-45 (tm246)* showed that only the *vps-45* mutants demonstrated a temperature sensitive moulting lethal phenotype whereas *unc-51* mutants would normally develop to adulthood irrespective of culturing temperature. This outcome suggests that VPS-45 is not directly influencing the process of autophagy or that it only has a mild influence on it (Section 3.4). It is also possible that is acting entirely independently of UNC-51, since no similarities are observed between the two mutants regarding the temperature sensitive lethality. Previous studies do point to an involvement of VPS-45 in the regulation of autophagy in yeast but not being essential for autophagy (Chen *et al*. 2014). Further to this, the data do support previously identified temperature sensitive

phenotypes identified in *Vps45* (Shanks et al. 2012) and *Vps21* yeast mutants, the latter of which exhibit similar autophagy defects as *Vps45* mutants (Chen et al. 2014).

Further experiments demonstrated that *C. elegans* carrying the *vps-45 (tm246)* allele exhibited higher embryonic lethality compared to the wild type both at the non-permissive and permissive temperatures for the moulting lethality. The wild type strain exhibited some embryonic lethality at 15°C, which was almost eradicated at the higher temperature of 25°C. A higher lethality was observed for all strains at the lower culturing temperature, suggesting that in all cases 15°C did not provide an ideal environment for the embryonic development of *C. elegans*. At 25°C, where wild type embryos exhibited a higher survival, it was observed that there was a small difference even in the case of the *unc-51 (e369)* mutant which showed a small lethality, however, not as big as in the case of the *vps-45 (tm246)* mutant (Section 3.3). This difference between the two mutants suggest that although both *vps-45* and *unc-51* can affect embryonic viability, the two must have different functions in embryonic development. Indeed it has been suggested that components of the autophagic machinery, including *unc-51*, take part in the clearance of apoptotic cell corpses which accumulate during embryonic development in *C.elegans* (Huang et al. 2013). Inability to effectively clear these corpses could possibility result in embryonic death. On the other hand, the *vps-45 (tm246)* embryonic lethality can potentially be explained by the defective trafficking of the yolk proteins to the developing embryo (Gengyo-Ando et al. 2007).

Following the above, it was assumed that shut down of both processes in *C. elegans* would potentially result in an additive effect. To investigate this, a double mutant was constructed by crossing the *unc-51 (e369)* and *vps-45 (tm246)* mutants (Section 3.5). The double mutant exhibited a very obvious phenotype of a much smaller body size compared to any of the other mutants. All strains, including the double mutant were accurately measured for their length. As such it became evident that the *vps-45 (tm246)* mutant was smaller compared to the N2 wild type strain followed by the *unc-51 (e369)* mutant and finally the double mutant which, exhibited a much smaller body size suggesting a more than additive effect of the two mutant phenotypes. This could potentially suggest a functional relation between the genes as well as the two processes in *C. elegans* development, potentially in moulting.

The double mutant phenotype was rarely encountered and could not produce any progeny by itself. Very often, the double homozygotic mutant would die during the early larval stages and not actually reach the adult stage at which size measurements were made. Only

a small proportion reached the adult stage, and animals would often burst while handling them for microscopy. Even at the rare occasion when these animals were able to reach adulthood, they would die without producing any progeny (Section 3.6). Therefore, while *C. elegans* can survive when either *vps-45* or *unc-51* function is lost, there is a mutual requirement for function. If *vps-45* is lost, *unc-51* (and autophagy) is essential for survival. When *unc-51* function is lost, *vps-45* becomes essential and presumably accurate targeting and fusion of vesicles is much more important when autophagy is defective.

In addition to this, it was observed that the *vps-45(tm246)* and *unc-51(e369)* mutants exhibited different moulting profiles compared to the wild type strain. In more detail, both the *vps-45* and *unc-51* mutants started their L1-L2 moult with a delay of 2-3 hours compared to the wild type strain. This delay in the onset of the L1-L2 moult can most likely be extended to each of the subsequent moults judging by the time each of the mutants required to reach adulthood. Both mutants exhibited a longer period of larval development taking longer to reach the adult stage, however for different reasons. In the case of the *vps-45* mutant a longer moulting period was identified compared to the wild type, whereas in the case of the *unc-51* mutant the duration of the moult was almost the same as for the wild type strain. The *unc-51* was also identified to potentially have longer intermoult periods. The above suggest that *vps-45* is needed during lethargus/moulting as lethargus takes longer in the mutant and that *unc-51* potentially plays a more important role at the exit from lethargus/moult and the intermoult periods (Section 3.9). These observations were verified via further experiments of the moulting time of individual animals for each of the strains as well as the fact that the *unc-51* mutant animals lost synchrony after several hours of development, whereas the other two did not with approximately only 55% of the population being at the same stage. Furthermore, the *unc-51 (e369)* and *vps-45(tm246)* mutants had a delayed development to adulthood. Generally it is, known that a family of genes, known as heterochronic genes are responsible for the regulation of temporal events in *C. elegans* [reviewed in (Ambros & Moss 1994)]. Moulting is included in these events, and mutation on the heterochronic transcription factor *lin-42* can affect the duration of moults. It is unknown what the internal cues are for the activation of *lin-42* however according to the data presented in this work it is at least possible that autophagy and or the endosomal system could play a role in its regulation (Monsalve et al. 2011). Collectively, these results, coupled with the fact that the mutants exhibited a much shorter lifespan compared to the wildtype strains in both the permissive (15°C) and non-permissive temperatures (25°C) (Section 3.10), suggest that both autophagy and endosomal trafficking plays an important role in the post embryonic

development of *C. elegans* and more specifically transit through the moult and return to the intermoult stages.

Overall, it is important to note that a synthetic effect was observed in the *unc-51 vps-45* double mutant which enforces the idea of some functional relation between autophagy and endosomal trafficking, potentially in moulting. In yeast, *vps-45* function has been associated with the regulation of autophagy where in the absence of functional Vps45, autophagosome clusters accumulate around the vacuole but do not fuse with it (Chen et al. 2014). It is possible that such an intersection between the two processes is also present in the more complex model of *C. elegans* and that *vps-45 (tm246)* would exhibit a similar phenotype with a mildly reduced autophagy. If that is the case, it is easy to understand the synthetic effect of the *unc-51 vps-45* double mutant as both proteins will be acting on the same process but in different steps. It is possible that *vps-45* acts in the trafficking of components required for the secretion of the cuticle during lethargus and that autophagy takes place subsequently for the clearance/removal of any residual material not effectively secreted during lethargus. During lethargus when the cuticle components are being secreted in a *vps-45* mutant at permissive temperature 15°C, lethargus takes longer than in the wild type, but animals survive. At 25°C this might be exacerbated and animals die. In the double mutant where autophagy is defective, animals die even at the permissive temperature of 15°C sometimes even by bursting indicating the extreme fragility of the cuticle. Therefore, autophagy is essential to survival in *vps-45* mutants, and the reason for death might relate to defects in cuticle synthesis as a result of incorrect or delayed protein trafficking.

7.3 Autophagy is developmentally regulated during moulting and is required for the survival of *vps-45 (tm246)* mutants.

As discussed in the previous section (Section 7.1), the *unc-51 vps-45* double mutant exhibited a synthetic lethality with severe irregularities in the body shape and size. Research from Singh and Sulston has suggested the genesis of new organelles during moulting, which have Golgi like characteristics (Singh & Sulston 1978). Here, the requirement for autophagy for the degradation of these structures after moulting is complete when the animal transits back to the next intermoult phase, is proposed. Furthermore, as discussed in the previous section there is strong evidence to suggest the

involvement of endosomal trafficking and autophagy in the moulting process. To investigate this idea, the *unc-51 (e369)* and *vps-45 (tm246)* mutants were utilised along with the LGG-1::GFP autophagy marker. LGG-1, is the homologue of the mammalian LC3, it can be found on the autophagosome membrane and is rapidly degraded with the organelle after the completion of autophagy (Ladoire et al. 2012; Abeliovich et al. 2000; Suzuki & Ohsumi 2007) as a result it can act as a marker for the presence of autophagy and the formation of autophagosomes

Consistent with my original hypothesis for an involvement of autophagy during the moult, higher expression of the LGG-1::GFP marker was observed shortly after the worms entered lethargus (Section 4.3). This was the case for all three strains, wild type and both the *unc-51 (e369)* and *vps-45 (tm246)* mutants. All three strains exhibited different times to entry into lethargus from L1 larval arrest (Section 4.4). However, LGG-1::GFP accumulation in the seam cells only appeared after entry into lethargus for each strain. Thus in each of these strains, although the length of time taken to enter lethargus varies, in each case the association of accumulation of LGG-1::GFP at the start of lethargus is retained. Thus, the accumulation of LGG-1::GFP in the seam cells is developmentally regulated and tightly associated with lethargus. Seam cells are part of the epithelial tissue responsible for the secretion of collagen components of the cuticle (Sulston & Horvitz 1977; Singh & Sulston 1978; Thein et al. 2003). The fact that the LGG-1 localizes in those cells during lethargus further strengthens the idea for the involvement of autophagy in moulting and specifically suggests the seam cells as the place for this process. That this accumulation is specific to moulting, and not to the seam cell divisions that occur at the end of each moult is supported by the following observation. In addition to the seam cell divisions that happen at the end of each moult, there is also a seam cell division that occurs in L1 larvae approximately 5 hours post-hatch (Shemer & Podbilewicz 2000; Podbilewicz & White 1994). No accumulation of LGG-1::GFP was observed at this seam cell division (Section 4.7). This result suggests that the accumulation of LGG-1::GFP in seam cells is not associated with cell division, but rather lethargus and moulting. This is also consistent with previous reports suggesting degradation of the midbodies after the cell-division in *C. elegans* in a macroautophagy independent way (Fazeli et al. 2016). The LGG-1 fluorescence rapidly disappeared from the seam cell shortly after the worms shed their cuticle through ecdysis (within 1 hour), with the only exception being in the *unc-51* mutant in which the GFP persisted in the seam after the end of the moult for 2 to 3 hours. This was to be expected since for the LGG-1 protein to be degraded autophagosomes need to be formed and degraded with their content via the autophagic process, and as such due to the

reduced autophagy in this strain the LGG-1 protein would persist longer after the end of the moult in a diffuse state (Section 4.4). The data obtained also suggest a requirement for higher levels of autophagy as a result of the *vps-45 (tm246)* mutant. Initially, our data suggested that there was a slightly faster degradation of the LGG-1 marker in the seam cells of the *vps-45 (tm246)* mutant post-moult. Upon measuring the whole body's total fluorescence of the LGG-1::GFP marker in the two mutants and the wild type strain it was observed that both mutants exhibited higher levels of fluorescence and therefore higher levels of *lgg-1* expression compared to the wild type, with the *unc-51 (e369)* mutant showing the highest. For the autophagy mutant that can be explained as previously due to the low incorporation of LGG-1 in autophagosomes as a result of a reduced induction of autophagy. In the case of the *vps-45 (tm246)* mutant, however, since the LGG-1 is degraded rapidly after autophagy, it would suggest that the *vps-45 (tm246)* mutant has higher demands for autophagy, probably due to the defects in endosomal sorting and the accumulation of vesicle, suggesting that autophagy is the mechanism which allows for the survival and development of these animals despite the problems in the endocytic pathway (Section 4.9).

To get a better idea of the differences in the induction of autophagy the number of autophagosomes in the seam cells in lethargic animals was counted. As previously stated, LGG-1 localizes in the seam cells where it becomes part of the membrane of the forming autophagosomes (Aladzcity et al. 2007). A low number of LGG-1::GFP foci (believed to represent formed autophagosomes) was observed at the beginning of lethargus when the protein first accumulated in the cells. As the moult was coming to an end and the seam cells start dividing the number of autophagosomes increased in the wild type strain. In the case of the *vps-45 (tm246)* mutant the autophagosome count was higher in the pre-division seam cells compared to the wild type. The number of autophagosomes was increased in the *vps-45 (tm246)* mutant during the end of the moult and the seam cell division. However, the number was less than that in the cells of the wild type strain during the same process. In the *unc-51 (e369)* mutant on the other hand, the number of autophagosomes remained low throughout the process. The above data, once again imply that autophagy is required particularly at the end of moult near the ecdysis phase. The fact that the *vps-45* mutant had a higher number of autophagosomes at the beginning of lethargus enforces the idea that higher levels of basal autophagy are required by this strain to aid with the possible defects of endosomal trafficking. However, the fact that the number of autophagosomes did not increase as much as in the wild type strain could suggest that this mutant cannot form this many autophagosomes, potentially due to the absence of a functional *vps-45 (tm246)* if it

would act as a regulator of autophagy (Chen et al. 2014), or that because of the requirement of autophagy for the clearance aberrant vesicles cause the diversion of resources (Section 4.5).

Similar experiments conducted in embryos throughout their developmental stages, further support the idea that during the secretion of the cuticle autophagy is required, at any stage of development, and that the *vps-45 (tm246)* mutant has higher demands for autophagy. The number of autophagosomes could not be counted in this case, however the total fluorescence levels in embryos mirror the result obtained by the adult animals (Section 4.8, 4.9).

Overall it was demonstrated that, autophagy takes place at the end of the moult in the seam cells, promoting the idea that autophagy is required for the rapid clearance of the secretory Golgi like structures formed in the hypodermis after the secretion of the cuticle (Singh & Sulston 1978), and returning the animal to the intermoult phases. This claim is further strengthened by the fact that autophagy was only induced in the seam cells at the end of the molt and not because of the division of the seam cells (Section 4.7). Further to this, *vps-45 (tm246)* mutants exhibited higher levels of LGG-1::GFP expression both as an adult and during embryonic development, aiding to the idea that autophagy is in higher demand in mutants lacking VPS45 probably as a survival mechanism. This is also consistent with the previously identified synthetic lethality. Autophagy is induced throughout lethargus/molting in *C. elegans* when VPS-45 is absent. Thus, the *vps-45* mutants might need autophagy to survive (Section 7.1), explaining the *unc-51 vps-45* synthetic lethality.

7.4 Investigating oxidative imbalances and resistance to oxidative stress in *unc-51 (e369)* and *vps-45 (tm246)* mutants

While comparing the *vps-45* and *unc-51* single mutants and the double mutant, it was observed that the intestinal lumen appears to be enlarged in all three cases (Section 3.8). This is consistent with defects in the function on the intestine. Furthermore, the enlarged intestinal lumen could suggest problems in the digestion for both mutants and possibly problems in the detoxification process since the intestine is the main detoxification organ of *C. elegans* with a number of antioxidant genes expressed in intestinal cells (An & Blackwell 2003; Freedman et al. 1993; Slice et al. 1990; Swain et al. 2004) .

Possibly both mutations could be affecting the oxidative state of the tissues and consequently the aging process [Reviewed in (Finkel & Holbrook 2000)] hence the shorter lifespan. A more oxidised state in the cells can be a result of the increased stress in the ER as a consequence of the high number of structures that are potentially accumulating in both mutants [(Cullinan et al. 2003; Plaisance et al. 2016), reviewed in (Ron 2002)]. In the case of *vps-45(tm246)* mutant this could be the result of the ineffective endosomal fusion which could produce aberrant or misfolded structures which could result in ER stress. In the case of *unc-51 (e369)* mutant, the lack of an effective clearance mechanism for misfolded proteins and other aberrant structures would be the cause for the oxidised environment once again due to the accumulation of misfolded proteins. Additionally the reduced lifespan exhibited by the both mutant could be due to an increased oxidative/ER stress previously mentioned (Bensaad et al. 2009).

Furthermore, accelerated rates of apoptosis has been observed in neutrophils of patients carrying the homozygous mutation T224N in the human VPS45 gene (P. Stepensky et al. 2013). Experiments in *vps-45* yeast mutants have shown that they are more sensitive to oxidative stress caused by the action of hydrogen peroxide (Cowan, 2014). As such, the possibility of a similar sensitivity in *C. elegans* was investigated possibly as a result of ER stress (Harding et al. 2003; Malhotra & Kaufman 2007b; Plaisance et al. 2016) due to the accumulation of mistargeted proteins by the endocytic system, or insufficient degradation of proteins.

Initially, an ER marker was employed to explore the possibility of ER redox imbalances, that could potentially also cause a susceptibility to oxidative stress. In the permissive temperature, for the *vps-45* moulting death, both mutant exhibited a reduced environment in the ER compared to the wild type strain. The autophagy defective *unc-51* mutant exhibited a more reduced environment to the *vps-45* mutant. The measurement of the ER redox state in a double homozygotic mutant for both alleles was not possible due to the synthetic lethality.

When the same measurements were repeated at the non-permissive temperature of 25°C for all strains, an increased in the oxidation state was observed for all mutants, especially in the case of the *vps-45* mutant. In this case, the *unc-51 (e369)* mutant appeared to exhibit similar oxidation levels to the wild type strain. However, the *vps-45(tm246)* mutants showed a much more oxidised environment compared to either one of the other strains (Section 5.3).

From these results, it might be expected that the *vps-45 (tm246)* mutant be more susceptible to oxidative stress. However, the killing assay demonstrated that the *unc-51 (e369)* mutant died faster than both the *vps-45* mutant and wild type strain when exposed to two concentrations of H₂O₂ for 4 hours. The *vps-45 (tm246)* mutant however, was more susceptible than the wild type strain (Section 5.4). To further understand how they reacted to oxidative stress three GFP markers were utilised, namely SOD-3::GFP, GST-4::GFP, and GCS-1::GFP, all three of which act at different points of the detoxification response.

For the SOD-3 marker the data indicate a stronger basal induction (in the absence of H₂O₂ treatment) from the *unc-51* mutant when compared to the wild type. Since SOD-3 has the role of converting oxygen anions to hydrogen peroxide it is suggested that there is an increased accumulation of free radicals in the cytoplasm of this strains cells, which was worsened by the further exposure to H₂O₂. This could potentially imply an ER stress. A mildly increased, however non-significant, response was also observed for the *vps-45* mutant. It is possible that the reason for this response is the accumulation of aberrant structures, organelles and proteins as a result of defective autophagy which cannot degrade them or due to incomplete endosomal sorting in the case of *vps-45*. Both of which could potentially cause an ER stress to a different degree, thus explaining the difference in the redox state of the ER in the two mutants (Madeo et al. 1999; Tu & Weissman 2004; Malhotra & Kaufman 2007a). Furthermore, SOD-3 is not only regulated exclusively by oxidative stress, but from starvation as well, since the insulin/IGF-1 signalling and *daf-16* are also responsible for its upregulation (Lee et al. 2001). As such, a mild oxidative stress might not be enough for a great upregulation of the enzyme (Section 5.5).

In the case of GST-4 all strains exhibited very similar responses across the board. GST-4 is a phase II detoxification enzyme, much like GCS-1 which will be discussed later and are controlled by the transcription factor SKN-1 (An & Blackwell 2003; Blackwell et al. 2015). In the case of GCS-1 only the *unc-51 (e369)* mutant showed a higher response to hydrogen peroxide induced oxidative stress and all other strains and conditions exhibited a similar response. This is unexpected considering that both these enzymes are controlled via similar pathways and respond to similar stimuli. However, it is important to note that GST-4 has a much broader spectrum of targets (Hayes et al. 2005; Nebert & Vasiliou 2004), and its action involves the conjugation of reduced GSH to its target oxidising compounds. GCS-1 on the other hand is involved in the first step of GSH biosynthesis, as such although it is also regulated by SKN-1 it acts earlier in the detoxification pathway as it will be providing the GSH required for GST-4 to act (Schulz et al. 2000) (Section 5.5).

Collectively, data suggest that both *unc-51 (e369)* and *vps-45 (tm246)* mutants are more sensitive to oxidative stress since both exhibited lower survival after treatment with H₂O₂. The *unc-51 (e369)* mutant was more sensitive of the two, something which can further be supported by the induction of oxidative stress markers in that mutant which was greater compared to the other two which overall exhibited similar responses. It is possible that in both cases accumulation of membranes, organelles and proteins is the cause of this stress, possibly as a result of ER stress. One of the marks of ER stress is the redox imbalance in the ER lumen which, when it is too high, can lead to redox imbalances in the cytoplasm as well. It is possible to consider that since *vps-45* acts in the Golgi to lysosome trafficking pathway, a blockage in this trafficking caused by loss of VPS-45 function could also affect previous stages in the protein trafficking pathway, namely the ER where proteins are synthesized and folded. Such a bottle neck could potentially cause accumulation of certain protein, possibly targeted to lysosomes, in the ER which in turn would put extra burden in the ER causing the imbalance. This could result in misfolding of proteins which in turn would require a refolding process which would produce ROS and as such create a more oxidising environment. However, not to the point where it would cause leakage of calcium or ROS in the cytoplasm to result in a cell wide oxidation state. On the other hand, in the case of the *unc-51 (e369)* mutant, things could be more complex, and possibly affect the cell to a greater degree. The *unc-51 (e369)* mutation affects autophagy as a whole, and is not confined only to a single molecular pathway as is the case of *vps-45*. Autophagy can aid in the homeostasis of the cell by recycling cellular structures and molecules that are either not needed by the cell, or are defective having been damaged by stresses. If autophagy is greatly reduced, then a greater level of stress might fall upon the ER. This can possibly explain why the *unc-51* is more susceptible to hydrogen peroxide killing and exhibits a stronger response under stress as well as the shorter lifespan. Alternatively, since as shown here autophagy is associated with moulting in *C. elegans*, it is also possible that the cuticle might be in some manner defective, possibly more permeable to hydrogen peroxide.

7.5 Concluding remarks and future work

Using the LGG-1::GFP marker it was demonstrated that autophagy is induced in a developmental manner during lethargus in hypodermal seam cells which are highly active in secretion of collagens and other components of the cuticle during this period.

Furthermore, during the periods of lethargus which last approximately 4 hours in the wild type, first the LGG-1::GFP protein was found to accumulate in a diffuse presumed cytoplasmic localisation and then towards the end of lethargus form distinct foci that are believed to be active autophagosomes. This is consistent with a model where the autophagy protein LGG-1 accumulates at the start of lethargus in a developmentally regulated way in preparation for an active period of autophagy, and then late in lethargus is converted into its active form driving a period of autophagy. This is supported by the finding that when the UNC-51/ATG kinase is mutated that the presumed active LGG-1::GFP foci do not form. In conclusion, the synthetic lethality described in this work demonstrates that autophagy is essential for organismal viability in *C.elegans* in the absence of the SM protein VPS-45.

The known viability of *vps-45* null mutants, which in both yeast and *C. elegans* have this unusual behaviour of temperature sensitivity, is hard to explain. The conclusion is that where the SM protein VPS-45 is an essential protein for viability at slightly elevated temperatures in both organisms, it is not necessary for viability at lower temperatures. Why the basic cell biology behaves in this way is unclear. However, the synthetic lethality demonstrated by the *unc-51; vps-45* double mutant is potentially interesting in this respect. It demonstrates that in *C. elegans*, the viability of a *vps-45* null mutant at 15°C requires functional autophagy. Thus, possibly high levels of defective vesicle/membrane fusions do occur in the *vps-45* mutant even at low temperatures, but cells (and animals) survive by utilising autophagy to recycle components trapped in defective fused vehicles and organelles. Evidence was found to suggest a possible upregulation of autophagy during the early phases of lethargus in the *vps-45* mutant, by using the LGG-1::GFP marker.

The molecular basis of the extra-genetic suppression of *vps-45* mutants of *C. elegans* was not elucidated. Full genome sequencing, despite working properly from a technical standpoint, failed to identify a single suppressor. However, via the utilisation of genetic mapping and phenotypic analysis, the existence of more than one suppressors in two subpopulations of our suppressed lines was inferred. Thus, a second round of sequencing in

the two distinct sub-populations (fast and slow growing suppressors) could help verify that this is the case and identify the suppressors. This is future research for this project.

While the molecular basis of the *vps-45* lethality suppression is not currently known, it is possible that the synthetic lethality with *unc-51* might provide an avenue of possible future research. Since we know now that autophagy is necessary for survival of *vps-45* mutants at 15°C, could upregulation of autophagy underpin the suppression of *vps-45* lethality at 25°C? This might easily be tested by crossing suppressed *vps-45* mutant lines with the LGG-1::GFP marker strain and using this to assess levels of autophagy in the suppressed and non-suppressed lines. Additionally, a new EMS screen using the *vps-45 (tm246)* LGG-1::GFP expressing strain could be carried out to isolate suppressed lines which will be expressing the transgene. This could be used to investigate if the frequent suppression of the *vps-45 (tm246)* mutant is associated with altered autophagy.

Finally, to investigate the possible role for autophagy in removing the expanded network of secretory apparatus that accumulate in seam cells during lethargus, electron microscopy of the wild type and *unc-51* mutant *C. elegans* during and after the moult could be used. If autophagy is indeed used to remove these organelles and return the hypodermis to its non-secretory intermoult state, persistence of these secretory structures after the moult would be anticipated in the *unc-51* mutant.

References

- Abeliovich, H. et al., 2000. Dissection of autophagosome biogenesis into distinct nucleation and expansion steps. *The Journal of cell biology*, 151(5), pp.1025–34. Available at: <http://www.ncbi.nlm.nih.gov/pubmed/11086004> [Accessed May 21, 2017].
- Abeliovich, H., Darsow, T. & Emr, S.D., 1999. Cytoplasm to vacuole trafficking of aminopeptidase I requires a t-SNARE-Sec1p complex composed of Tlg2p and Vps45p. *The EMBO journal*, 18(21), pp.6005–16. Available at: <http://emboj.embopress.org/cgi/doi/10.1093/emboj/18.21.6005> [Accessed May 18, 2017].
- Agnello, M. et al., 2015. *Cell Death - Autophagy, Apoptosis and Necrosis* T. M. Ntuli, ed., InTech. Available at: <http://www.intechopen.com/books/cell-death-autophagy-apoptosis-and-necrosis/the-role-of-autophagy-and-apoptosis-during-embryo-development> [Accessed February 13, 2017].
- Ahringer, J., 2006. Reverse genetics. Available at: <https://www.ncbi.nlm.nih.gov/books/NBK19711/> [Accessed January 27, 2017].
- Aladzcity, I. et al., 2007. Autophagy genes unc-51 and bec-1 are required for normal cell size in *Caenorhabditis elegans*. *Genetics*, 177(1), pp.655–660. Available at: <http://www.ncbi.nlm.nih.gov/pubmed/17890369>.
- Ambros, V. & Moss, E.G., 1994. Heterochronic genes and the temporal control of *C. elegans* development. *Trends in Genetics*, 10(4), pp.123–127. Available at: <http://linkinghub.elsevier.com/retrieve/pii/0168952594902135> [Accessed June 25, 2017].
- An, J.H. & Blackwell, T.K., 2003. SKN-1 links *C. elegans* mesendodermal specification to a conserved oxidative stress response. *Genes & development*, 17(15), pp.1882–93. Available at: <http://www.pubmedcentral.nih.gov/articlerender.fcgi?artid=196237&tool=pmcentrez&rendertype=abstract> [Accessed February 8, 2016].
- Ang, A.L. et al., 2004. Recycling endosomes can serve as intermediates during transport from the Golgi to the plasma membrane of MDCK cells. *The Journal of Cell Biology*, 167(3). Available at: <http://jcb.rupress.org/content/167/3/531.short> [Accessed May 24, 2017].
- Antonin, W. et al., 2002. Crystal structure of the endosomal SNARE complex reveals common structural principles of all SNAREs. *Nature structural biology*, 9(2), pp.107–11. Available at: <http://dx.doi.org/10.1038/nsb746> [Accessed October 24, 2016].
- Axe, E.L. et al., 2008. Autophagosome formation from membrane compartments enriched in phosphatidylinositol 3-phosphate and dynamically connected to the endoplasmic reticulum. *The Journal of cell biology*, 182(4), pp.685–701. Available at: <http://www.ncbi.nlm.nih.gov/pubmed/18725538> [Accessed May 22, 2017].
- Baba, M. et al., 1997. Two distinct pathways for targeting proteins from the cytoplasm to the vacuole/lysosome. *The Journal of cell biology*, 139(7), pp.1687–95. Available at: <http://www.ncbi.nlm.nih.gov/pubmed/9412464> [Accessed May 22, 2017].
- Baba, M., Osumi, M. & Ohsumi, Y., 1995. Analysis of the Membrane Structures Involved in Autophagy in Yeast by Freeze-Replica Method. *Cell Structure and Function*, 20(6), pp.465–471. Available at:

- <http://joi.jlc.jst.go.jp/JST.Journalarchive/csf1975/20.465?from=CrossRef> [Accessed May 21, 2017].
- Bazan, G.C. & Hillers, K.J., 2011. SNP-based mapping of crossover recombination in *Caenorhabditis elegans*. *Methods in molecular biology (Clifton, N.J.)*, 745, pp.207–22. Available at: <http://www.ncbi.nlm.nih.gov/pubmed/21660697> [Accessed February 10, 2016].
- Bennett, M., Calakos, N. & Scheller, R., 1992. Syntaxin: a synaptic protein implicated in docking of synaptic vesicles at presynaptic active zones. *Science*, 257(5067). Available at: <http://science.sciencemag.org/content/257/5067/255> [Accessed May 20, 2017].
- Bensaad, K., Cheung, E.C. & Vousden, K.H., 2009. Modulation of intracellular ROS levels by TIGAR controls autophagy. *The EMBO Journal*, 28(19), pp.3015–3026. Available at: <http://www.ncbi.nlm.nih.gov/pubmed/19713938> [Accessed May 18, 2017].
- Benson, K.F. et al., 2003. Mutations associated with neutropenia in dogs and humans disrupt intracellular transport of neutrophil elastase. *Nature genetics*, 35(1), pp.90–6. Available at: <http://www.ncbi.nlm.nih.gov/pubmed/12897784> [Accessed January 19, 2017].
- Betz, C. et al., 2013. Feature Article: mTOR complex 2-Akt signaling at mitochondria-associated endoplasmic reticulum membranes (MAM) regulates mitochondrial physiology. *Proceedings of the National Academy of Sciences of the United States of America*, 110(31), pp.12526–34. Available at: <http://www.pubmedcentral.nih.gov/articlerender.fcgi?artid=3732980&tool=pmcentrez&rendertype=abstract> [Accessed January 16, 2017].
- Biazik, J. et al., 2015. Ultrastructural relationship of the phagophore with surrounding organelles. *Autophagy*, 11(3), pp.439–451. Available at: <http://www.ncbi.nlm.nih.gov/pubmed/25714487> [Accessed July 19, 2017].
- Blackwell, T.K. et al., 2015. SKN-1/Nrf, stress responses, and aging in *Caenorhabditis elegans*. *Free radical biology & medicine*, 88(Pt B), pp.290–301. Available at: <http://www.pubmedcentral.nih.gov/articlerender.fcgi?artid=4809198&tool=pmcentrez&rendertype=abstract> [Accessed January 27, 2017].
- Boztug, K. et al., 2009. A Syndrome with Congenital Neutropenia and Mutations in G6PC3. Available at: <http://www.nejm.org/doi/full/10.1056/NEJMoa0805051> [Accessed February 13, 2017].
- Brabin, C. & Woollard, A., 2012. Finding a niche for seam cells? *Worm*, 1(2), pp.107–111. Available at: <http://www.ncbi.nlm.nih.gov/pubmed/24058832> [Accessed March 7, 2017].
- Brenner, S., 1974. The genetics of *Caenorhabditis elegans*. *Genetics*, 77(1), pp.71–94. Available at: <http://www.pubmedcentral.nih.gov/articlerender.fcgi?artid=1213120&tool=pmcentrez&rendertype=abstract> [Accessed January 20, 2017].
- Brickner, J.H. et al., 2001. The Tlg SNARE complex is required for TGN homotypic fusion. *The Journal of cell biology*, 155(6), pp.969–78. Available at: <http://www.pubmedcentral.nih.gov/articlerender.fcgi?artid=2150899&tool=pmcentrez&rendertype=abstract> [Accessed September 13, 2016].

- Bruinsma, P., Spelbrink, R.G. & Nothwehr, S.F., 2004. Retrograde transport of the mannosyltransferase Och1p to the early Golgi requires a component of the COG transport complex. *The Journal of biological chemistry*, 279(38), pp.39814–23. Available at: <http://www.ncbi.nlm.nih.gov/pubmed/15229219> [Accessed June 16, 2017].
- Bryant, N.J. & James, D.E., 2001. Vps45p stabilizes the syntaxin homologue Tlg2p and positively regulates SNARE complex formation. *The EMBO journal*, 20(13), pp.3380–8. Available at: <http://www.pubmedcentral.nih.gov/articlerender.fcgi?artid=125511&tool=pmcentrez&rendertype=abstract> [Accessed September 13, 2016].
- Bucher, E.A. & Seydoux, G., 1994. Gastrulation in the nematode *Caenorhabditis elegans*. *Seminars in Developmental Biology*, 5(2), pp.121–130. Available at: <http://linkinghub.elsevier.com/retrieve/pii/S1044578184710164> [Accessed January 29, 2017].
- Burd, C.G. et al., 1997. A novel Sec18p/NSF-dependent complex required for Golgi-to-endosome transport in yeast. *Molecular Biology of the Cell*, 8(6), pp.1089–1104. Available at: <http://europepmc.org/articles/PMC305716/?report=abstract> [Accessed January 20, 2017].
- Burkhardt, P. et al., 2008. Munc18a controls SNARE assembly through its interaction with the syntaxin N-peptide. *The EMBO journal*, 27(7), pp.923–33. Available at: <http://www.pubmedcentral.nih.gov/articlerender.fcgi?artid=2323264&tool=pmcentrez&rendertype=abstract> [Accessed February 5, 2017].
- Byerly, L., Cassada, R.C. & Russell, R.L., 1976. The life cycle of the nematode *Caenorhabditis elegans*. *Developmental Biology*, 51(1), pp.23–33. Available at: <http://linkinghub.elsevier.com/retrieve/pii/0012160676901196> [Accessed April 15, 2017].
- C. elegans Sequencing Consortium, 1998. Genome sequence of the nematode *C. elegans*: a platform for investigating biology. *Science (New York, N.Y.)*, 282(5396), pp.2012–8. Available at: <http://www.ncbi.nlm.nih.gov/pubmed/9851916> [Accessed January 27, 2017].
- Carpp, L.N. et al., 2007. Cellular levels of the syntaxin Tlg2p are regulated by a single mode of binding to Vps45p. *Biochem Biophys Res Commun*, 363(3), pp.857–860. Available at: <http://www.ncbi.nlm.nih.gov/pubmed/17904527>.
- Carr, C.M. & Rizo, J., 2010. At the junction of SNARE and SM protein function. *Current Opinion in Cell Biology*, 22(4), pp.519–527.
- Cassada, R.C. & Russell, R.L., 1975. The dauerlarva, a post-embryonic developmental variant of the nematode *Caenorhabditis elegans*. *Developmental Biology*, 46(2), pp.326–342. Available at: <http://linkinghub.elsevier.com/retrieve/pii/0012160675901098> [Accessed May 19, 2017].
- Chasnov, J.R. & Chow, K.L., 2002. Why are there males in the hermaphroditic species *Caenorhabditis elegans*? *Genetics*, 160(3), pp.983–94. Available at: <http://www.pubmedcentral.nih.gov/articlerender.fcgi?artid=1462001&tool=pmcentrez&rendertype=abstract> [Accessed January 26, 2017].
- Chen, W. et al., 1998. Rab11 is required for trans-golgi network-to-plasma membrane transport and a preferential target for GDP dissociation inhibitor. *Molecular biology*

- of the cell*, 9(11), pp.3241–57. Available at:
<http://www.ncbi.nlm.nih.gov/pubmed/9802909> [Accessed May 24, 2017].
- Chen, Y. et al., 2014. A Vps21 endocytic module regulates autophagy. *Molecular biology of the cell*, 25(20), pp.3166–77. Available at:
<http://www.pubmedcentral.nih.gov/articlerender.fcgi?artid=4196867&tool=pmcentrez&rendertype=abstract> [Accessed February 8, 2016].
- Cheng, S. et al., 2013. Autophagy genes coordinate with the class II PI/PtdIns 3-kinase PIKI-1 to regulate apoptotic cell clearance in *C. elegans*. *Autophagy*, 9(12), pp.2022–32. Available at: <http://www.tandfonline.com/doi/abs/10.4161/auto.26323> [Accessed January 16, 2017].
- Costa, M., Draper, B.W. & Priess, J.R., 1997. The role of actin filaments in patterning the *Caenorhabditis elegans* cuticle. *Developmental biology*, 184(2), pp.373–84. Available at: <http://www.ncbi.nlm.nih.gov/pubmed/9133443> [Accessed February 10, 2016].
- Cowan, M., 2014. A ROLE FOR THE ENDOSOMAL SNARE COMPLEX AND TETHERS IN AUTOPHAGY. Available at:
<http://theses.gla.ac.uk/5046/1/2013cowanphd.pdf> [Accessed July 20, 2017].
- Cowles, C.R., Emr, S.D. & Horazdovsky, B.F., 1994. Mutations in the VPS45 gene, a SEC1 homologue, result in vacuolar protein sorting defects and accumulation of membrane vesicles. *Journal of cell science*, 107 (Pt 1, pp.3449–59. Available at:
<http://www.ncbi.nlm.nih.gov/pubmed/7706396> [Accessed August 15, 2016].
- Cox, G.N., Kusch, M. & Edgar, R.S., 1981. Cuticle of *Caenorhabditis elegans*: its isolation and partial characterization. *The Journal of cell biology*, 90(1), pp.7–17. Available at:
<http://www.pubmedcentral.nih.gov/articlerender.fcgi?artid=2111847&tool=pmcentrez&rendertype=abstract> [Accessed January 20, 2017].
- Cox, G.N., Staprans, S. & Edgar, R.S., 1981. The cuticle of *Caenorhabditis elegans*. II. Stage-specific changes in ultrastructure and protein composition during postembryonic development. *Developmental biology*, 86(2), pp.456–70. Available at:
<http://www.ncbi.nlm.nih.gov/pubmed/6269931> [Accessed January 20, 2017].
- Cullinan, S.B. et al., 2003. Nrf2 Is a Direct PERK Substrate and Effector of PERK-Dependent Cell Survival. *Molecular and Cellular Biology*, 23(20), pp.7198–7209. Available at: <http://mcb.asm.org/content/23/20/7198.full> [Accessed February 6, 2017].
- Cutter, A.D., Avilés, L. & Ward, S., 2003. The proximate determinants of sex ratio in *C. elegans* populations. *Genetical research*, 81(2), pp.91–102. Available at:
<http://www.ncbi.nlm.nih.gov/pubmed/12872911> [Accessed January 26, 2017].
- Dalley, B.K. & Golomb, M., 1992. Gene expression in the *Caenorhabditis elegans* dauer larva: Developmental regulation of Hsp90 and other genes. *Developmental Biology*, 151(1), pp.80–90. Available at:
<http://linkinghub.elsevier.com/retrieve/pii/0012160692902153> [Accessed May 19, 2017].
- Degenhardt, K. et al., 2006. Autophagy promotes tumor cell survival and restricts necrosis, inflammation, and tumorigenesis. *Cancer Cell*, 10(1), pp.51–64. Available at:
<http://www.ncbi.nlm.nih.gov/pubmed/16843265> [Accessed August 28, 2017].
- DePristo, M.A. et al., 2011. A framework for variation discovery and genotyping using next-generation DNA sequencing data. *Nature genetics*, 43(5), pp.491–8. Available

- at: <http://dx.doi.org/10.1038/ng.806> [Accessed November 11, 2016].
- Djeddi, A. et al., 2012. Induction of autophagy in ESCRT mutants is an adaptive response for cell survival in *C. elegans*. *Journal of cell science*, 125(Pt 3), pp.685–94. Available at: <http://jcs.biologists.org/content/125/3/685> [Accessed August 17, 2016].
- Doitsidou, M. et al., 2010a. *C. elegans* mutant identification with a one-step whole-genome-sequencing and SNP mapping strategy. *PloS one*, 5(11), p.e15435. Available at: <http://www.pubmedcentral.nih.gov/articlerender.fcgi?artid=2975709&tool=pmcentrez&rendertype=abstract> [Accessed January 22, 2016].
- Doitsidou, M. et al., 2010b. *C. elegans* mutant identification with a one-step whole-genome-sequencing and SNP mapping strategy. *PloS one*, 5(11), p.e15435. Available at: <http://journals.plos.org/plosone/article?id=10.1371/journal.pone.0015435> [Accessed January 22, 2016].
- Dou, Z. et al., 2013. Class IA PI3K p110 β Subunit Promotes Autophagy through Rab5 Small GTPase in Response to Growth Factor Limitation. *Molecular Cell*, 50(1), pp.29–42. Available at: <http://www.ncbi.nlm.nih.gov/pubmed/23434372> [Accessed May 21, 2017].
- Dulubova, I. et al., 1999. A conformational switch in syntaxin during exocytosis: role of munc18. *The EMBO journal*, 18(16), pp.4372–82. Available at: <http://emboj.embopress.org/content/18/16/4372.abstract> [Accessed February 5, 2017].
- Dulubova, I. et al., 2002. How Tlg2p/syntaxin 16 “snares” Vps45. *The EMBO journal*, 21(14), pp.3620–31. Available at: <http://www.pubmedcentral.nih.gov/articlerender.fcgi?artid=126126&tool=pmcentrez&rendertype=abstract> [Accessed February 10, 2016].
- Elkin, S.R., Lakoduk, A.M. & Schmid, S.L., 2016. Endocytic pathways and endosomal trafficking: a primer. *Wiener Medizinische Wochenschrift*, 166(7–8), pp.196–204. Available at: <http://www.ncbi.nlm.nih.gov/pubmed/26861668> [Accessed June 15, 2017].
- Erdélyi, P. et al., 2011. Shared developmental roles and transcriptional control of autophagy and apoptosis in *Caenorhabditis elegans*. *Journal of Cell Science*, 124(9). Available at: <http://jcs.biologists.org/content/124/9/1510> [Accessed March 31, 2017].
- Fader, C.M. et al., 2009. TI-VAMP/VAMP7 and VAMP3/cellubrevin: two v-SNARE proteins involved in specific steps of the autophagy/multivesicular body pathways. *Biochimica et Biophysica Acta (BBA) - Molecular Cell Research*, 1793(12), pp.1901–1916. Available at: <http://www.ncbi.nlm.nih.gov/pubmed/19781582> [Accessed May 21, 2017].
- Fan, W., Nassiri, A. & Zhong, Q., 2011. Autophagosome targeting and membrane curvature sensing by Barkor/Atg14(L). *Proceedings of the National Academy of Sciences of the United States of America*, 108(19), pp.7769–74. Available at: <http://www.pubmedcentral.nih.gov/articlerender.fcgi?artid=3093500&tool=pmcentrez&rendertype=abstract> [Accessed January 16, 2017].
- Fasshauer, D. et al., 1998. Conserved structural features of the synaptic fusion complex: SNARE proteins reclassified as Q- and R-SNAREs. *Proceedings of the National Academy of Sciences of the United States of America*, 95(26), pp.15781–6. Available at: <http://www.ncbi.nlm.nih.gov/pubmed/9861047> [Accessed June 19, 2017].

- Fay, D.S., 2013. Classical genetic methods. *WormBook : the online review of C. elegans biology*, pp.1–58. Available at: <https://www.ncbi.nlm.nih.gov/books/NBK179229/> [Accessed January 27, 2017].
- Fazeli, G. et al., 2016. C. elegans midbodies are released, phagocytosed and undergo LC3-dependent degradation independent of macroautophagy. *Journal of Cell Science*, 129(20). Available at: <http://jcs.biologists.org/content/129/20/3721> [Accessed May 30, 2017].
- Fielding, C.A. et al., 2008. IL-6 Regulates Neutrophil Trafficking during Acute Inflammation via STAT3. *The Journal of Immunology*, 181(3), pp.2189–2195. Available at: <http://www.jimmunol.org/content/181/3/2189.full> [Accessed March 20, 2016].
- Finch, C.E. & Ruvkun, G., 2001. The genetics of aging. *Annual review of genomics and human genetics*, 2, pp.435–62. Available at: <http://www.annualreviews.org/doi/abs/10.1146/annurev.genom.2.1.435> [Accessed January 13, 2017].
- Finkel, T. & Holbrook, N.J., 2000. Oxidants, oxidative stress and the biology of ageing. *Nature*, 408(6809), pp.239–47. Available at: <http://dx.doi.org/10.1038/35041687> [Accessed January 12, 2015].
- Fire, A. et al., 1998. Potent and specific genetic interference by double-stranded RNA in *Caenorhabditis elegans*. *Nature*, 391(6669), pp.806–11. Available at: <http://www.ncbi.nlm.nih.gov/pubmed/9486653> [Accessed November 15, 2016].
- Frand, A.R., Russel, S. & Ruvkun, G., 2005. Functional genomic analysis of C. elegans molting. *PLoS biology*, 3(10), p.e312. Available at: <http://www.pubmedcentral.nih.gov/articlerender.fcgi?artid=1233573&tool=pmcentrez&rendertype=abstract> [Accessed January 24, 2017].
- Freedman, J.H. et al., 1993. The novel metallothionein genes of *Caenorhabditis elegans*. Structural organization and inducible, cell-specific expression. *The Journal of biological chemistry*, 268(4), pp.2554–64. Available at: <http://www.ncbi.nlm.nih.gov/pubmed/8428932> [Accessed May 18, 2017].
- Fridovich, I., 1995. Superoxide radical and superoxide dismutases. *Annual review of biochemistry*, 64, pp.97–112. Available at: <http://www.ncbi.nlm.nih.gov/pubmed/7574505> [Accessed January 27, 2017].
- Friedland, A.E. et al., 2013. Heritable genome editing in C. elegans via a CRISPR-Cas9 system. *Nature methods*, 10(8), pp.741–3. Available at: <http://www.pubmedcentral.nih.gov/articlerender.fcgi?artid=3822328&tool=pmcentrez&rendertype=abstract> [Accessed October 13, 2016].
- Fujita, N. et al., 2008. An Atg4B mutant hampers the lipidation of LC3 paralogues and causes defects in autophagosome closure. *Molecular biology of the cell*, 19(11), pp.4651–9. Available at: <http://www.pubmedcentral.nih.gov/articlerender.fcgi?artid=2575160&tool=pmcentrez&rendertype=abstract> [Accessed January 16, 2017].
- Furgason, M.L. et al., 2009. The N-terminal peptide of the syntaxin Tlg2p modulates binding of its closed conformation to Vps45p. *Proc Natl Acad Sci U S A*, 106(34), pp.14303–14308. Available at: <http://www.ncbi.nlm.nih.gov/pubmed/19667197>.
- Furuta, N. et al., 2010. Combinational Soluble N-Ethylmaleimide-sensitive Factor

- Attachment Protein Receptor Proteins VAMP8 and Vti1b Mediate Fusion of Antimicrobial and Canonical Autophagosomes with Lysosomes. *Molecular Biology of the Cell*, 21(6), pp.1001–1010. Available at: <http://www.ncbi.nlm.nih.gov/pubmed/20089838> [Accessed May 21, 2017].
- Futter, C.E. et al., 1995. Newly synthesized transferrin receptors can be detected in the endosome before they appear on the cell surface. *Journal of Biological Chemistry*, 270(18), pp.10999–11003. Available at: <http://www.jbc.org/cgi/doi/10.1074/jbc.270.18.10999> [Accessed May 24, 2017].
- Ganley, I.G. et al., 2011. Distinct Autophagosomal-Lysosomal Fusion Mechanism Revealed by Thapsigargin-Induced Autophagy Arrest. *Molecular Cell*, 42(6), pp.731–743. Available at: <http://www.ncbi.nlm.nih.gov/pubmed/21700220> [Accessed May 21, 2017].
- Garofalo, R.S., 2002. Genetic analysis of insulin signaling in Drosophila. *Trends in Endocrinology & Metabolism*, 13(4), pp.156–162. Available at: <http://www.sciencedirect.com/science/article/pii/S1043276001005483> [Accessed January 13, 2017].
- Geng, J. & Klionsky, D.J., 2008. The Atg8 and Atg12 ubiquitin-like conjugation systems in macroautophagy. “Protein modifications: beyond the usual suspects” review series. *EMBO reports*, 9(9), pp.859–64. Available at: <http://www.pubmedcentral.nih.gov/articlerender.fcgi?artid=2529362&tool=pmcentrez&rendertype=abstract> [Accessed January 16, 2017].
- Gengyo-Ando, K. et al., 2007. The SM protein VPS-45 is required for RAB-5-dependent endocytic transport in Caenorhabditis elegans. *Embo Reports*, 8(2), pp.152–157.
- Gillooly, D.J. et al., 2000. Localization of phosphatidylinositol 3-phosphate in yeast and mammalian cells. *The EMBO Journal*, 19(17), pp.4577–4588. Available at: <http://www.ncbi.nlm.nih.gov/pubmed/10970851> [Accessed May 21, 2017].
- Goedert, M., Clavaguera, F. & Tolnay, M., 2010. The propagation of prion-like protein inclusions in neurodegenerative diseases. *Trends in neurosciences*, 33(7), pp.317–25. Available at: <http://www.cell.com/article/S016622361000055X/fulltext> [Accessed November 4, 2016].
- Grenda, D.S. et al., 2007. Mutations of the ELA2 gene found in patients with severe congenital neutropenia induce the unfolded protein response and cellular apoptosis. *Blood*, 110(13), pp.4179–87. Available at: <http://www.bloodjournal.org/content/110/13/4179.short> [Accessed February 13, 2017].
- Grenda, D.S. et al., 2009. neutropenia induce the unfolded protein response and cellular Mutations of the ELA2 gene found in patients with severe congenital neutropenia induce the unfolded protein response and cellular apoptosis. *Blood*, 110(13), pp.4179–4187. Available at: <http://www.bloodjournal.org/content/110/13/4179.short> [Accessed May 20, 2017].
- Gurunathan, S. et al., 2000. Yeast exocytic v-SNAREs confer endocytosis. *Molecular biology of the cell*, 11(10), pp.3629–43. Available at: <http://www.ncbi.nlm.nih.gov/pubmed/11029060> [Accessed May 20, 2017].
- Hanada, T. et al., 2007. The Atg12-Atg5 conjugate has a novel E3-like activity for protein lipidation in autophagy. *The Journal of biological chemistry*, 282(52), pp.37298–302. Available at: <http://www.ncbi.nlm.nih.gov/pubmed/17986448> [Accessed May 21,

2017].

- Hanson, G.T. et al., 2004. Investigating mitochondrial redox potential with redox-sensitive green fluorescent protein indicators. *The Journal of biological chemistry*, 279(13), pp.13044–53. Available at: <http://www.ncbi.nlm.nih.gov/pubmed/14722062> [Accessed January 14, 2016].
- Hanson, P.I. et al., 1995. The N-Ethylmaleimide-sensitive Fusion Protein and -SNAP Induce a Conformational Change in Syntaxin. *Journal of Biological Chemistry*, 270(28), pp.16955–16961. Available at: <http://europepmc.org/abstract/MED/7622514> [Accessed February 5, 2017].
- Hara, T. et al., 2006. Suppression of basal autophagy in neural cells causes neurodegenerative disease in mice. *Nature*, 441(7095), pp.885–9. Available at: <http://dx.doi.org/10.1038/nature04724> [Accessed October 25, 2016].
- Harding, H.P. et al., 2003. An integrated stress response regulates amino acid metabolism and resistance to oxidative stress. *Molecular cell*, 11(3), pp.619–33. Available at: <http://www.ncbi.nlm.nih.gov/pubmed/12667446> [Accessed May 18, 2017].
- Harsay, E. & Schekman, R., 2002. A subset of yeast vacuolar protein sorting mutants is blocked in one branch of the exocytic pathway. *The Journal of Cell Biology*, 156(2), pp.271–286. Available at: <http://www.ncbi.nlm.nih.gov/pubmed/11807092> [Accessed May 24, 2017].
- Hayes, J.D., Flanagan, J.U. & Jowsey, I.R., 2005. Glutathione transferases. *Annual review of pharmacology and toxicology*, 45, pp.51–88. Available at: <http://annualreviews.org/doi/abs/10.1146/annurev.pharmtox.45.120403.095857> [Accessed October 23, 2016].
- He, C. et al., 2012. Exercise-induced BCL2-regulated autophagy is required for muscle glucose homeostasis. *Nature*, 481(7382), pp.511–5. Available at: <http://dx.doi.org/10.1038/nature10758> [Accessed January 17, 2017].
- He, C. et al., 2006. Recruitment of Atg9 to the preautophagosomal structure by Atg11 is essential for selective autophagy in budding yeast. *The Journal of cell biology*, 175(6), pp.925–35. Available at: <http://www.ncbi.nlm.nih.gov/pubmed/17178909> [Accessed May 21, 2017].
- Hieb, W.F. & Rothstein, M., 1968. Sterol requirement for reproduction of a free-living nematode. *Science (New York, N.Y.)*, 160(3829), pp.778–80. Available at: <http://www.ncbi.nlm.nih.gov/pubmed/4869093> [Accessed May 18, 2017].
- Hodgkin, J., 2005. Introduction to genetics and genomics. *WormBook*. Available at: http://www.wormbook.org/chapters/www_introgeneticsgenomics/IntroGenetGenom.html [Accessed May 25, 2017].
- Hodgkin, J., 1983. Male Phenotypes and Mating Efficiency in CAENORHABDITIS ELEGANS. *Genetics*, 103(1), pp.43–64. Available at: <http://europepmc.org/articles/PMC1202023/?report=abstract> [Accessed January 26, 2017].
- Hodgkin, J. & Doniach, T., 1997. Natural variation and copulatory plug formation in *Caenorhabditis elegans*. *Genetics*, 146(1), pp.149–64. Available at: <http://www.pubmedcentral.nih.gov/articlerender.fcgi?artid=1207933&tool=pmcentrez&rendertype=abstract> [Accessed January 26, 2017].
- Hoeven, R. van der et al., 2011. Ce-Duox1/BLI-3 generated reactive oxygen species

- trigger protective SKN-1 activity via p38 MAPK signaling during infection in *C. elegans*. *PLoS pathogens*, 7(12), p.e1002453. Available at: <http://www.pubmedcentral.nih.gov/articlerender.fcgi?artid=3245310&tool=pmcentrez&rendertype=abstract> [Accessed February 8, 2016].
- Holzenberger, M. et al., 2003. IGF-1 receptor regulates lifespan and resistance to oxidative stress in mice. *Nature*, 421(6919), pp.182–7. Available at: <http://dx.doi.org/10.1038/nature01298> [Accessed January 13, 2017].
- Honda, Y. & Honda, S., 1999. The daf-2 gene network for longevity regulates oxidative stress resistance and Mn-superoxide dismutase gene expression in *Caenorhabditis elegans*. *FASEB journal : official publication of the Federation of American Societies for Experimental Biology*, 13(11), pp.1385–93. Available at: <http://www.ncbi.nlm.nih.gov/pubmed/10428762> [Accessed January 13, 2017].
- Hong, W., 2005. SNAREs and traffic. *Biochimica et biophysica acta*, 1744(2), pp.120–44. Available at: <http://www.sciencedirect.com/science/article/pii/S0167488905000571> [Accessed November 13, 2016].
- Huang, S. et al., 2013. Autophagy genes function in apoptotic cell corpse clearance during *C. elegans* embryonic development. *Autophagy*, 9(2), pp.138–49. Available at: <http://www.ncbi.nlm.nih.gov/pubmed/23108454> [Accessed September 19, 2017].
- Huang, W.P. et al., 2000. The itinerary of a vesicle component, Aut7p/Cvt5p, terminates in the yeast vacuole via the autophagy/Cvt pathways. *The Journal of biological chemistry*, 275(8), pp.5845–51. Available at: <http://www.ncbi.nlm.nih.gov/pubmed/10681575> [Accessed July 25, 2017].
- Hunter, C.P. et al., 1999. Hox gene expression in a single *Caenorhabditis elegans* cell is regulated by a caudal homolog and intercellular signals that inhibit wnt signaling. *Development*, 126(4). Available at: <http://dev.biologists.org/content/126/4/805.long> [Accessed May 19, 2017].
- Itakura, E., Kishi-Itakura, C. & Mizushima, N., 2012. The Hairpin-type Tail-Anchored SNARE Syntaxin 17 Targets to Autophagosomes for Fusion with Endosomes/Lysosomes. *Cell*, 151(6), pp.1256–1269. Available at: <http://www.ncbi.nlm.nih.gov/pubmed/23217709> [Accessed May 21, 2017].
- Itakura, E. & Mizushima, N., 2010. Characterization of autophagosome formation site by a hierarchical analysis of mammalian Atg proteins. *Autophagy*, 6(6), pp.764–76. Available at: <http://www.pubmedcentral.nih.gov/articlerender.fcgi?artid=3321844&tool=pmcentrez&rendertype=abstract> [Accessed January 16, 2017].
- Jahn, R. & Scheller, R.H., 2006. SNAREs--engines for membrane fusion. *Nature reviews. Molecular cell biology*, 7, pp.631–643.
- Jahn, R. & Südhof, T.C., 2003. Membrane Fusion and Exocytosis. Available at: <http://www.annualreviews.org/doi/abs/10.1146/annurev.biochem.68.1.863?journalCode=biochem> [Accessed February 4, 2017].
- Jahn, R. & Südhof, T.C., 1999. Membrane fusion and exocytosis. *Annual review of biochemistry*, 68, pp.863–911. Available at: <http://www.ncbi.nlm.nih.gov/pubmed/10872468> [Accessed February 4, 2017].
- Jao, C.C. et al., 2013. A HORMA domain in Atg13 mediates PI 3-kinase recruitment in autophagy. *Proceedings of the National Academy of Sciences*, 110(14), pp.5486–

5491. Available at: <http://www.pnas.org/content/110/14/5486.full.pdf> [Accessed May 21, 2017].
- Jewell, J.L., Russell, R.C. & Guan, K.-L., 2013. Amino acid signalling upstream of mTOR. *Nature reviews. Molecular cell biology*, 14(3), pp.133–9. Available at: <http://www.pubmedcentral.nih.gov/articlerender.fcgi?artid=3988467&tool=pmcentrez&rendertype=abstract> [Accessed January 16, 2017].
- Jiang, P. et al., 2014. The HOPS complex mediates autophagosome-lysosome fusion through interaction with syntaxin 17. *Molecular biology of the cell*, 25(8), pp.1327–37. Available at: <http://www.ncbi.nlm.nih.gov/pubmed/24554770> [Accessed May 23, 2017].
- Johnstone, I.L., 2000. Cuticle collagen genes. Expression in *Caenorhabditis elegans*. *Trends in genetics : TIG*, 16(1), pp.21–7. Available at: <http://www.ncbi.nlm.nih.gov/pubmed/10637627> [Accessed February 8, 2016].
- Johnstone, I.L., 1994. The cuticle of the nematode *Caenorhabditis elegans*: a complex collagen structure. *BioEssays : news and reviews in molecular, cellular and developmental biology*, 16(3), pp.171–8. Available at: <http://www.ncbi.nlm.nih.gov/pubmed/8166670> [Accessed January 20, 2017].
- Johnstone, I.L. & Barry, J.D., 1996. Temporal reiteration of a precise gene expression pattern during nematode development. *The EMBO journal*, 15(14), pp.3633–9. Available at: <http://www.pubmedcentral.nih.gov/articlerender.fcgi?artid=451985&tool=pmcentrez&rendertype=abstract> [Accessed January 24, 2017].
- Kabeya, Y. et al., 2005. Atg17 Functions in Cooperation with Atg1 and Atg13 in Yeast Autophagy. *Molecular Biology of the Cell*, 16(5), pp.2544–2553. Available at: <http://www.ncbi.nlm.nih.gov/pubmed/15743910> [Accessed May 21, 2017].
- Kabeya, Y. et al., 2009. *Characterization of the Atg17–Atg29–Atg31 complex specifically required for starvation-induced autophagy in Saccharomyces cerevisiae*, Available at: <http://www.sciencedirect.com/science/article/pii/S0006291X09018221> [Accessed May 21, 2017].
- Kabeya, Y. et al., 2000. LC3, a mammalian homologue of yeast Apg8p, is localized in autophagosome membranes after processing. *The EMBO journal*, 19(21), pp.5720–8. Available at: <http://www.pubmedcentral.nih.gov/articlerender.fcgi?artid=305793&tool=pmcentrez&rendertype=abstract> [Accessed September 27, 2016].
- Kamada, Y. et al., 2000. Tor-mediated induction of autophagy via an Apg1 protein kinase complex. *The Journal of cell biology*, 150(6), pp.1507–13. Available at: <http://www.ncbi.nlm.nih.gov/pubmed/10995454> [Accessed May 21, 2017].
- Kamada, Y. & Ohsumi, Y., 2010. The TOR-Mediated Regulation of Autophagy in the Yeast *Saccharomyces cerevisiae*. In pp. 143–165. Available at: <http://linkinghub.elsevier.com/retrieve/pii/S1874604710280071> [Accessed May 21, 2017].
- Kamber, R.A., Shoemaker, C.J. & Denic, V., 2015. Receptor-Bound Targets of Selective Autophagy Use a Scaffold Protein to Activate the Atg1 Kinase. *Molecular Cell*, 59(3), pp.372–381. Available at: <http://www.ncbi.nlm.nih.gov/pubmed/26166702> [Accessed May 22, 2017].

- Kanazawa, T. et al., 2004. Amino acids and insulin control autophagic proteolysis through different signaling pathways in relation to mTOR in isolated rat hepatocytes. *The Journal of biological chemistry*, 279(9), pp.8452–9. Available at: <http://www.ncbi.nlm.nih.gov/pubmed/14610086> [Accessed January 16, 2017].
- Kaplan, R.E.W. & Baugh, L.R., 2016. L1 arrest, *daf-16* /FoxO and nonautonomous control of post-embryonic development. *Worm*, 5(2), p.e1175196. Available at: <http://www.ncbi.nlm.nih.gov/pubmed/27383290> [Accessed March 10, 2017].
- Karanasios, E. et al., 2013. Dynamic association of the ULK1 complex with omegasomes during autophagy induction. *Journal of cell science*, 126(Pt 22), pp.5224–38. Available at: <http://jcs.biologists.org/content/126/22/5224> [Accessed January 16, 2017].
- Khalfan, W.A. & Klionsky, D.J., 2002. Molecular machinery required for autophagy and the cytoplasm to vacuole targeting (Cvt) pathway in *S. cerevisiae*. *Current opinion in cell biology*, 14(4), pp.468–75. Available at: <http://www.ncbi.nlm.nih.gov/pubmed/12383798> [Accessed May 22, 2017].
- Kijanska, M. et al., 2010. Activation of Atg1 kinase in autophagy by regulated phosphorylation. *Autophagy*, 6(8), pp.1168–78. Available at: <http://www.ncbi.nlm.nih.gov/pubmed/20953146> [Accessed September 13, 2016].
- Kim, J. et al., 2011. AMPK and mTOR regulate autophagy through direct phosphorylation of Ulk1. *Nature cell biology*, 13(2), pp.132–41. Available at: <http://www.pubmedcentral.nih.gov/articlerender.fcgi?artid=3987946&tool=pmcentrez&rendertype=abstract> [Accessed November 24, 2016].
- Kim, J. et al., 2002. Convergence of multiple autophagy and cytoplasm to vacuole targeting components to a perivacuolar membrane compartment prior to de novo vesicle formation. *The Journal of biological chemistry*, 277(1), pp.763–73. Available at: <http://www.ncbi.nlm.nih.gov/pubmed/11675395> [Accessed May 20, 2017].
- Kim, J. et al., 2001. Cvt9/Gsa9 Functions in Sequestering Selective Cytosolic Cargo Destined for the Vacuole. *The Journal of Cell Biology*, 153(2). Available at: <http://jcb.rupress.org/content/153/2/381> [Accessed May 21, 2017].
- Kim, M.S. et al., 2011. Expressional and mutational analyses of ATG5 gene in prostate cancers. *APMIS : acta pathologica, microbiologica, et immunologica Scandinavica*, 119(11), pp.802–7. Available at: <http://www.ncbi.nlm.nih.gov/pubmed/21995634> [Accessed January 17, 2017].
- Kim, Y.G., Cha, J. & Chandrasegaran, S., 1996. Hybrid restriction enzymes: zinc finger fusions to Fok I cleavage domain. *Proceedings of the National Academy of Sciences of the United States of America*, 93(3), pp.1156–60. Available at: <http://www.pubmedcentral.nih.gov/articlerender.fcgi?artid=40048&tool=pmcentrez&rendertype=abstract> [Accessed January 28, 2017].
- Kirisako, T. et al., 1999. Formation Process of Autophagosome Is Traced with Apg8/Aut7p in Yeast. *The Journal of Cell Biology*, 147(2). Available at: <http://jcb.rupress.org/content/147/2/435> [Accessed May 20, 2017].
- KLASS, M. & HIRSH, D., 1976. Non-ageing developmental variant of *Caenorhabditis elegans*. *Nature*, 260(5551), pp.523–525. Available at: <http://www.nature.com/doi/10.1038/260523a0> [Accessed May 19, 2017].
- Köppen, M. et al., 2001. Cooperative regulation of AJM-1 controls junctional integrity in

- Caenorhabditis elegans epithelia. *Nature cell biology*, 3(11), pp.983–91. Available at: <http://www.nature.com/doi/10.1038/ncb1101-983> [Accessed March 28, 2017].
- Koyama-Honda, I. et al., 2013. Temporal analysis of recruitment of mammalian ATG proteins to the autophagosome formation site. *Autophagy*. Available at: <http://www.tandfonline.com/doi/abs/10.4161/auto.25529> [Accessed January 16, 2017].
- Kuervers, L.M. et al., 2003. The sterol modifying enzyme LET-767 is essential for growth, reproduction and development in *Caenorhabditis elegans*. *Molecular genetics and genomics : MGG*, 270(2), pp.121–31. Available at: <http://www.ncbi.nlm.nih.gov/pubmed/12905072> [Accessed January 24, 2017].
- Kuma, A., Matsui, M. & Mizushima, N., 2007. LC3, an Autophagosome Marker, Can be Incorporated into Protein Aggregates Independent of Autophagy: Caution in the Interpretation of LC3 Localization. *Autophagy*, 3(4), pp.323–328. Available at: <http://www.tandfonline.com/doi/abs/10.4161/auto.4012> [Accessed August 15, 2017].
- Kuroyanagi, H. et al., 1998. Human ULK1, a novel serine/threonine kinase related to UNC-51 kinase of *Caenorhabditis elegans*: cDNA cloning, expression, and chromosomal assignment. *Genomics*, 51(1), pp.76–85. Available at: <http://www.ncbi.nlm.nih.gov/pubmed/9693035> [Accessed January 16, 2017].
- Kutscher, L.M. & Shaham, S., 2014. Forward and reverse mutagenesis in *C. elegans*. *WormBook : the online review of C. elegans biology*, pp.1–26. Available at: <http://www.pubmedcentral.nih.gov/articlerender.fcgi?artid=4078664&tool=pmcentrez&rendertype=abstract> [Accessed January 27, 2017].
- Ladoire, S. et al., 2012. Immunohistochemical detection of cytoplasmic LC3 puncta in human cancer specimens. *Autophagy*, 8(8), pp.1175–84. Available at: <http://www.tandfonline.com/doi/abs/10.4161/auto.20353> [Accessed January 17, 2017].
- Lamb, C.A., Yoshimori, T. & Tooze, S.A., 2013. The autophagosome: origins unknown, biogenesis complex. *Nature reviews. Molecular cell biology*, 14(12), pp.759–74. Available at: <http://dx.doi.org/10.1038/nrm3696> [Accessed August 24, 2016].
- Langmead, B. et al., 2009. Ultrafast and memory-efficient alignment of short DNA sequences to the human genome. *Genome biology*, 10(3), p.R25. Available at: <http://genomebiology.biomedcentral.com/articles/10.1186/gb-2009-10-3-r25> [Accessed August 21, 2016].
- Laplante, M. & Sabatini, D.M., 2012. mTOR signaling in growth control and disease. *Cell*, 149(2), pp.274–93. Available at: <http://www.pubmedcentral.nih.gov/articlerender.fcgi?artid=3331679&tool=pmcentrez&rendertype=abstract> [Accessed October 18, 2016].
- Lee, R., Hench, J. & Ruvkun, G., 2001. Regulation of *C. elegans* DAF-16 and its human ortholog FKHRL1 by the daf-2 insulin-like signaling pathway. *Current Biology*. Available at: <http://www.sciencedirect.com/science/article/pii/S0960982201005954> [Accessed January 13, 2017].
- Levine, B. & Kroemer, G., 2008. Autophagy in the pathogenesis of disease. *Cell*, 132(1), pp.27–42. Available at: <http://www.cell.com/article/S0092867407016856/fulltext> [Accessed December 13, 2016].
- Li, H. et al., 2009. The Sequence Alignment/Map format and SAMtools. *Bioinformatics*

- (Oxford, England), 25(16), pp.2078–9. Available at: <http://www.pubmedcentral.nih.gov/articlerender.fcgi?artid=2723002&tool=pmcentrez&rendertype=abstract> [Accessed August 20, 2016].
- Liang, C. et al., 2008. Beclin1-binding UVRAG targets the class C Vps complex to coordinate autophagosome maturation and endocytic trafficking. *Nature Cell Biology*, 10(7), pp.776–787. Available at: <http://www.ncbi.nlm.nih.gov/pubmed/18552835> [Accessed May 21, 2017].
- Lin, R.C. & Scheller, R.H., 2000. Mechanisms of synaptic vesicle exocytosis. *Annual review of cell and developmental biology*, 16, pp.19–49. Available at: <http://www.ncbi.nlm.nih.gov/pubmed/11031229> [Accessed February 5, 2017].
- Lohman, J.. & Remington, S.J., 2008. Development of a family of redox-sensitive green fluorescent protein indicators for use in relatively oxidizing subcellular environments. *Biochemistry*, 47, pp.8678–8688. Available at: <http://www.rcsb.org/pdb/explore.do?structureId=3cd1> [Accessed February 13, 2017].
- Ma, J.-F. et al., 2010. Immunohistochemical evidence for macroautophagy in neurones and endothelial cells in Alzheimer’s disease. *Neuropathology and applied neurobiology*, 36(4), pp.312–9. Available at: <http://www.ncbi.nlm.nih.gov/pubmed/20102518> [Accessed January 17, 2017].
- Mack, H.I.D. et al., 2012. AMPK-dependent phosphorylation of ULK1 regulates ATG9 localization. *Autophagy*, 8(8), pp.1197–1214. Available at: <http://www.ncbi.nlm.nih.gov/pubmed/22932492> [Accessed May 21, 2017].
- Madeo, F. et al., 1999. Oxygen stress: a regulator of apoptosis in yeast. *The Journal of cell biology*, 145(4), pp.757–67. Available at: <http://www.pubmedcentral.nih.gov/articlerender.fcgi?artid=2133192&tool=pmcentrez&rendertype=abstract> [Accessed February 13, 2017].
- Malhotra, J.D. & Kaufman, R.J., 2007a. Endoplasmic reticulum stress and oxidative stress: a vicious cycle or a double-edged sword? *Antioxidants & redox signaling*, 9(12), pp.2277–93. Available at: <http://www.ncbi.nlm.nih.gov/pubmed/17979528> [Accessed February 10, 2016].
- Malhotra, J.D. & Kaufman, R.J., 2007b. Endoplasmic Reticulum Stress and Oxidative Stress: A Vicious Cycle or a Double-Edged Sword? *Antioxidants & Redox Signaling*, 9(12), pp.2277–2294. Available at: <http://www.liebertonline.com/doi/abs/10.1089/ars.2007.1782> [Accessed May 23, 2017].
- Matsunaga, K. et al., 2010. Autophagy requires endoplasmic reticulum targeting of the PI3-kinase complex via Atg14L. *The Journal of cell biology*, 190(4), pp.511–21. Available at: <http://www.ncbi.nlm.nih.gov/pubmed/20713597> [Accessed January 16, 2017].
- Matsuura, A. et al., 1997. Apg1p, a novel protein kinase required for the autophagic process in *Saccharomyces cerevisiae*. *Gene*, 192(2), pp.245–250. Available at: <http://www.sciencedirect.com/science/article/pii/S037811199700084X> [Accessed May 21, 2017].
- Matyash, V. et al., 2004. Sterol-derived hormone(s) controls entry into diapause in *Caenorhabditis elegans* by consecutive activation of DAF-12 and DAF-16. *PLoS biology*, 2(10), p.e280. Available at: <http://europepmc.org/articles/PMC517820/?report=abstract> [Accessed January 24,

- 2017].
- Mayer, A. & Wickner, W., 1997. Docking of yeast vacuoles is catalyzed by the Ras-like GTPase Ypt7p after symmetric priming by Sec18p (NSF). *The Journal of cell biology*, 136(2), pp.307–17. Available at: <http://www.ncbi.nlm.nih.gov/pubmed/9015302> [Accessed August 24, 2017].
- McCloy, R.A. et al., 2014. Partial inhibition of Cdk1 in G 2 phase overrides the SAC and decouples mitotic events. *Cell cycle (Georgetown, Tex.)*, 13(9), pp.1400–12. Available at: <http://www.tandfonline.com/doi/abs/10.4161/cc.28401> [Accessed May 25, 2016].
- McMahon, L. et al., 2003. Two sets of interacting collagens form functionally distinct substructures within a *Caenorhabditis elegans* extracellular matrix. *Molecular biology of the cell*, 14(4), pp.1366–78. Available at: <http://www.pubmedcentral.nih.gov/articlerender.fcgi?artid=153107&tool=pmcentrez&rendertype=abstract> [Accessed February 8, 2016].
- Meléndez, A. et al., 2003. Autophagy genes are essential for dauer development and life-span extension in *C. elegans*. *Science (New York, N.Y.)*, 301(5638), pp.1387–91. Available at: <http://science.sciencemag.org/content/301/5638/1387.abstract> [Accessed January 16, 2017].
- Meléndez, A. & Levine, B., 2009. Autophagy in *C. elegans*. *WormBook*, pp.1–26. Available at: <http://www.ncbi.nlm.nih.gov/pubmed/19705512> [Accessed May 21, 2017].
- Minevich, G. et al., 2012. CloudMap: a cloud-based pipeline for analysis of mutant genome sequences. *Genetics*, 192(4), pp.1249–69. Available at: <http://www.pubmedcentral.nih.gov/articlerender.fcgi?artid=3512137&tool=pmcentrez&rendertype=abstract> [Accessed January 22, 2016].
- Misura, K.M.S., Scheller, R.H. & Weis, W.I., 2000. Three-dimensional structure of the neuronal-Sec1–syntaxin 1a complex. *Nature*, 404(6776), pp.355–362. Available at: <http://www.ncbi.nlm.nih.gov/pubmed/10746715> [Accessed May 22, 2017].
- Mizushima, N. et al., 1998. A new protein conjugation system in human. The counterpart of the yeast Apg12p conjugation system essential for autophagy. *The Journal of biological chemistry*, 273(51), pp.33889–92. Available at: <http://www.ncbi.nlm.nih.gov/pubmed/9852036> [Accessed January 16, 2017].
- Mizushima, N., 2007. Autophagy: process and function. *Genes & development*, 21(22), pp.2861–73. Available at: <http://www.ncbi.nlm.nih.gov/pubmed/18006683> [Accessed May 21, 2017].
- Mizushima, N. et al., 2008. Autophagy fights disease through cellular self-digestion. *Nature*, 451(7182), pp.1069–75. Available at: <http://www.ncbi.nlm.nih.gov/pubmed/18305538> [Accessed May 20, 2017].
- Mizushima, N. & Klionsky, D.J., 2007. Protein turnover via autophagy: implications for metabolism. *Annual review of nutrition*, 27, pp.19–40. Available at: <http://www.ncbi.nlm.nih.gov/pubmed/17311494> [Accessed January 16, 2017].
- Monsalve, G.C. et al., 2011. LIN-42/PERIOD controls cyclical and developmental progression of *C. elegans* molts. *Current biology : CB*, 21(24), pp.2033–45. Available at: <http://www.ncbi.nlm.nih.gov/pubmed/22137474> [Accessed June 26, 2017].
- Nair, U. et al., 2012. A role for Atg8–PE deconjugation in autophagosome biogenesis.

- Autophagy*, 8(5), pp.780–793. Available at:
<http://www.ncbi.nlm.nih.gov/pubmed/22622160> [Accessed May 21, 2017].
- Nair, U. et al., 2011. SNARE proteins are required for macroautophagy. *Cell*, 146(2), pp.290–302. Available at: <http://www.ncbi.nlm.nih.gov/pubmed/21784249> [Accessed May 13, 2017].
- Nair, U. & Klionsky, D.J., 2011. Autophagosome biogenesis requires SNAREs. *Autophagy*, 7(12), pp.1570–2. Available at:
<http://www.pubmedcentral.nih.gov/articlerender.fcgi?artid=3327624&tool=pmcentrez&rendertype=abstract> [Accessed February 10, 2016].
- Nakatogawa, H., Ichimura, Y. & Ohsumi, Y., 2007. Atg8, a Ubiquitin-like Protein Required for Autophagosome Formation, Mediates Membrane Tethering and Hemifusion. *Cell*, 130(1), pp.165–178. Available at:
<http://www.sciencedirect.com/science/article/pii/S0092867407006587> [Accessed May 21, 2017].
- Nebert, D.W. & Vasiliou, V., 2004. Analysis of the glutathione S-transferase (GST) gene family. *Human Genomics*, 1(6), p.460. Available at:
<http://humgenomics.biomedcentral.com/articles/10.1186/1479-7364-1-6-460> [Accessed January 27, 2017].
- Nielsen, E. et al., 2000. Rabenosyn-5, a novel Rab5 effector, is complexed with hVPS45 and recruited to endosomes through a FYVE finger domain. *The Journal of cell biology*, 151(3), pp.601–12. Available at:
<http://www.pubmedcentral.nih.gov/articlerender.fcgi?artid=2185588&tool=pmcentrez&rendertype=abstract> [Accessed February 19, 2016].
- Noda, T. et al., 2000. Apg9p/Cvt7p is an integral membrane protein required for transport vesicle formation in the Cvt and autophagy pathways. *The Journal of cell biology*, 148(3), pp.465–80. Available at: <http://www.ncbi.nlm.nih.gov/pubmed/10662773> [Accessed May 13, 2017].
- Noda, T. & Ohsumi, Y., 1998. Tor, a phosphatidylinositol kinase homologue, controls autophagy in yeast. *The Journal of biological chemistry*, 273(7), pp.3963–6. Available at: <http://www.ncbi.nlm.nih.gov/pubmed/9461583> [Accessed January 16, 2017].
- Ogura, K., Wicky, C., Magnenat, L., Tobler, H., Mori, I., Müller, F., et al., 1994. *Caenorhabditis elegans* unc-51 gene required for axonal elongation encodes a novel serine/threonine kinase. , 8(20). Available at:
<http://www.genesdev.org/cgi/doi/10.1101/gad.8.20.2389> [Accessed March 10, 2017].
- Ogura, K., Wicky, C., Magnenat, L., Tobler, H., Mori, I., Muller, F., et al., 1994. *Caenorhabditis elegans* unc-51 gene required for axonal elongation encodes a novel serine/threonine kinase. *Genes & Development*, 8(20), pp.2389–2400. Available at:
<http://www.genesdev.org/cgi/doi/10.1101/gad.8.20.2389> [Accessed March 24, 2017].
- Ohashi, Y. & Munro, S., 2010. Membrane delivery to the yeast autophagosome from the Golgi-endosomal system. *Molecular biology of the cell*, 21(22), pp.3998–4008. Available at:
<http://www.pubmedcentral.nih.gov/articlerender.fcgi?artid=2982105&tool=pmcentrez&rendertype=abstract> [Accessed September 13, 2016].
- Ohsumi, Y., 2000. Kamada 2000, Tor-mediated induction of autophagy via an Apg1 protein kinase complex. *Journal of Cell Biology*, 150(6), pp.1507–1513. Available at:

- <http://jcb.rupress.org/content/150/6/1507.full> [Accessed May 21, 2017].
- Ookawara, T. et al., 2002. Nuclear translocation of extracellular superoxide dismutase. *Biochemical and Biophysical Research Communications*, 296(1), pp.54–61. Available at: <http://www.sciencedirect.com/science/article/pii/S0006291X02008045> [Accessed January 27, 2017].
- Orsi, A. et al., 2012. Dynamic and transient interactions of Atg9 with autophagosomes, but not membrane integration, are required for autophagy. *Molecular biology of the cell*, 23(10), pp.1860–73. Available at: <http://www.pubmedcentral.nih.gov/articlerender.fcgi?artid=3350551&tool=pmcentrez&rendertype=abstract> [Accessed January 16, 2017].
- Oury, T.D., Day, B.J. & Crapo, J.D., 1996. Extracellular superoxide dismutase in vessels and airways of humans and baboons. *Free Radical Biology and Medicine*, 20(7), pp.957–965. Available at: <http://www.sciencedirect.com/science/article/pii/0891584995022228> [Accessed January 27, 2017].
- Peixoto, C.A., Kramer, J.M. & de Souza, W., 1997. Caenorhabditis elegans cuticle: a description of new elements of the fibrous layer. *The Journal of parasitology*, 83(3), pp.368–72. Available at: <http://www.ncbi.nlm.nih.gov/pubmed/9194814> [Accessed March 27, 2017].
- Piper, R.C., Whitters, E.A. & Stevens, T.H., 1994. Yeast Vps45p is a Sec1p-like protein required for the consumption of vacuole-targeted, post-Golgi transport vesicles. *European journal of cell biology*, 65(2), pp.305–18. Available at: <http://www.ncbi.nlm.nih.gov/pubmed/7720726> [Accessed September 13, 2016].
- Plaisance, V. et al., 2016. Endoplasmic Reticulum Stress Links Oxidative Stress to Impaired Pancreatic Beta-Cell Function Caused by Human Oxidized LDL A. Nadal, ed. *PLOS ONE*, 11(9), p.e0163046. Available at: <http://dx.plos.org/10.1371/journal.pone.0163046> [Accessed May 23, 2017].
- Podbilewicz, B. & White, J.G., 1994. Cell Fusions in the Developing Epithelia of *C. elegans*. *Developmental Biology*, 161(2), pp.408–424. Available at: <http://www.sciencedirect.com/science/article/pii/S0012160684710414> [Accessed April 27, 2016].
- Pollard, M.G., Travers, K.J. & Weissman, J.S., 1998. Ero1p: a novel and ubiquitous protein with an essential role in oxidative protein folding in the endoplasmic reticulum. *Molecular cell*, 1(2), pp.171–82. Available at: <http://www.ncbi.nlm.nih.gov/pubmed/9659914> [Accessed May 18, 2017].
- Possik, E. & Pause, A., 2015. Measuring Oxidative Stress Resistance of Caenorhabditis elegans in 96-well Microtiter Plates. *Journal of Visualized Experiments*, (99), p.1367520. Available at: <http://www.jove.com/video/52746/measuring-oxidative-stress-resistance-caenorhabditis-elegans-96-well> [Accessed February 8, 2016].
- Poteryaev, D. et al., 2010. Identification of the switch in early-to-late endosome transition. *Cell*, 141(3), pp.497–508. Available at: <http://www.sciencedirect.com/science/article/pii/S0092867410002473> [Accessed March 2, 2016].
- Qu, X. et al., 2007. Autophagy Gene-Dependent Clearance of Apoptotic Cells during Embryonic Development. *Cell*, 128(5), pp.931–946. Available at: <http://www.ncbi.nlm.nih.gov/pubmed/17350577> [Accessed May 20, 2017].

- Raymond, C.K. et al., 1992. Morphological classification of the yeast vacuolar protein sorting mutants: evidence for a prevacuolar compartment in class E vps mutants. *Molecular biology of the cell*, 3(12), pp.1389–402. Available at: <http://www.ncbi.nlm.nih.gov/pubmed/1493335> [Accessed June 20, 2017].
- Reggiori, F. et al., 2004. The Atg1-Atg13 complex regulates Atg9 and Atg23 retrieval transport from the pre-autophagosomal structure. *Developmental cell*, 6(1), pp.79–90. Available at: <http://www.ncbi.nlm.nih.gov/pubmed/14723849> [Accessed May 20, 2017].
- Reggiori, F. & Klionsky, D.J., 2006. Atg9 sorting from mitochondria is impaired in early secretion and VFT-complex mutants in *Saccharomyces cerevisiae*. *Journal of Cell Science*, 119(14). Available at: <http://jcs.biologists.org/content/119/14/2903> [Accessed May 20, 2017].
- Reggiori, F. & Klionsky, D.J., 2002. Autophagy in the Eukaryotic Cell. *Eukaryotic Cell*, 1(1), pp.11–21. Available at: <http://ec.asm.org/content/1/1/11.full> [Accessed August 13, 2016].
- Robinson, J.S. et al., 1988. Protein sorting in *Saccharomyces cerevisiae*: isolation of mutants defective in the delivery and processing of multiple vacuolar hydrolases. *Molecular and cellular biology*, 8(11), pp.4936–48. Available at: <http://www.pubmedcentral.nih.gov/articlerender.fcgi?artid=365587&tool=pmcentrez&rendertype=abstract> [Accessed September 13, 2016].
- Ron, D., 2002. Translational control in the endoplasmic reticulum stress response. *The Journal of clinical investigation*, 110(10), pp.1383–8. Available at: <http://www.jci.org/articles/view/16784> [Accessed February 6, 2017].
- Rubinsztein, D.C., Codogno, P. & Levine, B., 2012. Autophagy modulation as a potential therapeutic target for diverse diseases. *Nature reviews. Drug discovery*, 11(9), pp.709–30. Available at: <http://dx.doi.org/10.1038/nrd3802> [Accessed September 21, 2016].
- Samuelson, A. V, Carr, C.E. & Ruvkun, G., 2007. Gene activities that mediate increased life span of *C. elegans* insulin-like signaling mutants. *Genes & development*, 21(22), pp.2976–94. Available at: <http://genesdev.cshlp.org/content/21/22/2976.abstract> [Accessed January 13, 2017].
- Sato, K. et al., 2014. *C. elegans* as a model for membrane traffic. *WormBook : the online review of C. elegans biology*, pp.1–47. Available at: <http://www.ncbi.nlm.nih.gov/pubmed/24778088> [Accessed March 27, 2017].
- Sato, M. et al., 2011. Degradation of paternal mitochondria by fertilization-triggered autophagy in *C. elegans* embryos. *Science (New York, N.Y.)*, 334(6059), pp.1141–4. Available at: <http://www.ncbi.nlm.nih.gov/pubmed/21998252> [Accessed July 1, 2016].
- Schneeberger, K. et al., 2009. SHOREmap: simultaneous mapping and mutation identification by deep sequencing. *Nature methods*, 6(8), pp.550–1. Available at: <http://dx.doi.org/10.1038/nmeth0809-550> [Accessed February 7, 2017].
- Schneider, C.A., Rasband, W.S. & Eliceiri, K.W., 2012. NIH Image to ImageJ: 25 years of image analysis. *Nature Methods*, 9(7), pp.671–675. Available at: <http://www.nature.com/doi/10.1038/nmeth.2089> [Accessed March 10, 2017].
- Schulz, J.B. et al., 2000. Glutathione, oxidative stress and neurodegeneration. *European*

- Journal of Biochemistry*, 267(16), pp.4904–4911. Available at: <http://doi.wiley.com/10.1046/j.1432-1327.2000.01595.x> [Accessed January 27, 2017].
- Scott, R.C., Juhász, G. & Neufeld, T.P., 2007. Direct Induction of Autophagy by Atg1 Inhibits Cell Growth and Induces Apoptotic Cell Death. *Current Biology*, 17(1), pp.1–11. Available at: <http://www.ncbi.nlm.nih.gov/pubmed/17208179> [Accessed May 20, 2017].
- Scott, S. V et al., 1996. Cytoplasm-to-vacuole targeting and autophagy employ the same machinery to deliver proteins to the yeast vacuole. *Proceedings of the National Academy of Sciences of the United States of America*, 93(22), pp.12304–8. Available at: <http://www.ncbi.nlm.nih.gov/pubmed/8901576> [Accessed May 22, 2017].
- Seals, D.F. et al., 2000. A Ypt/Rab effector complex containing the Sec1 homolog Vps33p is required for homotypic vacuole fusion. *Proceedings of the National Academy of Sciences*, 97(17), pp.9402–9407. Available at: <http://www.pnas.org/cgi/doi/10.1073/pnas.97.17.9402> [Accessed May 23, 2017].
- Seidel, H.S., Rockman, M. V & Kruglyak, L., 2008. Widespread genetic incompatibility in *C. elegans* maintained by balancing selection. *Science (New York, N.Y.)*, 319(5863), pp.589–94. Available at: <http://www.pubmedcentral.nih.gov/articlerender.fcgi?artid=2421010&tool=pmcentrez&rendertype=abstract> [Accessed November 24, 2016].
- Séron, K. et al., 1998. A yeast t-SNARE involved in endocytosis. *Molecular biology of the cell*, 9(10), pp.2873–89. Available at: <http://www.ncbi.nlm.nih.gov/pubmed/9763449> [Accessed May 20, 2017].
- Shanks, S.G. et al., 2012. The Sec1/Munc18 Protein Vps45 Regulates Cellular Levels of Its SNARE Binding Partners Tlg2 and Snc2 in *Saccharomyces cerevisiae* W. Hong, ed. *PLoS ONE*, 7(11), p.e49628. Available at: https://www.researchgate.net/publication/233725644_The_Sec1Munc18_Protein_Vps45_Regulates_Cellular_Levels_of_Its_SNARE_Binding_Partners_Tlg2_and_Snc2_in_Saccharomyces_cerevisiae [Accessed April 26, 2016].
- Shemer, G. et al., 2004. EFF-1 Is Sufficient to Initiate and Execute Tissue-Specific Cell Fusion in *C. elegans*. *Current Biology*, 14(17), pp.1587–1591. Available at: <http://linkinghub.elsevier.com/retrieve/pii/S0960982204005585> [Accessed May 19, 2017].
- Shemer, G. & Podbilewicz, B., 2000. Fusomorphogenesis: cell fusion in organ formation. *Developmental dynamics : an official publication of the American Association of Anatomists*, 218(1), pp.30–51. Available at: <http://www.ncbi.nlm.nih.gov/pubmed/10822258> [Accessed April 27, 2016].
- Shin, H.-W. et al., 2005. An enzymatic cascade of Rab5 effectors regulates phosphoinositide turnover in the endocytic pathway. *The Journal of Cell Biology*, 170(4), pp.607–618. Available at: <http://www.ncbi.nlm.nih.gov/pubmed/16103228> [Accessed May 21, 2017].
- Simonsen, A. et al., 1999. The Rab5 effector EEA1 interacts directly with syntaxin-6. *The Journal of biological chemistry*, 274(41), pp.28857–60. Available at: <http://www.ncbi.nlm.nih.gov/pubmed/10506127> [Accessed May 23, 2017].
- Singh, B. & Bhat, H.K., 2012. Superoxide dismutase 3 is induced by antioxidants, inhibits oxidative DNA damage and is associated with inhibition of estrogen-induced breast cancer. *Carcinogenesis*, 33(12), pp.2601–10. Available at:

- <http://www.pubmedcentral.nih.gov/articlerender.fcgi?artid=3510741&tool=pmcentrez&rendertype=abstract> [Accessed February 10, 2016].
- Singh, R.N. & Sulston, J.E., 1978. Some Observations On Moulting in *Caenorhabditis Elegans*. *Nematologica*, 24(1), pp.63–71. Available at: <http://booksandjournals.brillonline.com/content/journals/10.1163/187529278x00074> [Accessed February 8, 2016].
- Slice, L.W., Freedman, J.H. & Rubin, C.S., 1990. Purification, characterization, and cDNA cloning of a novel metallothionein-like, cadmium-binding protein from *Caenorhabditis elegans*. *The Journal of biological chemistry*, 265(1), pp.256–63. Available at: <http://www.ncbi.nlm.nih.gov/pubmed/2294106> [Accessed May 18, 2017].
- Solinger, J.A. & Spang, A., 2014. Loss of the Sec1/Munc18-family proteins VPS-33.2 and VPS-33.1 bypasses a block in endosome maturation in *Caenorhabditis elegans*. *Molecular biology of the cell*, 25(24), pp.3909–25. Available at: <http://www.ncbi.nlm.nih.gov/pubmed/25273556> [Accessed February 27, 2016].
- Solinger, J.A. & Spang, A., 2013. Tethering complexes in the endocytic pathway: CORVET and HOPS. *The FEBS journal*, 280(12), pp.2743–57. Available at: <http://www.ncbi.nlm.nih.gov/pubmed/23351085> [Accessed February 8, 2016].
- St Onge, R.P. et al., 2007. Systematic pathway analysis using high-resolution fitness profiling of combinatorial gene deletions. *Nature genetics*, 39(2), pp.199–206. Available at: http://www.tdi.ox.ac.uk/_asset/file/6692.pdf [Accessed April 19, 2017].
- Stenmark, H., 2009. Rab GTPases as coordinators of vesicle traffic. *Nature Reviews Molecular Cell Biology*, 10(8), pp.513–525. Available at: <http://www.nature.com/doi/10.1038/nrm2728> [Accessed May 21, 2017].
- Stepensky, P. et al., 2013. The Thr224Asn mutation in the VPS45 gene is associated with the congenital neutropenia and primary myelofibrosis of infancy. *Blood*, 121(25), pp.5078–5087. Available at: <http://www.ncbi.nlm.nih.gov/pubmed/23599270> [Accessed May 20, 2017].
- Stepensky, P. et al., 2013. VPS 45-associated primary infantile myelofibrosis - Successful treatment with hematopoietic stem cell transplantation. *Pediatr Transplant*, 17(8), pp.820–825. Available at: <http://www.ncbi.nlm.nih.gov/pubmed/24164830>.
- Stiernagle, T., 2006. Maintenance of *C. elegans*. *WormBook*. Available at: http://www.wormbook.org/chapters/www_strainmaintain/strainmaintain.html [Accessed March 10, 2017].
- Struthers, M.S. et al., 2009. Functional homology of mammalian syntaxin 16 and yeast Tlg2p reveals a conserved regulatory mechanism. *J Cell Sci*, 122(Pt 13), pp.2292–2299. Available at: <http://www.ncbi.nlm.nih.gov/pubmed/19509055>.
- Sudhof, T.C. et al., 2009. Membrane fusion: grappling with SNARE and SM proteins. *Science (New York, N.Y.)*, 323(5913), pp.474–7. Available at: <http://science.sciencemag.org/content/323/5913/474.abstract> [Accessed January 17, 2017].
- Sudhof, T.C. & Rothman, J.E., 2009. Membrane Fusion: Grappling with SNARE and SM Proteins. *Science*, 323(5913), pp.474–477. Available at: <https://www.ncbi.nlm.nih.gov/pmc/articles/PMC3736821/pdf/nihms494840.pdf> [Accessed May 22, 2017].

- Sulston, J.E. et al., 1983. The embryonic cell lineage of the nematode *Caenorhabditis elegans*. *Developmental biology*, 100(1), pp.64–119. Available at: http://wormatlas.org/ver1/Sulstonemblin_1983/toc.html [Accessed January 12, 2017].
- Sulston, J.E. & Horvitz, H.R., 1977. Post-embryonic cell lineages of the nematode, *Caenorhabditis elegans*. *Developmental biology*, 56(1), pp.110–56. Available at: <http://www.ncbi.nlm.nih.gov/pubmed/838129> [Accessed January 13, 2017].
- Sun, Q. et al., 2010. Rubicon controls endosome maturation as a Rab7 effector. *Proceedings of the National Academy of Sciences of the United States of America*, 107(45), pp.19338–43. Available at: <http://www.ncbi.nlm.nih.gov/pubmed/20974968> [Accessed May 21, 2017].
- Suzuki, K. et al., 2007. Hierarchy of Atg proteins in pre-autophagosomal structure organization. *Genes to Cells*, 12(2), pp.209–218. Available at: <http://www.ncbi.nlm.nih.gov/pubmed/17295840> [Accessed May 21, 2017].
- Suzuki, K. et al., 2002. Studies of cargo delivery to the vacuole mediated by autophagosomes in *Saccharomyces cerevisiae*. *Developmental cell*, 3(6), pp.815–24. Available at: <http://www.ncbi.nlm.nih.gov/pubmed/12479807> [Accessed May 21, 2017].
- Suzuki, K. et al., 2001. The pre-autophagosomal structure organized by concerted functions of APG genes is essential for autophagosome formation. *The EMBO Journal*, 20(21), pp.5971–5981. Available at: <http://www.ncbi.nlm.nih.gov/pubmed/11689437> [Accessed May 20, 2017].
- Suzuki, K. & Ohsumi, Y., 2007. Molecular machinery of autophagosome formation in yeast, *Saccharomyces cerevisiae*. *FEBS Letters*, 581(11), pp.2156–2161. Available at: <http://doi.wiley.com/10.1016/j.febslet.2007.01.096> [Accessed May 21, 2017].
- Swain, S.C. et al., 2004. *C.elegans* Metallothioneins: New Insights into the Phenotypic Effects of Cadmium Toxicosis. *Journal of Molecular Biology*, 341(4), pp.951–959. Available at: <http://linkinghub.elsevier.com/retrieve/pii/S0022283604007545> [Accessed May 18, 2017].
- Tabara, H., Grishok, A. & Mello, C.C., 1998. RNAi in *C. elegans*: soaking in the genome sequence. *Science (New York, N.Y.)*, 282(5388), pp.430–1. Available at: <http://www.ncbi.nlm.nih.gov/pubmed/9841401> [Accessed May 19, 2017].
- Takacs-Vellai, K. et al., 2005. Inactivation of the Autophagy Gene *bec-1* Triggers Apoptotic Cell Death in *C. elegans*. *Current Biology*, 15(16), pp.1513–1517. Available at: <http://www.ncbi.nlm.nih.gov/pubmed/16111945> [Accessed May 20, 2017].
- Takeshige, K. et al., 1992. Autophagy in yeast demonstrated with proteinase-deficient mutants and conditions for its induction. *The Journal of cell biology*, 119(2), pp.301–11. Available at: <http://www.ncbi.nlm.nih.gov/pubmed/1400575> [Accessed May 18, 2016].
- Tanida, I. et al., 2002. Human Apg3p/Aut1p homologue is an authentic E2 enzyme for multiple substrates, GATE-16, GABARAP, and MAP-LC3, and facilitates the conjugation of hApg12p to hApg5p. *The Journal of biological chemistry*, 277(16), pp.13739–44. Available at: <http://www.ncbi.nlm.nih.gov/pubmed/11825910> [Accessed January 16, 2017].
- Tanida, I. et al., 2005. Lysosomal turnover, but not a cellular level, of endogenous LC3 is a

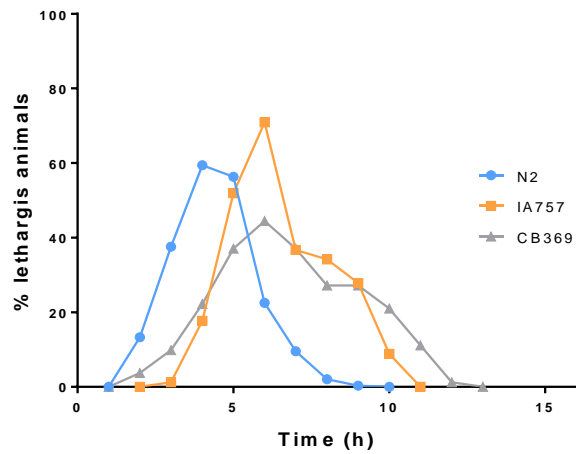
- marker for autophagy. *Autophagy*, 1(2), pp.84–91. Available at: <http://www.ncbi.nlm.nih.gov/pubmed/16874052> [Accessed July 25, 2017].
- Thein, M.C. et al., 2003. Caenorhabditis elegans exoskeleton collagen COL-19: an adult-specific marker for collagen modification and assembly, and the analysis of organismal morphology. *Developmental dynamics : an official publication of the American Association of Anatomists*, 226(3), pp.523–39. Available at: <http://www.ncbi.nlm.nih.gov/pubmed/12619137> [Accessed January 13, 2017].
- Thoreen, C.C. et al., 2009. An ATP-competitive mammalian target of rapamycin inhibitor reveals rapamycin-resistant functions of mTORC1. *The Journal of biological chemistry*, 284(12), pp.8023–32. Available at: <http://www.pubmedcentral.nih.gov/articlerender.fcgi?artid=2658096&tool=pmcentrez&rendertype=abstract> [Accessed January 16, 2017].
- Tian, E. et al., 2009. epg-1 functions in autophagy-regulated processes and may encode a highly divergent Atg13 homolog in *C. elegans*. *Autophagy*, 5(5), pp.608–15. Available at: <http://www.ncbi.nlm.nih.gov/pubmed/19377305> [Accessed May 21, 2017].
- Timmons, L., Court, D.L. & Fire, A., 2001. Ingestion of bacterially expressed dsRNAs can produce specific and potent genetic interference in *Caenorhabditis elegans*. *Gene*, 263(1–2), pp.103–12. Available at: <http://www.ncbi.nlm.nih.gov/pubmed/11223248> [Accessed May 19, 2017].
- Tsukada, M. & Ohsumi, Y., 1993. Isolation and characterization of autophagy-defective mutants of *Saccharomyces cerevisiae*. *FEBS letters*, 333(1–2), pp.169–74. Available at: <http://www.ncbi.nlm.nih.gov/pubmed/8224160> [Accessed May 20, 2017].
- Tu, B.P. & Weissman, J.S., 2004. Oxidative protein folding in eukaryotes: mechanisms and consequences. *The Journal of cell biology*, 164(3), pp.341–6. Available at: <http://jcb.rupress.org/content/164/3/341> [Accessed February 6, 2017].
- Vanfleteren, J.R. & De Vreese, A., 1995. The gerontogenes age-1 and daf-2 determine metabolic rate potential in aging *Caenorhabditis elegans*. *FASEB journal : official publication of the Federation of American Societies for Experimental Biology*, 9(13), pp.1355–61. Available at: <http://www.ncbi.nlm.nih.gov/pubmed/7557026> [Accessed May 19, 2017].
- VanRheenen, S.M. et al., 1999. Sec34p, a protein required for vesicle tethering to the yeast Golgi apparatus, is in a complex with Sec35p. *The Journal of cell biology*, 147(4), pp.729–42. Available at: <http://www.ncbi.nlm.nih.gov/pubmed/10562277> [Accessed June 16, 2017].
- VanRheenen, S.M. et al., 1998. Sec35p, a novel peripheral membrane protein, is required for ER to Golgi vesicle docking. *The Journal of cell biology*, 141(5), pp.1107–19. Available at: <http://www.ncbi.nlm.nih.gov/pubmed/9606204> [Accessed June 16, 2017].
- Vilboux, T. et al., 2013. A congenital neutrophil defect syndrome associated with mutations in VPS45. *N Engl J Med*, 369(1), pp.54–65. Available at: <http://www.ncbi.nlm.nih.gov/pubmed/23738510>.
- Ward, E.S. et al., 2005. From Sorting Endosomes to Exocytosis: Association of Rab4 and Rab11 GTPases with the Fc Receptor, FcRn, during Recycling. *Molecular Biology of the Cell*, 16(4), pp.2028–2038. Available at: <http://www.molbiolcell.org/cgi/doi/10.1091/mbc.E04-08-0735> [Accessed May 23,

- 2017].
- Waring, D.A. et al., 1990. Selective silencing of cell communication influences anteroposterior pattern formation in *C. elegans*. *Cell*, 60(1), pp.123–31. Available at: <http://www.ncbi.nlm.nih.gov/pubmed/2295086> [Accessed May 19, 2017].
- Wartosch, L. et al., 2015. Recruitment of VPS33A to HOPS by VPS16 Is Required for Lysosome Fusion with Endosomes and Autophagosomes. *Traffic (Copenhagen, Denmark)*, 16(7), pp.727–42. Available at: <http://www.ncbi.nlm.nih.gov/pubmed/25783203> [Accessed May 12, 2017].
- Webb, G.C. et al., 1997. Genetic interactions between a pep7 mutation and the PEP12 and VPS45 genes: evidence for a novel SNARE component in transport between the *Saccharomyces cerevisiae* Golgi complex and endosome. *Genetics*, 147(2), pp.467–78. Available at: <http://europepmc.org/articles/PMC1208171/?report=abstract> [Accessed January 20, 2017].
- Weimbs, T. et al., 1997. A conserved domain is present in different families of vesicular fusion proteins: A new superfamily. *Proceedings of the National Academy of Sciences*, 94(7), pp.3046–3051. Available at: http://www.pnas.org/content/94/7/3046.abstract?ijkey=92d3e590273b91c8179f6c1ba93910d6afb6f1a9&keytype2=tf_ipsecsha [Accessed February 5, 2017].
- Wicks, S.R. et al., 2001. Rapid gene mapping in *Caenorhabditis elegans* using a high density polymorphism map. *Nature genetics*, 28(2), pp.160–4. Available at: <http://dx.doi.org/10.1038/88878> [Accessed February 3, 2017].
- Williams, B.D. et al., 1992. A genetic mapping system in *Caenorhabditis elegans* based on polymorphic sequence-tagged sites. *Genetics*, 131(3), pp.609–24. Available at: <http://www.pubmedcentral.nih.gov/articlerender.fcgi?artid=1205034&tool=pmcentrez&rendertype=abstract> [Accessed February 7, 2017].
- Wright, H.L. et al., 2010. Neutrophil function in inflammation and inflammatory diseases. *Rheumatology (Oxford, England)*, 49(9), pp.1618–31. Available at: <http://rheumatology.oxfordjournals.org/content/49/9/1618.full> [Accessed September 11, 2016].
- Xiao, R. et al., 2015. RNAi Interrogation of Dietary Modulation of Development, Metabolism, Behavior, and Aging in *C. elegans*. *Cell Reports*, 11(7), pp.1123–1133. Available at: <http://www.ncbi.nlm.nih.gov/pubmed/25959815> [Accessed July 28, 2017].
- Yamaguchi, T. et al., 2002. Sly1 Binds to Golgi and ER Syntaxins via a Conserved N-Terminal Peptide Motif. *Developmental Cell*, 2(3), pp.295–305. Available at: <http://www.sciencedirect.com/science/article/pii/S1534580702001259> [Accessed May 20, 2017].
- Yan, J. et al., 1998. Identification of mouse ULK1, a novel protein kinase structurally related to *C. elegans* UNC-51. *Biochemical and biophysical research communications*, 246(1), pp.222–7. Available at: <http://www.ncbi.nlm.nih.gov/pubmed/9600096> [Accessed January 16, 2017].
- Yang, P. & Zhang, H., 2011. The coiled-coil domain protein EPG-8 plays an essential role in the autophagy pathway in *C. elegans*. *Autophagy*, 7(2), pp.159–65. Available at: <http://www.ncbi.nlm.nih.gov/pubmed/21116129> [Accessed May 21, 2017].
- Yen, W.-L. et al., 2007. Atg27 is required for autophagy-dependent cycling of Atg9.

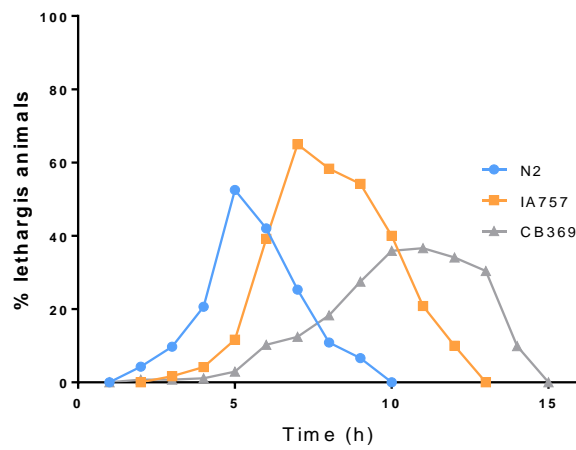
- Molecular biology of the cell*, 18(2), pp.581–93. Available at: <http://www.ncbi.nlm.nih.gov/pubmed/17135291> [Accessed May 20, 2017].
- Yen, W.L. et al., 2010. The conserved oligomeric Golgi complex is involved in double-membrane vesicle formation during autophagy. *J Cell Biol*, 188(1), pp.101–114. Available at: <http://www.ncbi.nlm.nih.gov/pubmed/20065092>.
- Yochem, J. et al., 1999. A gp330/megalin-related protein is required in the major epidermis of *Caenorhabditis elegans* for completion of molting. *Development (Cambridge, England)*, 126(3), pp.597–606. Available at: <http://www.ncbi.nlm.nih.gov/pubmed/9876188> [Accessed January 24, 2017].
- Yorimitsu, T. & Klionsky, D.J., 2005. Atg11 Links Cargo to the Vesicle-forming Machinery in the Cytoplasm to Vacuole Targeting Pathway. *Molecular Biology of the Cell*, 16, pp.1593–1605. Available at: <http://www.molbiolcell.org/content/16/4/1593.full.pdf> [Accessed May 21, 2017].
- Young, A.R.J. et al., 2006. Starvation and ULK1-dependent cycling of mammalian Atg9 between the TGN and endosomes. *Journal of Cell Science*, 119(18). Available at: <http://jcs.biologists.org/content/119/18/3888.short> [Accessed May 21, 2017].
- Yu, Z.-Q. et al., 2012. Dual roles of Atg8–PE deconjugation by Atg4 in autophagy. *Autophagy*, 8(6), pp.883–892. Available at: <http://www.ncbi.nlm.nih.gov/pubmed/22652539> [Accessed May 21, 2017].
- Zarkower, D., 2006. Somatic sex determination. *WormBook : the online review of C. elegans biology*, pp.1–12. Available at: http://www.wormbook.org/chapters/www_somaticsexdeterm/somaticsexdeterm.html [Accessed January 20, 2017].
- Zerial, M. et al., 1999. The Rab5 effector EEA1 is a core component of endosome docking. *Nature*, 397(6720), pp.621–625. Available at: <http://www.ncbi.nlm.nih.gov/pubmed/10050856> [Accessed August 24, 2017].
- Zhang, B. et al., 2015. Environmental Temperature Differentially Modulates *C. elegans* Longevity through a Thermosensitive TRP Channel. *Cell Reports*, 11(9), pp.1414–1424. Available at: [http://www.cell.com/cell-reports/pdf/S2211-1247\(15\)00498-2.pdf](http://www.cell.com/cell-reports/pdf/S2211-1247(15)00498-2.pdf) [Accessed April 19, 2017].
- Zhu, D. et al., 2015. Munc18c mediates exocytosis of pre-docked and newcomer insulin granules underlying biphasic glucose stimulated insulin secretion in human pancreatic beta-cells. *Molecular Metabolism*, 4(5), pp.418–426. Available at: <http://www.ncbi.nlm.nih.gov/pubmed/25973389> [Accessed May 12, 2017].
- Zolov, S.N. & Lupashin, V. V., 2005. Cog3p depletion blocks vesicle-mediated Golgi retrograde trafficking in HeLa cells. *The Journal of cell biology*, 168(5), pp.747–59. Available at: <http://www.ncbi.nlm.nih.gov/pubmed/15728195> [Accessed June 16, 2017].

Appendices

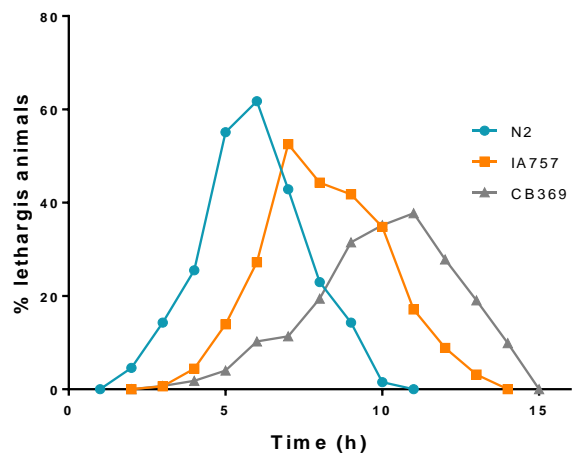
A)



B)



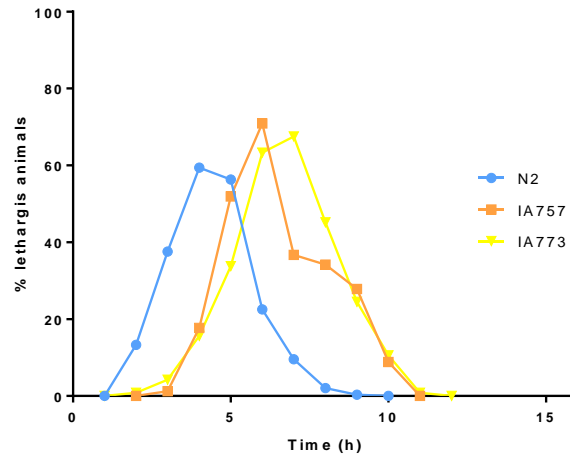
C)



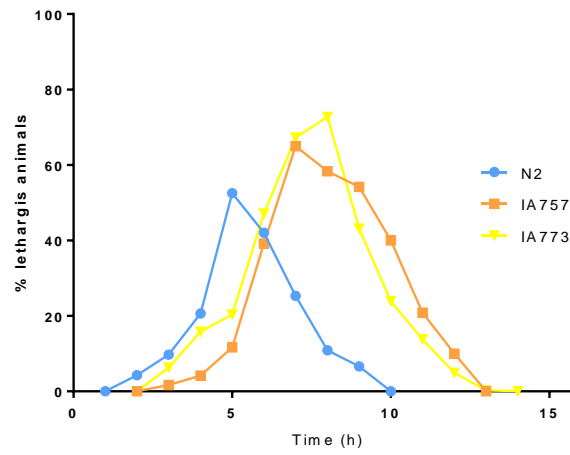
Appendix 1: Molting profiles of wild type (N2), *vps-45 (tm246)* (IA757), *unc-51 (e369)* (CB369) strains during the L1-L2 molt at 15°C.

Three individual experiments are shown (A-C).

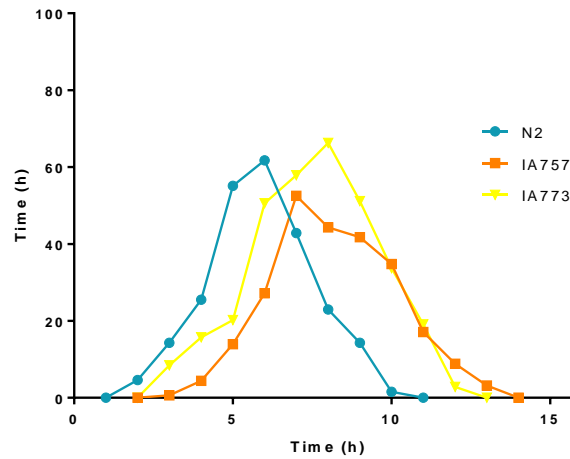
A)



B)

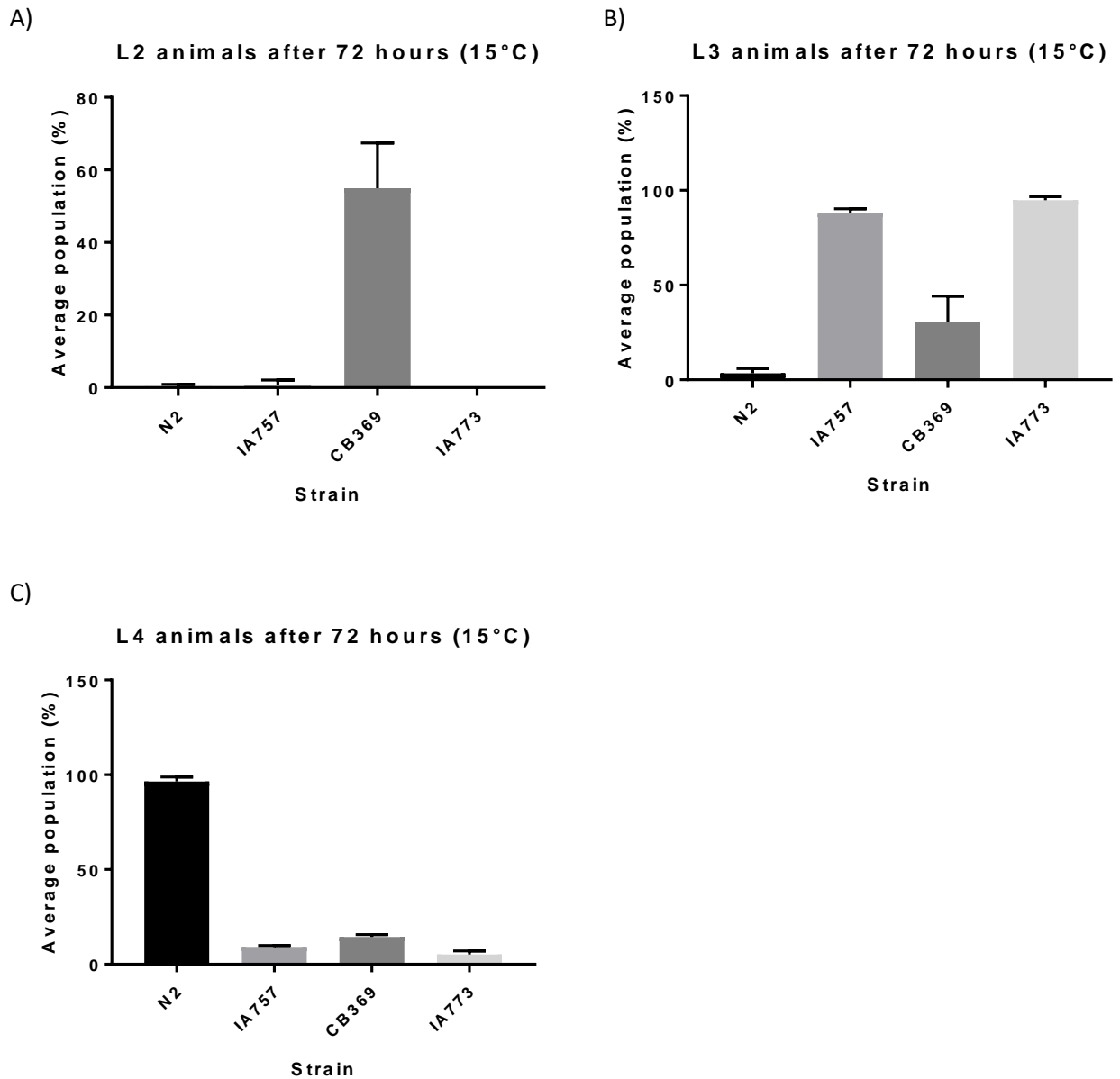


C)

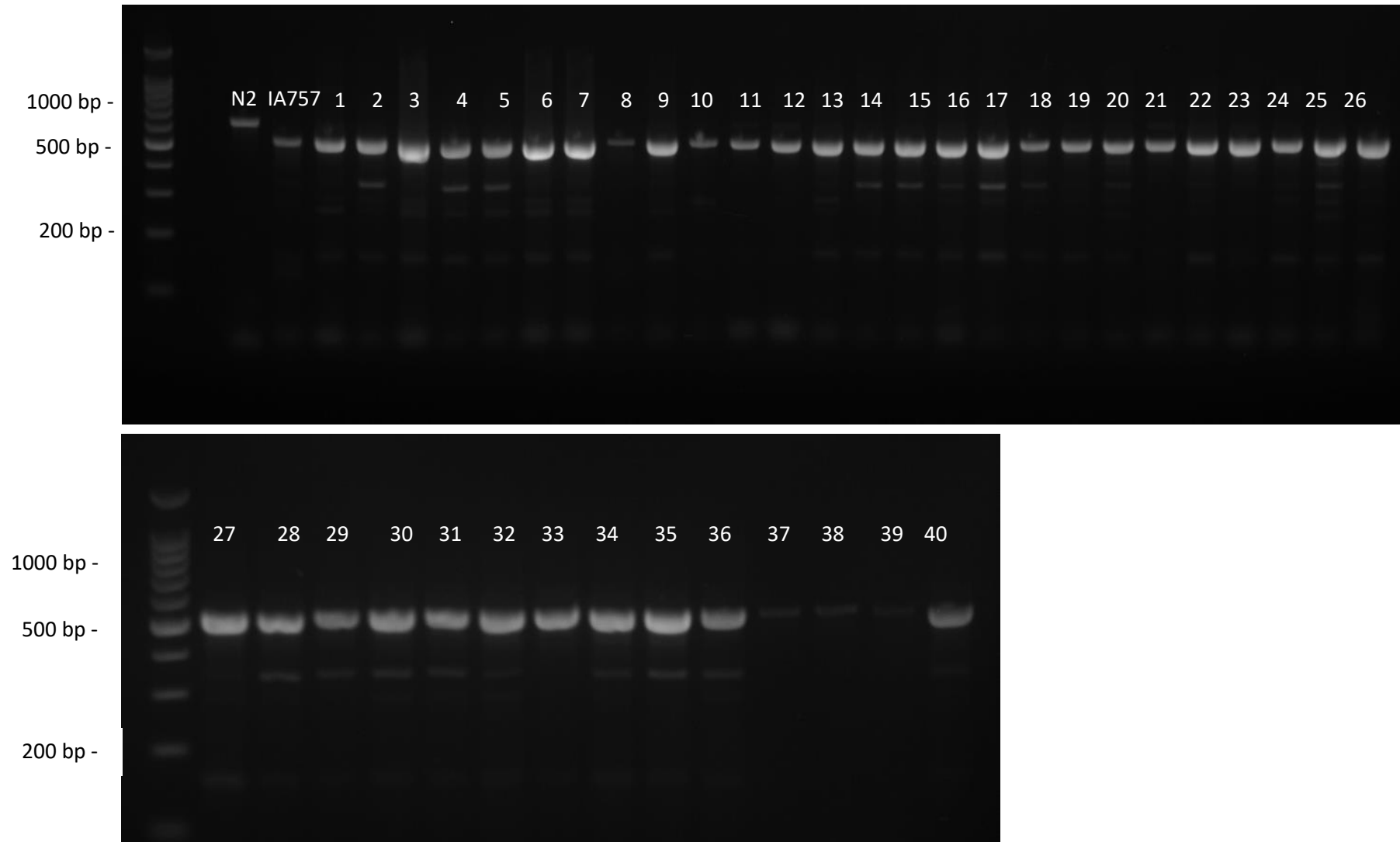


Appendix 2: Molting profiles of adult wild type (N2), *vps-45* (tm246) strain (IA757), *svp* (*ij117*) strain (IA773) during the L1-L2 molt at 15°C.

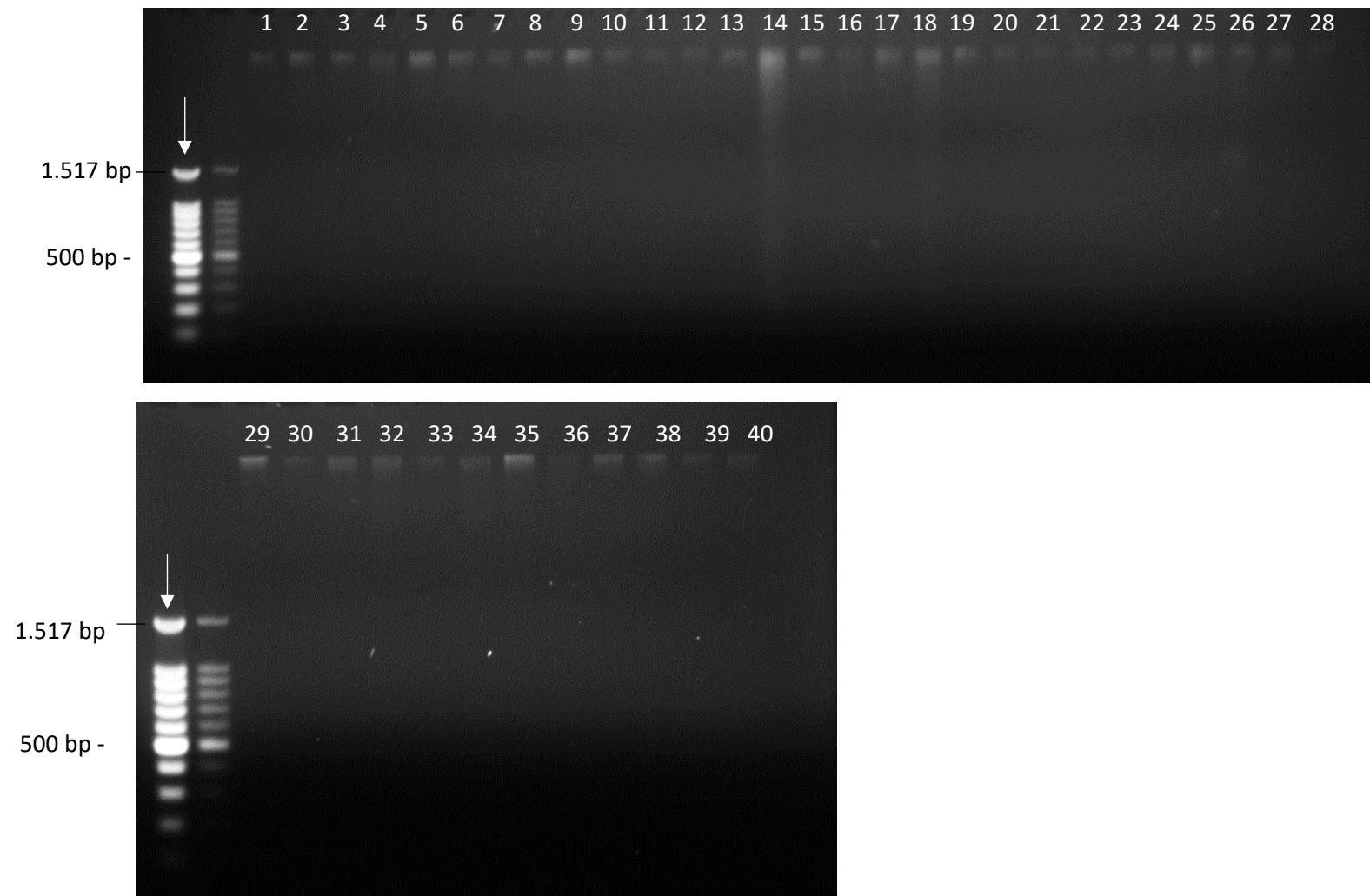
Three individual experiments are shown (A-C). Both IA757 and IA773 populations start molting at 1-2 hours later than the wild type stain.



Appendix 3: Average percentage of animals at a specific developmental stage for each strain after 72 hours of culturing at 15°C. Average of three experiments for each strain is shown. A) Percentage of animals at the L2 stage (\pm SD). Tukey's multiple comparison test N2 vs IA757, $P=0.9998$. N2 vs CB369, $P<0.0001$. IA757 vs CB369, $P<0.0001$. N2 vs IA773, $P=0.9999$. IA757 vs IA773, $P=0.9987$. B) Percentage of animals at the L3 stage (\pm SD). Tukey's multiple comparison test N2 vs IA757, $P<0.0001$. N2 vs CB369, $P=0.0066$. IA757 vs CB369, $P<0.0001$. N2 vs IA773, $P<0.0001$. IA757 vs IA773, $P=0.6718$. C) Percentage of animals at the L4 stage (\pm SD). Tukey's multiple comparison test N2 vs IA757, $P<0.0001$. N2 vs CB369, $P<0.0001$. IA757 vs CB369, $P=0.0208$. N2 vs IA773, $P<0.0001$. IA757 vs IA773, $P=0.0784$.



Appendix 4: 40 homozygotic lines for the *vps-45(tm246)* after cross with the Hawaiian strain verified by PCR. Verification of the suppression for the molting death by survival at 25°C.



Appendix 5: Genomic isolates of the 40 suppressed lines for the *vps-45 (tm246)* molting death at 25°C, after treatment with RNase.

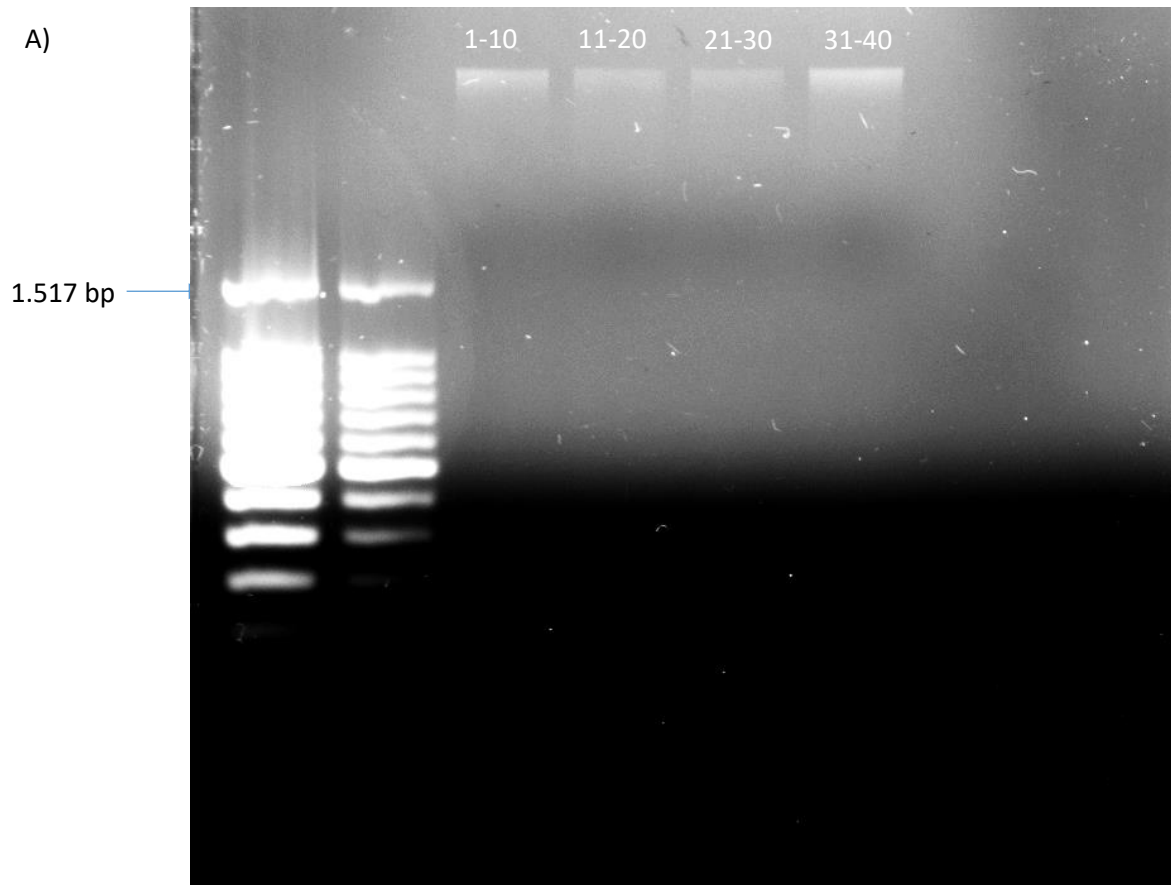
Isolates generated for full genome sequencing. Ladder was loaded at 10 μ l and 5 μ l. The 500 bp band from the ladder was used as the control for the quantification of the rest of the samples, the band has 97 ng of DNA.

Column 1			Column 2		
SAMPLE	ng/ μ l	volume for final mix (μ l)	SAMPLE	ng/ μ l	volume for final mix (μ l)
1	2.987747408	33.47003155	11	7.587182	13.18012422
2	4.458058435	22.43128964	12	7.832234	12.7677497
3	4.79736098	20.84479371	13	8.341188	11.98870056
4	5.34401508	18.71252205	14	11.32893	8.826955075
5	7.295004713	13.70801034	15	8.774741	11.39634801
6	6.889726673	14.51436389	16	7.615457	13.13118812
7	6.738925542	14.83916084	17	8.62394	11.59562842
8	11.27272727	8.870967742	18	9.245994	10.81549439
9	8.934967012	11.19198312	19	8.086711	12.36596737
10	7.747408106	12.90754258	20	7.210179	13.86928105
Total volume(μl)		171.4906654			119.9374369

Column 3			Column 4		
SAMPLE	ng/ μ l	volume for final mix (μ l)	SAMPLE	ng/ μ l	volume for final mix (μ l)
21	6.918002	14.45504087	31	3.426966	29.18032787
22	6.908577	14.47476126	32	3.445693	29.02173913
23	6.757776	14.79776848	33	2.84176	35.18945634
24	6.823751	14.65469613	34	3.03839	32.91217257
25	6.993402	14.29919137	35	3.77809	26.46840149
26	5.777568	17.30831974	36	6.208178	16.10778443
27	4.542884	22.01244813	37	2.570225	38.90710383
28	3.025448	33.0529595	38	2.275281	43.95061728
29	3.426966	29.18032787	39	1.348315	74.16666667
30	2.827715	35.36423841	40	0.828652	120.6779661
		209.5997518			446.5822357

Appendix 6: Table showing the concentration of each sample from the 40 sequencing lines genomic isolates, as it was quantified from the gel pictures.

Samples were mixed together in 4 tubes (10 samples per tube) with 100 ng/ μ l final concentration for each sample. The mix from each tube was passed through a DNA cleaning column to remove the RNase enzyme.

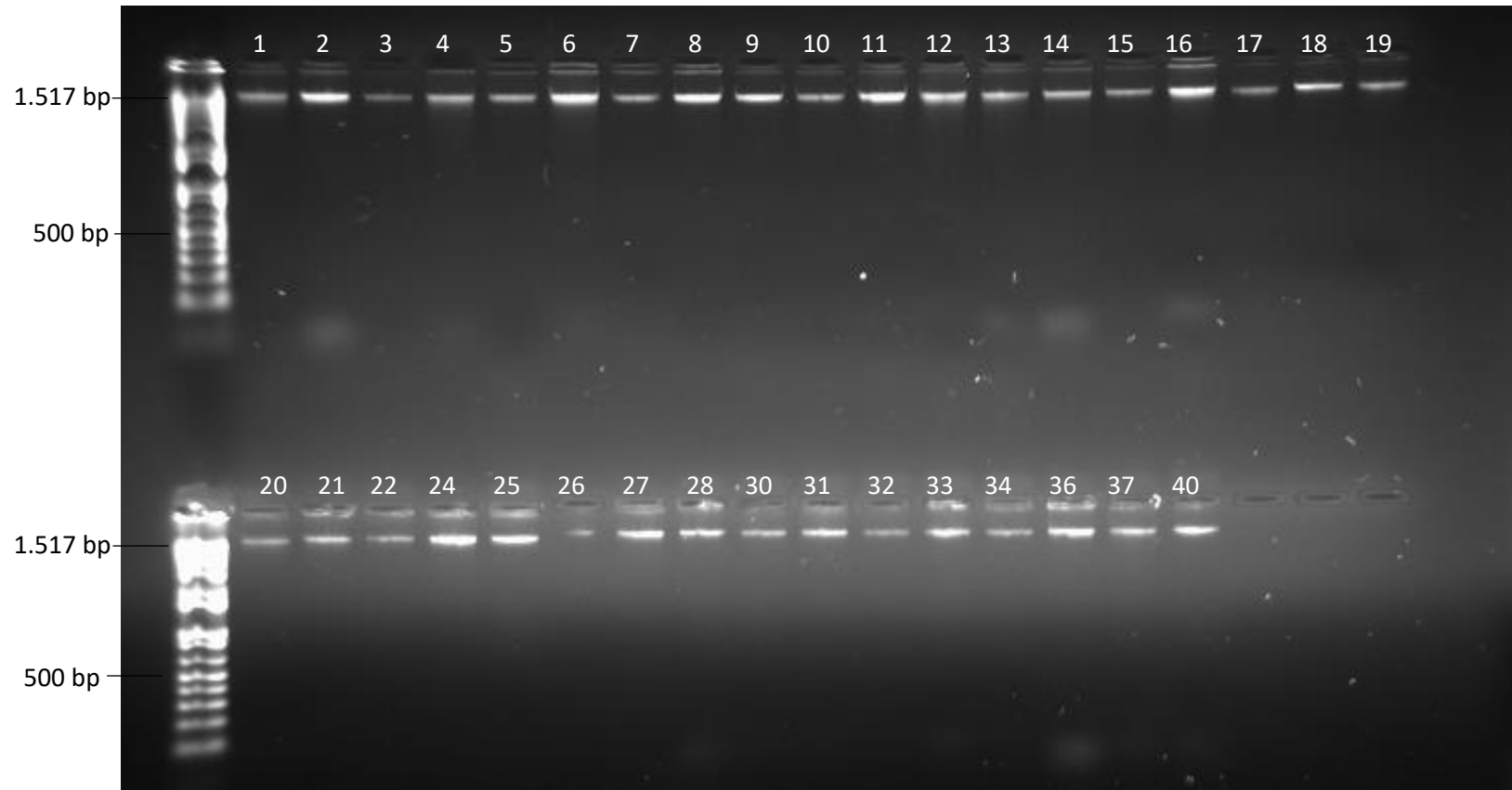


B)

SAMPLE	ng/ μ l (nanodrop)	Volume for final mix (μ l)
1-10	2.1	476
11-20	1.8	555
21-40	2.9	344
41-60	3.1	320
		Final volume: 1695 μ l

Appendix 7: Sample pools prior to final mix for full genome sequencing.

A) Genomic DNA of all 40 lines pulled together in 4 mixes, after removal of the RNase. B) Table after quantification of the 4 pulled samples for the sequencing with the nanodrop. Volumes required for the addition of 1000 ng from each sample.



Appendix 8: Genomic isolates of the 35 suppressed lines for the *vps-45 (tm246)* molting death at 25°C excluding the five slow growing lines, after treatment with RNase.

Isolates generated for the second round of full genome sequencing. Ladder was loaded at 10 μ l. The 500 bp band from the ladder was used as the control for the quantification of the rest of the samples, the band has 97 ng of DNA.

Column A			Column B		
SAMPLE	ng/μl	volume for final mix	SAMPLE	ng/μl	volume for final mix
1	21.39937373	14.01910186	8	29.38898	10.2079084
2	29.35723362	10.21894651	9	26.61252	11.27289073
3	16.12266202	18.60734906	10	21.86167	13.72264744
4	23.72794994	12.6433173	11	31.39324	9.556198699
5	21.32526165	14.0678227	12	29.5149	10.16435637
6	32.76058557	9.157345473	13	25.21992	11.89536046
7	20.61645979	14.55147989	14	24.19593	12.39877711

Total		93.2653628			79.21813921
volume(μl)					

Column C			Column D		
SAMPLE	ng/μl	volume for final mix	SAMPLE	ng/μl	volume for final mix
15	20.3086738	14.77201332	22	24.04400816	12.47712103
16	30.57985707	9.810379405	24	32.07471967	9.353160467
17	18.2422537	16.44533646	25	30.43289921	9.857752885
18	22.57470775	13.28920859	26	24.21954235	12.38669153
19	18.40736202	16.29782691	27	30.84353186	9.72651256
20	48.69255906	6.161105635	28	29.47836997	10.17695349
21	25.5539895	11.73984986	30	27.20854129	11.02594942

		88.51572018			75.00414138
--	--	--------------------	--	--	--------------------

Column E

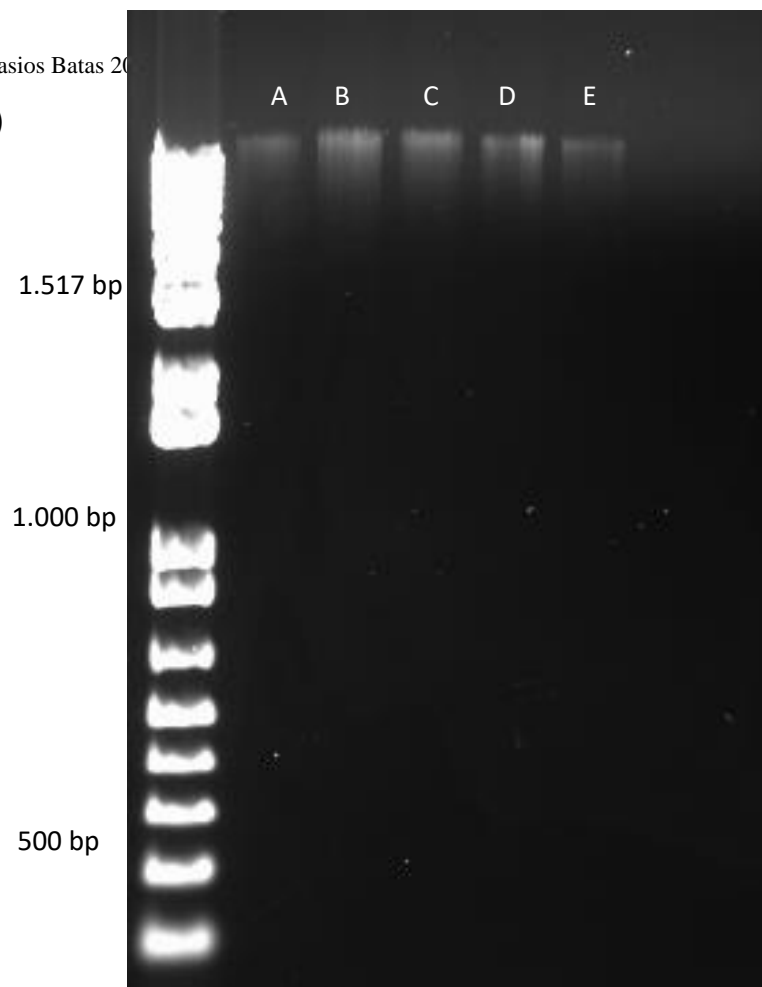
SAMPLE	ng/ μ l	volume for final mix
31	29.66812027	10.11186409
32	25.76589628	11.64329767
33	29.72941141	10.09101714
34	26.64130776	11.26070847
36	31.34359506	9.571333456
37	28.64796542	10.47194785
40	28.63165125	10.47791472

		73.6280834
--	--	-------------------

Appendix 9: Table showing the concentration of each sample from the genomic isolates, as it was quantified from the gel pictures for the second round for full genome sequencing.

Samples were mixed together in 5 tubes (7 samples per tube) with 100 ng/ μ l final concentration for each sample. The mix from each tube was passed through a DNA cleaning column to remove the RNase enzyme.

A)



B)

SAMPLE	ng/ μ l (nanodrop)	Volume for final mix (μ l)
A (1-7)	10.1	19.8
B (8-14)	8.3	24
C (15-21)	8.1	24
D (22-28, 30)	7.3	27
E (31-34, 36,3,40)	6.7	30
		Final volume:124.8 μ l

Appendix 10: Sample pools prior to final mix for the second round of full genome sequencing.

A) Genomic DNA of all 35 'fast growing' lines pulled together in 5 cleaning mixes, after removal of the RNase. B) Table after quantification of the 5 pulled samples for the sequencing with the nanodrop. Volumes required to achieve 200ng of DNA per sample.